****

******SRI SAI NADHAYA NAMAH **********

*****Sada nimba vrukshasya mooladhi vasat!***

***Sudha sravinam tikta mapya priyamtam ! ***

*** Tarum kalpavrukshadhikam sadhayantam! ***

*** Namameeswaram sadgurum sainadham ! ***

****

STUDIES ON FLOW INSTABILITIES AND NONLINEAR OSCILLATIONS IN NATURAL CIRCULATION BOILING SYSTEMS

A Thesis Submitted in
Partial Fulfillment of the Requirements
for the Degree of

DOCTOR OF PHILOSOPHY

by

Gonella V. Durga Prasad
(*Roll No. 02610302*)

DEPARTMENT OF MECHANICAL ENGINEERING
INDIAN INSTITUTE of TECHNOLOGY GUWAHATI
MARCH 2008

ACKNOWLEDGMENTS

I express my sincere gratitude and hearty thanks to my supervisor, Dr. Manmohan Pandey, for his valuable and inestimable guidance and constant encouragement. I am deeply inspired not only by his experience and knowledge, but also the way of approaching a problem, immense patience and utmost care. I am highly indebted to him for his untiring devotion and willingness. During my research work, he provided me with the most valuable ideas, which played a vital role in the completion of research work successfully. I enjoyed each and every moment working under his supervision and learnt a lot many things from him, which will be an asset for my future research.

I wish to express my warm and sincere thanks to my doctoral committee members Prof. Subhash C. Mishra, Prof. Anoop K. Dass and Dr. Ujjwal K. Saha for giving their valuable suggestions and encouragement during my research work.

I would like to express my sincere thanks to Prof. U. S. Dixit (H.O.D. Mechanical Engineering Department) for providing all the facilities needed during my research work. I take this opportunity to thank all the faculty members for their valuable suggestions and cooperation during my course work. I specially thank Mr. Amal Kalita for allotting a separate computer in the CAD lab for my research work.

I wish to express my warm and sincere thanks to Dr. S.K. Gupta (Director, SADD) and Mr. S.K. Pradhan of Atomic Energy Regulatory Board (AERB) for their valuable suggestions and encouragement. I also take this opportunity to specially thank Mr. S.K. Pradhan for his help in learning RELAP5/MOD3.4.

I am sincerely thankful to the Indian Institute of Technology Guwahati for providing me the sufficient funds and grants to have this research work done successfully. I am also greatly thankful to Atomic Energy Regulatory Board (AERB) for providing the financial support for the successful completion of my research work.

I express my sincere and respectful gratitude to my grandparents Sri G. Subba Rao and Smt. Suryakantamma garu who laid the foundation for my prospective career. I am very much indebted to their interminable loving care and affection on me during my childhood days as I was brought up under their supervision.

My deepest gratitude goes to my father Sri. G.S.R. Murthy and mother Smt. G. Prameela whose blessings and incessant support is the real impetus that continuously motivates me to produce my best. I extend my blessings and wishes to my siblings Smt.

A. Padmaja and Mr. Girish for their support and encouragement. I pray god for their glorious and prosperous future.

I reserve my heart full of affection and sincere gratitude to my wife Jnana Deepti for her love and patience during my research work. I take this opportunity to appreciate and thank her for the hardship she had undergone during the stressful moments of my research work. I wish to express my warm and sincere thanks to my parents-in-law Sri. D. Radhanga Pani and Smt. Kameswari for their support and encouragement.

I express my sincere thanks to each and all of my relatives and well-wishers who encouraged me to accomplish my research work.

I express my sincere thanks to my best friends Mr. Sankar Sastry, Mr. Kavala Veerababu Rao, Mr. Elaprolu Vishnu Vardhana Rao, Mr. B. Rama Raju, Mr. Vijay Kumar Pantangi and Mr. Jagu Srinivasa Rao for their constant support and making my stay pleasant at IIT Guwahati. I wish them all the best in their future endeavors.

All my lab buddies of Mechanical Engineering Department made it a convivial place for me to work. In particular, I would like to thank Mr. S.P. Lakshmanan (Laksh) for his constant support, friendship and help during my research work. All other folks, including Krishnayya, Ashok Kumar and Gopa Kishore, had supported me in research work through our interactions during the long hours in the lab.

I take this opportunity to express my sincere thanks to Smt. Divya Pandey for her kind hospitality and concern during our tough times. I extend my blessings and wishes to Master Subham Pandey. I wish him a glorious and prosperous future.

The chain of my gratitude would be definitely incomplete if I would forget to thank the divine force behind this accomplishment. I offer my respectful salutation to the holy sandals of my Sadguru, Sri Sai Baba, of Shirdi who drew me to himself and graced me with his supreme blessings. His perpetual blessings inspired and enriched me with my life's goal and afforded me this glorious chance to accomplish my Doctoral degree.

List of Publications from this thesis work

Journals

1. Durga Prasad, G.V., Pandey, M., Kalra, M.S. (2007). Review of research on flow instabilities in natural circulation boiling systems. Progress in Nuclear Energy 49, 429-451.

2. Durga Prasad, G.V., Pandey, M. (2008) Stability analysis and nonlinear dynamics of natural circulation boiling water reactors. Nuclear Engineering and Design 238, 229-240.

3. Durga Prasad, G.V., Pandey, M., Pradhan, S. K., Gupta, S. K. (2008) Study of flow instabilities in a double channel natural circulation boiling system. Nuclear Engineering and Design 238, 1750-1761.

4. Durga Prasad, G.V., Pandey, M. Parametric effects on reactivity instabilities and nonlinear oscillations in a nuclear-coupled double channel natural circulation boiling system . Annals of Nuclear Energy (communicated).

Conferences:

1. Durga Prasad, G.V., Pandey, M., Kalra, M.S. A Review of investigations on flow instabilities in natural circulation boiling loops. In: Proceedings of The 11th International topical meeting on Nuclear Reactor Thermal Hydraulics (NURETH-11), Avignon, France, October 2-6, 2005.

2. Durga Prasad, G.V, Pandey, M., Pradhan, S.K., Gupta S.K. Nonlinear dynamics of pressure tube type natural circulation boiling water reactor. In: Proceedings of The 12th International topical meeting on Nuclear Reactor Thermal Hydraulics (NURETH-12), Pittsburg, Pennsylvania, U.S.A, September 30-October 4, 2007.

3. Durga Prasad, G.V, Pandey, M. Instabilities and nonlinear oscillations of natural circulation boiling systems. In: Proceedings of 19th National and 8th ISHMT-ASME Heat and Mass Transfer Conference, Hyderabad, January 3-5, 2008.

4. Durga Prasad, G.V., Pandey, M., Pradhan, S.K., Gupta S.K. Numerical investigation of on-power refueling in a natural circulation boiling water reactor. ICONE16-48390, In: Proceedings of 16th International conference on Nuclear Engineering ICONE-16, Orlando, Florida, USA, May 11-15, 2008.

Abstract

The present work consists of numerical studies on flow instabilities in natural circulation boiling systems. An exhaustive review of literature has been carried out. Boiling systems have been modelled using two different approaches: lumped parameter modelling and RELAP5/MOD3.4 code. Thermal-hydraulic as well as coupled neutronic-thermohydraulic instabilities have been studied in single and double channel systems. Nonlinear oscillations, bifurcations and chaotic oscillations have also been investigated.

The latest generations boiling water reactors (BWRs) are designed with natural circulation as the operation mode under both normal and abnormal conditions. Use of natural circulation is very common in fossil-fuel boilers also. Natural circulation boiling systems are subjected to flow instabilities due to parametric fluctuations, inlet conditions etc., which may result in mechanical vibrations of components and system control problems and reduction in the critical heat flux. Analysis of these instabilities in natural circulation boiling loops is very important for the safety of nuclear reactors and other boiling systems. Linear stability theory is widely used to study the onset of instabilities and system behavior under small perturbations around a steady state. However, instabilities due to nonlinear effects become significant as the perturbations grow. A system stable for small perturbations may become unstable for large perturbations, if there is a repeller (e.g., an unstable limit cycle) in the state space. Perturbations in an unstable system may not grow indefinitely, and the system may approach an attractor (e.g., a stable limit cycle) in the state space. The limit cycle oscillations may amplify and undergo period doubling, and eventually lead to aperiodic or chaotic oscillations through a cascade of period-doubling bifurcations. In order to predict the frequency and amplitude of these oscillations, and their influence on the reactor stability, nonlinear dynamic analysis is required.

Safety concerns of nuclear reactors have attracted the attention of researchers on flow instabilities in natural circulation boiling loops. During the past three decades, a large number of experimental and numerical investigations have been conducted to study and understand the conditions for inception of flow instabilities, parametric effects on instabilities, and the system behaviour under such conditions. To review the state of the art, an exhaustive survey of literature has been carried out by reviewing over 100 contributions. Work done on instabilities due to channel thermal-hydraulics as well as neutronics thermal-hydraulics coupling has been discussed. Different methods of analysis used by researchers and results obtained by them have been reviewed. Various mathematical

models and numerical techniques adopted for developing computer codes have also been discussed. The findings reported in the investigations made in the past three decades have been summarized to present the state of the art of the understanding of flow instabilities in natural circulation boiling systems.

A single channel natural circulation boiling system is modelled using a lumped parameter mathematical model and RELAP5/MOD3.4 code. The thermal-hydraulic model in the present study has been obtained by non-dimensionalizing and integrating one-dimensional equations of mass, momentum and energy balances for the coolant, using the homogeneous equilibrium model for two-phase flow. The power dynamics in the lumped parameter model is represented by point neutron kinetics. Comparison studies are carried out using lumped parameter mathematical model and RELAP. Complete linear stability analysis is carried out with the lumped model. The effect of various geometrical parameters and feedback parameters on the stability of the system is studied in detail and discussed. Different, but seemingly contradictory findings reported in literature about the effects of void reactivity coefficient and fuel time constant on the stability of the system are resolved. The different findings reported by different authors may be either due to the different geometrical and neutronic parameters or due to the different approaches to mathematical modeling. To investigate this, three different system configurations have been analysed using the same mathematical model. The effect of fuel time constant and void reactivity coefficient on the stability of the system in Type-I and Type-II regions has been studied for the three system configurations. Stability maps have been plotted in a non-dimensional parameter plane and compared with the findings reported in literature. It is confirmed that the differences in the results reported in literature is due to the influence of system parameters and cannot be attributed to model uncertainties.

Nonlinear dynamics and bifurcations have been studied numerically, for one of the geometrical configurations, for boiling channels with and without riser. The possibility of existence of stable and unstable limit cycles, period doublings, and chaotic oscillations has been investigated. Stable as well as unstable limit cycles have been located by the autonomous shooting technique. The effect of VR on the nonlinear dynamics has been studied in the Type-I as well as Type-II regions. Further, the effects of void reactivity coefficient and fuel time constant on the occurrence of chaotic oscillations in Type-II region are investigated. The methods of limit cycle shooting, Fourier power spectra, Poincaré sections, and Lyapunov exponents have been used in this study.

Such single channel analysis is simple and appropriate for studying in-phase oscillations in a system of parallel channels with uniform power profile. However, single channel models are inadequate for simulating out-of-phase oscillations. Moreover, the power profile across the channels is not uniform and constant. Power fluctuations in some of the channels can trigger thermal-hydraulic oscillations in other channels due to closed loop boundary conditions. In order to study the transients due to channel-to-channel interactions and on-power refueling, a double channel system is modelled with a lumped parameter mathematical model (LPM) and with REALP5/MOD3.4. The lumped model of the single channel system is modified and extended to a double channel system. Stability and nonlinear dynamic analysis is carried out using the lumped parameter model. The oscillations modes of the two equal powered geometrically identical parallel channels are investigated in Type-I and Type-II regions. The effects of gravitational and frictional pressure drops and geometrical parameters on the oscillation modes are investigated. Channel-to-channel interaction and on-power refueling studies are carried out using RELAP model. During the refuelling process, there will not be power input to that channel. The flow area increases and single-phase liquid flows through this channel. During such conditions, complex channel-to-channel interactions exist, which may destabilize the system.

In boiling water reactors, there is coupling between the neutronics and thermal- hydraulics. The spatial distribution of neutrons in the reactor core and its interaction with thermal-hydraulics influences the types of instabilities observed in the reactor. In order to study the effects of such coupling, the double channel thermal-hydraulic model is coupled with a multi-point reactor kinetics model. The effects of various parameters (such as neutron interaction coefficient, fuel time constant and void reactivity coefficient and geometric parameters) on the stability of system and modes of oscillations at different operating conditions are investigated. Nonlinear dynamic analysis is carried out and the effect of the parameters on the types of bifurcation and chaotic oscillations is studied. The chaotic oscillations are confirmed by evaluating Lyapunov exponents, power spectral density and Poincaré sections.

In the study of single channel system, it was found that the effects of void reactivity coefficient and fuel time constant on system stability are influenced by the geometrical parameters and are different for different systems. Supercritical as well as subcritical Hopf bifurcations were observed in both Type I and Type II regions, for different ranges of void reactivity coefficient. Chaotic oscillations were observed under strong reactivity feed-

back in the Type-II region for boiling channels with and without riser. In the analysis of thermal-hydraulic instabilities in a double channel system, it was found that the two channels oscillate out-of-phase in Type-I region due to dominant gravitational pressure drop at low powers. In Type-II region, the channels oscillate in both in-phase and out-of-phase modes depending on the dominance of two-phase frictional pressure drop and the downcomer inertia. It was also observed that geometrical parameters influence the mode of oscillations in Type-II region, but not in Type-I region. In channel-to-channel interaction studies with RELAP, it was found that at low powers, disturbance in one channel does not have significant effect on the other channel. At higher powers, disturbances in one channel significantly affect the stability of other channels. During on-power refueling, a near-stagnation condition or low-velocity reverse flow can occur, the possibility of reverse flow being higher at lower pressures. In the study of coupled neutronic-thermohydraulic instabilities in a double channel system, it was found that the neutron interaction coefficient has a destabilizing effect in Type-II region and stabilizing effect in Type-I region. An increase in the absolute value of void reactivity coefficient increases the gain of neutronic feedback due to which in-phase oscillations occur. Fuel time constant has a strong influence on the modes of oscillations. Increase in fuel time constant increases delay and suppress the neutronic feedback. Consequently, the channels oscillate in out-of-phase mode. The delay effect of fuel time constant is strong at high powers and low absolute values of void reactivity coefficient. Strong neutron interaction between the channels causes in-phase oscillations. Increase in riser length and downcomer inertia causes out-of-phase oscillations. Subcritical and supercritical Hopf bifurcations are observed at different operating conditions. Strong neutron interaction between channels suppresses the chaotic oscillations.

Contents

List of Figures

List of Tables

Nomenclature

A	area in m^2
c	delayed neutron precursor density expressed in (W/m)
C_p	specific heat at constant pressure (J/kg)
D	diameter (m)
f	friction factor
g	acceleration due to gravity (m/s^2)
G	mass flux density ($kg/m^2.s$)
G_0	Steady state inlet mass flux density of first channel in multi channel system
h	enthalpy (J/kg)
H_f	effective heat transfer coefficient
j	auxiliary function
$j_{1,c,0}$	steady state void fraction in terms of auxiliary function
$j_{1,R,0}$	steady state riser void fraction in terms of auxiliary function
L	length (m)
N_{Fr}	Froud number = $(\frac{G_0}{\rho_l})^2/gL$
N_s	ratio of residence time and fuel time constant = $(4L_c\rho_l H_f)/(\rho_f G_0 D_f C_{pf})$
N_{sub}	Subcooling number = $(h_l - h_{ci})(\rho_l - \rho_g)/\rho_g(h_g - h_l)$
N_{Zu}	Zuber number = $q_0 L(\rho_l - \rho_g)/\rho_g G_0 A(h_g - h_l)$
N_ρ	Density number = ρ_g/ρ_l
P	Pressure (MPa)
ΔP_a	acceleration pressure drop
ΔP_f	frictional pressure drop
ΔP_g	gravitational pressure drop
ΔP_i	inertial pressure drop
ΔP_m	pressure drop due to minor losses

q'	neutron density expressed in linear power units (W/m)
q	Heat flux (W/m^2)
Q	Volumetric heat generation rate (W/m^3)
t	time (s)
t_{ref}	reference time (s) = $(L\rho_l)/(G_0)$
T	temperature (K)
U	Internal energy
v	velocity
V	Specific volume of two-phase mixture at equilibrim
X	steam quality
Z	axial position (m)

Greek Symbol

α	void fraction
β	delayed neutron fraction
Γ	diffusion coefficient
γ_a	void reactivity coefficient
γ_d	doppler coefficient
λ	delayed neutron precursor decay constant (s^-1)
Λ	neutron generation time (s); friction number
ρ	density (kg/m^3); reactivity
μ	Viscosity
τ	fuel time constant = $(D_f\rho_f C_{pf})/4H_f$
ξ	normalised length coordinate

Subscripts

av	average
bb	boiling boundary
C	core
ci	core inlet
ce	core exit
D	downcomer
Di	downcomer inlet
f	fuel
fi	feed water inlet
g	saturated vapor
k	phase (liquid or vapour)
j	number of channels
l	saturated liquid
n	node
R	riser
Ri	riser inlet
Re	riser exit
s	steam
sat	saturated
w	water
0	steady state

Superscript

*	non-dimensionalised

Abbreviations

NCBWR	Natural circulation boiling water reactor
PHT	Primary heat transport loop
LPM	Lumped parameter model
MSB	Marginal stability boundary
ODE	Ordinary differential equation
VR	Void reactivity coefficient

Chapter 1

Introduction

1.1 Motivation

The concept of nuclear power generation had started in 1950. Today according to IAEA statistics (www.iaea.org), there are 439 nuclear power plants in operation with a total net installed capacity of 371.855 GW(e). The nuclear reactors can be classified on the basis of generation which characterizes the evolution of nuclear power technology. Generation I reactors are basically proto-type reactors and are of the same type. In early 1970s different designs of commercial nuclear power reactors are developed which are categorized as generation-II reactors. The generation II reactors include PWR, BWR, CANDU etc. Generation III reactor are advanced versions of generation II reactors with standardized designs, improved fuel technology, and passive safety systems. The design of nuclear reactors based on forced circulation mode is complex due to the requirement of recirculation pumps and the related piping systems and hence, economically expensive. Further, events such as pump trips and loss of coolant accidents (LOCA) subject these reactors with stringent safety regulations. Hence, the demand for more economical and reliable reactors with simple designs lead to the development of generation III+ reactors (which are extensions of generation III) with advanced passive safety features.

Natural circulation cooling is a key issue in the design of generation III + boiling water reactors (BWRs) for its simplicity, inherent safety, and maintenance reduction features. In natural circulation BWR, the coolant flow is driven by the density difference between

the two-phase mixture (in the core and the riser sections) and the single-phase coolant (in the downcomer). This passive feature ensures coolant circulation as long as heat is generated in the core. The elimination of recirculation pumps and related piping equipment prevents the accidents such as pump trips. The economic simplified boiling water reactor (ESBWR) is a generation III+ reactor designed by GE, based on natural circulation. In India, advanced heavy water reactor (AHWR) which is a pressure tube type natural circulation boiling water reactor based on Thorium fuel cycle is being designed as a part of its third stage of nuclear power program (www.barc.ernet.in).

Natural circulation boiling water reactors (NCBWRs) are less stable compared to forced circulation. The presence of riser (used to enhance circulation flow) induces new region of instability (Type-I) at low powers, during start-up. The current research (experimental and numerical) in natural circulation boiling water reactors is focused on better design and operational methodologies in order to minimize the thermal-hydraulic instabilities during start-up and full power operating conditions.

Numerical investigations based on mathematical models (both distributed as well as lumped parameter approaches) are used extensively to investigate various transients that may occur in NCBWRs. Lumped parameter approach is widely used to study the dynamic response of the system under different operating conditions. The present work is one such numerical investigation, in which NCBWRs are modeled using lumped parameter approach as well as with a commercial software RELAP5/MOD3.4 (which is based on a one-dimensional two fluid model). The theory of nonlinear dynamics is used to investigate the parametric effects on the nonlinear behavior of NCBWR.

1.2 Objectives

- To develop a better insight into the parametric effects on the stability characteristics and nonlinear dynamic behavior of the natural circulation boiling water reactors under different operating conditions.

- To resolve the contradictory findings reported in literature about the stabilizing and destabilizing effects of void reactivity coefficient and fuel time constant on the system.

- To investigate the influence of geometrical configuration on: the effects of feedback and delay parameters on system stability, bifurcation characteristics, period doubling scenario, and chaotic oscillations.
- To investigate the parametric effects on the bifurcation scenario and chaos in Type-I and Type-II regions. Further, to study the possibilities of subharmonic and aperiodic behaviour by calculating the Poincaré sections, Fourier power spectra, and, where necessary, Lyapunov exponents.
- To investigate the stability characteristics and nonlinear oscillations in a double channel system using lumped parameter model.
- To investigate the effect of channel-to-channel interaction in a double channel system, and the transients occurring in the system during on-power refueling using a commercial software RELAP5/MOD3.4.
- To study the effect of parameters such as void reactivity coefficient, fuel time constant, neutron interaction coefficient, and geometrical configuration on the modes of oscillations in a double channel nuclear-coupled natural circulation system.

1.3 Outline of the thesis

The thesis is organized in the following manner.

A detailed review of the research carried out on instabilities in natural circulation boiling systems is discussed in Chapter 2. The findings reported in the past three decades have been summarized to present the state of the art of the understanding of flow instabilities in natural circulation boiling systems. The derivation of the lumped parameter mathematical model of the natural circulation system is presented in Chapter 3. A brief discussion about the code structure, numerical schemes, and different hydrodynamic components of RELAP5/MOD3.4 is also presented. Chapter 3 further discusses the comparison studies carried out for a pressure tube type NCBWR using the lumped parameter and RELAP5 models.

Stability analysis and nonlinear dynamics of a single channel natural circulation boiling water reactor using a lumped parameter model is presented in Chapter 4. Parametric

effects on stability, bifurcation characteristics, period doubling scenario, and chaotic oscillations are investigated. Chapter 5 discusses channel thermal-hydraulic instabilities in a simple double channel system using a lumped parameter and RELAP5 models. Parametric effects on the modes of thermal-hydraulic oscillations are investigated using the lumped parameter model. The channel-to-channel interaction and on-power refueling in the double channel system and a pressure tube type NCBWR are investigated using RELAP5 model and compared.

Chapter 6 discusses coupled neutronic-thermohydraulic instabilities in a double channel system. The effects of parameters such as void reactivity coefficient, fuel time constant, neutron interaction coefficient, riser length, and downcomer inertia on the stability, modes of oscillations, bifurcation characteristics, and chaotic oscillations are discussed. The summary of the work done and the conclusions reached, together with a few observations on the possible extension of the present work, are presented in Chapter 7.

Chapter 2

Review of Literature

Safety concerns of nuclear reactors have attracted the attention of researchers on flow instabilities in natural circulation boiling loops. This chapter presents the state of the art in this area by reviewing a number of contributions. A large number of experimental and numerical investigations have been conducted to study and understand the conditions for inception of flow instabilities, parametric effects on instabilities, and the system behaviour under such conditions. Work done on instabilities due to channel thermal hydraulics as well as neutronics thermal hydraulics coupling has been reviewed. Different methods of analysis used by researchers and results obtained by them have been discussed. Various mathematical models and numerical techniques adopted for developing computer codes have also been discussed. The findings reported in the investigations made in the past three decades have been summarized to present the state of the art of the understanding of flow instabilities in natural circulation boiling systems.

2.1 Introduction

Steam generation systems are subjected to flow instabilities due to parametric fluctuations, inlet conditions etc., which may result in mechanical vibrations of components and system control problems. Analysis of these instabilities in natural circulation boiling loops is very important for the safety of nuclear reactors and other boiling systems. Instabilities in boiling channel systems occur due to external and internal disturbances. External

disturbances (perturbation transients) include fluctuations in mass flow rates (due to recirculation pump trip), sudden increase in steam flow (increase in demand), fluctuations in inlet enthalpy, fluctuations in heat supply rate etc. Internal disturbances include flow pattern transition due to heat transfer to the fluid. These instabilities generally prevail during startup/shutdown transients, triggering large parametric fluctuations that may lead to accidents. Thus, the study of dynamic behavior of the system is essential to develop efficient control systems for safe operation.

Flow in boiling channels is driven by external source (forced circulation) or by buoyancy force due to density difference of two phases (natural circulation). Earlier, all boiling water reactors (BWRs) were operated with forced circulation only. However, natural circulation is an important mode of operation for removing shutdown decay heat during accidents in such reactors. The latest generations BWRs are designed with natural circulation as the operation mode under both normal and abnormal conditions. The economic simplified boiling water reactor (ESBWR) designed by GE (Hinds and Maslak, 2006) and the advanced heavy water reactor (AHWR) being developed in India (Sinha and Kakodkar, 2006) are natural circulation BWRs. The heat removal from the core of NCBWR takes place by natural circulation during start-up, power rising and accidental conditions in addition to the rated full power operating condition. Use of natural circulation is very common in fossil-fuel boilers also.

In this chapter, a detailed review of the research carried out on instabilities in natural circulation boiling systems, in the past three decades is presented. Section 2.2 discusses classification of instabilities and explains various types of instabilities. Various approaches to mathematical modeling of natural circulation boiling systems and different numerical codes are discussed in Section 2.3. Section 2.4 reviews the investigations on nonlinear dynamics of natural circulation boiling systems. Experimental investigations are discussed in Section 2.5. The paper ends with concluding remarks in Section 2.6.

2.2 Flow Instabilities

A boiling channel with subcooled inlet conditions, and heated along its length, will have two basic flow regions, one is the single phase region, which extends from channel inlet

to boiling boundary (the point at which boiling starts), and the second is two-phase flow region in which the vapor and liquid coexist. The two-phase mixture plays an important role in heat transfer process and pressure drop in boiling channels. A close coupling exists between hydrodynamic and heat transfer processes in two-phase flow systems. The addition and removal of heat from a two-phase flow causes variations in the amount and distribution of each phase and the flow pattern or topology of the flow. These changes, in turn, induce variations in local heat transfer processes. Because of the continuous change of all the thermal and hydraulic properties of the flow, the situation at any axial point in the channel can never be fully developed either thermally or hydrodynamically. As the flow is not in equilibrium, the flow properties fluctuate highly both upstream and downstream of the point considered (Collier, 1994). The parameters such as void fraction distribution, flow pattern and its transition, temperature distribution and heat transfer coefficient along the boiling channel play an important role in the system stability. The knowledge of their behavior under different operating conditions is important for design and safe operation of boiling systems, particularly nuclear reactors.

Natural circulation: Flow under natural circulation is inherently less stable and experiences flow instabilities compared to the forced circulation mode, due to relatively small hydraulic driving head. In natural circulation loop, the heating process in the heater section is the driving force for the flow. The heat supplied will generate buoyancy and the flow will be created in the loop such that, in steady state, the buoyancy is balanced by the pressure drop due to friction and two-phase acceleration. If the heating power is increased further, the flow rate will also increase. On further increasing the heating power, the flow speed may be so large that sufficient time is not available for the fluid to be heated, and subcooled fluid enters the riser section and the buoyancy force reduces. The flow gets decelerated and even reversed. Therefore, a self-sustained oscillation is created which may be chaotic if the inlet subcooling is sufficiently large at a given heating power. These thermal-hydraulic oscillations in the two-phase natural circulation loop are quite similar to Lorentzian water wheel (Wu et al., 1996).

Flow instabilities are of different types depending on the system configuration and operating conditions. One of the earlier works on flow oscillations was by Jain et al. (1966), whose experimental investigation provided detailed information on the onset of oscillatory behavior and the effect of riser and test section dimensions. On the basis of

primary features such as oscillation periods, amplitudes, and relationships between pressure drop and flow rate, flow instabilities have been classified into several types, which were first proposed by Boure et al. (1973). BWRs are generally susceptible to three types of instabilities, as classified by March-Leuba and Rey (1993).

1. **Control system instability**: This is due to the malfunction of reactor hardware. Suitable control mechanisms are provided to deal with this type of instability.

2. **Thermal-hydraulic instabilities**: caused by self-oscillation of two-phase flow heated channel due to density wave effects. These instabilities are primarily classified as static and dynamic. These instabilities are discussed in Sections 2.2.1 and 2.2.2. Some static and dynamic type instabilities occur particularly during start up conditions. These instabilities are discussed in Section 2.2.4.

3. **Coupled neutronic thermal-hydraulic instabilities**: Also called reactivity instabilities, are due to the void and power feedback effects on neutron kinetics and thermal hydraulics respectively. In channel thermal-hydraulic instability, only flow feedback due to density effects is present, whereas in coupled neutronic reactivity instability, there is a power feedback (fuel transfer function) in addition to the flow feedback. Instabilities due to coupled neutronics are discussed in Section 2.2.3.

Figure 2.1 briefly presents the summary of the classification of instabilities discussed by Boure et al. (1973) and March-Leuba and Rey (1993).

2.2.1 Static Instabilities

Static instability is characterized by sudden large amplitude excursion of flow, to a new stable operating condition. The mechanism and the threshold conditions are predicted using steady state characteristics of the system. Pressure drop characteristics of a flow channel, nucleation properties, and flow regime transitions play important roles on characterization of static instabilities. Critical heat flux (CHF), which limits the heat transfer capability of boiling systems, is influenced by the static instabilities. Ledinegg instability, flow pattern transition instability, geysering, chugging and vapor burst etc. are categorized as static instabilities (Boure et al., 1973)

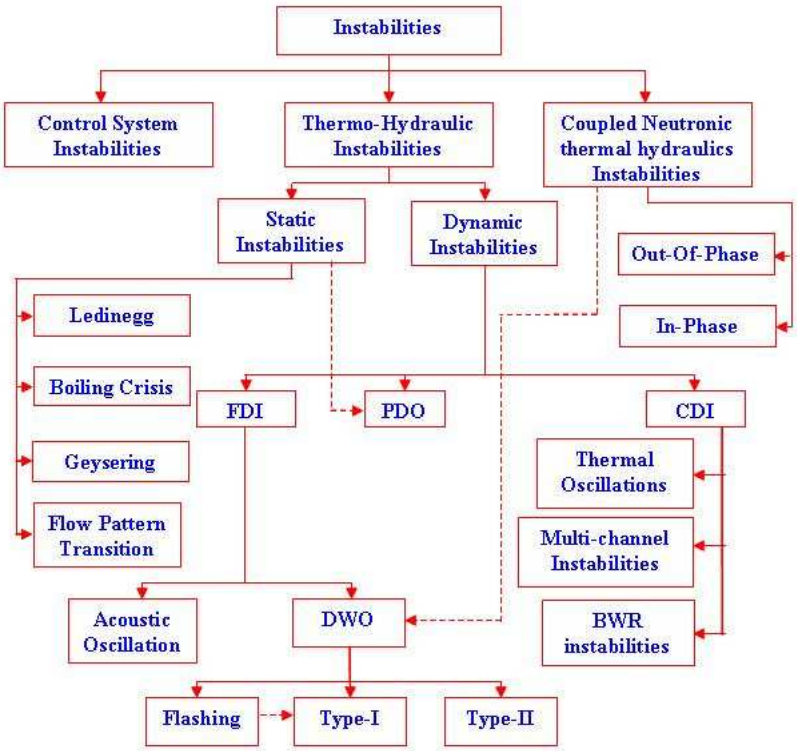

Figure 2.1: Flow instabilities tree

Ledinegg instability: It is characterized by a sudden change in the flow rate to a lower value or a flow reversal. This happens when the slope of channel demand pressure drop vs. flow rate curve (internal characteristic of channel) becomes algebraically smaller than the loop supply pressure drop vs. flow rate curve (external characteristics of channel). Physically, this behavior exists when the pressure drop decreases with increasing flow. Criterion or condition for Ledinegg instability (static instability) to occur is expressed by the inequality (Boure et al., 1973).

$$(\frac{\partial \Delta P}{\partial G})_{int} \leq (\frac{\partial \Delta P}{\partial G})_{ext} \tag{2.1}$$

Where P is the steady-state pressure drop along the flow channel, and G is mass velocity. Rao et al. (1995) concluded from their analysis that Ledinegg instability does not occur due to neutronic feedback and that it is pure channel thermo-hydraulic instability. According to Fukuda and Kobori (1979), hydrodynamic instabilities of two-phase flow are classified into at least eight types, three of which can be roughly classified into Ledinegg instability. Ledinegg instability can be avoided by making the slope of external characteristics steeper than that of the internal by providing inlet throttle valve (Boure et al., 1973)

or by increasing the system pressure.

The onset of Ledinegg instability may sometimes cause wall dryout, but often lies very close to the dryout point because the onset may be followed by limit cycle fluctuations in the flow. Kim et al. (1999) investigated the effect of flow oscillations on critical heat flux (CHF) for low flow and low pressure conditions and suggested CHF correction factors based on experimental data for forced and natural circulation flows. They observed that the flow circulation mode (natural or forced) does not affect the CHF as long as the flow is stable. However, the CHF reduces in the presence of flow oscillations, regardless of the circulation mode, the reduction being larger in case of natural circulation compared to forced circulation.

Flow pattern transition instability: This is mainly caused by the different pressure drop characteristics of various flow patterns. The mechanism can be explained as follows: when a system is operating close to the transition point between slug and annular flow, a small disturbance or reduction in flow rate increases the void fraction, which changes the flow pattern to annular flow. Annular flow has less pressure drop as compared to the slug flow. This will cause the flow to increase and hence the void fraction to reduce. As a result, the flow pattern changes again to slug flow (Boure et al., 1973).

Very little work has been done on flow pattern transition instability. Flow pattern instability and Ledinegg instability have similar characteristics and the former is of greater concern because it triggers CHF due to drastic flow changes from high to low value. Ledinegg instability occurs at lower power compared to the flow pattern instability at any subcooling Nayak et al. (1998).The two-phase flow pattern change significantly affects the flow rate of a natural circulation loop Jeng and Pan (1999).

2.2.2 Dynamic Instabilities

Dynamic instability is caused by the dynamic interaction between the flow rate, pressure drop, void fraction etc. The mechanism involves the propagation of disturbances by pressure and void or density waves. The stability boundary of this type is predicted based on the dynamic behavior or transient (time-dependant) characteristics of the system. Density wave oscillations (DWO), parallel channel instability, pressure drop oscillations (PDO)

etc. fall under this class (Boure et al., 1973). Natural circulation boiling systems are highly susceptible to DWOs and much research was focused on this type of instability.

Density wave oscillations (DWO): These oscillations are due to multiple regenerative feedbacks between the flow rate,vapor generation rate, and pressure drop (Boure et al., 1973). Under certain conditions, the feedback can become 180^o out-of phase with the perturbation and result in self-sustained oscillations. Fukuda and Kobori (1979) conducted experiments both on forced and natural circulation conditions in two parallel channels to study DWOs. They classified DWOs into two types: Type I and Type II.

1. ***Type I instability*** : This type of instability occurs at very low steam quality condition (At low power and high inlet subcooling) and is of specific importance in natural circulation BWRs. At low pressure and low flow quality, the hydrostatic head (as imposed by the core and riser void fraction) is very sensitive to flow-rate fluctuations. These are low frequency type oscillations dominated by gravity effects in unheated riser section.

2. ***Type II instability***: These instabilities occurring at relatively high power, low coolant flow conditions (At high power and low inlet subcooling), are due to the interaction between the two-phase flow pressure loss, mass flux and void formation and propagation in the core. These are high frequency oscillations dominated by two-phase frictional pressure drop. This phenomenon is important both in forced and natural circulation reactors (van der Hagen et al., 2000).

The fact that different pressure drop terms are dominant in each type suggests the existence of other types, i.e., it can be implied that there can be other types of instabilities in which different pressure drop terms may be dominant at low and high steam quality conditions. There are at least 8 types of instabilities, according to Fukuda and Kobori (1979).

Parallel channel instabilities: Most two-phase heat exchangers consists of multiple parallel boiling channels where the channel-to-channel interactions significantly influence the density wave (DWO) instability phenomenon. Studies related to multiple parallel channels mostly involved forced flow boiling systems. However conclusions from these studies reveal that, in-phase and out-of-phase oscillations can be the normal oscillation modes for an identical double channel system. Guido et al. (1991) studied analytically, the density wave oscillations in parallel boiling channels. They observed that for identi-

cal channels the normal modes of oscillation are the in-phase and the out-of-phase ones. They also reported complex oscillation modes for non-identical channels. Clausse et al. (1989) studied analytically, the systems with parallel boiling channels coupled with an external loop using the theory of parameter perturbation to investigate the instability modes which can occur in such systems. They observed in-phase and out-of-phase oscillations in identical channels at different conditions. They further observed that, in the channels which are different, complex oscillation modes can be seen. These channel-to-channel interactions can drive the system more unstable with increased number of channels.

Clausse and Lahey (1991) developed a thermal-hydraulic lumped parameter model based on Galerkin nodal approximation method. Lee and Pan (1999) extended this nonlinear model to study the dynamics and stabilities of multiple parallel boiling channel systems. These studies involve forced flow systems. Lee and Pan (2005b) further extended their previous study to natural circulation systems. They observed that identical and equal power channels oscillate out-of-phase in Type-I region, where gravitational pressure drop dominates, and in-phase in Type-II region, where frictional pressure drop dominates. At high pressure conditions the dynamics could be different.

Pressure drop oscillations (PDO): These oscillations are categorized as compound dynamic instability and occur as secondary phenomenon triggered by static instability. PDO occurs in a system having compressible volume upstream or within the heated section and also when the system operates in the negative slope region of the pressure drop vs. flow rate curve (Boure et al., 1973). PDO exhibits a long oscillatory period and is always accompanied by high oscillation amplitude and jumps in wall-temperature. Guo et al. (2001) investigated experimentally the characteristics of PDO. They observed that PDO occurs only when there is compressible volume in the loop. They suggested that adding a throttling device upstream of the evaporator and maintaining uniform heat flux in the evaporator are some of the measures that can suppress PDO.

2.2.3 Coupled Neutronic Instabilities

Coupled neutronic thermal hydraulic instabilities (or reactivity instabilities) are generated due to reactivity effects of void generated in core. Caorso and Lasalle plant events in 1984 and 1988 respectively renewed the interests of many researchers in this type of instability

in BWRs (March-Leuba and Rey, 1993).

Neutron thermal hydraulic coupling : In boiling water reactors, water serves as coolant and moderator. The moderator thermalizes the neutrons to increase the probability of neutron participation in chain reaction. Void generation in core reduces the moderator quantity (reduction in moderator-to-fuel ratio) and hence its moderating capacity. The effective multiplication factor k_{eff} , which is a function of moderator-to-fuel ratio, also reduces. This, in a water-moderated system, results in a change in reactivity, and hence a change in reactor power. Thus, there is a direct coupling between neutronics and thermal hydraulics, which is termed as void reactivity feedback.

Feedback mechanism: In natural circulation systems, mass flow rate is not an independent variable and depends on the power, operating pressure, and geometry. Thus, a small perturbation in power or any other parameter perturbs the inlet mass flow rate (van Bragt and van der Hagen, 1998a). A typical feedback mechanism of a natural circulation BWR is shown in Figure 2.2. The three feedback effects are

1. Thermal hydraulic feedback through void generation in core. This effects the reactivity term in neutron kinetics through void reactivity feedback term.

2. Fuel dynamics and heat transfer feedback through Doppler reactivity. This loop acts as a filter of power perturbations and introduce time delays between power production and coolant flow heating.

3. Power feedback on the core thermal hydraulics. This effects the rate of void generation and mass flow rate (in natural circulation system).

Types of reactivity instabilities: These instabilities are of two types, namely, core wide and out-of-phase.

1. ***Core wide reactivity instabilities***: In this mode, the whole core behaves as one and the oscillations are in-phase. The neutronic feedback is large and the flow feedback is less because of the damping effect of friction in the recirculation loop of the system (March-Leuba and Blakeman, 1991).

2. ***Out-of-phase reactivity instabilities***: In this mode one half of the core behaves out-of-phase from other half and average power remains constant (March-Leuba and Rey,

1993). The gain of inlet flow feedback is large compared to neutronic feedback.

Different neutron kinetics models are proposed in literature to study the regional instabilities (out-of-phase) in BWRs. March-Leuba and Blakeman (1991) examined the stability of subcritical neutronic modes which could result in out-of-phase power oscillations and employed the subcritical reactivity (subcriticality) of the spatial harmonic mode as another indication of the stability. They showed the stability boundaries with the subcriticality as a parameter. Munoz-Cobo et al. (1996) studied the global and regional instabilities using modal kinetic equations (discussed in Section 2.3.1) based on λ-modes. They showed that global oscillations only appear when the first harmonic mode does not have enough thermal-hydraulic feedback to overcome the eigenvalue separation. Further, they showed that self-sustained regional oscillations could arise due to the different thermal-hydraulic properties of the reactor planar halves, if the modal reactivities have appropriate feedback gains.

Kengo et al. (1997) developed a neutronic model for linear multi-channel analysis of out-of-phase (regional) instability in a BWR core. Turso et al. (1997) developed a low order model of BWR using modal point kinetics equations and investigated the out-of-phase oscillations of Lasalle BWR. Nayak et al. (2000) used coupled multi-point kinetics model. They considered each subcore as subcritical and a constant interaction coefficient, based on the multiplication factor of each subcore, was used. This model is useful in the analysis of an NCBWR with multiple channels or subcores with different flux distributions. Nayak et al. (2000) also compared the stability maps plotted using coupled multi-point kinetics model and the modal point kinetics model (which uses a single value of subcriticality to all subcores irrespective of their flux distribution). They observed that both the models gave the same threshold power for stability. Lee and Pan (2005a) used multi-point reactor kinetics model to investigate the regional instability and non-linear dynamics of a system of multiple nuclear-coupled boiling channels.

The influence of nuclear feedback (void reactivity coefficient) and the delay (fuel time constant) on the stability of the system were investigated by many researchers.It could be inferred from the observations of van Bragt and van der Hagen (1998b), Nayak et al. (2000), Lee and Pan (2005c) that in systems with low frequency oscillations (Lower than 0.1 Hz), an increase in the values of void reactivity coefficient(in absolute sence) and fuel time constant has stabilizing and destabilizing effects respectively. On the other hand in

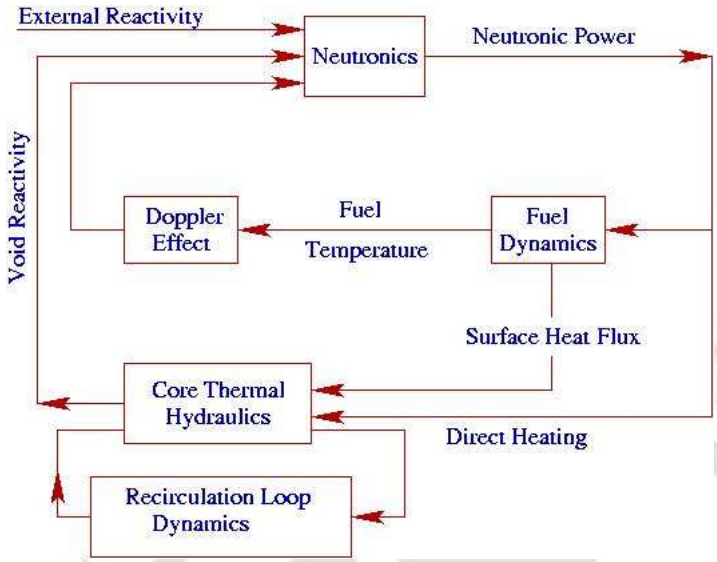

Figure 2.2: Feedback loop of natural circulation BWR

systems with high frequency oscillations (of the order of 1 Hz), an increase in the values of void reactivity coefficient (in absolute sence) and fuel time constant has destabilizing and stabilizing effects respectively. The effect of void reactivity coefficient and fuel time constant on the stability characteristics is significantly influenced by geometrical parameters, as discussed in Section 4.3.2.

Effect of fuel dynamics: Fuel dynamics introduces some time delay in the transfer of nuclear heat in the core and has a great influence on DWOs due to nuclear coupling. This delay is characterized by fuel time constant τ. This time constant is of the order of the oscillation period of DWOs. This time delay makes a negative void reactivity system less stable or a positive void reactivity system more stable to DWOs. For a very small fuel-time-constant, however, a negative void reactivity coefficient would stabilize the system, which is explained by the fact that an increase in void fraction would cause a decrease in power that would suppress further increase in void fraction. This suggests that the time delay of the nuclear heat is the most important factor in the mechanism of the nuclear-thermal coupled instability (Rao et al., 1995).

2.2.4 Startup Transients

Natural circulation systems may undergo thermal-hydraulic instabilities, under low-power and low-pressure conditions, which occur during startup. At low pressures, a natural cir-

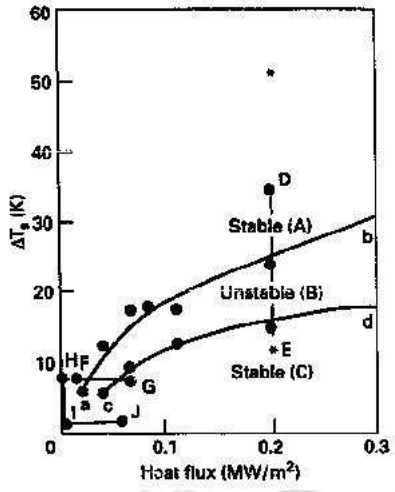

Figure 2.3: Stability map for 5 MW reactor at 1.5 MPa Operating point of the reactor shown by * :(Jiang et al., 1995)

culation loop typically has three operation ranges: (A) single-phase stable region, (B) two-phase unstable region and (C) two-phase stable region as shown in Figure 2.3. The void reactivity feedback and void fraction fluctuations in the reactor core would create power oscillations during start-up. Three kinds of thermal-hydraulic instabilities may occur during start up in natural circulation BWRs, which are: (1) geysering induced by condensation, (2) natural circulation instability induced by hydrostatic head fluctuation in steam separators, and (3) density wave instabilities. It has been found that geysering occurs with flashing, which is of high amplitude and low frequency type (Aritomi et al., 1992). Well-defined start-up procedures like pressurization using external source are devised to avoid start-up instabilities. Manera (2003) proposed efficient start-up procedures to avoid these instabilities.

Geysering: This phenomenon occurs at low powers and low circulation flow rates. It occurs due to bubble formation, growth and its subsequent collapse during start-up. It has been observed in a variety of closed end, vertical columns of liquid, which are heated at the base. The mechanism can be explained as follows (Paniagua et al., 1999). In vertical channels during start-up, with high inlet subcooling, voids are generated and a large slug of bubbles forms, which grows into large bubble due to decrease in hydrostatic pressure head as it moves towards exit. The vapor then mixes with the liquid in the subcooled riser and is condensed there. The condensed liquid re-enters the channel and restores non-boiling conditions. This process repeats periodically and causes flow oscillations. In case of parallel channels, if the condensation rate is higher than the circulation rate, then flow

reversal can occur (Jiang et al., 1995). During start-up conditions, inlet subcooling is the main parameter, which causes geysering. High inlet subcooling results in subcooled riser section and triggers geysering. If inlet subcooling is low enough, saturated conditions may prevail in the riser, thereby suppressing the condensation induced geysering (Paniagua et al., 1999).

The phenomenon of geysering in single channel was experimentally investigated by Jiang et al. (1995). They observed that the basic mechanism of geysering in the single channel is similar to that of multiple channel case, but has no constant period and amplitude. Geysering occurs at certain inlet subcooling region. The mass flow rate oscillates with high peak values, like pulses without a regular period. Very loud explosion-like sounds occur as vapor condenses in the inlet of the riser. The condensation of the subcooled vapor results in a strong flow disturbance, which acts as a pressure wave, and propagates in the system at the velocity of sound. The energy of the pressure wave is released when it passes through the valves and other components in the system. This results in strong mechanical vibrations in the system (Jiang et al., 1995).

Aritomi et al. (1992) studied experimentally the instabilities during startup in natural circulation BWRs in twin parallel channels. They studied experimentally, the effect of parameters such as inlet subcooling and inlet throttling on geysering. During start-up conditions, inlet subcooling is the main parameter, which causes geysering. High inlet subcooling results in subcooled riser section and triggers geysering. At high inlet subcooling, geysering occurs at very low velocities (Aritomi et al., 1993). If inlet subcooling is low enough, saturated conditions may prevail in the riser, thereby suppressing the condensation induced geysering. Flow reversal rate influences greatly, the occurrence of geysering, but it is independent of inlet subcooling in both natural and forced circulation. It is observed that geysering is more pronounced in boiling channels with longer risers. The rate of flow reversals also increase as riser length increases. Inlet throttling aggravates the geysering as the natural circulation rate is reduced.

In their subsequent work, Aritomi et al. (1993) studied the phenomenon of geysering in parallel channels in both natural and forced circulation under different conditions of heat input, inlet subcooling and adiabatic riser lengths. They observed that an increase in heat fliux suppresses geysering and stabilizes flow in case of forced circulation. However in natural circulation, another inphase instabilitity appears which superimposes geysering

(this will be discussed in following paragraphs). This is true for both single and multiple channel cases in natural circulation. The basic mechanism of occurrence of geysering is same for both single and parallel channels. Some of the differences are: a) in parallel channels, geysering is induced at higher velocities than in a single channel. b) geysering in single channel has no constant period and amplitude, However, geysering in parallel channels was observed to be periodic. Boiling channels with longer riser are more pronounced to geysering. The rate of flow reversal also increase as riser length increases. The basic mechanism of occurrence of geysering is same for both single and parallel channels. Some of the differences are: a) in parallel channels, geysering is induced at higher velocities than in a single channel. b) geysering in single channel has no constant period and amplitude, However, geysering in parallel channels was observed to be periodic (Aritomi et al., 1993).

When geysering occurs, the thermal neutron flux in the core may greatly fluctuate due to the channel becoming filled with water and vapor alternatively. In multi-channel case, geysering occurs randomly in the channels and does not occur simultaneously in all the channels. When out-of-phase geysering occurs in neighboring fuel assemblies, the neutron fluctuation due to geysering is not significant, but when in-phase geysering occurs in neighboring channels, the fluctuation of neutron flux will be very high. The effect of system pressure on geysering under both natural and forced circulation was studied by Chiang et al. (1994). It is observed that, as system pressure increases, geysering is suppressed. This is because, as system pressure increases, the saturation temperature rises, which suppresses the formation of large bubbles and thus leads to less oscillatory flow behavior (Chaiko and Blythe, 1993, Paniagua et al., 1999).

Natural circulation instability: As the heat input is increased, geysering is suppressed and another instability called ‘natural circulation instability’ is induced due to hydrostatic head fluctuation (PDO), which varies natural circulation force. As heat flux is further increased, density wave instabilities appear. Aritomi et al. (1992) also observed that, under certain conditions, the three kinds of instabilities appear in one cycle of flow oscillation, but they did not describe the specific condition at which this occurs. Density wave instability is superimposed onto natural circulation instability, and geysering suddenly occurs, when the natural circulation rate increases, and the condition in the outlet plenum comes to subcooled because of heat balance. This indicates that geysering does

not occur under a low velocity condition only.

Chiang et al. (1993) studied experimentally the features of in phase natural circulation oscillations, the description of which cannot be found in Boure et al. (1973) classification. The period of natural circulation oscillations is much longer than that of density wave instabilities, and reduces with an increase in heat flux and with a decrease in inlet subcooling. They studied the behavior of natural circulation oscillations experimentally using a two-channel test facility. They observed that the oscillation of the total circulation rate was synchronous with flow oscillations in both the heated channels but was shifted by about 180° against the PDOs between the outlet plenum and separator. As soon as the vaporization rate increases, the natural circulation oscillations will be suppressed. The period of natural circulation oscillations reduces as system pressure increases (Chiang et al., 1994).

Flashing: Flashing was first reported by Wissler et al. in 1956 (Manera, 2003). When hot liquid flows from a higher to a lower pressure region, the saturation temperature decreases considerably, due to which a part of the liquid is converted into steam. This phenomenon is termed as flashing. At startup conditions, both system pressure and heating power are low, which implies large differences in saturation temperature between the inlet and the outlet of the adiabatic section. At low powers, the coolant, which is heated up in the heated section of the natural circulation loop, may not reach saturation conditions in the core itself. However, due to the strong variation of saturation temperature along the system, flashing can occur in the adiabatic section, leading to an enhancement of the natural circulation flow rate. In dynamic conditions, this phenomenon can cause self-sustained oscillations. These flow oscillations make the operation of the reactor during startup rather difficult and could cause strong mechanical vibrations of the reactor's internal components (Manera et al., 2001).The flashing instability occurs at lower inlet subcooling which means flashing instability occurs after geysering.

Flashing can be categorized as a type of density wave instability due to similarities such as the phase difference of temperatures of boiling region and the non-boiling region, and the oscillation period, which has been observed to be near the time required for fluid to pass through the chimney (Inada et al., 2000). van der Hagen et al. (2000) reported that the phenomenon of flashing influences Type I instability. It was observed from their experiments that flashing drives the flow start-up conditions. Hence, they advised to in-

corporate flashing (to include flashing number N_{flash}) in the physical model to study Type I instability. The effects of various parameters on the stability of boiling channels are briefly listed in Table 2.1.

2.3 Mathematical Modeling

A model is a mathematical representation of the real process in a system. There are different modeling approaches. A lumped parameter approach is generally used to study the dynamic behaviour of the system using a low-order model comprising a system of ODEs. Distributed parameter models consist of PDEs with respect to time and space, and are used when the spatial variation of the variables has to be studied. These two models are developed from physical principles. There is another empirical approach based on input-output data in which a black box model of reasonable complexity is developed using system identification technique, which can describe the system well in specific operating conditions. These models are valid for specified operating conditions only. March-Leuba et al. (1986a) applied this technique and developed a simple model to study the nonlinear dynamics of boiling water reactors. In this section, various modeling concepts used in the context of boiling channels are discussed.

A mathematical model of boiling channel includes power dynamics and thermal-hydraulics. Power dynamics consists of the kinetics of nuclear chain reaction and heat generation in the fuel rods. Thermal-hydraulics comprises mass, energy, and momentum balances for the coolant.

2.3.1 Power Dynamics

The simplest way to model this part is to assume constant and axially uniform heat flux. In fossil-fuel boiler applications, this approximation is reasonable, although the combustion and heat transfer processes may have some influence on boiler dynamics. This approximation has also been used to study the dynamics of BWRs, where power oscillations due to void feedback effects are present. However, the assumption of constant heat flux ignores the coupling between neutronics and thermal-hydraulics, which can be incorporated

Table 2.1: Effects of Parametric variation on flow instabilities

Parameter increase	Effect on stability	Reason	Remarks and References
System pressure	Stability increases	Density difference decrease thus reducing the effect of gravitational pressure drop.	Guanghui et al. (2002)
Mass flow rate	Stability increases	Critical power at which oscillations are generated increases. Avoids bubble agglutination.	Guanghui et al. (2002)
Inlet subcooling	Destabilizes the flow at small subcoolings	Due to significant response delay in void formation with increment in transit time.	At very low subcooling, system exhibits high stability (Boure et al., 1973, Nair et al., 1996, Rao et al., 1995)
	Stabilizes at medium and high subcoolings	Reduces void fraction and increases non-boiling length and its transit time.	
Inlet resistance	Stability increases	Single phase friction increases which is in phase with change in inlet flow and thus provides damping effect on the increasing flow.	Guanghui et al. (2001), Prasad et al. (1995)
Exit resistance	Stability reduces	Increases two-phase friction, which is out of phase with change of inlet flow.	Boure et al. (1973), Prasad et al. (1995)
Riser Length	Stability reduces	Increases two phase gravitational pressure drop. Destabilizes the system in Type-I region and stabilizes in Type II region.	van Bragt and van der Hagen (1998b), Chang and Lahey Jr (1997)
Negative void reactivity coefficient	Destabilizes Type II instabilities	Increase in gain of void feedback loop.	Rao et al. (1995)
	Stabilizes Type I instabilities	Phase lags in channel and fuel are relatively small due to low resonance frequency	van Bragt and van der Hagen (1998b)
Fuel time constant	Stabilizes Type II instabilities	Filtering of high frequency oscillations in void reactivity feedback loop.	Rao et al. (1995)
	Destabilizes Type I instabilities	Break frequency of fuel transfer function will shift towards lower frequency and increases phase shift.	van Bragt and van der Hagen (1998b)
Froude number (with void reactivity feedback)	Stability increases	Froude number appears in the denominator of the gravitational term. Smaller the Froude number higher the gravitational effect.	Without feedback, Froude number has no effect on stability boundary (Rao et al., 1995)

in the model by including neutron kinetics equations.

The time dependent behaviour of neutron population in a reactor can be modeled by neutron transport theory. This method allows a precise representation of neutron interactions with a minimum of assumptions. The mathematical representation of kinetic equations is complex due to explicit dependency on neutron energy, direction of motion, and position (i.e., three space coordinates) in addition to time. Nevertheless, such 3D formulations are used in some numerical codes, which will be discussed in Section 3.4.

It would be conceptually and computationally easier to handle the equations if they were dependent only on time. Under certain conditions, the energy, direction and position variables can be averaged out from the time dependent kinetic equations, resulting in a set of ODEs with respect to time. Point neutron kinetic equations (two ODEs, if one group of delayed neutron precursors is modeled) represent the neutron kinetics in the simplest form (Lewins, 1977).Because of their simplicity, point kinetics equations have been widely used to study instabilities in BWRs. Many numerical codes also use point neutron kinetics.

Out-of-phase (regional) oscillations cannot be modeled by point kinetics equations, but use of 3D neutron kinetics is computationally very expensive. March-Leuba and Blakeman (1991) developed a lumped parameter model to study the out-of-phase oscillations by considering the spatial harmonic modes of the neutron kinetic equations. The general solution of a linear partial differential equation can be expanded in terms of their inherent spatial modes as

$$\Phi(t,r,\theta,z) = \sum_{m=0}^{\infty} n_m(t)\phi_m(r,\theta,z) \tag{2.2}$$

Where ϕ_m is the spatial mode and n_m is the neutron density of m^{th} mode.

Using this method March-Leuba and Blakeman (1991) proposed a modal kinetic equation (in ODE form) using the time dependent part of the solution of n_m (neutron density of m^{th} mode). The number of modal kinetics equations depend on the number of harmonic modes considered. If only fundamental mode is considered then we get the point neutron kinetics equations. Munoz-Cobo et al. (2000) used modal kinetic equations for fundamental and first subcritical modes with two groups of delayed neutron precursors to

study the out-of-phase DWOs in parallel channels.

2.3.2 Thermal Hydraulics

The fluid behaviour in the channel can be described using the basic conservation equations of mass energy and momentum in differential form. The boiling channel constitutes single-phase region (extends from core or channel inlet to the point where the boiling starts) and two-phase region (from boiling boundary to core or channel exit). In single phase region, the application of conservation equations is straightforward. The behaviour of fluid in two-phase region is rather complicated, as mentioned in Section 2.2, and needs special treatment. In two-phase region, the void fraction, steam quality, pressure, enthalpy of steam and liquid phases and the velocities of the two phases are main quantities to be considered while developing state equations.

3D two-fluid modeling is the most general form of representing two-phase flow. In this formulation (Kleinstreuer, 2003), the balance equations of mass, momentum, and energy are applied to the two phases separately, resulting in a system of 10 PDEs (in 3D space and time), which are supplemented by additional equations such as constitutive relations, equations of state, and the law of heat conduction. These equations are applicable only within each phase. Moreover in two-phase flow there will be exchange of mass, momentum and energy between the phases, which can be considered using five interfacial jump equations. In addition to these, the knowledge of boundary and initial conditions is needed to solve these equations. However, it is very difficult to provide the initial conditions because that would require knowledge of location of each phase interface, which is difficult because of complex interface geometry. Averaging techniques are applied to modify these equations into more convenient form for solving (Kleinstreuer, 2003).

The modeling of two-phase flow can be simplified by considering 1D formulation supported with correlations developed from experimental investigations. Much research has been done, experimentally and numerically, on two-phase flow and efficient models were proposed to model accurately the flow behaviour in the two-phase region. The 1D models widely used in the literature are separated flow model (two fluid model), drift flux model, and homogeneous equilibrium mixture (HEM) model (Wallis, 1969).

In the 1D two-fluid model, the two phases are modeled separately, resulting in six balance equations for mass, momentum and energy fields, supplemented by correlations for two-phase frictional multiplier, void fraction, and heat transfer coefficient. For simplicity the two phases are assumed to be in thermal equilibrium.i.e. vapor generation starts only when the liquid bulk temperature reaches the saturation value and beyond that all the heat added to the system goes to generate vapor. However, in reality, there exists a thermal boundary layer near the heated surface, which causes vapor generation even if the liquid bulk temperature is below saturation. This increases the two-phase mixture region, but reduces the rate of vapor generation locally because a part of the heat added is utilized to increase the bulk temperature of the liquid. Saha and Zuber (1978) developed a non-equilibrium model analytically incorporating the above non-equilibrium aspects of the two-phase flow to study its effects on system stability. Comparing with the previous experimental work (Saha et al., 1976), they osbserved that model with non-equilibrium theory predicts more accurately than the equilibrium theory. Numerical Codes like RAMONA, TRAC etc are equipped with thermal non-equilibrium effects.

Zuber and Findlay in 1965 proposed Drift flux model in which a combined momentum balance is written for the two-phase mixture, and the slip between the phases is accounted for by additional relations. The number of equations can be reduced to five, four or three (Manera, 2003). In this model the void fraction is a function of total and vapor superficial velocities, phase distribution parameter and drift velocity. These parameters are obtained by the correlations derived from experimental data at various operating conditions.Thus correct prediction of void transport in the system depends on the accuracy of these correlations. Coddington and Macian (2002) conducted a detailed study on the accuracy of a range of widely used void fraction correlations based on the Zuber-Findlay drift flux model. They observed that out of the 25 different correlations published between 1965 1995, 13 correlations produced acceptable results over the whole range of data. Many of the correlations are satisfactory with in the conditions similar to those from which they were derived. Proper selection depends on the operating pressure and system configuration. The simplest model is the HEM model, which assumes thermal equilibrium and no-slip between the phases, and treats the two-phase mixture as a pseudo-fluid with pseudo-properties. Drift flux model inherits the simplicity of HEM model and accuracy of two-fluid model.

Choice of mathematical model depends on the type of instability to be studied. For example, flashing takes place due to decrease in saturation temperature, resulting from decrease in pressure. Therefore, the dependence of thermodynamic properties on the local pressure is the key factor in modeling flashing instabilities. Dykhuizen et al. (1986) used 1D two-fluid model with slip between phases and thermal non equilibrium conditions. Inada et al. (2000) developed a drift flux model assuming thermal equilibrium conditions in the riser section and van Bragt et al. (2002) developed a 1D HEM model to simulate flashing. Jeng and Pan (1999) used drift flux model, taking flow pattern change and subcooled boiling into consideration to investigate the steady state characteristics of a two-phase natural circulation loop. The liquid density in the single-phase region was considered as a function of temperature, based on Boussinesq approximation, to include the buoyant effect.

2.3.3 Numerical Codes

Numerous thermal-hydraulics and neutronics codes have been developed to deal with the stability issues. These codes range from system analysis codes that can simulate plant behaviour, to simple models like single channel HEM model to study basic physical phenomena. The numerical codes can be classified into two groups as follows. Frequency domain codes: These codes are developed by linearization and Laplace transformation of the governing equations, which are based on two-phase mass, momentum and energy balances. These codes are primarily used for linear stability analysis of boiling systems, and are better in predicting stability inception and margins. LAPUR5, FABLE, ODYSY, and MATSTAB are some of the frequency domain codes. Time domain codes: These codes are developed based on the PDE formulations. These are capable of predicting the behavior of nonlinearities by numerical integration of the nonlinear form of modeling equations over time. RAMONA-3B, RELAP5, RETRAN-3D, and TRAC are some of the time domain codes (Hanggi, 2001). The numerical codes can be further classified as thermal hydraulic system codes (THSC), neutron kinetics codes (NKC), severe accident analysis codes (SAA) etc based on the field of application. Some of these codes with brief description are listed in Tables 2.2 and 2.3. The list is by no means exhaustive but can serve as an information of the type of codes available today. THSC codes have built-in neutron kinetics modules or coupled with NKC codes.These codes are developed using the

Table 2.2: List of time domain codes

Code	Thermal hydraulics	Neutronic/ Features
RAMONA-4B	Four equation 1D drift flux model with thermal non-equilibrium between the two-phases Liquid can be subcooled, saturated or superheated but vapor is considered to be saturated and uses explicit numerical scheme Rohatgi et al. (1997).	Uses 3D neutron kinetics. Consideres local pressure dependencies. Can simulate start up transients compared to its earlier version RAMONA Paniagua et al. (1999)
RETRAN-3D	5 equation model with slip between phases	1D neutron kinetics
RELAP5	6 equation two-fluid model. Uses semi implicit finite difference technique. Provides an option to select implicit finite difference technique.	Point neutron kinetics.Offers special process models.Widest international acceptance RELAP (1995).
TRACG	6 equation two-fluid model and uses explicit numerical schemes.Its earlier version TRAC has built in numerical damping to achieve stable solutions. This renders the simulation of instabilities non-conservative.	3D neutron kinetics
TRAC-PFI	6 equation two-fluid model and has 3D thermal hydraulics capability. Modified version TRAC-PFI/MOD2 has the capability of 1D,2D and 3D analysis of thermal-hydraulics.	3D Neutron kinetics
ATHLET	Five-equation drift flux model and accounts for thermal and mechanical non-equilibrium. Uses fully implicit numerical scheme.	Can be coupled with NKC. Developed for analysis of anticipated and abnormal plant transients, small and intermediate leaks, and large breaks in LWRs.
CATHARE-2	6 equation two-fluid model. All kinds of two-phase flow patterns can be treated. Zero, 1D,2D modules are available	3D Neutron kinetics
POLCA-T	5 equation drift flux model with thermal non-equilibrium between phases. Used to analyse scenarios such as control rod failures, boron shutdown etc.	3D Neutron kinetics
COBRA-IIIC/MIT2	3 equation homogeneous model. It is used for DNBR (departure from nucleate boiling ratio) analysis in LWR sub-channels	Coupled with 3D neutronic code SIMULA
FLOCAL	1D four equation drift flux model consisting of momentum, energy and mass balance equations for mixture along with additional mass balance for vapur phase.	Pure Thermal-hydraulic code primarily developed to simulate instabilities in natural circulation system. Code was validated with experimental results of CIRCUS test facility (Manera et al., 2005)

Table 2.3: List of 3D Neutron kinetic and Severe accident codes

3D Neutron kinetics codes		
Code	Description	Features
DYN3D	3D neutronic kinetics based on nodal expansion method for solving the two-group neutron diffusion equation.	Burn upcalculation. Option of external coupling with thermal hydraulic code ATHLET
NEM	3D neutronic kinetics with multi group nodes.	option for modeling 3D cartesian, cylindrical and hexagonal geometries. coupled with TRAC-PFI thermal hydraulic code
PARCS	3D neutronic kinetics. Code applicable to both PWR and BWR cores loaded with rectangular or hexagonal fuel assemblies	Can be coupled with TRAC-M and RELAP5
NESTLE	A multi dimensional neutronics code. Can solve 2 or 4 group neutron diffusion equations in cartesian or hexagonal geometries.	Several different core symmetry options are available including quarter, half and full core options for Cartesian geometry and 1/6, 1/3 and full core options for hexagonal geometry.
SIMULA	3-D neutron kinetics with one, two or six groups.solves the neutron diffusion equations in one or two groups, on 3-D coarse-mesh nodes (quarter or full fuel assemblies) using a linear-discontinuous finite-difference scheme.	Coupled with thermal hydraulic code COBRA-IIIC/MIT2
Severe accident codes		
VICTORIA	Developed to analyse fission product behaviour within the reactor coolant system (RCS) during severe accident situation (Bixer et al., 1992).	It can predict in detail, the release of radionuclides and radioactive materials from fuel and transport in the RCS during core degradation
SCDAP	Models the core behaviour during a severe accident. It works in combination with RELAP5/MOD3 to describe the overall RCS thermal hydraulic response, core damage progression, and fission product re1ease and transport during severe accidents up to the point of reactor vessel or the system failure (Allison et al., 1992).	It uses the detailed fission product code VICTORIA to describe the fission product release and transport during severe accidents. The code includes many generic component models from which the general systems can be simulated (SCDAP/RELAP5, 1997).
MELCOR	A fully integrated code that models all phases of the progression of severe accidents in LWRs (Madni, 1992). Can model wide range of phenomena and their interactions	Models have been coded with optional adjustable parameters to facilitate uncertainty analysis and sensitivity studies (Summers et al., 1992).

formulations of two-phase mass, momentum, and energy balances by a system of PDEs. Different models as discussed in section 2.3.2 are used in these codes. The advanced versions of these codes are modified to accurately predict various thermal hydraulic transients. For example to correctly predict the possible start-up instabilities like geysering and flashing, the pressure dependency of the vapor generation and its collapse along the channel should be considered to predict the phenomena accurately. This is achieved by estimating the thermophysical properties at the local pressure. Paniagua et al. (1999) developed a new code TWOPHASE based on non-homogeneous, non-equilibrium drift flux formulation with momentum integral method and equipped with an option of basing all local thermophysical properties either on system average pressure or on local pressure. It was observed that, when the code uses local pressure distribution for evaluating the local properties, the percentage of over prediction and under prediction of frequency and amplitude reduces considerably.

The neutron kinetics codes (NKC) are developed using detailed 3D neutron diffusion equations with multi precursor groups.DYN3D, NEM, NESTLE, PARCS, QUABOX etc. are some of the neutronic codes with 3D neutron kinetic equations. These codes are coupled with thermal-hydraulic system codes to study the reactor dynamics. The severe accident codes (SAA) are developed to model the reactor transients during severe accidents. Accidents occur due to various chemical and physical processes during reactor operation. These include core uncovering (loss of coolant), fuel heat up, cladding oxidation, fuel degradation (loss of rod geometry), core-concrete attack and ensuing aerosol generation, in-vessel and ex-vessel hydrogen production, transport, and combustion, fission product release (aerosol and vapor) its transport and deposition etc. Core material melting and relocation is another phenomenon which results in heating up of reactor vessel lower head. This results in thermal and mechanical loading and failure of the vessel lower head and transfer of core materials to the reactor vessel cavity. A broad spectrum of these phenomena in both boiling and pressurized water reactors can be simulated using severe accident codes like MELCOR, MAAP, RELAP/SCDAPSIM/MOD3.1 etc (Kmetyk, 1994, Leonard et al., 1996, Allison et al., 1992, Summers et al., 1992).

The earlier codes were developed with a detailed modeling of thermal hydraulics, limiting the neutron kinetics to 1D or point kinetics because the coupling of 3D neutron kinetics with thermal-hydraulics would have been computationally very expensive. How-

ever coupling of full 3-D NKC with the THSC codes allows the best estimate simulations of interactions between reactor core behaviour and plant dynamics and it is a powerful tool to analyze the severe accident scenarios during which there exists strong coupling between the core neutronics and the primary circuit thermal-hydraulics. With the present fast computing facilities, the coupling technique has become much easier.This method of coupling THSC and NKC is usually achieved as either internal coupling or external coupling. In internal coupling, each neutron kinetic node is coupled with thermal hydraulic cell in the system code (OECD, 2004). This method allows detailed and direct calculations. However, it requires major modifications in the neutronic and thermal hydraulic codes. In external coupling, the neutron kinetics code is combined with a separate core thermal-hydraulic model (OECD, 2004). It is then coupled to the full thermal-hydraulic system code by passing boundary conditions at the top and bottom of the core. This method requires little or no modifications in both the codes, but suffers with numerical instabilities and slow convergence. Parallel processing allows the codes to be run separately, on different processors, and exchange data during the calculation. (OECD, 2004) This approach uses parallel virtual machine (PVM) environment. PVM is a powerful tool for coupling of large codes and performs calculations on multiple processors with significant reduction in computational time. However, PVM environment requires development of an interface routine to interact with the parallel codes (OECD, 2004). Bousbia-Salah and D'Auria (2007) discussed the salient features and limitations of coupled code technique.

2.4 Nonlinear Dynamics

Linear and nonlinear stability methods are used to predict the stability of boiling channel. Linear stability theory is widely used to study the onset of instabilities and system behavior under small perturbations around a steady state. Linear stability analysis can be done in time domain or frequency domain. However, instabilities due to nonlinear effects become significant as the perturbations grow. During abnormal operating conditions like reactor trip, loss of coolant accident etc., the perturbations in the system variables are so large that the effects of nonlinearities amplify and the system may suddenly jump to new region (e.g., a limit cycle) in the phase space, far away from the original equilibrium

state. The limit cycle oscillations may amplify and undergo period doubling, and eventually lead to aperiodic or chaotic states through a cascade of period-doubling bifurcations. Linear theory cannot predict the amplitude and frequency of these nonlinear oscillations. Therefore, in order to predict the frequency and amplitude of these perturbations, and their influence on the reactor stability, nonlinear dynamic analysis is required (Chang and Lahey Jr, 1997, Chaiko and Blythe, 1993).

The theory of nonlinear dynamics (bifurcation and chaos) is used successfully by many researchers to study the system behavior under wide operating conditions and for large parametric fluctuations. Some of the references are Achard et al. (1985), March-Leuba et al. (1986a), March-Leuba et al. (1986b), Tsuji et al. (1993), Clausse and Lahey (1991). Nonlinear study is carried out with low dimensional models in ODEs that are derived by integrating the governing PDEs along the boiling loop. Once the stability margin is established, the bifurcation analysis is applied across the stability margin and deep into the unstable region. Bifurcation characteristics can be studied by transient simulations for operating conditions deep in the unstable region. However this method is laborious and special nonlinear techniques like shooting method, center manifold reduction method etc. are applied to study the bifurcation characteristics. DERPAR (Kubicek and Marek, 1983), BIFOR2 (Hassard, 1981), BIFDD (van Bragt et al., 1999), codes can be used for applying center manifold reduction method. DERPAR code searches the real and Hopf bifurcation points directly. BIFOR2 code reduces the higher dimension system to the two-dimensional system on the center manifold and subsequently transforms the reduced dimension model to Poincaré normal form.

Dynamic (Hopf) bifurcation is an important type of bifurcation in BWR system stability. Hopf bifurcation occurs when a pair of complex conjugate eigenvalues of the Jacobian matrix (the real part of all other eigenvalues being negative) of the dynamical system crosses the imaginary axis with a non zero speed as the control parameter is varied slowly. When system experiences Hopf bifurcation, a family of periodic solutions exist in the neighborhood of stability boundary. The case when the periodic solution lies on the stable side of the stability boundary is called a subcritical Hopf bifurcation, and the case when the periodic solution lies on the unstable side is called a supercritical Hopf bifurcation. On stability point of view, subcritical Hopf bifurcation is more dangerous. When operating in the stable region for the subcritical case, sufficiently large perturba-

tions diverge the system from steady state proving it to be an unsafe operating condition. Karve et al. (1997) observed the existence of unstable limit cycle near the stable fixed point.

March-Leuba et al. (1986a) developed a reduced order nonlinear model of BWR and investigated the evolution of stable limit cycles, series of period doubling which eventually led to chaotic oscillations, deep in the unstable region. (Munoz-Cobo and Verdu, 1991) used this model to study the limit cycle oscillations in BWR by applying Hopf bifurcation theory and center manifold reduction method. van Bragt et al. (1999) studied in detail, the bifurcation characteristics of a NCBWR using BIFDD code. Recently Rizwan-Uddin (2006) used the nonlinear model (March-Leuba et al., 1986a) and conducted semi-analytical bifurcation analysis using BIFDD code. Tsuji et al. (1993) analyzed the in-phase power oscillations (core-wide reactivity instability) of BWR using center manifold reduction method and Poincaré normal form. Padki et al. (1992) investigated PDOs and Ledinegg instability from the viewpoint of bifurcation theory. They observed that the PDO limit cycles occur after a supercritical Hopf bifurcation and Ledinegg instability occurs after a saddle-node bifurcation as heat input is increased.

Chaotic behavior of boiling systems has been observed numerically as well as experimentally. Chang and Lahey Jr (1997) observed in their numerical investigation that, under constant heat flux conditions, a boiling channel with riser can experience chaotic oscillations at some operating conditions. In contrast, a boiling channel without riser exhibits stable behavior at the same operating condition. Wu et al. (1996) experimentally observed chaotic oscillations in a low pressure two-phase natural circulation loop under low power and high inlet subcooling. Schuster et al. (2000) studied the nonlinear effects of flow instabilities in natural circulation loop DANTON (test facility). They studied the effect of nonlinearities in natural circulation by using various methods like auto-correlation function, fast Fourier transformation and estimation of a temporal Lyapunov-exponent.

Bifurcation characteristics of NCBWR are significantly influenced by parameters like void reactivity feedback, Froude number, subcooling number, axial power profile and void distribution parameter. The system experiences both subcritical and supercritical bifurcations at certain ranges of parameter values (van Bragt et al., 1999, van Bragt et al., 2000). The nodalization scheme adopted also influence the bifurcation characteristics. van Bragt et al. (1999) observed that in Type-I region the nature of Hopf bifurcation

change from subcritical to supercritical as the number of riser nodes are increased.

2.5 Experimental Investigations

Experimental investigations give clear insight of the physical phenomenon occurring, serves as a benchmark for validation of numerical codes. The experimental data is used to develop correlations which can be used as constitutive equations in numerical codes. However most of the experimental data is proprietary and not available in open literature. Reduced scale integral system test facilities are developed world wide to simulate and study the natural circulation phenomena. Some of the sophisticated test facilities and their features are listed in Table 2.4.

Scaling criteria: Experimental test facilities are designed by suitable thermal hydraulic scaling. The general objective of a scaling analysis is to obtain the physical dimensions and operating conditions of a reduced scale test facility capable of simulating the important flow and heat transfer behavior of the system under investigation. A general scaling methodology involves 1. Identification of thermal hydraulic processes to be modelled. 2. establishing the similarity criteria between the test facility and the full-scale prototype. 3. Evaluation of test facility specifications based on the similarity criteria. 4. Quantification of the biases due to scaling distortions.

Similarity analysis: This analysis is carried out through appropriate non-dimensionalization of the balance and constitutive equations of two-phase natural circulation flow. However due to the complexity of formulations and the two-phase flow correlations, this process is difficult compared to single phase Ishii and Kataoka (1984) used drift flux model to develop similarity parameters for two-phase natural circulation. Basic non-dimensional numbers that govern the dynamics of natural circulation boiling loops are: Froude number, Reynolds number, subcooling number, phase-change number, drift number, density number, friction number etc. (Nair et al., 1996). The time lag effect in the heated liquid region due to the subcooling of liquid entering the heated duct is taken care of by the subcooling number. Phase-change number scales the change of phase due to the heat transfer to the system and decides the time lag in the heated mixture region. Drift number accounts for the diffusion effects due to the relative motion of fluids and characterizes flow pattern.

Table 2.4: Experimental test facilities

Test facility	Configuration	Features
DESIRE (IRI, Delft University Netherlands)	A scaled facility for Dodeward NCBWR.Use Freon as working fluid Possibility to adjust local friction at core inlet and riser exit. Variable riser length.	Radially asymmetric power distribution which can be used to compare the 3D thermal -hydraulic and CFD codes. Have artificial neutronic feedback
CIRCUS (IRI, Delft University Netherlands)	A full height scaled model of Dodeward reactor. 4 electrically heated fuel channels and 4 bypass channels and one common riser.Flexibility in use of number of risers and facility to adjust inlet friction and subcooling.	Designed to study the thermal-hydraulic stability of a natural circulation BWR at low pressure conditions typical for startup.
PANDA (Switzerland)	A large scale thermal- hydraulic test facility with 6 cylindrical pressure vessels. The installed power is 1.5 MW generated by a bundle of heater rods.	Designed for 10 bar pressure and 200° C.
CLOTAIRE (CEA, France)	Developed to study two-phase flow phenomena in the secondary side of PWR steam generators.Can simulate steam-water at a pressure of 75 bar with the use of Freon-114.	With slight modifications the test facility can be used to BWR studies.
PUMA (Purdue University, USA)	Design consists of 4 parallel channels in core with bypass channels Detailed instrument system. Electrical heating mechanism	Designed to simulate the transient response following various LOCA scenarios and to simulate transients where the pressure id below 1.03 MPa
SIRIUS-N	A reduced scale test facility which resembles a typical NCBWR. The loop consists of 2 channels, 2 chimneys, an upper plenum, a downcomer, asublooler and a pre heater.	Can simulate accurately the regional and core wide instabilities of BWRs.Equpped with void feedback reactivity simulation facility Furuya et al. (2005a).
CAPCN (Argentina)	Test facility with full height relative to CAREM reactor and a volume scale of 1:280. The operating pressure is 12 MPa and maximum power of 300 kW.	Simulate the dynamic phenomena of CAREM reactor coolant system near normal operating conditions.
ITL (BARC, India)	Full height test facility with a volume scaling of 1:452. It has a design pressure of 100 bar and temperature 315° C.	Designed in BARC India to simulate natural circulation phenomena in Advanced Heavy Water Reactor (AHWR).
PLC (BARC, India)	A parallel channel (4 channels) test facility developed by BARC. PLC has a design pressure of 20 bar and temperature 220° C and can operate at 200 kW.	Can simulate steady state behavior of AHWR with channels at same or different powers. Artificial neutronic feedback simulation.
NCTF (IIT Bombay, India)	A 1/4th length scale test facility resembling AHWR. It consists of two loops with four risers and two steam drums representing the four loops of AHWR (Iyer and Kadengal, 2003).	Designed and fabricated in IIT Bombay to study the dynamics of AHWR. Studies on single and multiple channels, and integrated system studies can be carried out.

Density number scales the system pressure (Nair et al., 1996). These scaling parameters are used to develop the similarity criteria between the model and the prototype.

Numerous experimental investigations on natural circulation boiling systems are reported in literature. Jain et al. (1966), Saha et al. (1976), Dijkman (1971), Qui et al. (2003), Jiang et al. (1995), Kyung and Lee (1994), Lorenzini et al. (1991), Unal (1981), Unal (1980), France et al. (1986), Unal (1985), Guanghui et al. (2002) are some of the experimental works on self sustained density wave oscillations. These investigations were carried out on different scaled test facilities with different configurations and at different operating conditions. The effect of various geometrical parameters on the density wave instabilities were investigated. They developed some correlations to predict the inception of DWOs. However these correlations are applicable only to those configurations and operating conditions which are similar to conditions from which they were derived.

van der Hagen et al. (1997) conducted experiments on Dodeward natural circulation boiling water reactor and generated experimental database covering the entire operational range, i.e., low-power low-pressure (startup condition), high-power high-pressure (normal condition) and low-power high-pressure (shutdown condition). The current and future generation BWRs have natural circulation as the normal operation mode. More comprehensive experimental investigation is needed to visualize natural circulation instability phenomena under wide operating conditions. A Freon-based scaled version (GENESIS test facility) of the economical simplified boiling water reactor (ESBWR) is designed and constructed based on the derived scaling rules (Marcel et al., 2008). The knowledge thus gained can be used in design of future BWRs. de Kruijf et al. (2003, 2004), Aguirre et al. (2005), Furuya et al. (2005b), and Marcel et al. (2008) are some of the recent experimental works being carried out in this direction.

2.6 Summary

A large number of numerical and experimental investigations on two-phase flow instabilities in natural circulation boiling channels have been reported in literature. Many numerical codes, in time domain as well as frequency domain, have been developed, using various mathematical modeling techniques. Both lumped parameter as well as distributed

parameter (usually 1D) models have been used. The power dynamics has been modeled using either constant heat flux assumption or neutron kinetics (point kinetics is the most common, but 1D and even 3D kinetics are also used in some numerical codes). Different models of two-phase flow have been employed for modeling thermal-hydraulics. HEM model (three-equation model) is widely used in numerical studies due to its simplicity, but more comprehensive models, ranging from 4 to 6 equations, are used to achieve better accuracy. Drift flux model is used to account for the slip between phases while exploiting the simplicity of models with 3 or 4 equations. Dependence of properties on local pressure is commonly ignored, but has to be considered for simulating instabilities like flashing and geysering. Numerical studies of two-phase flow instabilities use techniques of linear stability theory as well as nonlinear dynamics and bifurcation theory.

Extensive research has taken place on linear analysis of instabilities in natural circulation boiling systems, but there is further scope for nonlinear analysis of instabilities using techniques of nonlinear dynamics and bifurcation theory. In particular, start-up transients need to be investigated using nonlinear dynamics methods. The knowledge gained form nonlinear analysis can be used for designing better control systems and safety measures. Different types of instabilities have been studied separately, experimentally and numerically, which makes it desirable to develop a unified stability map covering the entire parameter space and all types of instabilities. Many numerical codes have been developed to simulate neutronics and thermal-hydraulics, but development of user-friendly software with graphic user interface remains to be done. This will facilitate extensive numerical simulations of instabilities and thus help in improving reactor safety.

Chapter 3

Modeling of Natural Circulation Boiling Systems

3.1 Introduction

The study of dynamic behavior of natural circulation boiling water reactors (NCBWR) involves several interrelated steps. These include the selection of an adequate set of state variables characterizing the neutronic and thermal-hydraulic processes, the formulation of time-dependent equations that interrelate the different variables, and the solution of analytical and numerical techniques. Different mathematical modeling techniques are available in literature as discussed in Section 2.3.

The theory of nonlinear dynamics and chaos is based on the analysis of system of ordinary differential equations (lumped parameter model). The basic governing equations, which are in PDE (partial differential equations) form, can be transformed into an equivalent nonlinear system of ordinary differential equations (ODEs) by nodalization and spatial integration.

In this chapter, we describe the mathematical modeling of the natural circulation boiling systems using two different approaches (Lumped parameter modeling and RELAP5 /MOD3.4). The lumped parameter model (LPM) is derived from the basic governing equations of mass momentum and energy. The model is derived with different state variables and compared. The boiling systems are also modeled using a commercial software

RELAP5/MOD3.4. Parametric studies are carried out using both the models (LPM and RELAP5) and the results are compared.

3.2 Lumped parameter model

The lumped parameter mathematical model can be divided into three parts: Power dynamics which describes the dynamics of heat generation in fuel rod; Heater wall dynamics which models the heat transfer from the fuel rod surface to the coolant; Thermal hydraulics which models the fluid (single phase or two-phase) flow in the boiling system.

3.2.1 Power dynamics

In nuclear reactors, the heat is generated due to chain reactions. Neutron transport theory (Henry, 1975) is generally used to treat the time dependent behavior of neutron population in the reactor. This theory allows a precise representation of neutron interactions with a minimum of assumptions. The resulting equations are however, mathematically complex due to their explicit dependence on neutron energy, direction of motion, and position, in addition to time. The kinetic equations would be conceptually easier to handle if they were dependent only on time. Under certain conditions, it is possible and widely useful to suitably integrate or average out energy, direction and position variables from the time-dependent transport theory equations, resulting in a set of ordinary differential equations with respect to time, in which the delayed neutrons (which are known to effect the reactor dynamics significantly both quantitatively and qualitatively) can be retained if desired (Pandey, 1996).

It is recognized that the delayed neutron emitters have widely different decay constant and are better represented by six group of delayed neutron precursors. It is convenient and satisfactory (and most widely used in lumped parameter models) to treat the delayed neutron precursors using one precursor group model. This simplifies the equations by representing all the delayed neutrons as though they had a single mean life time or decay constant. Further simplification is possible by the effective life time model or Λ' approximation, and the prompt jump approximation. These approximations reduce the dimension

of the system and have been frequently employed both in linear as well as nonlinear studies of reactor dynamics. Pandey (1996) studied both qualitatively and quantitatively the effect of these approximations on the bifurcation characteristics and critical bifurcation parameter.

The resultant point reactor kinetics equations are coupled with suitably reduced-order thermal-hydraulic model of the reactor core, with appropriate reactivity feedback mechanism, to yield a lumped parameter model. Point reactor kinetics model with one group of delayed neutrons is widely used in linear and nonlinear analysis of nuclear coupled thermal-hydraulic analysis of natural circulation boiling water reactors. During out-of-phase instability, neutron diffusion from channel to channel may be an important factor due to change in void fraction among the channels which the point kinetics model does not take into account. For this purpose, spatial neutron kinetics models such as multi-point reactor kinetics (Lee and Pan, 2005c) and multi-modal kinetics (Munoz-Cobo et al., 1996) etc., are used. In the following sections, the point kinetics model and multi-point reactor kinetics model are discussed briefly.

Point neutron kinetics

The point neutron kinetics equations with one group of delay neutrons can be written in terms of linear power as

$$\frac{dq'(t)}{dt} = \frac{\rho(t) - \beta}{\Lambda} q'(t) + \lambda c(t) \tag{3.1}$$

$$\frac{dc(t)}{dt} = \frac{\beta}{\Lambda} q'(t) - \lambda c(t) \tag{3.2}$$

where, $q'(t)$ and c(t) are neutron density and delayed neutron precursors defined in terms of linear power units (W/m). The reactor kinetics is coupled with the fuel rod dynamics and thermal-hydraulics through the reactivity feedback due to fuel temperature and void fraction, respectively. The reactivity $\rho(t)$ in Eq. 3.1 is defined as

$$\rho(t) = \gamma_a(\alpha_{cav}(t) - \alpha_{cav,0}) + \gamma_d(T_f(t) - T_{f,0}) \tag{3.3}$$

where, γ_a is void reactivity coefficient and γ_d is Doppler reactivity coefficient. These equations are non-dimensionalised using the following translation and scaling of the state

variables and time.

$$q'^{*} = \frac{q' - q'_0}{q'_0}; \qquad c^{*} = \frac{c - c_0}{c_0}; \qquad t^{*} = \frac{tG_0}{L\rho_L} \tag{3.4}$$

hence, the point kinetic equations in non-dimensional form are given as

$$\frac{dq'^{*}(t^{*})}{dt^{*}} = t_{ref}\left[\frac{(\rho(t^{*}) - \beta)}{\Lambda}q'^{*}(t^{*}) + \frac{\beta}{\Lambda}c^{*}(t) + \frac{\beta}{\Lambda}\right] \tag{3.5}$$

$$\frac{dc^{*}(t^{*})}{dt^{*}} = \lambda t_{ref}\left[q'^{*}(t^{*}) - c^{*}(t^{*})\right] \tag{3.6}$$

Here the reference time is given as $t_{ref} = \frac{L\rho_l}{G_0}$. The reactivity $\rho(t^{*})$ is now defined in non-dimensional form as

$$\rho(t^{*}) = \gamma'_a(j_{1,c}(t^{*}) - j_{1,c,0}) + \gamma'_d(T^{*}_f(t^{*}) - T^{*}_{f,0}) \tag{3.7}$$

where, $\gamma'_a = \frac{\gamma_a}{(1-N_\rho)}$, $\gamma'_d = \frac{\gamma_d}{(T_{f,0}-T_{sat})}$ and 'j_1' is an auxiliary function defined in Section 3.2.3.

Multi-point reactor kinetics

This model considers the neutron interactions among subcores with equal or unequal power generation rates. The dynamic equations of neutron density and delayed neutrons (in terms of linear power units) in the j^{th} subcore can be expressed as

$$\frac{dq'_j(t)}{dt} = \frac{\rho_j(t) + H_{jj} - \beta - 1}{\Lambda}q'_j(t) + \lambda c_j(t) + \sum_{m\neq j}^{M}\frac{H_{jm}}{\Lambda}q'_m(t) \tag{3.8}$$

$$\frac{dc_j(t)}{dt} = \frac{\beta}{\Lambda}q'_j(t) - \lambda c_j(t) \tag{3.9}$$

where, j=1,2,...,M. The third term in the RHS of Eq. 3.8 accounts for the neutrons generated in the m^{th} subcore migrating to the j^{th} subcore. The interaction coefficient H_{jm}, accounts for the fraction of neutrons generated in the m^{th} subcore that migrate to the j^{th}

subcore. Uehiro et al. (1996) proposed that

$$H_{jm} = \frac{exp(-\varepsilon_{jm})}{\sum_{k=1}^{M} exp(\varepsilon_{jk})} \tag{3.10}$$

where, ε_{jm} is the neutron interaction coefficient which is expressed as $\varepsilon_{jm} = \frac{|r_j - r_m|}{L_n}$. The term $|r_j - r_m|$ is the distance between the j^{th} and m^{th} subcores and L_n is the neutron migration length. The definition given by Eq. 3.10 however, cannot satisfy the steady state condition of Eq. 3.8 at time $t = 0$ when each subcore has a different steady state heat generation rate (Lee and Pan, 2005a). Hence, Lee and Pan (2005a) proposed that

$$H_{jm} = \frac{q'_{j0} exp(-\varepsilon_{jm})}{\sum_{k=1}^{M} q'_{k0} exp(\varepsilon_{jk})} \tag{3.11}$$

Equation 3.11 satisfies the steady state condition of equations 3.8 and 3.9 when the subcores have equal or unequal heat generation rates. Under steady state conditions from the equations 3.8 and 3.9, the term H_{jj} is given as

$$H_{jj} = 1 - \sum_{m \neq j}^{M} H_{jm} \frac{q'_{m0}}{q'_{j0}} \tag{3.12}$$

using the transformations defined in Eq. 3.4, the multi-point equations can be written in non-dimensional form as

$$\frac{dq'^{*}_{j}(t^*)}{dt^*} = t_{ref} \left[\frac{\rho_j(t^*) + H_{jj} - \beta - 1}{\Lambda} q'^{*}_{j}(t^*) + \frac{\beta}{\lambda} c^{*}_{j}(t^*) + \frac{\rho_j(t^*) + H_{jj} - 1}{\Lambda} \right] + t_{ref} \left[\sum_{m \neq j}^{M} \frac{q'_{m0} H_{jm}}{q'_{j0} \Lambda} q'^{*}_{m}(t^*) + \sum_{m \neq j}^{M} \frac{q'_{m0} H_{jm}}{q'_{j0} \Lambda} \right] \tag{3.13}$$

$$\frac{dc^{*}_{j}(t^*)}{dt^*} = \lambda t_{ref} \left[q'^{*}_{j}(t^*) - c^{*}_{j}(t^*) \right] \tag{3.14}$$

the reactivity $\rho(t^*)$ is given by Eq. 3.7.

3.2.2 Heater wall dynamics

The heat transfer from the fuel rod to the coolant is defined by heater wall dynamics. The internal thermal resistance of the fuel rod is assumed to be negligible compared to the external resistance to heat transfer between the heater and coolant. Hence, the temperature distribution in the fuel rod is neglected and the fuel rod is considered as a lump having uniform temperature. The effects of heat conduction through the fuel rod cladding, gap conductance, and heat diffusion through the fuel pellet have been neglected for simplicity. A more detailed model of heater wall dynamics would consider these effects (Lin et al., 1998). Applying energy balance to fuel rod surface and coolant,

$$\rho_f V C_f \frac{dT_f}{dt} = q' L_f - q'' \pi D_f L_f \tag{3.15}$$

Here V is volume of fuel rod. Under steady state conditions

$$q'_0 = q''_0 \pi D_f \tag{3.16}$$

substituting Eq. 3.16 in Eq. 3.15 and applying Newton's law of cooling, $q'' = H_f(T_f - T_{sat})$, the dynamic equation of fuel temperature is given by

$$\frac{dT_f}{dt} = \frac{1}{\tau_f}\left[\frac{q'}{\pi D_f H_f} - (T_f - T_{sat})\right] \tag{3.17}$$

where, $\tau_f = \frac{\rho_f D_f C_{pf}}{4H_f}$ is defined as the fuel time constant. The heat transferred to the coolant is given by

$$q'_c = \pi D_f H_f (T_f - T_{sat}) \tag{3.18}$$

using the scales defined in Eq. 3.4 and defining $T^*_f = \frac{T_f - T_{sat}}{T_{f0} - T_{sat}}$, the above Eq. 3.17 can be written in non-dimensional form for j^{th} channel as

$$\frac{dT^*_{f,j}}{dt^*} = N_S \left[q'^*_j - T^*_{f,j} + 1\right] \tag{3.19}$$

where, $N_S = \frac{t_{ref}}{\tau_f}$ is the ratio of reference time to the fuel time constant. Here the reference time is given as $t_{ref} = \frac{L\rho_l}{G_0}$.

3.2.3 Thermal hydraulics

The lumped parameter thermal-hydraulic model developed by van Bragt and van der Hagen (1998a) is used in the present study. The model has been modified and extended to a multi-channel system. van Bragt and van der Hagen (1998a) developed the lumped parameter thermal-hydraulic model in dimensional form, from the basic one-dimensional unsteady state equations of mass, momentum and energy. The model was then nondimensionalised using suitable scales. However, in the present study, the one-dimensional unsteady governing equations of mass, momentum and energy are first nondimensionalised using appropriate scaling parameters. The nondimensionalised equations are then integrated along the boiling system to derive a generalized lumped parameter thermal-hydraulic model for a multi-channel system. The resulting equations are the same as those given by van Bragt and van der Hagen (1998a). The assumptions made in deriving the thermal-hydraulic model are listed below:

- One-dimensional HEM model for two-phase flow.
- Thermo-physical properties are evaluated at the system pressure.
- Incompressibility of the phases (a reasonable assumption under normal operating conditions)
- Viscous dissipation, change in kinetic energy, potential energy, and flow work are neglected.
- Linear axial variation of enthalpy in single and two-phase regions.

Hence, the one-dimensional governing equations of mass, momentum, and energy balances are given as

$$\frac{\partial \rho}{\partial t} + \frac{\partial G}{\partial z} = 0 \tag{3.20}$$

where, $G = \rho u$ is the mass flux density ($kg/m^2.s$)

$$-\frac{\partial P}{\partial z} = -\frac{\partial \rho u}{\partial t} - \frac{\partial \rho u^2}{\partial z} - \frac{f}{2D}\rho u^2 - \rho g \tag{3.21}$$

$$\frac{\partial \rho h}{\partial t} + \frac{\partial G h}{\partial z} = \frac{q'}{A} \tag{3.22}$$

where, q' is the linear heat transfer rate (W/m). In boiling water reactor, the heat generated due to nuclear chain reaction is transferred from fuel rod surface to the coolant in boiling channel. Hence, when neutron kinetics and heater wall dynamics are considered in the mathematical model, then q' in the energy Eq. 3.22 is the linear rate of heat transfer to the coolant from the fuel rod i.e., $q' = q'_c$. When constant heat flux to the boiling channel is assumed, the neutron kinetics and heater wall dynamics are not considered. In this case, q' in the energy Eq. 3.22 is the heat generation rate and $q' = q'_g$.

The above governing equations are non-dimensionalized using the following scales.

$$\rho^* = \frac{\rho(t)}{\rho_l}, \qquad G^* = \frac{G(t)}{G_0}, \qquad h^* = \frac{h - h_{ci}}{h_l - h_{ci}}, \qquad t^* = \frac{tG_0}{\rho_l L}, \qquad P^* = \frac{\rho_l P}{G_0^2} \tag{3.23}$$

hence, the governing equations in non-dimensional form can be written as

$$\frac{\partial \rho^*}{\partial t^*} + \frac{\partial G^*}{\partial z^*} = 0 \tag{3.24}$$

$$-\frac{\partial P^*}{\partial z^*} = -\frac{\partial G^*}{\partial t^*} - \frac{1}{\rho^*}\left[\frac{\partial G^{*2}}{\partial z^*}\right] - \Lambda\frac{(G^*)^2}{\rho^*} - \frac{\rho^*}{N_{Fr}} \tag{3.25}$$

$$\frac{\partial(\rho^* h^*)}{\partial t^*} + \frac{\partial(G^* h^*)}{\partial z^*} = \frac{N_{Zu} T_f^*}{N_{sub}} \tag{3.26}$$

The energy equation for constant heat flux conditions is given as

$$\frac{\partial(\rho^* h^*)}{\partial t^*} + \frac{\partial(G^* h^*)}{\partial z^*} = \frac{N_{Zu}}{N_{sub}} \tag{3.27}$$

These non-dimensional governing equations are integrated along each component of a natural circulation boiling system. The derivation of the lumped parameter thermal-hydraulic model of a multi-channel natural circulation boiling system is discussed below. It is assumed that all the channels have the same inlet subcooling. The basic components of natural circulation boiling system are the core, the riser, steam drum, feedwater mixer, and downcomer.

Core

Core consists of parallel boiling channels with fuel rods embedded in them. The heat generated in the fuel rods is taken away by the coolant flowing in the channels and a two-

phase mixture is formed. Hence, core can be divided into two regions: The single phase region, which extends from core inlet to the point where boiling starts; and the two-phase region, which extends from boiling boundary to the exit of core.

In the single phase region, the mass flux density is constant (from continuity Eq. 3.24). Hence, integrating the energy Eq. 3.26 from the core inlet to the boiling boundary, the equation for the dynamic behavior of boiling boundary in the j^{th} channel of the core is

$$\frac{dz^*_{bb,j}(t^*)}{dt^*} = 2\left[G^*_{ci,j}(t^*) - \frac{z^*_{bb,j}(t^*)T^*_{f,j}(t^*)N_{Zu,j}}{N_{sub}}\right] \tag{3.28}$$

where, it is assumed that all the channels have the same inlet subcooling. In the two-phase region, the mixture density is given by

$$\rho_m = \rho_g\alpha + \rho_l(1-\alpha) \tag{3.29}$$

further this Eq. 3.29 can be written in non-dimensional form as

$$\rho^*_m = 1 + (1-N_\rho)\alpha \tag{3.30}$$

where, $N_\rho = \frac{\rho_g}{\rho_l}$ is the density number. Hence, the continuity Eq. 3.24 can be written as

$$\frac{\partial j_1(z^*,t^*)}{\partial t^*} = \frac{\partial G^*}{\partial z^*} \tag{3.31}$$

where j_1 is an auxiliary function defined as $j_1(z^*,t^*) = (1-N_\rho)\alpha(z^*,t^*)$. In the core, the average core void fraction can be defined as $\alpha_{cav} = \int_{ci}^{ce}\alpha(z^*,t^*)\,dz^*$ and hence, the auxiliary function for the core j_{1cav} can be defined on the basis of core average void fraction as $j_{1cav} = (1-N_\rho)\alpha_{cav}$. Now integrating the modified continuity Eq. 3.31 from the core inlet to the core exit, the dynamic equation of the average core void fraction in the j^{th} channel is derived as

$$\frac{dj_{1cav,j}(t^*)}{dt^*} = (G^*_{ce,j} - G^*_{ci,j}) \tag{3.32}$$

where, $j_{1cav,j}(t^*) = \int_0^1 j_{1c,j}(z^*,t^*),dz^*$.

The relation between inlet and outlet mass flux densities is obtained by integrating the

energy Eq. 3.26 in the two-phase region, as follows

$$G^*_{ci,j}(t^*) = G^*_{ce,j}(t^*) + [1 + j_{2cav,j}(t^*)] - N_{Zu,j}T^*_{f,j}(t^*)[1 - z^*_{bb,j}(t^*)] \tag{3.33}$$

where, $j_{2cav,j}(t^*) = X^*_{ce,j}(t^*)[N_{Zu,j} - N_{sub}]$.

Riser

The two-phase mixture from the core enters the riser where there is no heat supply. The riser is divided into N_R nodes of equal length. Integrating the continuity Eq. 3.31 over a riser node gives the dynamic behavior of the void fraction as

$$\frac{dj_{1Rav,n,j}(t^*)}{dt^*} = \left[G^*_{R,n,j}(t^*) - G^*_{R,n-1,j}(t^*)\right]\frac{N_R}{L^*_R} \tag{3.34}$$

where, $j_{1Rav,n,j}(t^*) = (1-N_\rho)\alpha_{Rav,n,j}$. Equating the RHS of energy Eq. 3.26 to zero (since there is no heat supply in the riser) and integrating over a riser node, the nodal mass flux density is given by

$$G^*_{R,n-1}(t^*)[1 + j_{2Rav,n-1}(t^*)] = G^*_{R,n}(t^*)[1 + j_{2Rav,n}(t^*)] \tag{3.35}$$

where, $j_{2Rav,n,j}(t^*) = X^*_{Rn,j}(t^*)[N_{Zu,j} - N_{sub}]$.

Void fraction in two-phase region

The void fraction in the two-phase region can be expressed in terms of mass quality as

$$\alpha(z,t) = \frac{\rho_l X(z,t)}{\rho_g + (\rho_l - \rho_g)X(z,t)} \tag{3.36}$$

assuming that the mass quality varies linearly (Astrom and Bell, 2000) along the length of the two-phase region in the core, the mass quality can be expressed in terms of exit quality as

$$X(z,t) = X_{ce}(t)\xi \tag{3.37}$$

where, ξ is the normalised length coordinate along the core in the two-phase region. Hence, Eq. 3.36 can be written in terms of the exit quality as

$$\alpha(\xi,t) = \frac{\rho_l X_{ce}(t)\xi}{\rho_g + (\rho_l - \rho_g)X_{ce}(t)\xi} \tag{3.38}$$

this Eq. 3.38 can be further written in non-dimensional form as

$$j_1(\xi,t^*) = \frac{\xi}{\frac{1}{(N_{Zu}-N_{sub})X^*_{ce}(t^*)} + \xi} \tag{3.39}$$

this Eq. 3.39 is obtained by using the relation $(N_{Zu} - N_{sub})X^*_{ce}(t^*) = \frac{\rho_l - \rho_g}{\rho_g}X_{ce}(t)$. Hence, Integrating Eq. 3.39 in the two-phase region along core, the relation between the void fraction and mass quality in the j^{th} channel is given as

$$j_{1c,j}(t^*) = \left[1 - \frac{ln(1 + j_{2c,j}(t^*))}{j_{2c,j}(t^*)}\right] \tag{3.40}$$

In terms of core average void fraction, the above relation can be re-written as

$$j_{1cav,j}(t^*) = \left[1 - z^*_{bb,j}(t^*)\right]\left[1 - \frac{ln\left(1 + j_{2cav,j}(t^*)\right)}{j_{2cav,j}(t^*)}\right] \tag{3.41}$$

similarly, the relation between average void fraction and quality in a riser node can be derived as

$$j_{1Rav,n,j}(t^*) = \left[1 - \frac{1}{(j_{2Rav,n,j} - j_{2Rav,n-1,j})} ln\left\{1 + \frac{j_{2Rav,n,j} - j_{2Rav,n-1,j}}{1 + j_{2Rav,n-1,j}}\right\}\right] \tag{3.42}$$

Steam drum

The two-phase mixture from riser enters the steam drum where the steam is separated and the saturated water from the steam drum mixes with feedwater and flows into the downcomer. The time scale of drum dynamics is very less compared to the time scale of neutronics and thermal-hydraulics, and hence can be assumed steady. Further, it is assumed that the amount of feedwater is equal to the amount of steam separated in the steam drum, which means that the steam drum is under steady state condition. Hence, applying steady mass and energy balances to the steam drum and feedwater system, an

expression for feedwater inlet subcooling is given as

$$N_{sub} = \left(\frac{h_l - h_{fi}}{h_g - h_{fi}}\right) N_{Zu} \tag{3.43}$$

Hence, in natural circulation systems, the subcooling number depends on the Zuber number and the feedwater inlet enthalpy. A detailed derivation of steam drum statics is given in Appendix A.

Momentum dynamics

In multi-channel systems, there are a number of closed loops each consisting of the core, the riser and a common downcomer. Since all the loops are closed, the LHS in the momentum Eq. 3.25 becomes zero and the RHS expresses various contributions (inertial, frictional, gravitational, acceleration and minor losses) to the pressure drop in different sections of each closed loop. These pressure drop terms are derived by integrating the respective terms of the one-dimensional momentum Eq. 3.25 along the components of each channel and the common downcomer of a multi-channel boiling system. The derivations of these pressure drop terms are discussed in Appendix B.

In multi-channel system, the momentum dynamics is described by the summation of the dynamic pressure drop through each closed loop which is equal to zero.

$$\left(\sum \Delta P\right)_{C,j} + \left(\sum \Delta P\right)_{R,j} + \left(\sum \Delta P\right)_{D} = 0 \tag{3.44}$$

where, $(\sum \Delta P) = \Delta P_i + \Delta P_a + \Delta P_g + \Delta P_f + \Delta P_m$ and the expression of each term is listed in Appendix B. The coupling between each closed loop is given by the relation

$$G^*_{Di} A^*_D = G^*_{ci,1} + \sum_{j=2}^{M} G^*_{ci,j} \left(\frac{A_{C,j}}{A_{C,1}}\right) \tag{3.45}$$

further, if the channels are identical, then the total pressure drop across any two channels is equal. Hence, for any two channels (say j and m),

$$\left(\sum \Delta P\right)_{C,j} + \left(\sum \Delta P\right)_{R,j} = \left(\sum \Delta P\right)_{C,m} + \left(\sum \Delta P\right)_{R,m} \tag{3.46}$$

The ordinary differential equations (ODEs) 3.28, 3.32, 3.34, 3.44 along with the nonlinear algebraic equations 3.33, 3.41, 3.42 3.35 constitute the lumped parameter thermal-hydraulic model of a natural circulation multi-channel system. The state variables of this model (referred as LPM1 in the present work) are $z^*_{bb,j}$, $j_{1c,j}$, $j^*_{1R,n,j}$, $G^*_{ci,j}$. The number of these state variables depends on the number of channels and number of riser nodes. For a single channel system with two riser nodes, the number of state variables in the thermal-hydraulic lumped parameter model (LPM1) are five. In LPM1, the algebraic equations defined by 3.41, 3.42 are to be solved in every iteration. This increases the computational time in multi-channel studies. Further, the algebraic Eq. 3.42 suffers singularity at steady state condition due to the logarithmic term. Hence, a truncated Taylor series expansion is needed. A much better option in order to avert the above said problem is to use the core exit quality $X^*_{ce,j}$ and the nodal quality in the riser $X^*_{R,n,j}$ as state variables instead of using $j_{1c,j}$ and $j_{1R,n,j}$ in the two-phase region. This can be done as follows.

Differentiating the algebraic Eq. 3.41 with respect to non-dimensional time and rearrangement of the terms, the dynamics of the core exit quality in the two-phase region is given as

$$\frac{dX^*_{ce,j}}{dt^*} = \frac{\left[\frac{dj_{1c,j}}{dt^*} + \left(\frac{j_{2c,j}-\ln\left(1+j_{2c,j}\right)}{j_{2c,j}}\right)\frac{dz^*_{bb,j}}{dt^*}\right]\left(1+j_{2c,j}\right)j^2_{2c,j}}{\left(1-z^*_{bb,j}\right)\left(N_{Zu,j}-N_{sub}\right)\left[\left(1+j_{2c,j}\right)\ln\left(1+j_{2c,j}\right)-j_{2c,j}\right]} \tag{3.47}$$

similarly differentiating the algebraic Eq. 3.42 with respect to non-dimensional time, the dynamics of vapor mass quality in a riser node is given by

$$\frac{dX^*_{R,n,j}}{dt^*} = \frac{A_{n,j}\left(\frac{dXR,n-1,j^*}{dt^*}\right) - B_{n,j}\left(\frac{dj_{1R,n,j}}{dt^*}\right)}{1+\left[1+\left(N_{Zu,j}-N_{sub}\right)X^*_{R,n,j}\right]\left(j_{1R,n,j}-1\right)} \tag{3.48}$$

where, $A_{n,j} = \left(j_{1R,n,j}-1\right)\left[1+\left(N_{Zu,j}-N_{sub}\right)X^*_{R,n,j}\right] + \left[1+\frac{\left(N_{Zu,j}-N_{sub}\right)\left(X^*_{R,n,j}-X_{R,n-1,j}\right)}{\left[1+\left(N_{Zu,j}-N_{sub}\right)X^*_{R,n,j}\right]}\right]$ and $B_{n,j} = \left[\left(X^*_{R,n,j}-X^*_{R,n-1,j}\right)\left(1+\left(N_{Zu,j}-N_{sub}\right)X^*_{R,n,j}\right)\right]$.

This change in the state variables of the two-phase region eliminates the necessity to solve the algebraic equations and hence, the lumped parameter thermal-hydraulic model (referred as LPM2 in the present work) consists of only ODEs given by equations 3.28, 3.47, 3.48, 3.44. The LPM2 is simple and computationally faster compared to the LPM1

and the application of nonlinear dynamics becomes easy with the LPM2. However, the LPM1 and LPM2 are mathematically equivalent and expected to give identical results. In the present work both the models are used.

3.3 RELAP5/MOD3.4 model

Numerical codes are used for the transient analysis studies, severe accident prediction studies and as probabilistic risk assessment (PRA) tools. The classifications and the features of these codes are discussed in detail in Section 2.3.3. These codes are used by regulating agencies to support rulemaking, licensing audit calculations, evaluation of accident mitigation strategies, evaluation of operator guidelines, and experiment planning analysis. RELAP5 is a light water reactor (LWR) transient analysis code (Shieh et al., 1994), developed at the Idaho National Engineering Laboratory (INEL). Its specific applications included simulations of transients in LWR systems such as loss of coolant, anticipated transients without SCRAM, and operational transients such as loss of feedwater, loss of off-site power, station blackout, and turbine trip. It can also be used for simulation of a wide variety of hydraulic and thermal transients in both nuclear and non-nuclear systems involving mixtures of steam, water, non-condensable, and solute.

In RELAP5 the reactor dynamics is represented by point neutron kinetics and hydrodynamic model is a one-dimensional, transient, average two-fluid model for flow of a two-phase steam-water mixture that can contain non-condensable components in the steam phase and/or a soluble component in the water phase. The one dimensional average two-fluid model is obtained by reducing the multidimensional two-fluid equations by uaing a spatial averaging operator. Separate sets of conservation equations are used for each phase, resulting in six basic field equations of mass momentum, and energy balances (Shieh et al., 1994). The two-fluid model is briefly described here. The assumptions made in developing the one dimensional averaged two-fluid model are given below.

- It is assumed that the mean flow is aligned with the z coordinate direction. The velocity components and all the terms associated with other coordinate directions are neglected. This assumption reduces the number of auxiliary parameters of the momentum and energy equations.

- The turbulent parameters, Reynolds stresses, and the Reynolds heat flux are neglected. This is because the one-dimensional model retains only the component associated with axial diffusion whose effects are small compared to the axial mean flow convective flux of momentum and energy. However, the radial or transverse turbulent diffusion effects are included within the wall heat transfer and wall friction correlations.

- The phasic pressures are equal and it is assumed that the interfacial pressures are also equal to the phasic pressures.

- The interfacial momentum and energy storage, phasic viscous stresses and internal phasic heat transfer are neglected.

- The viscous and form drag which are major components of the interphase drag and are modeled using a Dracy-type friction factor formulation.

The one dimensional phasic mass balance for the k^{th} phase is given as

$$\frac{\partial \alpha_k \rho_k}{\partial t} + \left(\frac{L}{V}\right) \frac{\partial A \alpha_k \rho_k v_k}{\partial z} = \Gamma \tag{3.49}$$

where, L is the corresponding averaging scale and v_k is the scalar value of the velocity in the z- direction. Thus, the formulation is applicable to flow in a channel in which the cross section varies in the streamwise direction. The one dimensional average momentum equation of the two phases is given as below.

$$\begin{aligned} \frac{\partial \alpha_k \rho_k v_k}{\partial t} + \left(\frac{L}{V}\right) \frac{\partial A \alpha_k \rho_k V_k^2}{\partial z} + \partial_k \left(\frac{\partial P}{\partial z}\right) - \left(\frac{L}{V}\right) \frac{\partial A \alpha_k \tau_{zzk}}{\partial z} - \alpha_k \rho_k g_z \\ = \Gamma_k V_k^{\Gamma} + \left(M_{\sigma k}^{tv} + M_{wk}^{tv}\right) . n_z + M_{\sigma k}^{n\rho} . n_z \end{aligned} \tag{3.50}$$

Here, n_z represents the unit vector in z-direction, $M_{\sigma k}^{tv}$ and M_{wk}^{tv} are the phasic interface drag parameters and fluid friction at the wall respectively, $M_{\sigma k}^{n\rho}$ is the virtual mass effect, and V_k^T is the interfacial velocity associated with mass transfer. The one dimensional

average energy equation of the two phases is given as below.

$$\frac{\partial \alpha_k \rho_k U_k}{\partial t} + \left(\frac{L}{V}\right)\frac{\partial A \alpha_k \rho_k U_k^2}{\partial z} = -P_k\left[\frac{\partial \alpha_k}{\partial t}\right] + \left(\frac{L}{V}\right)\frac{\partial A \alpha_k V_k}{\partial z} + \Gamma_k\left(U_k + P/\rho_k\right)_\sigma + q_{\sigma k}A_\sigma + q_{wk}A_{wk} + \alpha_k Q_k + \alpha_k \mu_k \Phi_k^2 \quad (3.51)$$

where, suffix σ designates an interfacial value, $\mu\Phi^2$ is the viscous dissipation term, and $q_{\sigma k}A_\sigma$ and $q_{wk}A_{wk}$ are the averaged interfacial heat flux and heat flux at the wall, respectively. The viscous dissipation term in Eq. 3.51 should be interprited as all sources of dissipation resulting from viscous effects, including that from wall friction and interfacial friction, even though no viscous shear stresses appear directly (Shieh et al., 1994).

Closure of the field equations is provided through the use of constitutive relations and correlations for such processes as inter-phase friction, inter-phase heat transfer, wall friction, and wall heat transfer. These constitutive relations include models for defining flow regimes and flow-regime-related models for inter-phase drag and shear, the coefficient of virtual mass, wall friction, wall heat transfer, inter-phase heat and mass transfer, and direct (sensible) heat transfer. The RELAP5 hydrodynamic model contains several options for invoking simpler hydrodynamic models. These include homogeneous flow, thermal equilibrium, and frictionless flow models. These options can be used independently or in combination primarily to compare the code results with calculations from the older codes or different mathematical models like lumped parameter models based on the homogeneous equilibrium model. Semi-implicit and the nearly implicit schemes are used in RELAP5.

The basic two-fluid differential equations possess complex characteristic roots that give the system a partially elliptic character and thus constitute an ill-posed initial boundary value problem. In RELAP5, the numerical problem is rendered well-posed by the introduction of artificial viscosity terms in the difference equation formulation that damp the high frequency spatial components of the solution. The system model is solved numerically using a semi-implicit finite-difference technique. This scheme uses a direct sparse matrix solution technique for time step advancement and has a material Courant time step stability limit. However, there is an option for solving the system model using a nearly-implicit finite-difference technique, which allows violation of the material Courant limit.

This option is suitable for steady-state calculations and for slowly varying, quasi-steady transient calculations (RELAP, 2001a).

The programming design of the hydrodynamic calculation is primarily organized on volumes and junctions. The hydrodynamic components such as pipe, pump etc. which are modeled for specific application, are organized collections of these volumes and junctions. However, some components like pump, valves etc. need additional processing. A single volume component is simply one volume and all the components are modeled as combination of single volumes. A time-dependent volume is basically a single volume having its length, elevation change, and volume, set to zero during input processing. It is used whenever the entry and exit of fluid in a system is to be simulated. A single-junction component is simply one system junction. It is used to connect other components such as two pipes. Time dependent junctions can be used whenever the phasic velocities or phasic mass flow rates are known as a function of time or other time-advanced quantity. Time-dependent junctions can connect any system volumes, or a system volume and a time-dependent volume. A pipe component is a series of volumes and interior junctions, the number of junctions being one less than the number of volumes (RELAP, 2001b). A separator component is a black box model consisting of a special volume with junction flows. The inflowing steam-water mixture is separated by defining the quality of the outflow streams using empirical functions.

Numerous validation studies are reported in the literature. Vanttola et al. (2005) validated neutron kinetics/thermal-hydraulics codes (including RELAP5) with experimental data of different VVER type nuclear power plants. They found that general behavior of the transients calculated by codes match quite well with the experimental data. Kaliatka and Uspuras (2000) developed a RELAP5/MOD3 model of the main circulation circuit (MCC) of RBMK-1500 graphite moderated BWR. They carried out benchmark analysis of three different events which occurred at Ignalina nuclear power plant. The RELAP5 results compared well with plant data. Also in their subsequent analysis Kaliatka and Uspuras (2002) studied loss-of-coolant accident conditions in RBMK-1500 reactor using RELAP5 code. Based on the results, a management strategy was developed and implemented so that the plant is adequately protected from such accidents. Urbonas et al. (2003) validated RELAP5 with the experimental data of Electrogorsk E-108 test facility. Different phenomena such as, oscillatory flow pattern and CHF were studied using

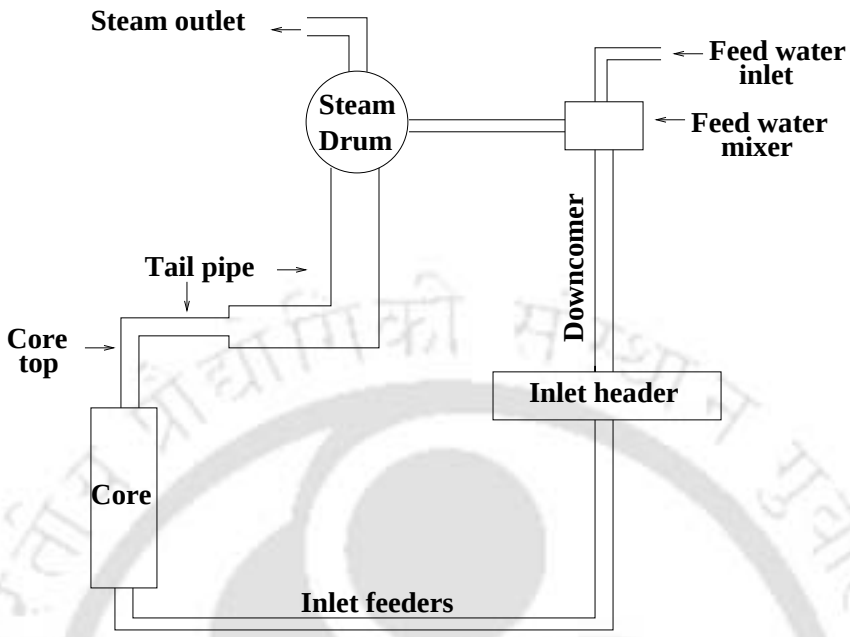

Figure 3.1: Schematic view of a pressure tube type NCBWR

RELAP5 models and E-108 test facility. They also compared specific RBMK tests (oscillatory behaviour, critical discharge, and CHF) with the RELAP5 models. They observed that RELAP5 results are compared well with experimental data.

In the present work single and double channel systems are modeled using RELAP5. Parametric studies are carried out with RELAP5 and lumped parameter model (LPM1 and LPM2) and the results are compared. The modeling and comparison of double channel system is discussed in Section 5.3.2.

3.4 Comparison studies

In this section, a pressure tube type natural circulation boiling water reactor (NCBWR) is modeled separately using lumped parameter model and RELAP5. A schematic view of the NCBWR is shown in Figure 3.1. The geometrical configuration is shown in Table 3.1. The primary heat transport loop consists of core, tail pipe (riser), steam drum, downcomer, inlet header and inlet feedwater pipes. Inlet feeder, core, core top and tail pipe consists of 113 channels through which the coolant flows. Subcooled liquid from the inlet header flows into the core through the inlet feeder pipes. In the core, heat is generated by nuclear

chain reaction. The coolant absorbs the heat and vapor is generated. The resultant two-phase mixture flows into the adiabatic riser section where there is no heat supply. The riser is divided into core top, horizontal and vertical tail pipes. The buoyancy effect due to the density difference between the riser and downcomer sections provides the necessary driving force. The two-phase mixture from riser enters into steam drum where the steam is separated and the saturated liquid flows into feedwater mixer. Subcooled feedwater mixes with saturated water in the mixer and the resultant subcooled water flows into the downcomer.

Assumptions:

1. A constant and axially uniform heat flux in the core.
2. All the channels are averaged into a single equivalent channel assuming that all the channels get the same power. The flow area of a single channel is equivalent to the flow area of 113 channels. The hydraulic diameter is calculated as four times the cross sectional area divided by wetted perimeter which is independent of number of channels modeled. The mass flow rate used is the total mass flow rate through 113 channels and gives the correct mass flow when divided by the cross sectional area. This makes the model a single channel type.
3. No carry under i.e., only single phase liquid flows into the downcomer.
4. The amount of subcooled feedwater is equal to the amount of outlet saturated steam flow from the steam drum. Thus the feedwater mixer is assumed to be steady.
5. Steam drum is very large compared to other components. It is assumed that the drum level is maintained constant. Hence, the steam drum dynamics is assumed to be steady.

3.4.1 Modeling of single channel NCBWR

The thermal-hydraulics of the primary heat transport loop of pressure tube type NCBWR (Figure 3.1) is modeled using the lumped parameter model and RELAP5 software as discussed in Sections 3.2.3 and 3.3, respectively.

Table 3.1: Geometrical configuration of pressure tube type NCBWR

Component	Length (m)	Volume flow area (one channel) (m^2)
Inlet feeder	10.62 vertical length and 7.11 horizontal	0.0074
Core bottom	4.9	0.002732
Active core	3.5	0.0048
Core top	3.9	0.0033
Horizontal tail pipe 1	3.5	0.00326
Horizontal tail pipe 2	19.8	0.0117
Vertical tail pipe	25.7	0.0117
Downcomer	26.8	0.262 (For 113 channels)
Inlet header	0.55	5.7 (For 113 channels)

Lumped parameter model

The core is divided into two regions: single phase region which extends from the core inlet to the point where boiling starts; and the two-phase region which extends form the boiling boundary to the core exit. The dynamics of the boiling boundary is described by the Eq. 3.28. Since the model is for a single channel, the suffix 'j' in Eq. 3.28 is equal to one.

The two-phase region is considered as one node and the dynamics of average core void fraction is described by Eq. 3.32. The relation between the core inlet-exit mass flux densities and that between the core average void fraction and exit quality are given by expressions 3.33 and 3.40, respectively. The riser section comprises coretop, horizontal and vertical tail pipes. The core top can be devided into n_{ct} nodes of equal length and the void dynamics in each node can be described by Eq. 3.34. The horizontal tailpipe is divided into two sections HP1 and HP2 based on flow area. Each section is divided into 'n' nodes (i.e. n_{HP1} and n_{HP2}) of equal length and the void dynamics in each horizontal section of horizontal tail pipe can be defined by Eq. 3.34. Similarly, the vertical tail pipe can be divided into n_{Vt} nodes and the void dynamics in each node can again be defined by Eq. 3.34. In steam drum, the saturated steam is separated and the saturated water flows into the feedwater mixer. A detailed derivation of steam drum statics is given in Appendix A.

Momentum dynamics is similar to that discussd in Section 3.2.3. The momentum dynamics is described by the sumation of the dynamic pressure drop through each closed loop which is equal to zero. In single channel system there is only one closed loop and

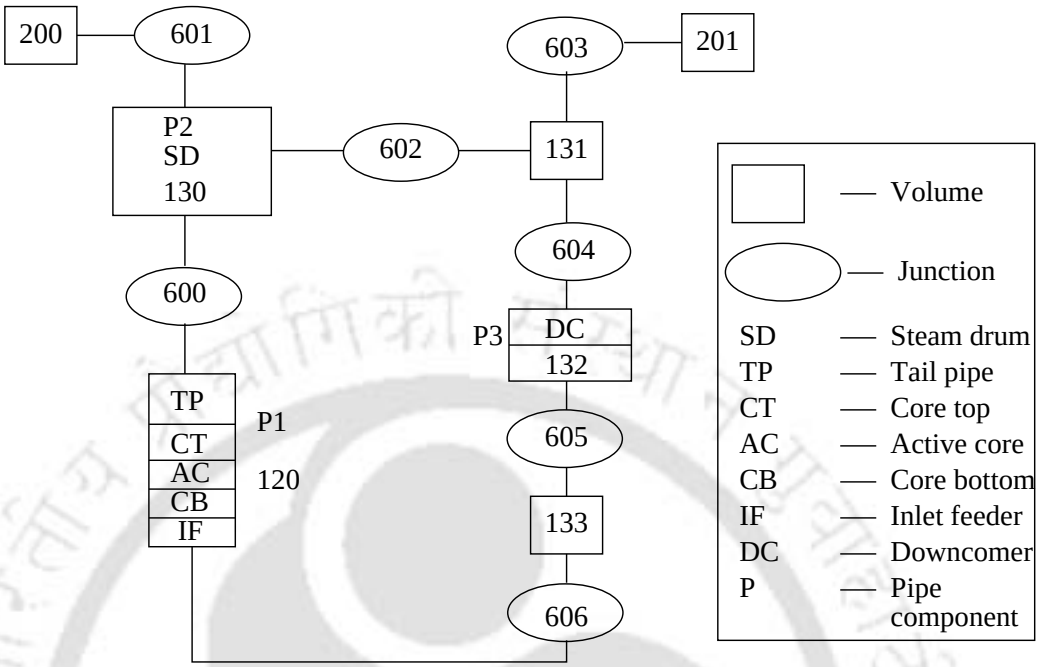

Figure 3.2: Nodalization scheme of RELAP5 model

the suffix 'j' in Eq. 3.44 is equal to one.

$$\left(\sum \Delta P\right)_C + \left(\sum \Delta P\right)_R + \left(\sum \Delta P\right)_D = 0 \tag{3.52}$$

where, $(\sum \Delta P) = \Delta P_i + \Delta P_a + \Delta P_g + \Delta P_f + \Delta P_m$. The expressions of each term along the core, riser sections (core top horizontal and vertical tail pipes) and downcomer are discussed in Appendix B.

RELAP5/MOD3.4 model

The primary heat transfer loop (PHT) of the pressure tube type NCBWR is modelled using RELAP5/MOD3.4 code. A detailed nodalization scheme for the PHT loop is shown in Figure 3.2. The components of the PHT loop are shown in Figure 3.1. The inlet feeders (IF), core bottom (CB), active core (AC), core top (CT), tail pipes (TP) are modelled in RELAP5 using pipe component (P1). The pipe component P1 is divided into 35 volumes. The first two volumes model the feedwater inlet pipe, the third volume models core bottom followed by 15 volumes for active core, one volume for core top, two volume for horizontal tail pipe followed by fourteen volumes for vertical tail pipe. The

steam drum (pipe component P2) is divided into ten volumes. The saturated water from the steam drum and the feedwater are mixed in single volume. The downcomer (Pipe component P3) is divided into ten volumes and the inlet header is modeled using single volume component. All the components are connected using single junction components. The boundary conditions i.e. steam outlet from steam drum and the feedwater inlet are defined using time dependent volumes. Control cards are used to adjust the amount of feedwater supply based on the amount of steam flow at the steam drum outlet. The heat supply to the active core is modeled using a heat structure component divided into fifteen volumes (equivalent to fifteen volumes of active core) and the constant power option (no neutronics) is used.

3.4.2 Studies with lumped parameter model

In this section, the effect of nodalization of riser section on the accuracy and complexity is studied and an optimum nodalization is selected. Further, marginal stability boundaries are plotted on $N_{Zu} - N_{sub}$ parameter plane using LPM1 and LPM2. It is to be noted that in these studies, it is assumed that the saturated liquid from the drum is completely cooled and liquid of desired subcooling flows into the downcomer. This assumption decouples the N_{sub} and N_{Zu} (i.e., Eq. A.7, is not used) and facilitates their use as independent parameters.

In the two-phase region, the mass quality varies along the length of the core. This makes it necessary to divide the riser section into nodes and integrate. van Bragt et al. (1999) studied the effect of nodalization on the marginal stability boundary. They compared the marginal stability boundary obtained by exact integration and observed that the MSB of nodalization approaches the exact MSB as the number of nodes are increased. However, this also increases the computation cost. Figure 3.3 shows the stability boundaries plotted using three different riser nodes for a pressure tube type NCBWR (Figure 3.1). In Type-I region the stability boundaries predicted by the three riser nodes matched well, but in Type-II region, there are minor differences. In the present study the riser of pressure tube type NCBWR is divided into 2 nodes. Marginal stability boundaries are plotted with models LPM1 and LPM2 as shown in Figure 3.4. The stability margins predicted by the two models perfectly matched. This is as expected because the two models

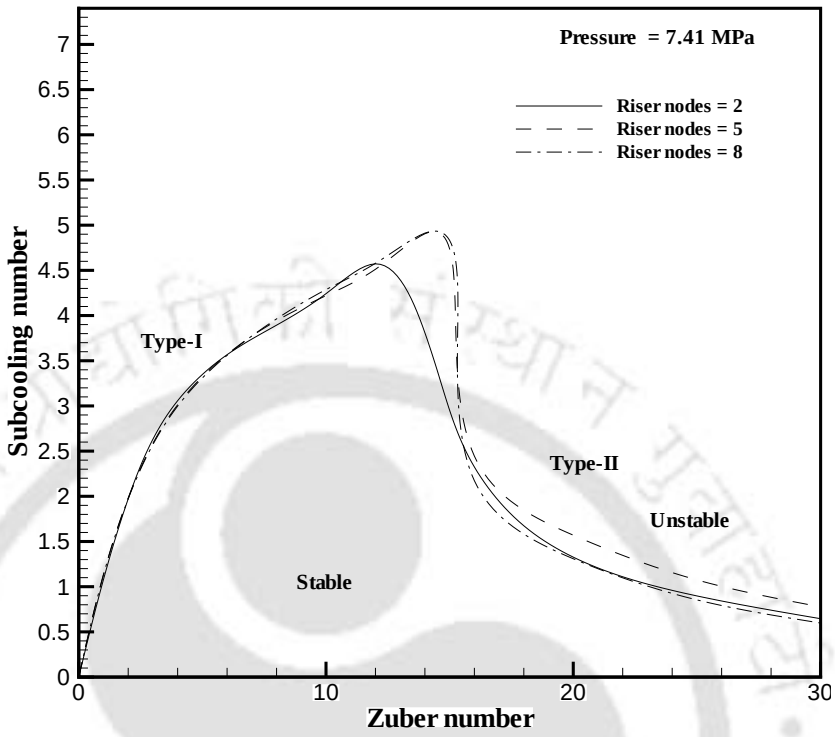

Figure 3.3: Effect of riser nodalization on stability

are mathematically equivalent. The computations using LPM2 are much faster compared to LPM1 due to the elimination of nonlinear algebraic equations.

3.4.3 Studies with RELAP5/MOD3.4 model

Nodal sensitivity test

RELAP5 uses a one-dimensional, transient, two-fluid model for the flow of a two-phase steam-water mixture. In the two-fluid non-equilibrium model, each phase is defined by separate mass, momentum and energy balance equations resulting in six basic field equations. The system of differential equations along with the linear equations of state and additional constitutive relations are solved simultaneously by a forward elimination scheme and subsequent direct solution for the pressure field. The numerical solution method for the hydrodynamic model uses a finite difference scheme having fixed, but staggered, spatial nodes. The predictions are generally sensitive to nodalization and the uncertainty in the results has to be kept within tolerable limits by an appropriate choice of nodalization.

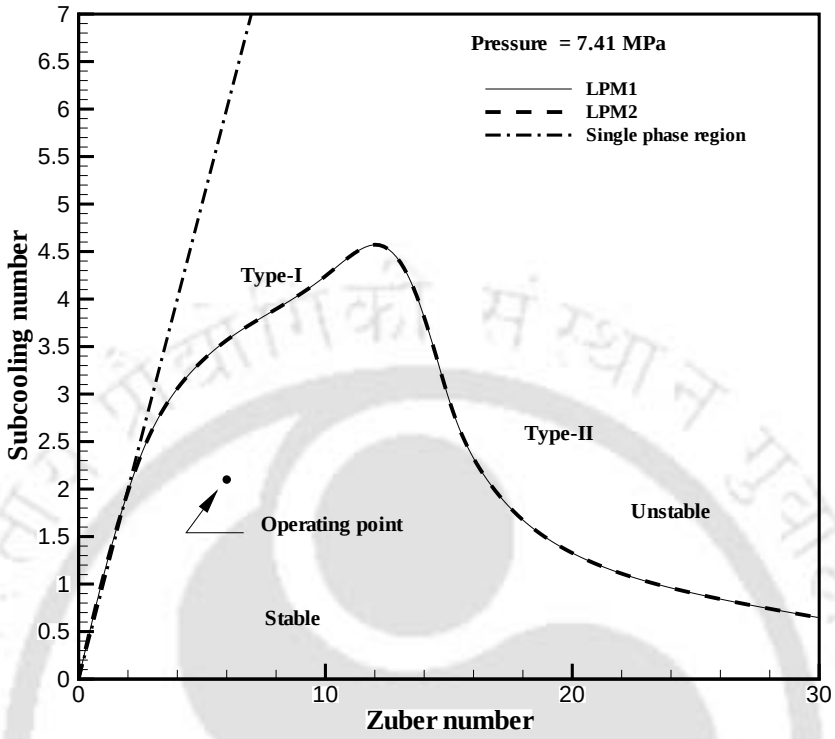

Figure 3.4: Comparison of stability boundaries plotted using LPM1 and LPM2

In this section the effect of nodalization on the predictions is studied.

Parametric studies are carried out at 7.41 MPa with six different nodalization schemes (denoted S1, S2, S3, S4, S5), having different nodalizations of the active core and riser (vertical tail pipe).

Figures 3.5 and 3.6(a) show the mass flow rate, void fraction and exit quality calculated at different powers for six different nodalization schemes (denoted S1, S2, S3, S4, S5) at 7.41 MPa pressure. At low powers, all the schemes predict very close values of the mass flow rate (Figure 3.5(a)). However, the difference in the predictions widens as the power increases. The effects of nodalization schemes on the mass flow rate, void fraction and the core exit quality are shown in Figures 3.5(a), 3.5(b) and 3.6(a), respectively. It is seen that all the nodalization schemes predict similar trends for the mass flow rate as a function of power. It can be further observed that the nodalization scheme affects quality at higher powers, but the void fraction is not much affected.

Comparing nodalization schemes S1, S3 and S4, it is found that the refinement of core nodes reduces nodal sensitivity. Similarly, comparison of schemes S2, S3 and S5

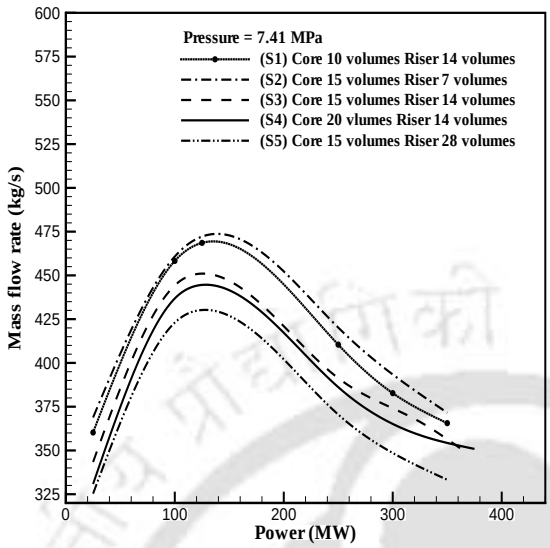

(a) Mass flow rate calculated for different powers using different nodalization schemes at 7.41 MPa

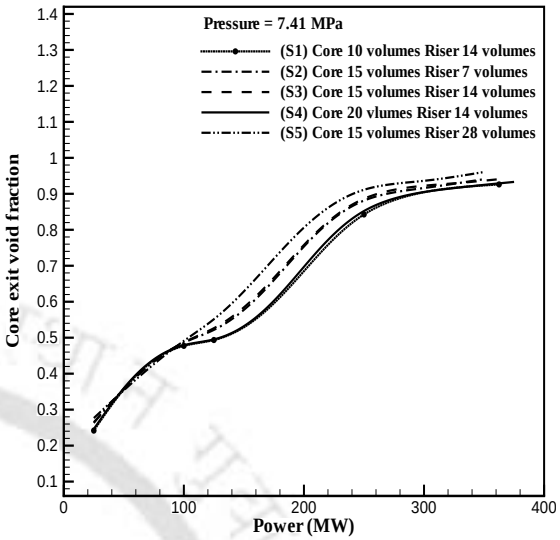

(b) Exit void fraction calculated for different powers using different nodalization schemes at 7.41 MPa

Figure 3.5: Nodal sensitivity test of RELAP5 model

shows that the refinement of riser nodes also reduces nodal sensitivity. However, there is considerable increase in CPU time for finer nodalization schemes. The trends in the steady state values obtained by all the schemes considered are similar. Based on these comparisons, it is decided to divide the core into 15 volumes and the riser into 14 volumes. Thus, we select Scheme S3 (with 15 core volumes, 1 volume for core top, 2 volumes for horizontal tail pipes, and 14 riser volumes). The predictions of the selected scheme (S3) may differ from finer schemes (S4 and S5) by upto 5 percent. This may be considered to be acceptable for verifying parametric trends predicted by the lumped parameter model and studying the nature of transients during on-power refueling in NCBWR.

Comparison of LPM1 and RELAP5

RELAP5 transient simulations are carried out at various operating conditions at 7.41 MPa pressure. Parametric studies are conducted using RELAP5 and steady state lumped parameter model and the results are compared. The core inlet mass flow rate at various channel powers simulated by LPM1 and RELAP5 is shown in Figure 3.6(b). It can be observed that the lumped parameter model overpredicts the mass flow rate, but the trends are similar to those observed in RELAP5 simulations. As the power is increased, the mass flow rate increases first and then decreases at higher powers. This can be explained as fol-

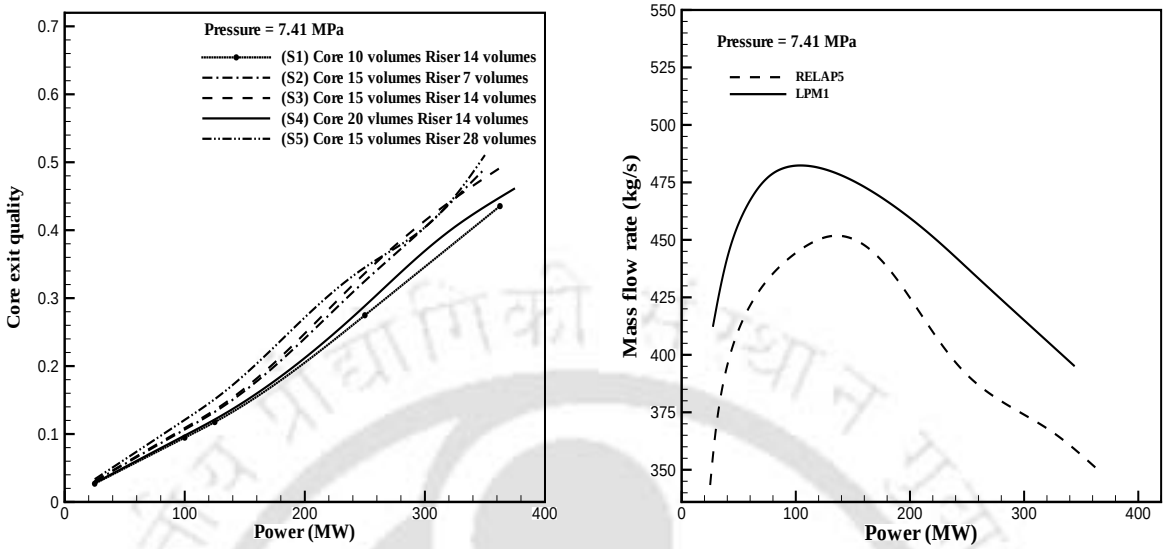

(a) Exit quality calculated for different powers using different nodalization schemes at 7.41 MPa

(b) Variation of mass flow rate with channel power at 7.41 MPa using RELAP5 and LPM1

Figure 3.6: Nodal sensitivity test and comparison between RELAP5 and LPM1

lows: as power is increased, the core exit quality and void fraction will increase (Figures 3.7(a) and 3.7(b)). This will have two effects. (1) Decrease in the gravitational pressure drop due to reduction in density because of increase in void fraction, which will tend to increase the mass flow rate. (2) Increase in two-phase frictional pressure drop due to increase in the void fraction, which tends to reduce the mass flow rate. Thus, as the power is increased, the net variation in mass flow rate depends on which of the two effects is dominant. At low powers, gravitational pressure drop is significant (due to generation of very low void fraction) compared to frictional pressure drop. The contribution of frictional pressure drop is small due to the low flow velocity. As the power is increased, the total pressure drop decreases due to reduction in the gravitational pressure drop. This results in an increase in mass flow rate. However, at higher powers, two-phase frictional pressure drop has a significant contribution. Consequently, the total pressure drop increases with the increase in power. Hence, the mass flow rate decreases.

The core exit quality predictions using lumped parameter model are in very good agreement with RELAP5 predictions at low powers, but deviate at high powers as shown in Figure 3.7(a). The void fraction predictions by RELAP5 and LPM are shown in Figure 3.7(b). It can be observed from Figures 3.7(a) and 3.7(b) that, the exit quality and core void fraction are under predicted by LPM1 when compared to RELAP5 simulations however, the trends are similar. Comparison studies are also carried out at5.21 MPa pressure

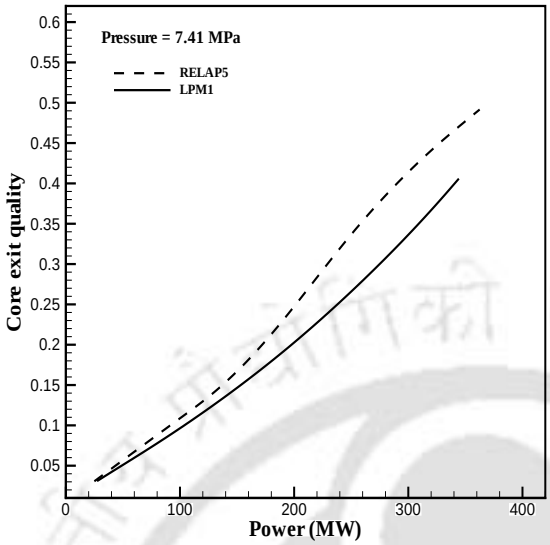

(a) Variation of exit quality with channel power at 7.41 MPa using RELAP5 and LPM1

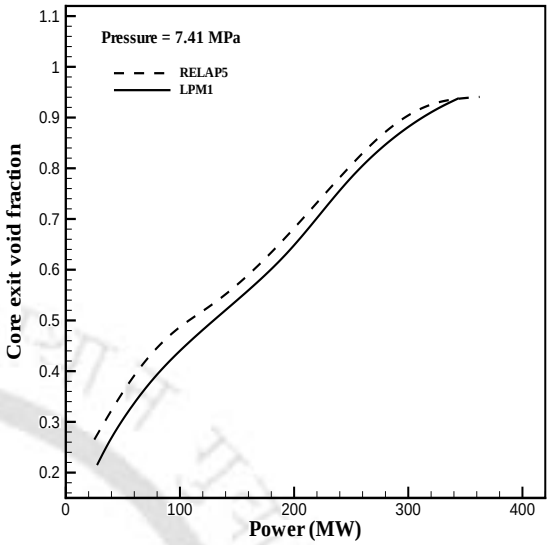

(b) Variation of void fraction with channel power at 7.41 MPa using RELAP5 and LPM

Figure 3.7: Variation of exit quality and void fraction with channel power at 7.41 MPa using RELAP5 and LPM1

as shown in Figures 3.8(a),3.8(b) and 3.8(c). It is observed that the LPM model over predicts, the mass flow rate and under predicts the void fraction and exit quality as compared to RELAP5 predictions; however, the trends obtained by LPM fairy match with those obtained by RELAP5. The differences can be due to the various simplifying assumptions made in the LPM.

The lumped parameter model (system of nonlinear ordinary differential equations) was linearised about its steady-state point and the eigenvalues of the Jacobian matrix are evaluated. The stability is determined by the nature of the eigenvalues of the Jacobian matrix. A marginal stability boundary is plotted on a channel power-feedwater inlet temperature plane at pressure 7.41 MPa. Similarly, RELAP5 transient simulations are carried out at various powers and feedwater inlet temperatures. The stability of the system is inferred from the nature of time evolutions of different variables like void fraction, quality and mass flow rate, and a marginal stability boundary is plotted accordingly. The marginal stability boundaries computed by LPM and RELAP5 are shown in Figure 3.8(d). It can be observed that, the stability boundaries developed by using LPM and RELAP5 fairly match. Despite many simplifying assumptions, the lumped parameter model is conservative.

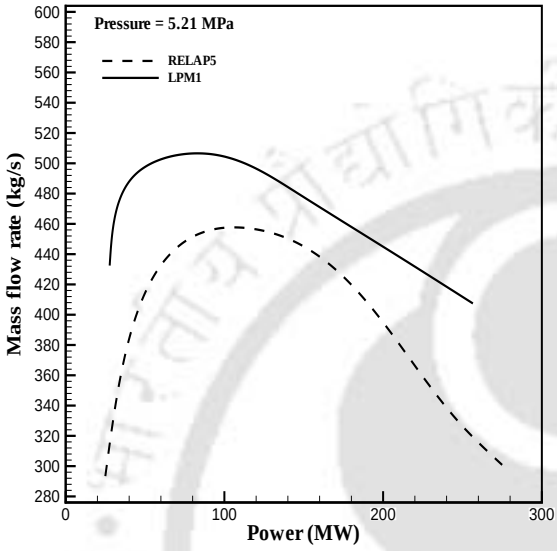

(a) Variation of mass flow rate with channel power at5.21 MPa using RELAP5 and LPM1

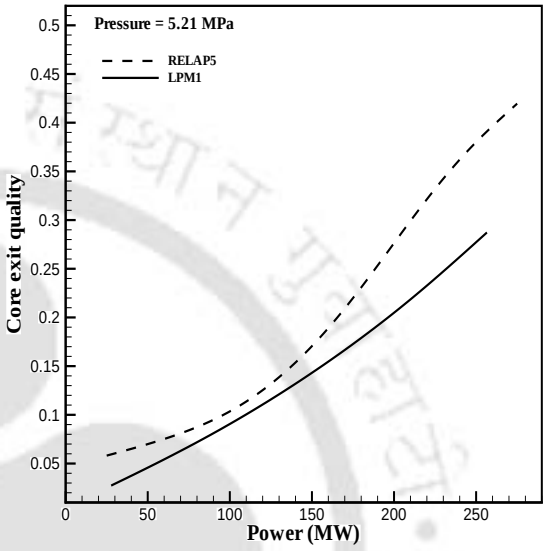

(b) Variation of exit quality with channel power at 5.21 MPa using RELAP5 and LPM

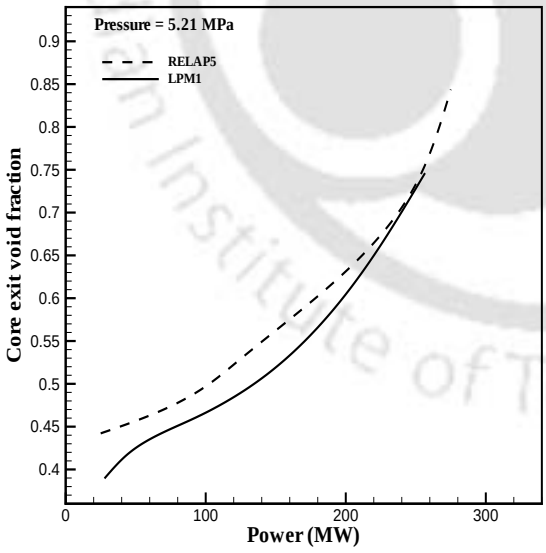

(c) Variation of exit void fraction with channel power at 5.21 MPa using RELAP5 and LPM1

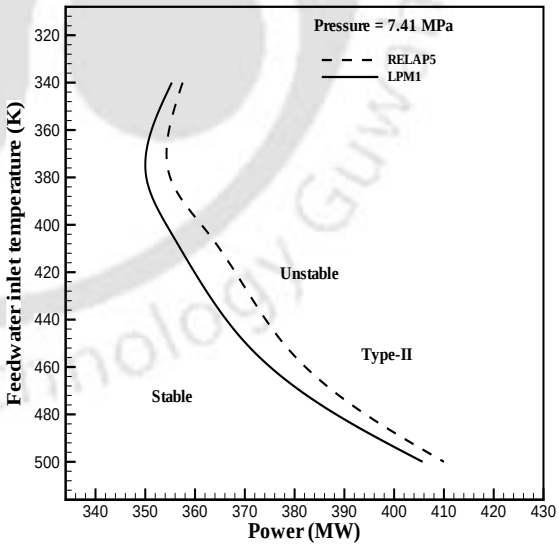

(d) Comparison of marginal stability boundary at 7.0 MPa

Figure 3.8: Comparison of parametric study at 5.21 MPa and marginal stability boundary at 7.41 MPa

3.5 Summary

The mathematical modeling of a natural circulation boiling system using two different approaches (lumped parameter modeling and RELAP5/MOD3.4) has been presented in this chapter. Starting from basic governing equations of mass, momentum, and energy balances, a lumped parameter model based on different state variables (named as LPM1 and LPM2) is derived. A pressure tube type NCBWR is modeled using LPM1 and LPM2. Stability analysis of the NCBWR was carried out with both models (LPM1 and LPM2) and compared. The stability boundaries predicted by both the models perfectly matched as expected. However, the LPM2 is much faster than the LPM1. The elimination of quadratic equations in the LPM2 model makes it computationally faster than the LPM1.

Furthermore, the NCBWR is modeled using RELAP5/MOD3.4 which is based on the two-fluid model. A detailed nodalization study was carried out and a suitable nodalization scheme was selected. Though the trends predicted by all the schemes are similar, the nodalization scheme has a significant effect on the parametric predictions and stability boundaries. Stability analysis and parametric studies are carried out using LPM1 and RELAP5 and the results are compared. The parametric trends and stability boundaries predicted by LPM1 and RELAP5 models matched well. The differences in the parametric predictions can be attributed to various simplifying assumptions used in LPM.

Chapter 4

Stability and Nonlinear Analysis of Single Channel Systems

4.1 Introduction

Any real system depends on physical parameters, which can vary over certain specific sets and affect the dynamics of the systems both qualitatively and quantitatively. A complete understanding of the effects of physical parameters on the dynamics of the real system is very important for safety, economics and operational efficiency. Parameter dependent mathematical models (both lumped and distributed parameter models) of the physical systems can be derived from basic physical laws. These models, in turn, can be used to study the dynamics of the system extensively and economically using different mathematical techniques. The lumped parameter model of natural circulation boiling water reactor (NCBWR) formulated in Section 3.2 is one such parameter dependent system.

Linear and nonlinear dynamics theories are widely used in literature to study the stability of boiling water reactors under different operating conditions. In the linear analysis using equations linearized around an operating point, the studies are necessarily confined to small transients. This study gives quantitative information about the stability of the system under different operating conditions and can be treated as predecessor to the nonlinear analysis. In mathematical models of NCBWRs, nonlinearities arise due to strong interactions between the neutronics and thermal-hydraulics. Under abnormal operating

conditions, the nonlinearities amplify and there can be a large departure from the intended steady state and the system may exhibit a response that has no counter part in the linear world. Furthermore, the parameter set that characterizes the NCBWR under such conditions will itself be significantly different, transforming the latter into a new dynamical system. Thus, a linearized study around an operating point alone is not likely to give an adequate insight into the full range of possible behaviors. It would, therefore, appear that a detailed nonlinear dynamic study of the NCBWR under different operating conditions, should benefit the understanding of the general intrinsic BWR dynamics. This would further help in developing better and safer reactor designs.The theory of nonlinear dynamics has been used by several researchers to investigate the bifurcation characteristics of the system across the marginal stability boundary (MSB). A detailed review of these investigations is given in Section 2.4.

In the present chapter, stability analysis and nonlinear dynamics of a single channel natural circulation boiling water reactor is studied in detail using a lumped parameter model (LPM1). The stability analysis is carried out to study: the effect of geometrical and feedback parameters on the stability of the system, the influence of system parameters on the stabilizing and destabilizing effects of feedback parameters such as fuel time constant (FTC) and void reactivity feedback (VR). For this purpose, three different system configurations (Table 4.1) have been analyzed using the same mathematical model.

The BWR loop considered in this study is a simplified form of the systems studied by van Bragt and van der Hagen (1998a), Nayak et al. (2000), and Lee and Pan (2005c). The dimensions of major components, e.g., core, riser and downcomer, inlet and exit loss coefficients, and neutronic parameters have been taken from these references. A common simplified geometry has been modeled and minor details have been omitted. For example, the horizontal tail pipe and the inlet header considered by Nayak et al. (2000) and the upper and lower downcomer, upper and lower plenum, etc. considered by Lee and Pan (2005c) are not included in this study. The neutronic parameters for system 2 have been taken from Sinha and Kakodkar (2006). Nonlinear dynamics and bifurcations have been studied numerically, for one of the geometrical configurations, for boiling channels with and without riser. The possibility of existence of stable and unstable limit cycles, period doublings, and chaotic oscillations have been investigated. An unstable limit cycle has been located by the autonomous shooting technique. The effect of parameters VR and

Table 4.1: Input data used in the study

Quantity	System 1	System 2	System 3
Length of channel (m)	4.0	3.5	3.81
Total area of flow (m2)	0.3925	3.264	5.681
Non-dimensional riser length L_R^*	1.71	7.714	0.787
Non-dimensional downcomer length L_d^*	2.71	8.714	1.787
Non-dimensional riser area A_R^*	2.25	1.620	1.833
Non-dimensional downcomer area A_d^*	2.88	0.3212	2.1123
Core inlet loss coefficient K_{ci}	3.46	20.0	20.0
Core exit loss coefficient K_{ce}	2.19	5.0	0.68
Riser exit loss coefficient K_{Re}	1.0	5.0	1.0
Downcomer inlet loss coefficient K_{di}	1.0	15.0	1.0
β	0.0061	0.003	0.0065
Λ	0.00005	0.00022	0.00001
λ	0.084	0.084	0.0781
Void reactivity coefficient (VR)	- 0.005 to - 0.5	- 0.005 to - 0.3	- 0.05 to - 0.3
Doppler reactivity coefficient	- 0.00002	- 0.00002	0.0
Fuel time constant (seconds)	2.0 to 16.0	2.0 to 16.0	2.0 to 10.0

fuel time constant on the nonlinear dynamics have been studied in the Type-I and Type-II regions. Furthermore, the effect of parameters such as VR, fuel time constant, core inlet and exit loss coefficients on the chaotic oscillations are investigated.

4.2 Mathematical Modeling

A schematic view of the simple boiling system is shown in Figure 4.1. The system comprises the basic components: the core, the riser and the downcomer. The boiling system is modeled using the lumped parameter model discussed in Section 3.2. Point reactor kinetics (equations 3.5, 3.6 and 3.7) with one group of delayed neutrons is used to represent power dynamics, a lumped parameter energy balance is used for the for the fuel rod (Eq. 3.19), and a lumped parameter thermal-hydraulics model, which is further explained here briefly.

The core comprises a number of parallel channels which are subjected to different powers. In the present analysis the flow area of all the channels in core is averaged into a single channel. This single channel approximation is optimum and computationally simple while investigating the core wide (in-phase) oscillations. The lumped parameter thermal-hydraulic model discussed in Section 3.2 can be directly used by omitting the suffix j, which represents the number of channels. The LPM1 dynamic equations are

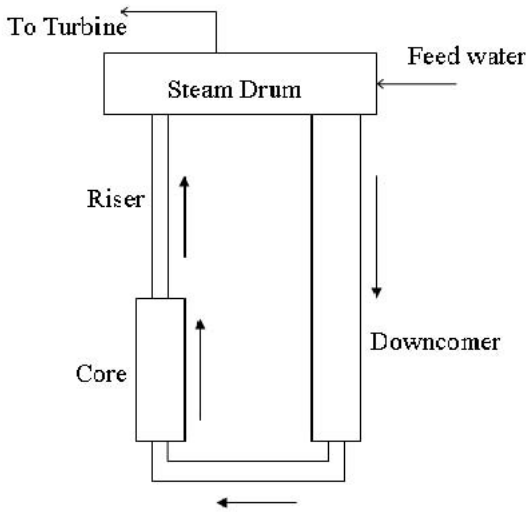

Figure 4.1: Schematic view of NCBWR

listed below.

The core is divided into two regions (single and two-phase regions). The single phase region is modeled as a single node and the dynamics of the boiling boundary (Eq. 3.28) is given as

$$\frac{dz^*_{bb}(t^*)}{dt^*} = 2\left[G^*_{ci}(t^*) - \frac{z^*_{bb}(t^*)T^*_f(t^*)N_{Zu}}{N_{sub}}\right] \tag{4.1}$$

The two-phase region is modeled as a single node and the average core void dynamics (Eq. 3.32) is described by the equation

$$\frac{dj_{1cav}(t^*)}{dt^*} = (G^*_{ce} - G^*_{ci}) \tag{4.2}$$

The adiabatic riser is divided into N_R nodes and the riser void dynamics (Eq. 3.34) is described by the equation

$$\frac{dj_{1Rav,n}(t^*)}{dt^*} = \left[G^*_{R,n}(t^*) - G^*_{R,n-1}(t^*)\right]\frac{N_R}{L^*_R} \tag{4.3}$$

Further, the relation between the core inlet and exit mass flux densities is given by Eq. 3.33 and the relations between the quality and void fraction in the core and the riser are given by equations 3.41 and 3.42, respectively. The flow in the downcomer is considered to be single phase and friction is neglected. It is further assumed that the subcooling number is independent of the Zuber number. The momentum dynamics is discussed in Section 3.2.3 and Appendix B.

4.3 Stability analysis

In this section stability analysis is carried out to investigate the parametric effects on the stability of the NCBWR. The parameters considered in the present study include geometrical and feedback parameters (such as fuel time constant and void reactivity feedback). Three different system configurations are used in this study. Geometrical configuration 1 (system1) was used in the study of parametric effects on stability discussed in Section 4.3.1. In order to resolve the contradictory results reported in literature about the effects of parameters such as void reactivity coefficient and fuel time constant on the stability of the system, stability studies are carried out using geometrical configurations 2 and 3 (Table 4.1) and compared. In order to investigate stability characteristics, the system of nonlinear differential equations governing the dynamics of the system was linearized about its steady-state point and the eigenvalues of the Jacobian matrix were evaluated. It was observed that, as the stability boundary is crossed in the parameter plane, a pair of complex conjugate eigenvalues crosses the imaginary axis in the complex plane. Stability maps were drawn in the Zuber number - subcooling number plane.

4.3.1 Parametric effects on stability

Effect of riser length

In NCBWRs riser enhances the natural circulation by increasing the gravity head in downcomer. The longer is the riser, the more is the driving head. The effect of riser length on the stability of the system is shown in Figure 4.2(a). It can be observed that the increase in riser length destabilizes the system in Type-I region and stabilizes in Type-II region. In

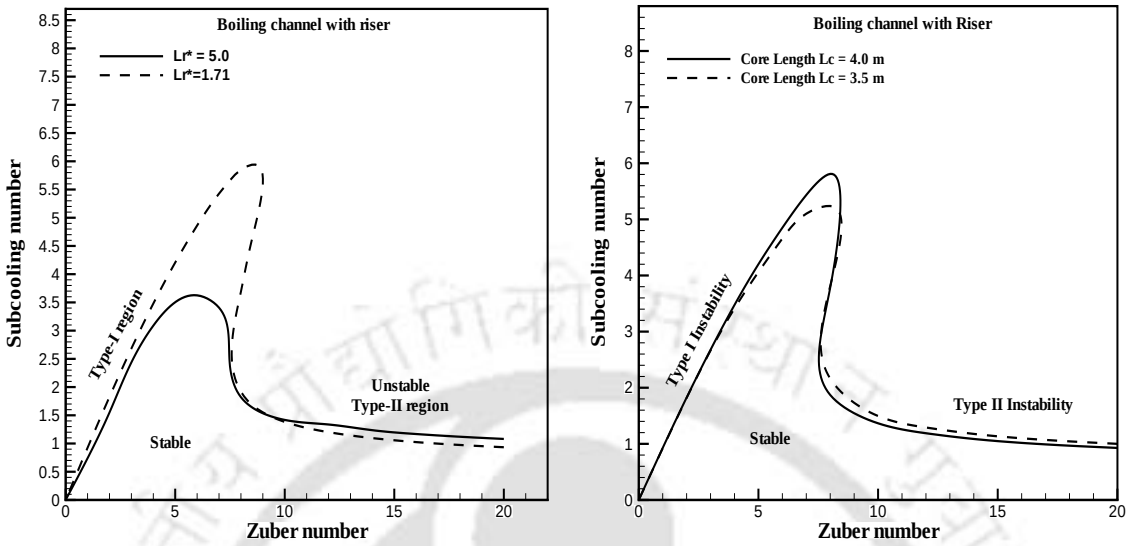

(a) Effect of riser length on stability of the system (b) Effect of core length on stability of the system

Figure 4.2: Effect of riser and core dimensions on stability

Type-I region, increase in riser length may have both stabilizing and destabilizing effects (van Bragt and van der Hagen, 1998b). The stabilizing effect is due to the enhanced circulation flow rate, which increases single-phase friction, and the destabilizing effect is due to increase in gravitational pressure drop and decrease in exit quality. In the present study the gravitational pressure drop is dominant and hence, increase in riser length has a destabilizing effect on Type-I region. In Type-II region, increase in riser length reduces the void fraction in the core (due to increase in circulation flow rate) and two-phase frictional pressure drop. Hence, increase in riser length stabilizes the system in Type-II region.

Effect of core length

The effect of the core length on the stability of the system is shown in Figure 4.2(b). Increase in the core length has a stabilizing effect in Type-I region and a destabilizing effect in Type-II region. An increase in core length increases the gravitational and two-phase frictional pressure drops.

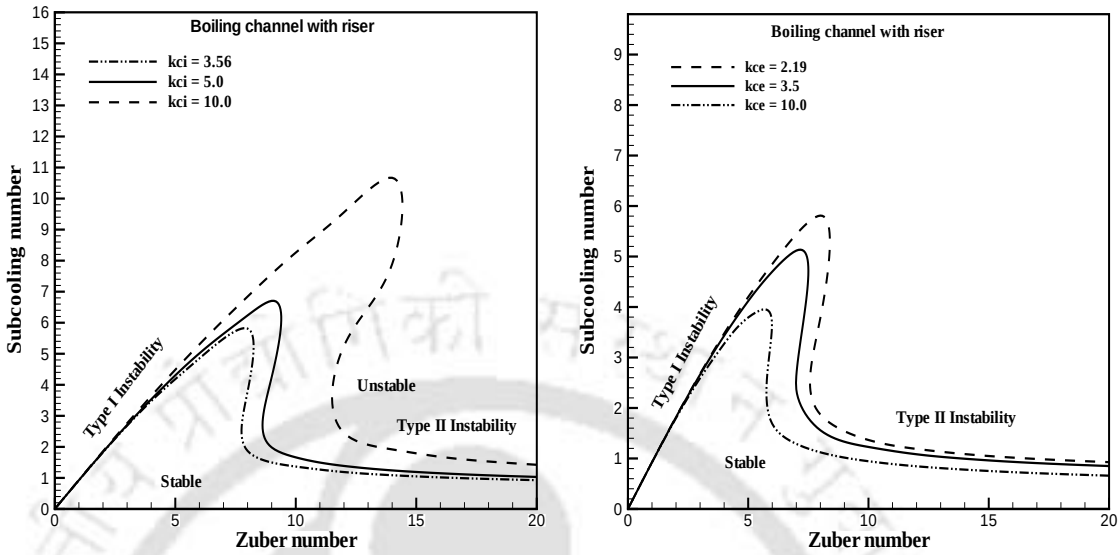

(a) Effect of inlet resistance (b) Effect of exit resistance

Figure 4.3: Effect of inlet and exit resistances on the stability of the system

Effect of inlet resistance

Increase in inlet resistance stabilizes the system both in Type-I and Type-II regions as shown in Figure 4.3(a). This is because, an increase in inlet resistance increases single-phase friction which is in-phase with the change of inlet flow. This increases the total pressure drop and reduces the inlet flow. Thus increase in inlet resistance provides damping effect on the increasing inlet flow and stabilizes the system (Boure et al., 1973).

Effect of exit resistance

Increase in exit resistance has a destabilizing effect in both Type-I and Type-II regions as shown in Figure 4.3(b)). Increase in exit resistance increases the two-phase friction (which is out-of-phase with the change of inlet flow) and decreases circulation flow. This results in increase in void generation and exit pressure drop, which further reduces the circulation flow (Boure et al., 1973). Hence, exit resistance has a destabilizing effect on the stability of the system. However, in some cases increase in exit resistance has a stabilizing effect in Type-I region as observed by Lee and Pan (2005b). The stabilizing effect is due to reduction in gravitational pressure drop. For the geometrical configuration considered in the present study, the destabilizing effect was dominant in Type-I region.

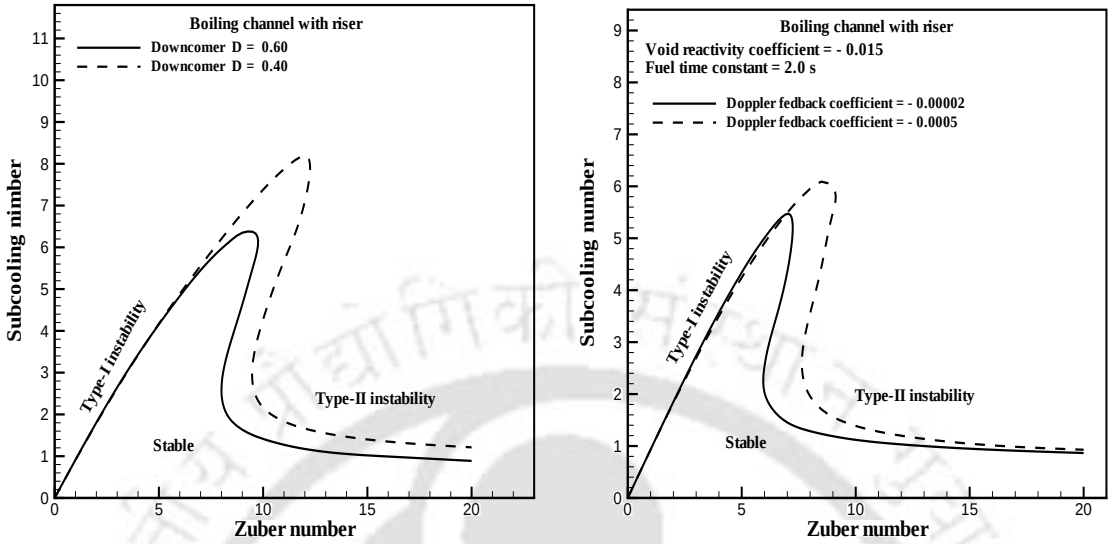

(a) Effect of downcomer diameter (b) Effect of Doppler feedback coefficient

Figure 4.4: Effect of downcomer inertia and Doppler feedback coefficient on the stability of the system

Effect of downcomer diameter

The effect of downcomer diameter is shown in Figure 4.4(a). An increase in diameter decreases the inertia in downcomer. It can be observed that, decrease in downcomer diameter stabilizes the system in Type-I and Type-II regions. The stabilizing effect is due to the suppression of inlet flow fluctuations.

Effect of Doppler feedback coefficient

The effect of Doppler feedback coefficient is shown in Figure 4.4(b). Increase in absolute value of Doppler feedback coefficient destabilizes the system in Type-I region and stabilizes the system in Type-II region.

4.3.2 Resolution of contradictory results

Numerous experimental and numerical investigations have been conducted on the effect of geometrical parameters and feedback parameters like fuel time constant and void reactivity coefficient (VR) on the dynamics of Type-I and Type-II instabilities. Different

findings were reported in literature regarding the effect of VR and fuel time constant on the stability of the system in Type-I and Type-II regions. van Bragt and van der Hagen (1998b) found that, an increase in the absolute value of VR has stabilizing and destabilizing effects in Type-I and Type-II regions, respectively. However, it has a stabilizing effect in both the regions according to Nayak et al. (2000), and a destabilizing effect in both the regions according to Lee and Pan (2005c). An increase in the fuel time constant has a stabilizing effect in Type- II region and a destabilizing effect in Type-I region according to van Bragt and van der Hagen (1998b), but, according to Nayak et al. (2000), it has a destabilizing effect in both the regions. These researchers worked on different designs of NCBWRs using different modeling approaches. Nayak et al. (2000) linearized the governing equations and integrated over various segments of the loop. The model used by Lee and Pan (2005c) is an extension of the mathematical model developed by Clausse and Lahey (1990) to natural circulation boiling systems. The governing equations are non-dimensionalized and discretized by dividing the channel into a number of spatial nodes with equal enthalpy change (but with moving boundaries), and then integrating over each node assuming a linear nodal enthalpy profile. van Bragt and van der Hagen (1998b) divided the heater section into single phase and two-phase regions and the local enthalpy is assumed to change simultaneously at all axial positions. They divided the adiabatic riser into nodes of equal length and assumed linear variation of quality within a node. Therefore, the different findings reported by different authors may be either due to the different geometrical and neutronic parameters or due to the different approaches to mathematical modeling. In order to investigate this phenomenon, three different system configurations have been used in the present work: system 1, system 2 and system 3 (Table 4.1). The results obtained for systems 1, 2 and 3 were compared with the stability characteristics reported by van Bragt and van der Hagen (1998a), Nayak et al. (2000), and Lee and Pan (2005c), respectively.

Effect of void reactivity coefficient

Figure 4.5 shows stability maps for system 1 with different values of VR. It is seen that increase in the absolute value of VR stabilizes the system in Type-I region but destabilizes the system in Type-II region. This agrees with the findings of van Bragt and van der Hagen (1998b). The effect of VR on stability for system 2 is shown in Figure 4.6. It

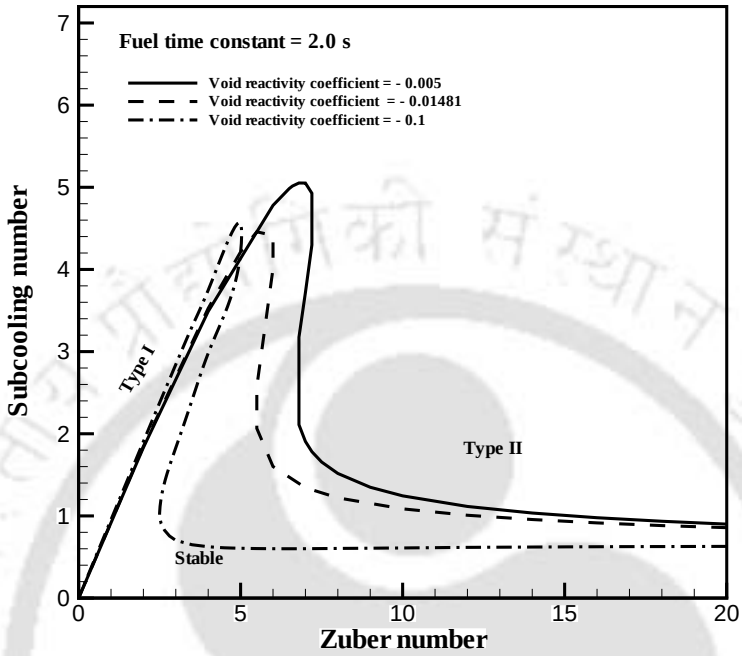

Figure 4.5: Effect of void reactivity coefficient on stability for system 1

shows that increasing the absolute value of the VR stabilizes both the Type-I and Type-II instabilities. This compares well with Nayak et al. (2000). However for system 3, an increase in absolute value of VR destabilizes both the Type-I and Type-II regions as shown in Figure 4.7, which is in agreement with the observations of Lee and Pan (2005c). The difference in the effect of the void coefficient on stability for systems 1, 2 and 3 is due to the influence of various geometric parameters, as will be discussed in subsequent Sections.

Effect of fuel time constant

The effect of fuel time constant is shown in Figures 4.8 to 4.10 for systems 1, 2 and 3. From Figure 4.8 it can be seen that, for system 1, as the fuel time constant is increased, the system is stabilized in Type-II region but destabilized in Type-I region. This agrees with the results of van Bragt and van der Hagen (1998b). For system 2, as the fuel time constant is increased, the system is destabilized in both Type-I as well as Type-II regions (Figure 4.9), which is in agreement with the findings of Nayak et al. (2000). However,

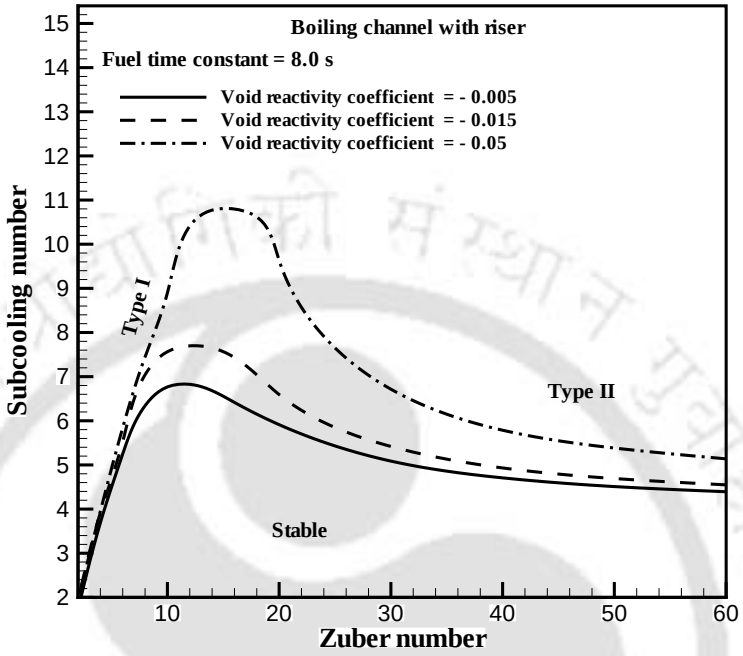

Figure 4.6: Effect of void reactivity coefficient on stability for system 2

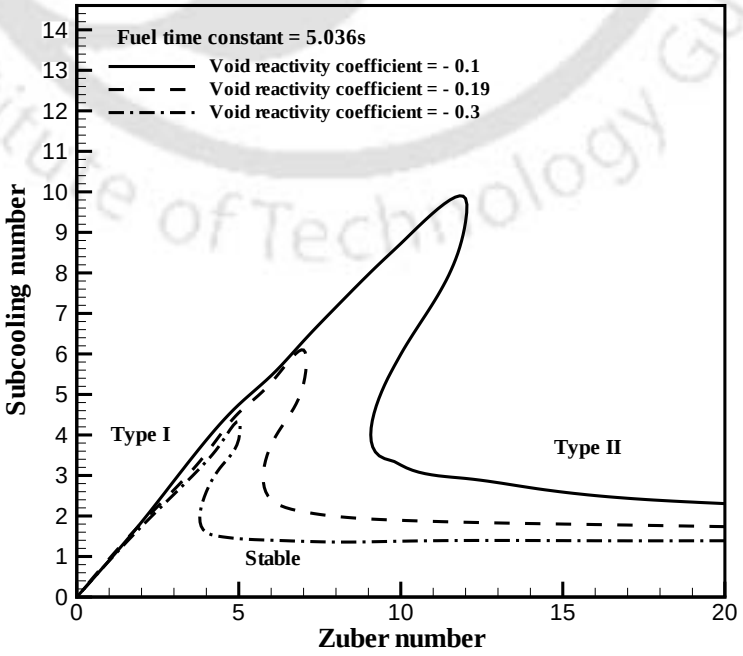

Figure 4.7: Effect of void reactivity coefficient on stability for system 3

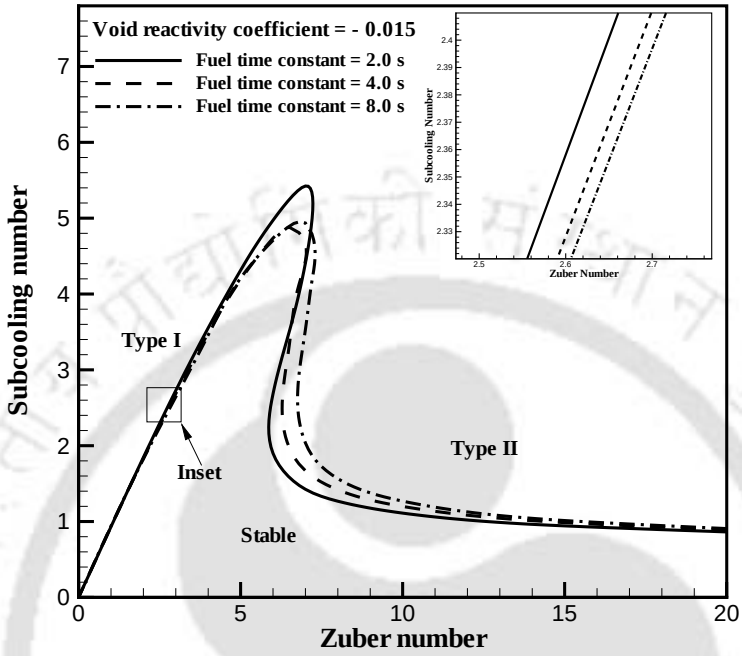

Figure 4.8: Effect of fuel time constant on stability for system 1

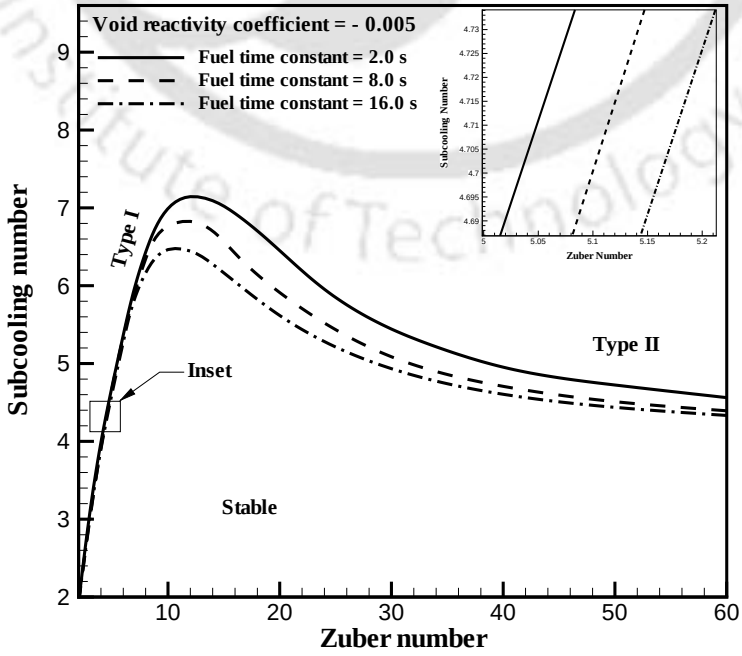

Figure 4.9: Effect of fuel time constant on stability for system 2

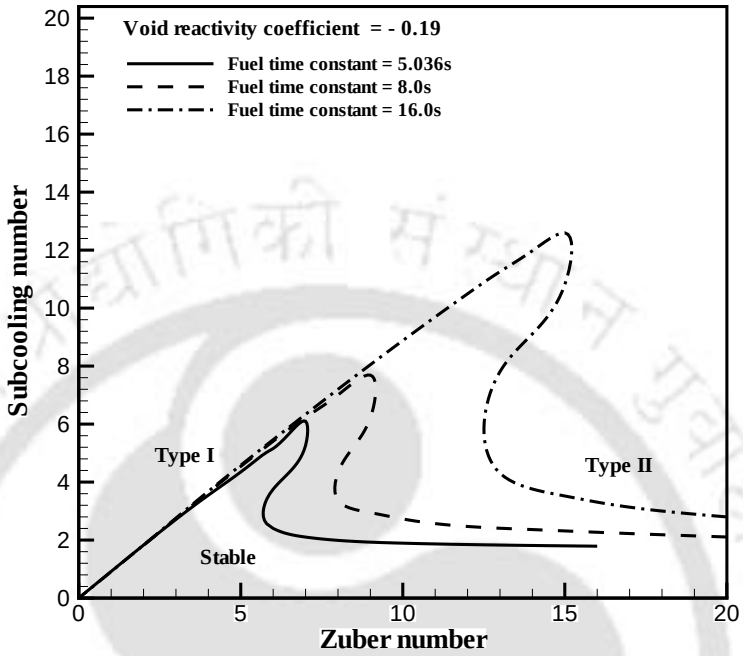

Figure 4.10: Effect of fuel time constant on stability for system 3

on increasing the fuel time constant, a stabilizing effect on Type-I and Type-II regions is observed in Figure 4.10 for system 3. This result could not be compared with literature because Lee and Pan (2005c) have not reported the effect of fuel time constant on stability. Thus, the effect of the fuel time constant on stability is different for systems 1, 2 and 3. This is due to the combined influence of various geometric parameters, as will be discussed in subsequent sections.

Influence of geometric parameters

As described in the above sections, the void reactivity coefficient as well as the fuel time constant have different effects on stability for systems 1, 2 and 3. These results agree with the findings reported in literature (van Bragt and van der Hagen, 1998b, Nayak et al., 2000, Lee and Pan, 2005c). Since the present study has been conducted by using the same mathematical model with the three system configurations, it is confirmed that the difference in the results cannot be attributed to model uncertainties. Systems 1, 2 and 3 have different geometric and neutronic parameters (Table 4.1). In order to investigate

the influence of neutronic parameters, the effect of void reactivity coefficient and fuel time constant was investigated for system 1 with the neutronic parameters of system 2. The results are shown in Figures 4.11(a) and 4.11(b), which are similar in the trend as Figures 4.5 and 4.8, respectively. This confirms that the neutronic parameters β, λ and Λ do not influence the nature of the effects of void reactivity coefficient and fuel time constant on the system stability. Thus, it follows that the difference in the results for systems 1, 2 and 3 is due to the influence of various geometric parameters. In order to determine whether this is due to the riser length, stability characteristics were studied for the riser length of system 2 and all other parameters of system 1. The results were similar to those for system 1, indicating that the difference arises due to a combined influence of various geometric parameters. These parameters determine the frequencies of oscillations in Type-I and Type-II regions. For example, an increase in the riser length or the inlet loss coefficient reduces the frequency of oscillations. In the present study, the frequency of oscillation at the point of onset of instability was calculated from the imaginary part of the eigenvalue pair crossing the imaginary axis. It was observed that the frequencies for system 2 are lower than those for system 1, while the frequencies for system 3 are higher (Table 4.2). According to March-Leuba and Rey (1993), increase in the fuel time constant has both stabilizing and destabilizing effects occurring simultaneously on the system. The stabilizing effect is due to the inherent filtering of the oscillation amplitude at higher frequencies and the destabilizing effect is due to the phase delay to the feedback. Thus, increase in the fuel time constant can stabilize or destabilize the system, depending on which of these two effects is dominant. March-Leuba and Rey (1993) have stated that the gain effect is generally dominant over the phase effect, hence increase in the fuel time constant has a stabilizing effect on the system. However, Nayak et al. (2000) have found that for the low frequency thermohydraulic oscillations observed in AHWR, the phase effect is more significant, hence an increase in the fuel time constant destabilizes the system. In a similar manner, increase in VR can have a destabilizing effect at high frequencies, due to increase in gain. It has a stabilizing effect at low frequencies due to the reduced phase lag (Nayak et al., 2000). This, along with Table 2, explains the difference in the effects of fuel time constant and VR on stability for systems 1, 2 and 3.

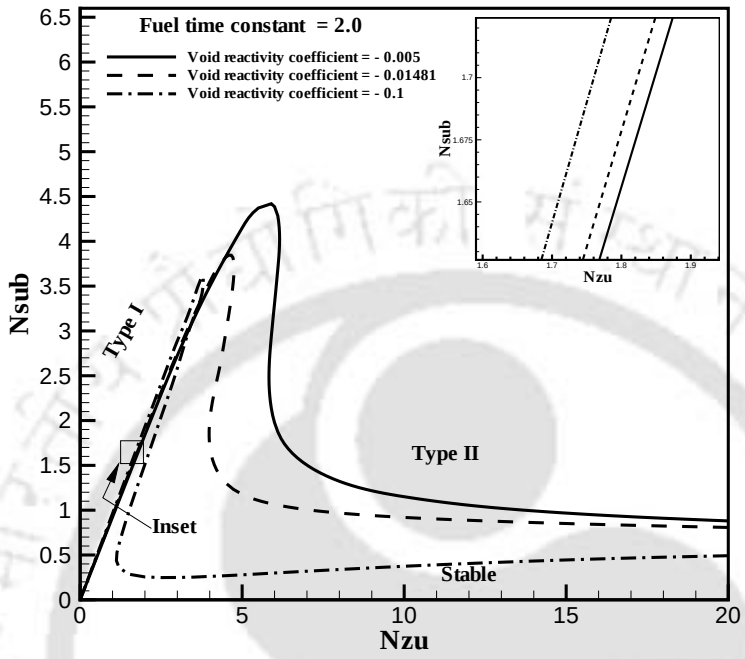

(a) Effect of void reactivity coefficient on stability for system 1 with neutronic parameters of system 2

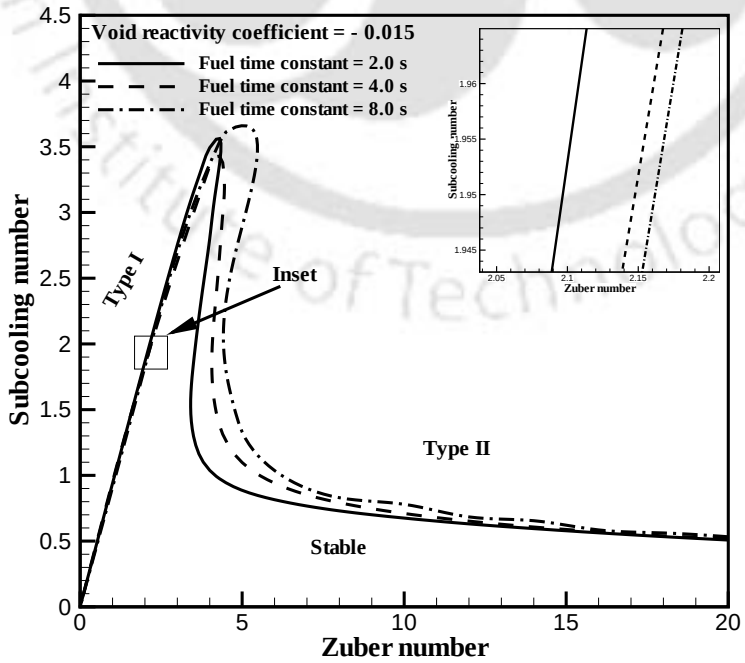

(b) Effect of fuel time constant on stability for system 1 with neutronic parameters of system 2

Figure 4.11: Effect of neutronic parameters

Table 4.2: Frequencies of oscillations for the three geometrical configurations

Type of instability	Range of frequencies of oscillations (Hz)		
	system 1	System 2	System 3
Type-I	0.1 to 0.2	0.02 to 0.1	0.4 to 0.7
Type-II	0.7 to 1.2	0.3 to 0.4	0.6 to 0.9

4.4 Nonlinear dynamics

It was observed that, as the stability boundary is crossed in the parameter plane, a pair of complex conjugate eigenvalues crosses the imaginary axis with non-zero speed in the complex plane. Therefore, according to the Hopf bifurcation theorem (Hassard, 1981), there is a possibility of existence of stable limit cycles in the unstable region or unstable limit cycles in the stable region. The regions of Type-I and Type-II instabilities were investigated for the existence of limit cycles, period doublings and chaotic oscillations. Boiling channels without as well as with riser were studied using system 1 with $N_{Zu} = 6.0$. Bifurcations in N_{Zu}–N_{sub} plane were studied by varying N_{sub}. The void reactivity coefficient was varied from -0.005 to -0.5 in order to study its effect on the bifurcation sequence. This analysis was done for system 1 and the fuel time constant was fixed at 2.0 s.

The transient simulations were done using a modified Bulirsch-Stoer algorithm applicable for stiff system of ODEs (Press et al., 1993). The stable and unstable periodic solutions were located using the limit cycle shooting technique (Parker and Chua, 1989). This technique, based on the Newton-Raphson method and the orthogonality condition, locates a point on a periodic orbit of an autonomous system and determines its period. Fourier power spectra were computed using an FFT algorithm (Parker and Chua, 1989) with the sampling interval carefully chosen to avoid the aliasing problem. A power spectrum containing sharp peaks at discrete frequencies indicates periodic oscillations while a continuous power spectrum indicates a chaotic or a quasiperiodic orbit. Poincaré sections (Parker and Chua, 1989) were computed by locating crossings of the trajectory with a hyperplane in the state-space. Poincaré section of a periodic orbit consists of finite number of points, while that of a chaotic or a quasiperiodic orbit contains infinite number of points. Aperiodicity (chaoticity) observed in different models of the NCBWR, for certain parameter range, results from the exponential divergence of initially close points on the limit set (asymptotic orbit). The rate of this divergence is characterized by Lyapunov

exponents. A system with one or more positive Lyapunov exponents is chaotic. In the present work, the Lyapunov exponents were computed using the algorithm proposed by Wolf et al. (1985), which uses Gram-Schimidt orthonormalization. The numerical techniques used in the present analysis are briefly discussed in Appendix C.

4.4.1 Boiling channel without riser

Initially, the region of Type-II instabilities in the boiling channel without riser with constant heat flux (using N_{Zu} = 6.0 – 20.0) was explored. Stable limit cycles with varying amplitudes and periods were observed, but no period doublings or chaotic oscillations were found. Next, the system with neutronics-thermohydraulics coupling was explored for void reactivity coefficient values between -0.005 to -0.4. Supercritical Hopf bifurcation and series of period doublings were observed as N_{sub} was increased. For the values of VR = -0.25 to -0.4, the system was found to become chaotic after a series of period-doublings as N_{sub} was increased.

A period doubling scenario observed in Type-II instability region at VR = -0.3 and fuel time constant = 2.0 s, for N_{Zu} = 6.0 and N_{sub} being the control parameter is discussed as follows. For $N_{sub} \leq 0.45$ (approximately), a simple limit cycle was found as can be seen in Figure 4.12. Figure 4.12(a) shows the time evolution of one of the state variables and Figure 4.12(b) shows a projection of its phase portrait. The closed loop confirms the presence of stable limit cycle. On further variation of bifurcation parameter N_{sub}, a period doubling was found at $N_{sub} = 0.450$ as shown in Figure 4.13, and another period doubling was found at $N_{sub} = 0.453$ (Figure 4.14) . This was followed by a series of period doublings (Figure 4.15) and eventually led to chaos at $N_{sub} = 0.475$ as shown in Figure 4.16 . The phase portrait Figure 4.16(b) appears to be chaotic. However, the final confirmation of the chaotic nature can be made by plotting the Poincaré section and by computing Lyapunov exponents at $N_{sub} = 0.475$.

The scattered nature of Poincaré section as shown in Figure 4.17(a) indicates chaotic behavior. Lyapunov exponents are computed using the method of Wolf et al. (1985). The Lyapunov exponents at $N_{sub} = 0.475$ were found to be 1.792, 0.000, -0.5699, -19.1223, -195.7815, -1359.2359. The calculations were done for non-dimensional time from 0 to 1000 and the iterations were found to converge within $\pm$ 0.0005. The convergence of

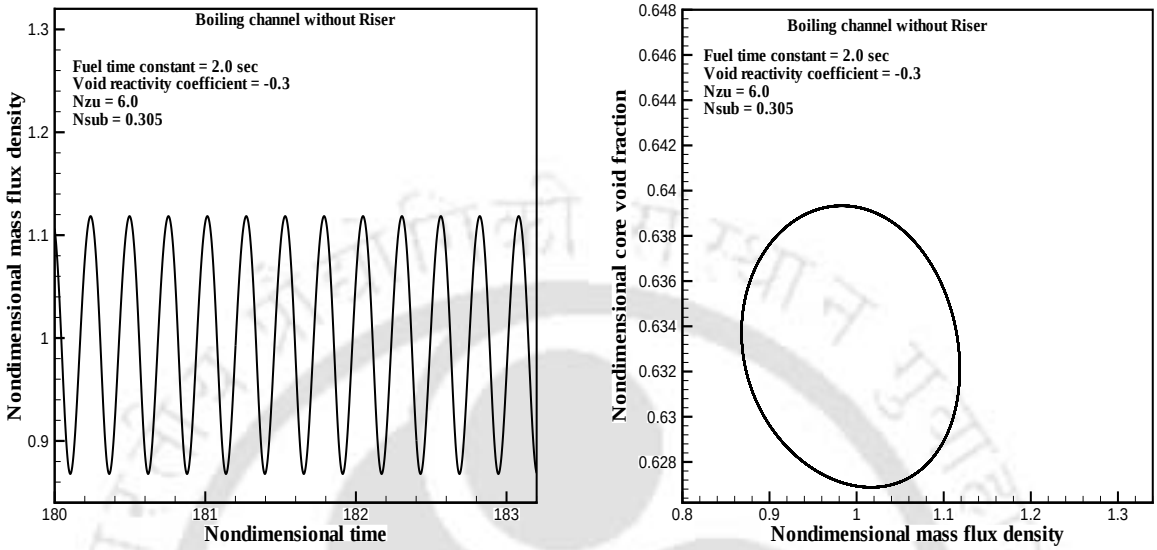

(a) Time evolution of limit cycle (b) Phase portrait

Figure 4.12: Stable limit cycle at N_{zu} = 6.0 and $N_{sub} = 0.305$ for VR = -0.3 and fuel time constant = 2.0 s

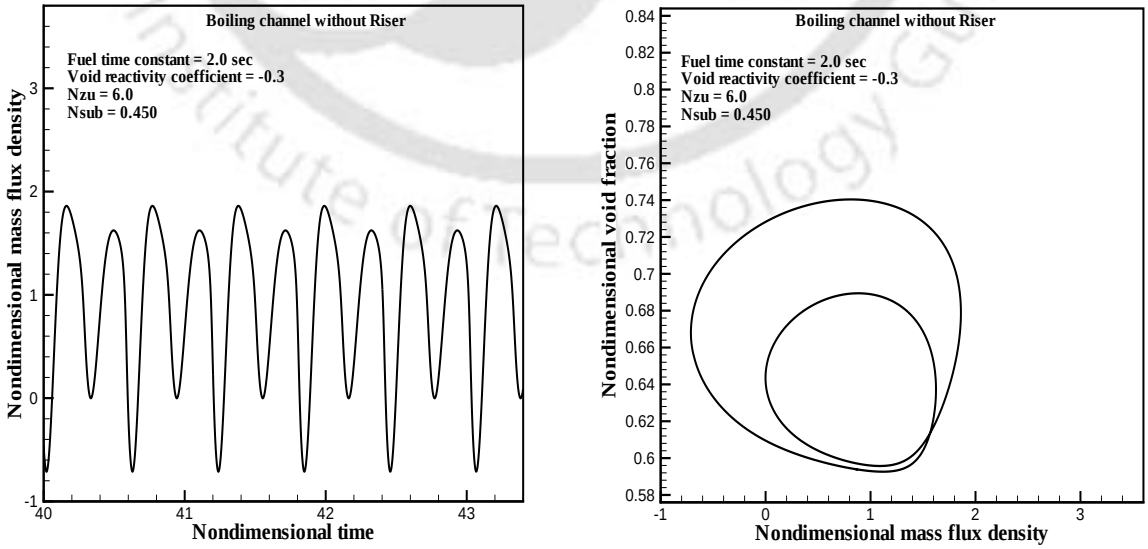

(a) Time evolution of limit cycle (b) Phase portrait

Figure 4.13: Period doubling at N_{zu} = 6.0 and $N_{sub} = 0.450$ for VR = -0.3 and fuel time constant = 2.0 s

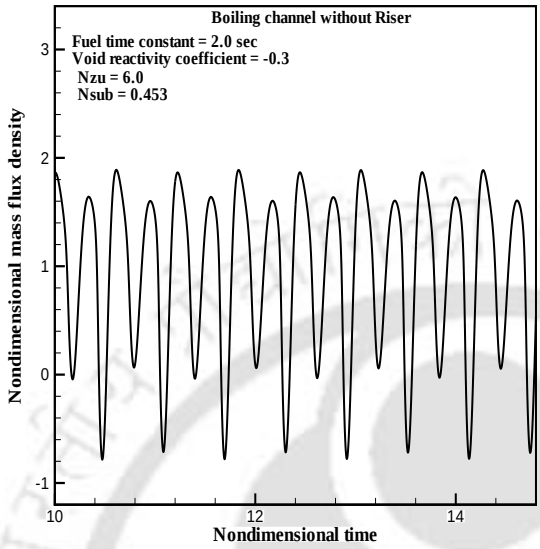

(a) Time evolution of limit cycle

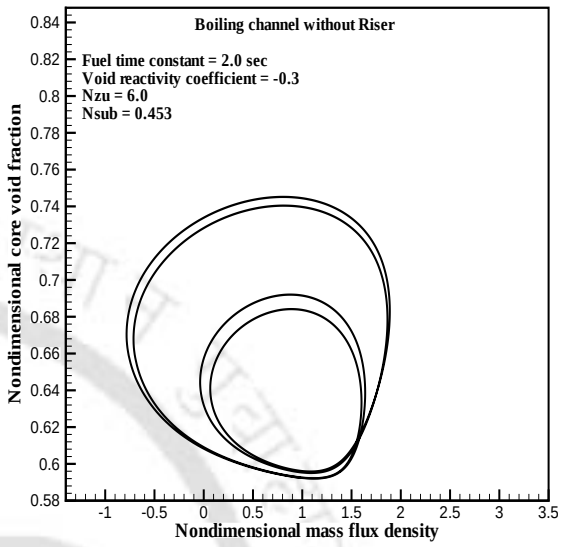

(b) Phase portrait

Figure 4.14: Second Period doubling at N_{zu} = 6.0 and $N_{sub} = 0.453$ for VR = -0.3 and fuel time constant = 2.0 s

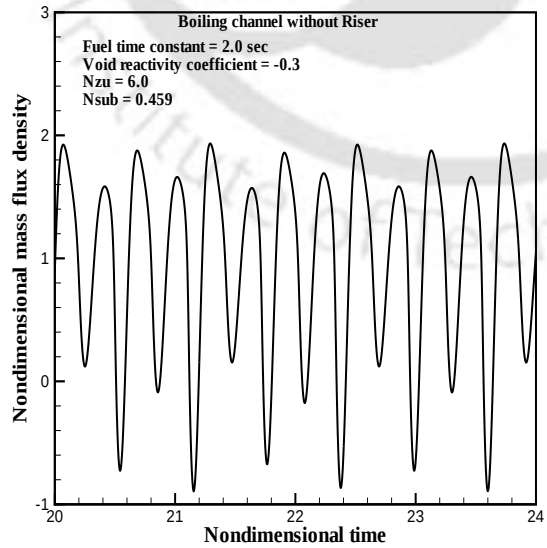

(a) Time evolution of limit cycle

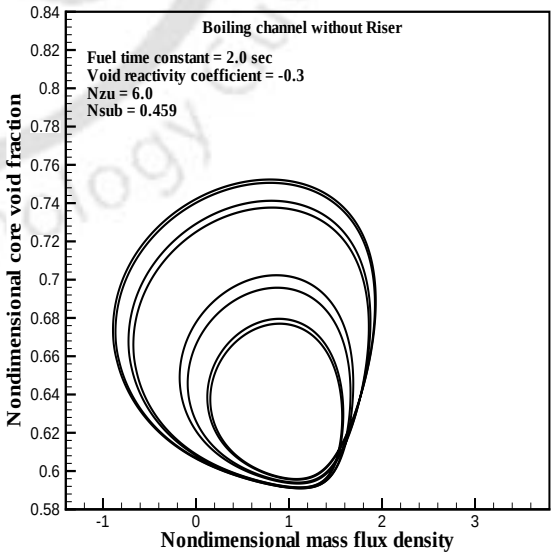

(b) Phase portrait

Figure 4.15: Third Period doubling at N_{zu} = 6.0 and $N_{sub} = 0.459$ for VR = -0.3 and fuel time constant = 2.0 s

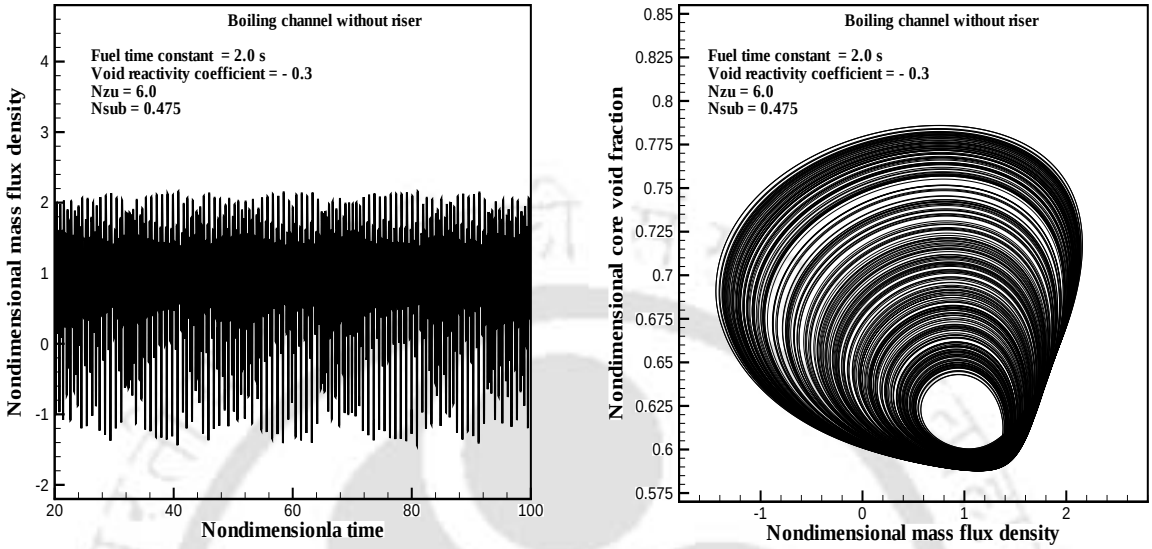

(a) Time evolution of limit cycle (b) Phase portrait

Figure 4.16: Chaos at N_{zu} = 6.0 and $N_{sub} = 0.475$ for VR = -0.3 and fuel time constant = 2.0 s

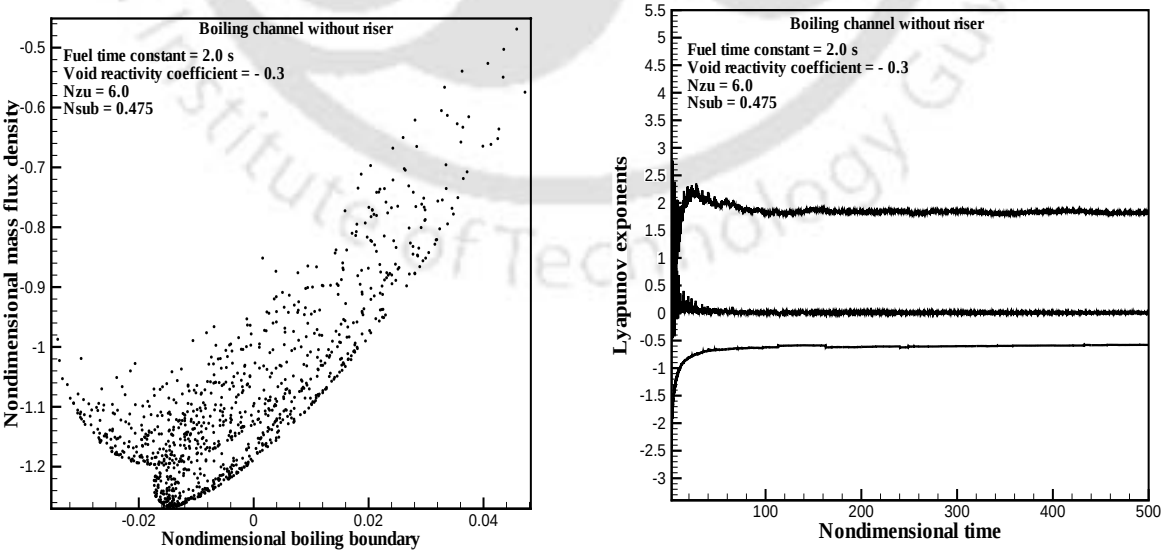

(a) Poincaré section plotted at $N_{sub} = 0.475$ (b) Three largest Lyapunov exponents computed at $N_{sub} = 0.475$

Figure 4.17: Confirmation of chaos at N_{zu} = 6.0 and $N_{sub} = 0.475$ for VR = -0.3 and fuel time constant = 2.0 s

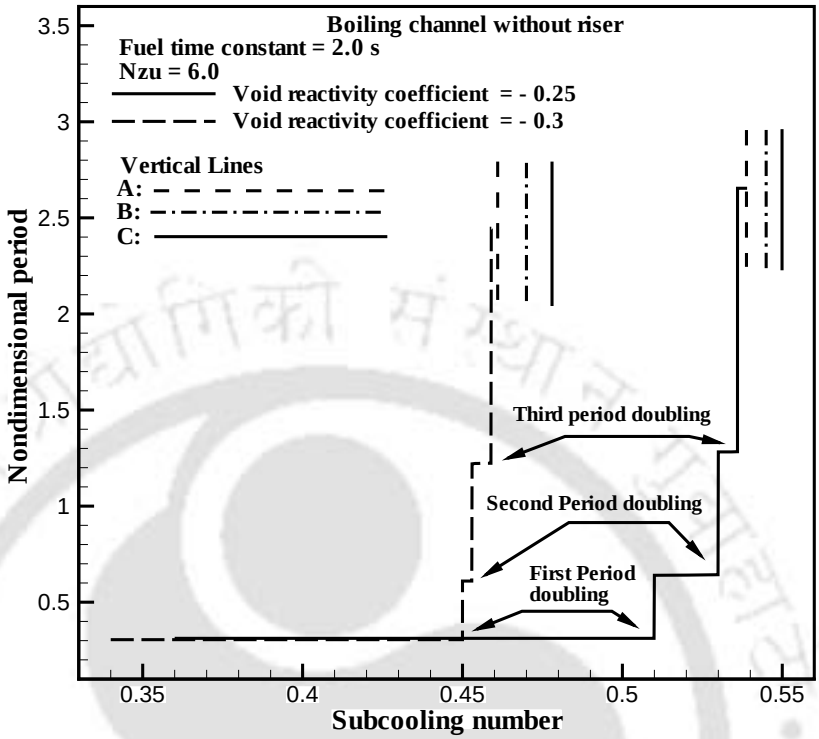

Figure 4.18: Period doubling scenario of boiling channel without riser at different VR values

three largest Lyapunov exponents is shown in Figure 4.17(b), which, for clarity, has been drawn for non-dimensional time from 0 to 500 only. The existence of a positive Lyapunov exponent confirms the chaotic behavior.

Bifurcation diagrams plotted on period vs control parameter (i.e., the subcooling number) give qualitative information of the parametric effects on the period doubling scenario. Figure 4.18 shows the period doubling scenario at two different values of VR. N_{sub} was varied slowly and the period was calculated by limit cycle shooting and cross checked by transient simulations. Thus the exact point of the period doubling on the parameter plane was located (Parker and Chua, 1989).

The region between vertical lines A and B (Figure 4.18) denotes a cascade of period doublings, the line B represents the onset of chaos, and the region between lines B and C is that in which the system was found to be chaotic. The chaotic nature of the system between points B and C was observed by plotting Poincaré sections and computing Lyapunov exponents. The chaotic oscillations shown in Figures 4.16 and 4.17 correspond to a point on line B (for VR = -0.3) in Figure 4.18. It can be further observed that an increase

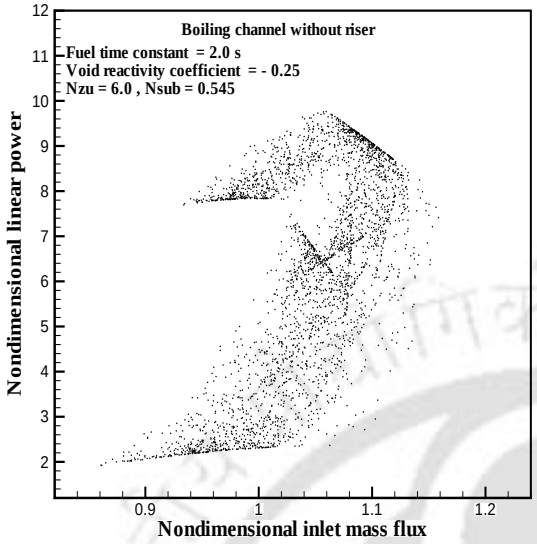

(a) Poincaré section plotted at $N_{sub} = 0.545$

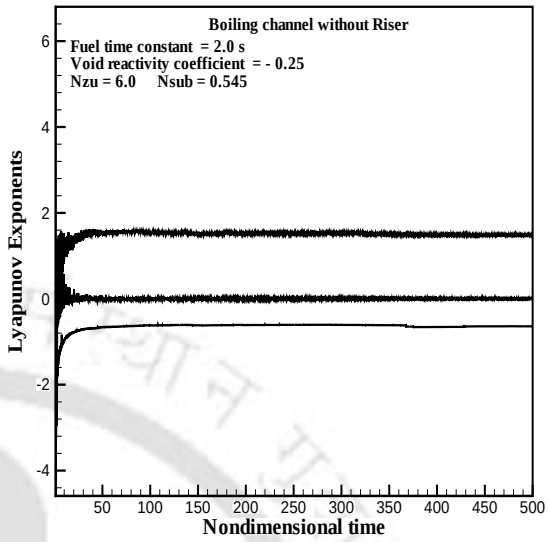

(b) Three largest Lyapunov exponents computed at $N_{sub} = 0.545$

Figure 4.19: Confirmation of chaos at N_{zu} = 6.0 and $N_{sub} = 0.545$ for VR = -0.25 and fuel time constant = 2.0 s

in absolute value of VR enhances the occurrence of chaotic oscillations. i.e. the chaotic oscillations occur at lower values of N_{sub} as the absolute value of VR is increased. The Poincaré section and the three largest Lyapunov exponents computed at a $N_{sub} = 0.545$ on line B (in Figure 4.18 for VR = -0.25) are shown in Figures 4.19(a) and 4.19(b), respectively. The Lyapunov exponents evaluated at $N_{sub} = 0.545$ and VR = -0.25 were found to be 1.472, 0.000, -0.607, -16.416, -196.801, -1355.823. The calculations were done for non-dimensional time from zero to 1000 and the iterations were found to converge within $\pm$ 0.005.

4.4.2 Boiling channel with riser

Boiling channel with riser experiences two types of instabilities, Type-I (at low power and high inlet subcooling) and Type-II (at high power and low inlet subcooling). van Bragt et al. (1999) studied extensively the effect of VR on the bifurcation characteristics in Type-I and Type-II regions using the Hopf bifurcation code BifDD. They observed both sub- and supercritical Hopf bifurcations in Type-I region for different ranges of VR. van der Hagen (1987) had suggested that the dynamics of Type-I instabilities could be studied by using large fuel time constants. Numerical simulations using the limit cycle

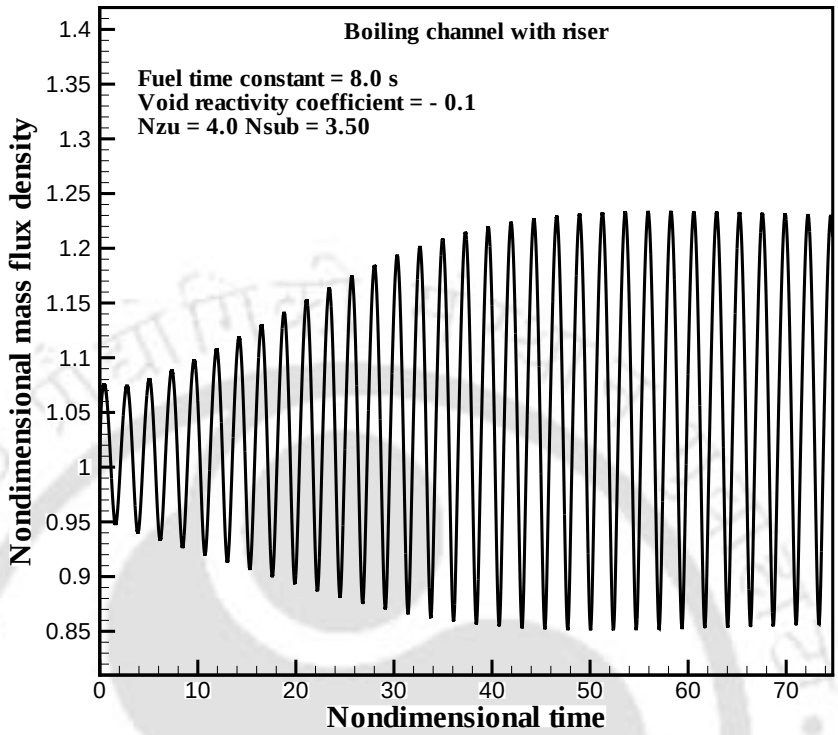

Figure 4.20: Time evolution of a stable limit cycle at parameter values of point $N_{Zu} = 4.0$ and $N_{sub} = 3.50$ for VR = -0.1 and fuel time constant = 8.0 s

shooting technique were done in both Type-I and Type-II regions to study the effects of VR and fuel time constant.

TYPE-I REGION

In Type-I region the Zuber number was fixed at N_{Zu} = 4.0 and the subcooling number N_{sub} was varied slowly across MSB from stable to unstable region. Simulations were carried out by varying the fuel time constant from 2.0 s to 16 s and VR from -0.002 to -0.3. The system was found to undergo both sub- and supercritical Hopf bifurcations. For fuel time constant = 8.0s and VR = -0.1, the system experiences supercritical Hopf bifurcation at Nsub= 3.417. Figure 4.20 shows the time evolution of a stable limit cycle in the unstable region (at N_{Zu} = 4.0 and N_{sub} = 3.50). On further increase in the N_{sub} value, the system diverged and no period doubling sequence was observed. An unstable limit cycle was detected in the stable region (at N_{Zu} = 4.0 and N_{sub} = 3.524) for fuel time constant = 2.0 s and VR = -0.015. Unlike stable limit cycles, it is not possible to obtain the phase-portraits

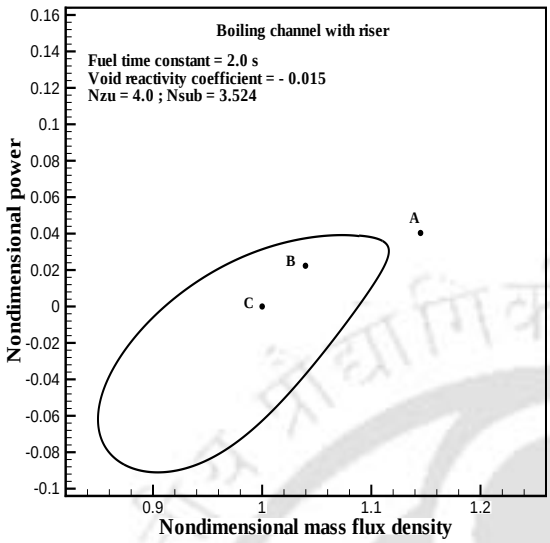

(a) A projection of the phase portrait of unstable limit cycle for parameter values of point $N_{Zu} = 4.0$ and $N_{sub} = 3.524$

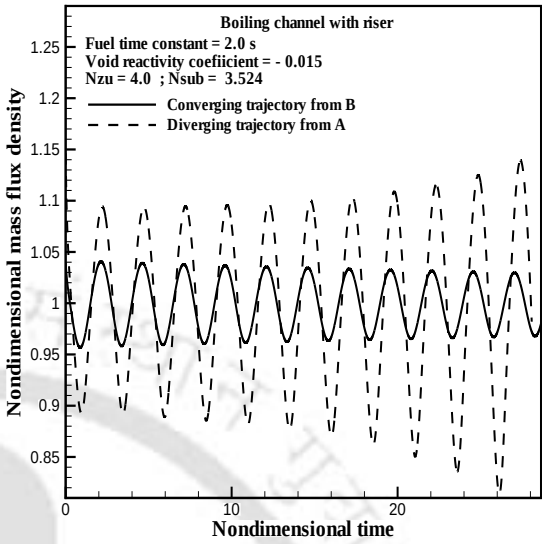

(b) Time evolution of a state variable at parameter values of point $N_{Zu} = 4.0$ and $N_{sub} = 3.524$ from two different initial conditions

Figure 4.21: Unstable periodic orbit at N_{zu} = 4.0 and $N_{sub} = 3.524$ for VR = -0.015 and fuel time constant = 2.0 s

of unstable limit cycles by numerical integration, unless the initial point is exactly on the limit cycle. Therefore, a point on the unstable limit cycle was located, and its period estimated, by the autonomous shooting method (Parker and Chua, 1989). Then its phase-portrait (Figure 4.21(a)) was obtained by numerical integration for one period, starting from the point found by shooting. Trajectories emanating from two initial conditions are shown in Figure 4.21(b). The trajectory emerging from point A diverges out, whereas the trajectory from point B converges to the fixed point C. This shows that the system can be unstable for large disturbances even though it is stable for small perturbations about its steady-state. It was observed that for values of fuel time constant lower than 4.0s, the system experiences a subcritical Hopf bifurcation for all the values of VR explored. On the other hand, for values of fuel time constant above 4.0s, the bifurcation was subcritical at values of VR greater (algebraically) than -0.09 and supercritical at values of VR less (algebraically) than -0.10. Thus, the fuel time constant has a significant influence on Type-I instability.

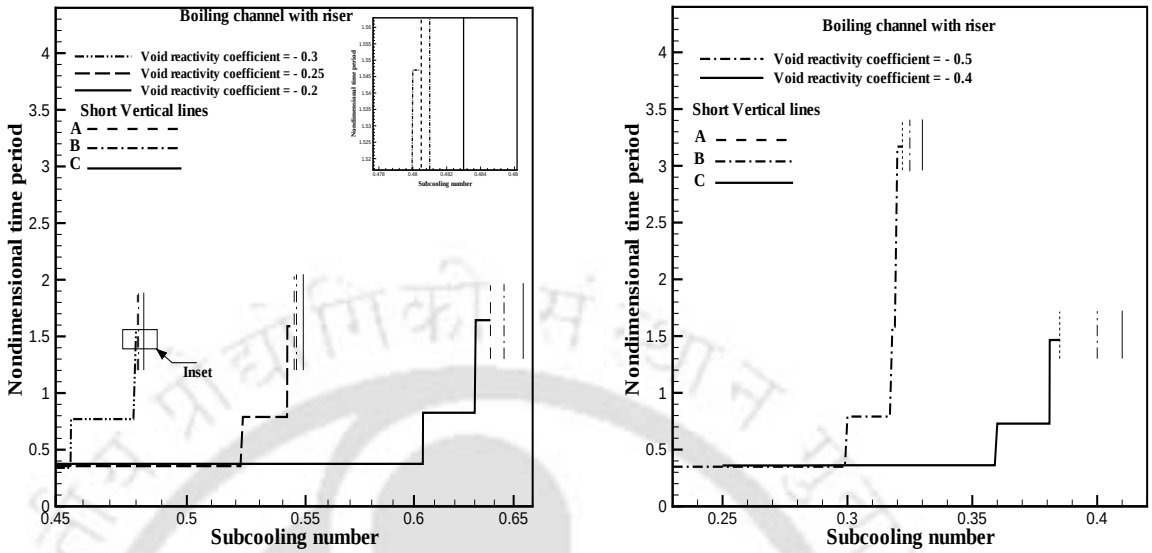

(a) Period doubling scenario of boiling channel with riser for VR = −0.2 to −0.3

(b) Period doubling scenario of boiling channel with riser for VR = −0.4 and −0.5

Figure 4.22: Effect of VR on period doubling scenario in boiling channel with riser

TYPE-II REGION

In Type-II region, the effects of various parameters like VR, fuel time constant, core inlet and exit loss coefficients, on the period doubling scenario and chaotic oscillations are investigated. The transient simulations are carried out for $N_{Zu} = 6.0$ and N_{sub} is the control parameter, which is varied slowly across MSB from stable to unstable region. The range of VR explored was from -0.005 to -0.5 and fuel time constant was varied from 2.0 to 10.0 seconds.

Effect of void reactivity coefficient (VR)

The system experienced supercritical Hopf bifurcation (the presence of stable limit cycle) for values of VR ranging between -0.005 to -0.18. Stable limit cycles and a period doubling were observed from transient simulations, but chaotic oscillations were not seen. For values of VR greater than -0.18 (in the absolute sense), the system experienced chaotic oscillations. Figures 4.22(a) and 4.22(b) show the period doubling scenario at $N_{Zu} = 6.0$ and VR range -0.1 to -0.5. The bifurcation parameter N_{sub} was varied slowly and the exact point of period doubling on the parameter plane was located using the method of limit cycle shooting. The region between vertical lines A and B denotes a cascade of

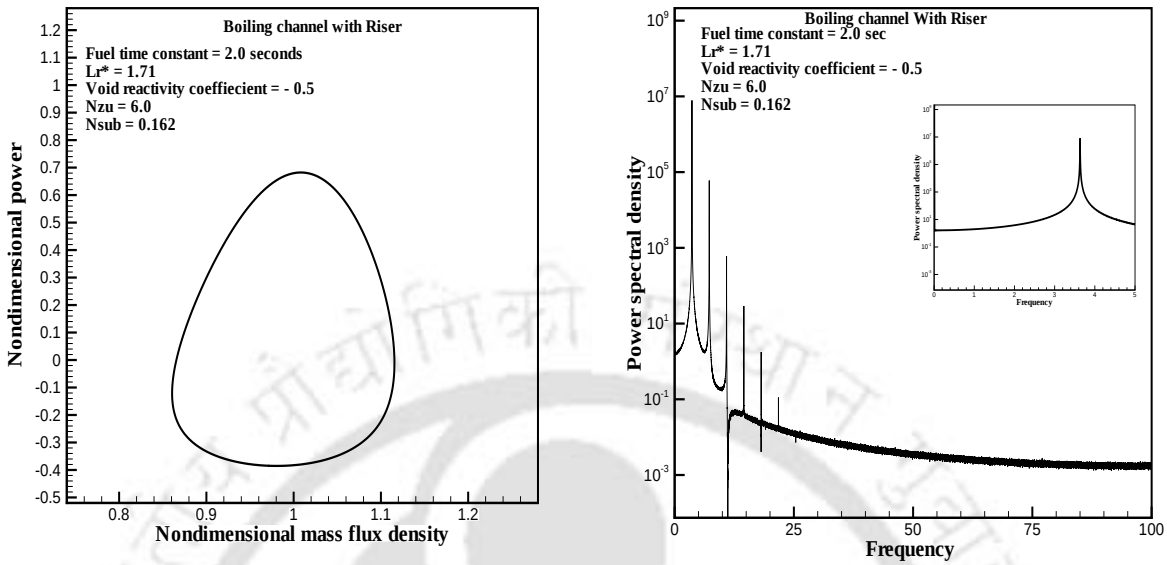

(a) Phase portrait (b) Fourier power spectrum

Figure 4.23: Simple limit cycle at $N_{sub} = 0.162$ for VR = -0.5 and fuel time constant = 2.0 s

period doublings, the line B represents the onset of chaos, and the region between lines B and C is that in which the system was found to be chaotic. From Figure 4.22 it can be observed that, as the absolute value of VR is increased, the chaotic oscillations are enhanced (i.e., the chaotic oscillations occur early).

The sequence of period doublings and chaotic nature of the system between points B and C of Figure 4.22 at different values of VR was observed by transient simulations and by plotting Fourier power spectra. The chaotic oscillations are further confirmed by computing Lyapunov exponents. The period doubling route to chaos for one of the values of VR (VR = -0.5 in Figure 4.22(b)) is presented here.

Fixing N_{Zu} at 6.0 and N_{sub} being the control parameter, as N_{sub} is varied in the unstable region, a simple limit cycle was observed up to $N_{sub} \leq 0.30$ (approximately). A simple limit cycle observed at $N_{sub} = 0.162$ is shown in Figure 4.23. The power spectrum of this limit cycle has sharp peaks at the fundamental frequency and its harmonics as shown in Figure 4.23(b). The sub-harmonics are absent as can be seen in the inset of Figure 4.23(b). As the control parameter is varied further a period doubling was found at $N_{sub} = 0.30$ (Figure 4.24) and another period doubling was found at $N_{sub} = 0.32$ (Figure 4.25). The first period doubling has one sub-harmonic peak and the second period doubling has three such sub-harmonic peaks as can be seen from the insets of Figures 4.24

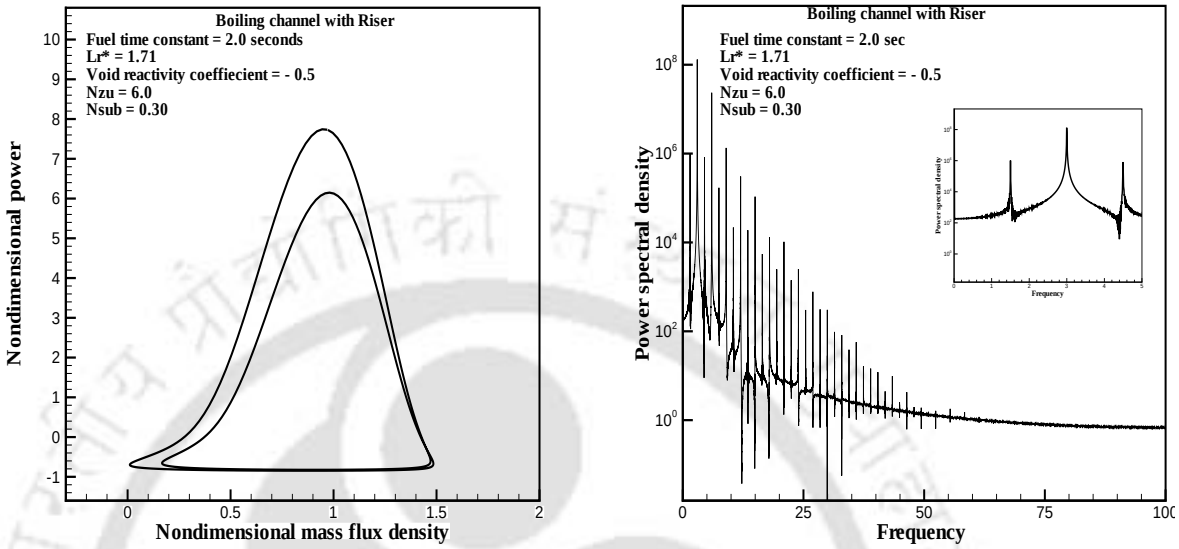

(a) Phase portrait (b) Fourier power spectrum

Figure 4.24: First period doubling at $N_{sub} = 0.30$ for VR = -0.5 and fuel time constant = 2.0 s

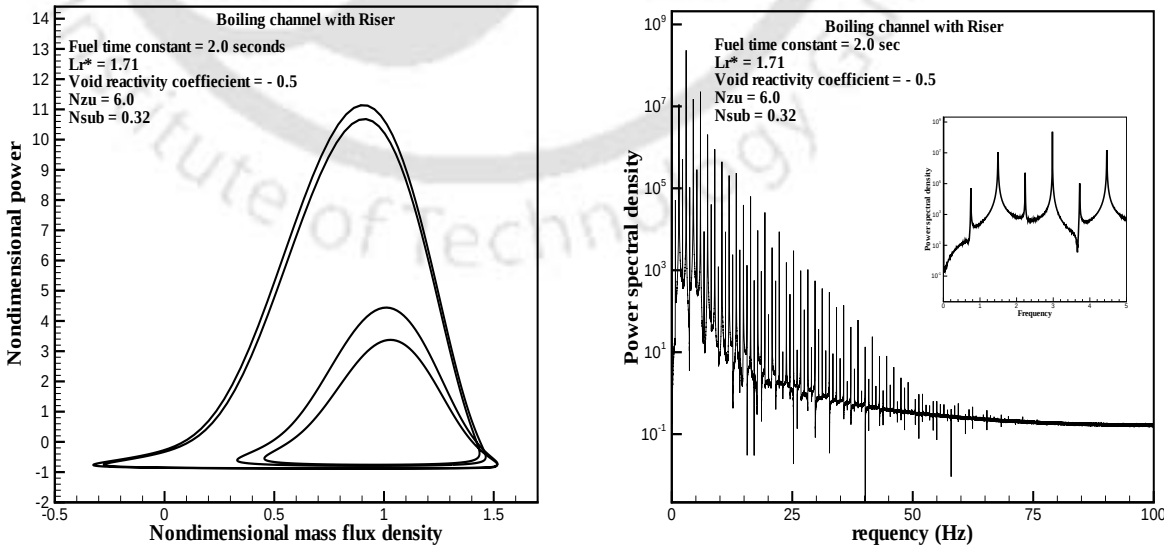

(a) Phase portrait (b) Fourier power spectrum

Figure 4.25: Second period doubling at $N_{sub} = 0.32$ for VR = -0.5 and fuel time constant = 2.0 s

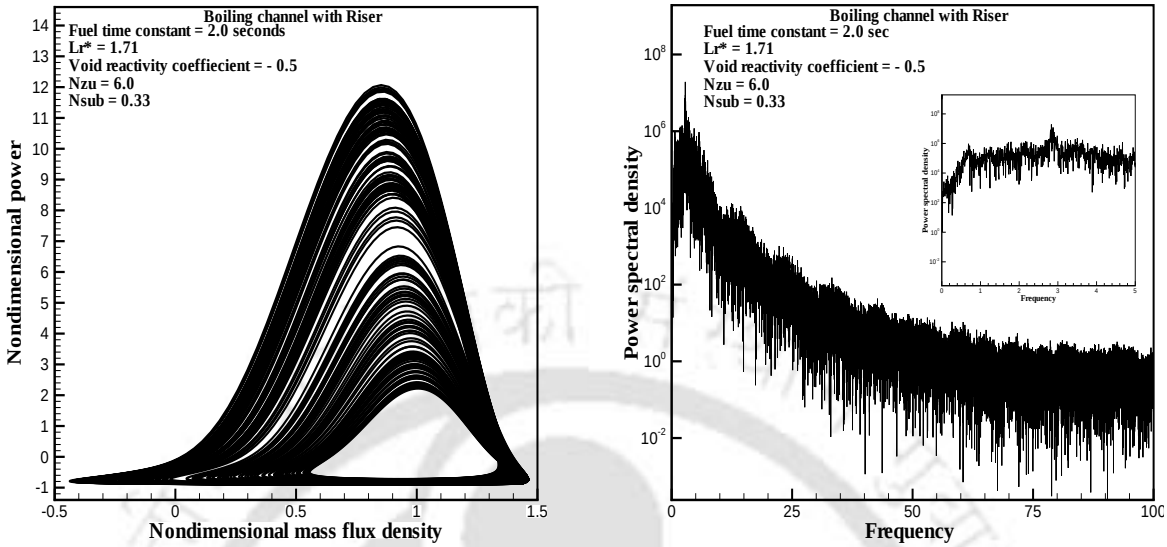

(a) Phase portrait (b) Fourier power spectrum

Figure 4.26: Chaotic oscillation at $N_{sub} = 0.33$ for VR = -0.5 and fuel time constant = 2.0 s

and 4.25 respectively. On further increase in N_{sub}, a series of period doublings occurred eventually leading to chaos at $N_{sub} = 0.330$. The continuous spectrum which can be seen from the inset of Figure 4.26(b) indicates chaotic oscillations. The chaotic behavior is further confirmed by computing Lyapunov exponents which were estimated to be 1.480165, 0.002259,-0.329870, -5.182020,-13.261220, -28.186296, -141.424419, and -1707.863442. The presence of positive exponent confirms chaotic behavior. Figure 4.27 shows the largest three Lyapunov exponents computed using Wolf et al. (1985) algorithm and the iterations were found to converge within $\pm$ 0.0003.

Effect of fuel time constant

Fuel time constant characterizes the delay in heat transfer from fuel rod surface to the coolant. Higher the fuel time constant, higher is the delay in heat transferred to the coolant. The effect of fuel time constant on period doubling scenario and chaotic oscillations is shown in Figure 4.28(a). In this study the fuel time constant is varied from 2.0s to 4.0s and all other parameters are kept constant (i.e., $k_{ci} = 3.46$, $k_{ce} = 2.19$, VR = -0.2) similar to that in Figure 4.22(a). It can be observed that, as fuel time constant is increased, the occurrence of period doubling is considerably delayed. For the fuel time constant = 4.0 s, the first period doubling occurred at higher N_{sub} compared to the fuel time constant

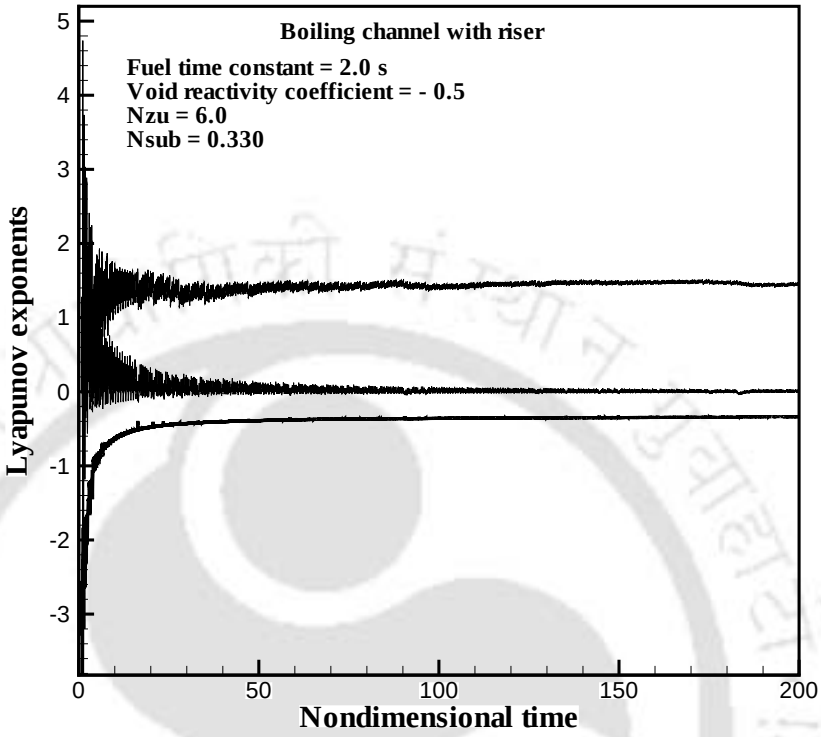

Figure 4.27: Lyapunov exponents at $N_{Zu} = 6.0$ and $N_{sub} = 0.330$ for VR = -0.5 and fuel time constant = 2.0 s

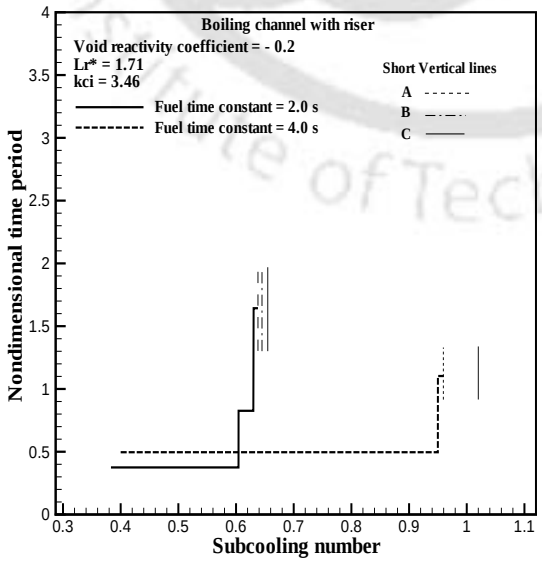

(a) Effect of fuel time constant on period doubling scenario and chaos

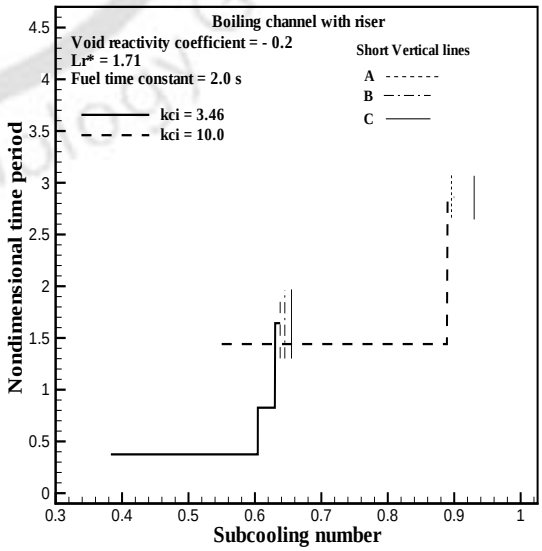

(b) Effect of core inlet loss coefficient k_{ci} on period doubling scenario and chaos

Figure 4.28: Effect of fuel time constant and k_{ci} on period doubling scenario and chaos

= 2.0 s. Consequently, series of period doublings occurred between $N_{sub} = 0.96$ and 1.02 indicated by small vertical lines A and C. However, chaotic oscillations did not occur. It can be further observed that the oscillation time period is higher for fuel time constant = 4.0 s. Hence, increase in fuel time constant increases the time period of the oscillations (in other words, the frequency of oscillations decreases as the fuel time constant increases).

Effect of core inlet loss coefficient (k_{ci})

As discussed in Section 4.3.1, increase in k_{ci} has a stabilizing effect on the system. The effect of k_{ci} on the period doubling scenario and chaos is shown in Figure 4.28(b). In this study, k_{ci} was increased from 3.46 to 10.0, keeping the other parameters constant (i.e., fuel time constant = 2.0 s, VR = -0.2, $k_{ce} = 2.19$). As k_{ci} is increased from 3.46 to 10.0, the first period doubling was delayed and occurred at $N_{sub} = 0.89$. Further a series of period doublings occurred between $N_{sub} = 0.89$ and 0.92 indicated by short vertical lines A and C. In this case also, chaotic oscillations did not occur. Further, it can be observed that, the time period of oscillations was increased (decrease in frequency of oscillations).

Effect of core exit loss coefficient (k_{ce})

Increase in k_{ce} has a destabilizing effect on the system as discussed in Section 4.3.1. Further, the effect of k_{ce} on the period doubling scenario and chaos is shown in Figure 4.29. In this study, the core exit loss coefficient k_{ce} was increased from 2.19 to 10.0, keeping the other parameters constant (i.e., fuel time constant = 2.0 s, VR = -0.2,$k_{ci} = 3.46$). As k_{ce} is increased from 2.19 to 10.0, the first period doubling was advanced and occurred at $N_{sub} = 0.48$ followed by cascade of period doublings between $N_{sub} = 0.50$ to 0.54. It is interesting to note that, though the period doubling scenario was advanced (or aggravated), chaotic oscillations were not observed. It can be further observed that, increase in core exit loss coefficient k_{ce} reduces the time period of the oscillations (i.e., increase in the frequency of oscillations).

From the above studies it can be concluded that the parameters (such as fuel time constant and core inlet loss coefficient) which has a stabilizing effect on the system delays the occurrence of period doubling and chaos. On the other hand the parameters (such as

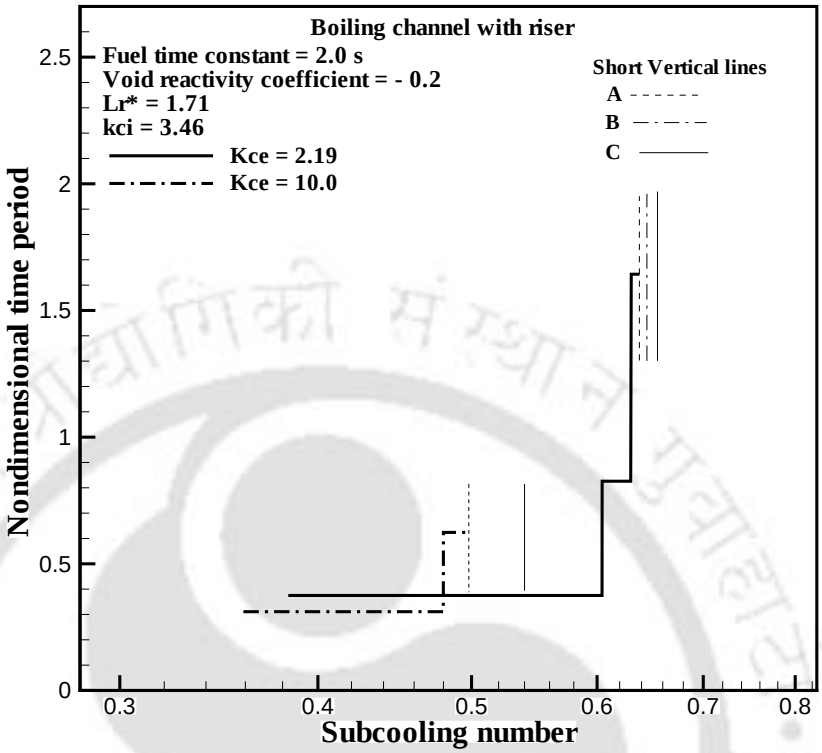

Figure 4.29: Effect of core exit loss coefficient k_{ce} on period doubling scenario and chaos

VR, core exit loss coefficient) which has a destabilizing effect on the system aggravates the occurrence of period doubling and chaos.

4.5 Summary

This chapter contains two numerical studies, one on stability analysis and the other on nonlinear dynamics of NCBWR. The purpose of the stability analysis was to study the effect of geometrical parameters and feedback parameters on the stability of the system and further to resolve different, seemingly contradictory parametric trends reported earlier in literature. The difference in the way the VR and the fuel time constant effect the system stability can be either due to the influence of various geometric and neutronic parameters or due to the difference in the modeling approaches. Since the present study has been conducted by using the same mathematical model with three different system configurations, and the results agree with the findings reported in literature, it is confirmed that the difference observed is not attributable to model uncertainties. It was also observed

that the neutronic parameters do not influence the nature of the effects of VR and fuel time constant on the system stability.

From the stability analysis, it follows that the effects of VR and fuel time constant are influenced by the geometrical parameters and are different for different systems. In systems with low frequency oscillations, an increase in absolute value of void reactivity coefficient stabilizes the system and an increase in fuel time constant destabilizes the system. On the other hand, for systems with high frequency oscillations, an increase in the absolute value of VR destabilizes and an increase in fuel time constant stabilizes the system.

Nonlinear analysis has been carried out for the boiling channels with and with out riser. Both constant heat flux and coupled neutronic cases are considered. One of the system configurations (system 1) has been used in the nonlinear studies. For constant heat flux case, transient simulations are carried out across the MSB in the Type-I and Type-II regions. It is observed the system experienced supercritical Hopf bifurcation across the MSB in Type-I and Type-II regions. Stable limit cycles are located but there is no period doubling scenario. Further, nonlinear analysis for coupled-neutronics case has been done to study the effect of parameters like VR, fuel time constant, core inlet and exit loss coefficients on the bifurcations and chaotic behavior of the system in Type-I and Type-II regions. Poincaré sections, Fourier power spectra and Lyapunov exponents were computed to confirm the chaotic behavior. It was observed that in the Type-I region, for fuel time constant values lower than 4.0s, the system experiences a subcritical Hopf bifurcation for all the values of VR explored. This leads to an unstable limit cycle, which was located by the shooting method. Therefore, the system is unstable for large disturbances, although being stable for small perturbations about its steady state. For values of fuel time constant above 4.0s, the bifurcation was subcritical at values of VR greater (algebraically) than -0.09 and supercritical at values of VR less (algebraically) than -0.10. However, period doubling scenario and chaos was not observed in Type-I region.

The boiling channels with and without riser experience chaotic oscillations under strong reactivity feedback in the Type-II region. Boiling channel with riser experiences chaotic oscillations at lower values of VR (in absolute sense) compared to boiling channel without riser. Further, the effect of VR, fuel time constant and geometric parameters like core inlet and exit resistances on the chaotic oscillations in Type-II region are investigated.

It is observed that, an increase in VR (absolute value) and core exit loss coefficient aggravates the chaotic oscillations. On the other hand, an increase in parameters such as fuel time constant and core inlet loss coefficient delayed the occurrence of period doubling and chaos. In other words, the parameters which have a stabilizing effect on the system delays the occurrence of period doubling and chaotic oscillations, and the parameters which destabilize the system aggravates the chaotic oscillations. It was further observed that in Type-II region, increase in parameters such as VR (absolute value), and core exit loss coefficient k_{ce} increases the frequency of oscillations, on the other hand, an increase in fuel time constant and core inlet loss coefficient k_{ci} decreases the frequency of oscillations.

Chapter 5

Thermal-Hydraulic Instabilities in Double Channel Systems

5.1 Introduction

Single channel analysis is simple and appropriate for studying the in-phase oscillations in a system of parallel channels with uniform power profile. However, in real reactors there are hundreds of channels having different flow conditions. The power profile across the channels is not uniform and constant, and the channels may have different modes of oscillations. Single channel models are inadequate for simulating the out-of-phase oscillations. Power fluctuations in some of the channels can trigger thermal-hydraulic oscillations in other channels due to common boundary conditions. Some of the new generation nuclear reactors are equipped with on-power refueling facility for efficient fuel management. In this process, when the reactor runs at full power, the spent fuel from a channel is removed and the new fuel is loaded. During refueling, there will not be power input to that channel. The flow area increases and single-phase liquid flows through this channel. During such conditions, in natural circulation systems, complex channel-to-channel interactions exist, which may destabilize the system. In order to study the transients due to channel-to-channel interactions and on-power refueling, a system of parallel channels needs to be modeled.

In this chapter, thermal-hydraulic instabilities in a double channel system and a pres-

sure tube type NCBWR are investigated. Initially, a simple double channel natural circulation system is modeled separately using RELAP5/MOD3.4 and a lumped parameter model (LPM). Based on the studies carried out by LPM and RELAP5, the present work is divided into two parts. A detailed study of instabilities and nonlinear oscillations are carried out using LPM. Channel-to-channel interaction studies are carried out using RELAP5. Further, a pressure tube type NCBWR is modeled using RELAP5 and on-power refueling studies are carried out in the similar way as done for the simple double channel system and the findings are compared. The chapter is organized as follows: Section 5.2 discusses the modeling of double channel boiling systems using LPM and RELAP5. Nodal sensitivity test of double channel RELAP5 model and comparison of LPM and RELAP5 are presented in Section 5.3. Section 5.4 discusses stability analysis and nonlinear oscillations using lumped parameter model. Channel-to-channel interaction and on-power refueling studies are presented in Section 5.5. Section 5.6 discusses the channel-to-channel interaction and on-power refueling studies for a pressure tube type NCBWR. Conclusions are presented in Section 5.7.

5.2 Modeling of double channel system

In order to investigate the channel-to-channel interaction and on-power refueling on the dynamics of the system, a simple double channel boiling loop is modeled using a lumped parameter model and RELAP5/MOD3.4. The schematic view of the simple double channel system is shown in Figure 5.1. It is a simplified version of a pressure tube type NCBWR (discussed in Section 3.4) in which only 2 channels are considered for modeling. The horizontal sections of the riser are eliminated and the riser length is reduced to 5.0 m. Further, the dimensions of the downcomer and inlet header are reduced accordingly. The geometrical configuration is briefly given in Section 5.2.2. The stability analysis and the nonlinear oscillations in the double channel system are investigated using a lumped parameter model (LPM2). The lumped parameter model (LPM2) for a multichannel system is derived in Chapter 3. It is further briefly presented in Section 5.2.1. The RELAP5 model and a detailed nodalization scheme of the double channel system are presented in the Section 5.2.2.

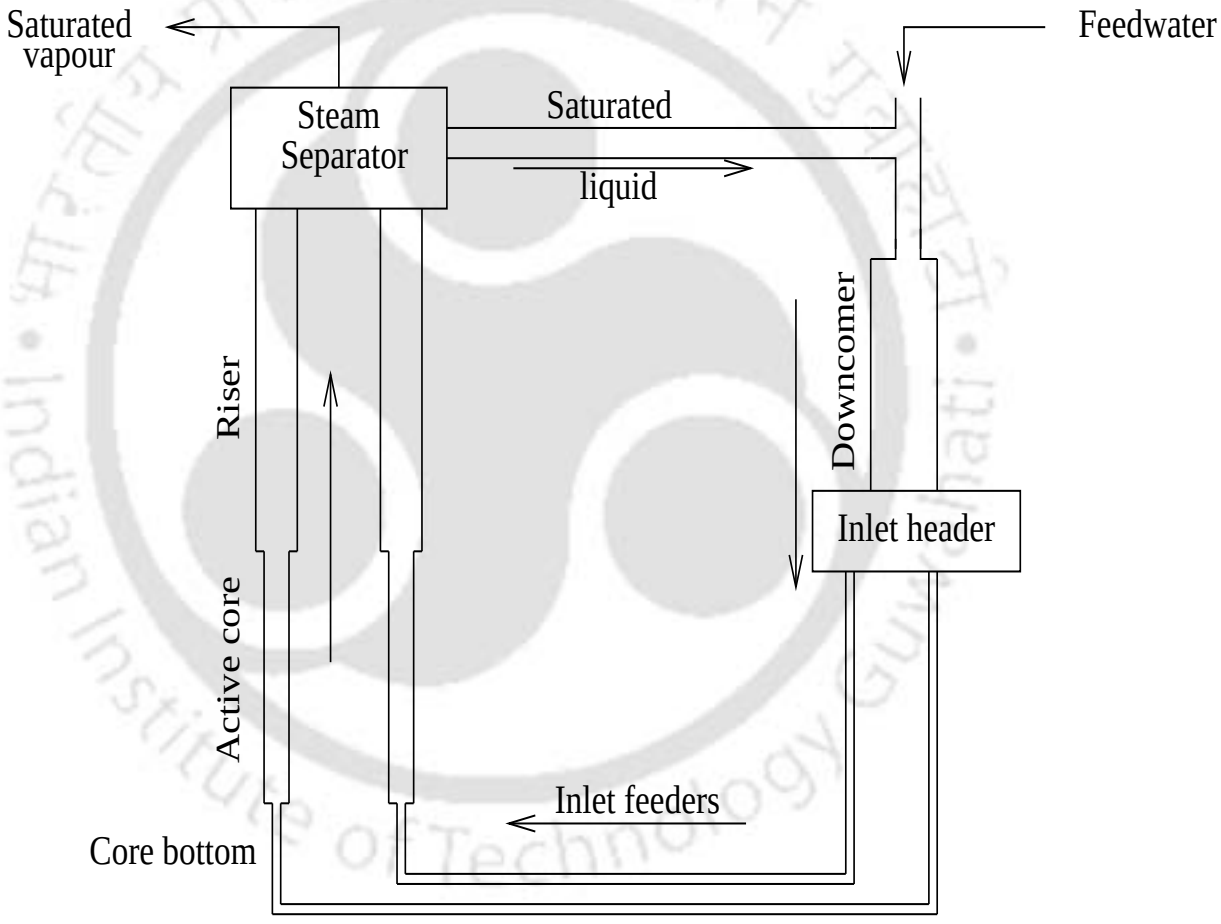

Figure 5.1: Schematic view of a simple double channel system

5.2.1 Lumped parameter model

A detailed derivation of LPM2 is given in Section 3.2. In the present study, it is assumed that the two channels are subjected to a constant and uniform heat flux (i.e., no neutronics case). The modeling of LPM in the present analysis directly starts from the thermal-hydraulic equations (omitting neutronics and heater wall dynamics). The single phase region in the core is modeled as a single node and the dynamics of the boiling boundary in j^{th} channel is given as

$$\frac{dz^*_{bb,j}(t^*)}{dt^*} = 2\left[G^*_{ci,j}(t^*) - \frac{z^*_{bb,j}(t^*)N_{Zu,j}}{N_{sub}}\right] \tag{5.1}$$

where,j = 1,2. The two-phase region is modeled as a single node and the average core void dynamics (Eq. 3.32) is given as

$$\frac{dj_{1cav,j}(t^*)}{dt^*} = (G^*_{ce,j} - G^*_{ci,j}) \tag{5.2}$$

where, $j_{1cav,j}(t^*) = (1-N_\rho)\alpha_{cav,j}$. Similarly, the riser void dynamics is given by Eq. 3.34, as below

$$\frac{dj_{1Rav,n,j}(t^*)}{dt^*} = \left[G^*_{R,n,j}(t^*) - G^*_{R,n-1,j}(t^*)\right]\frac{N_R}{L^*_R} \tag{5.3}$$

where, $j_{1Rav,n,j}(t^*) = (1-N_\rho)\alpha_{Rav,n,j}$.

The relation between the core inlet and outlet mass flux densities in each channel is obtained by integrating the energy Eq.3.27 in the two-phase region, as follows

$$G^*_{ci,j}(t^*) = G^*_{ce,j}(t^*) + [1 + j_{2cav,j}(t^*)] - N_{Zu,j}[1 - z^*_{bb,j}(t^*)] \tag{5.4}$$

where, $j_{2cav,j}(t^*) = X^*_{ce,j}(t^*)[N_{Zu,j} - N_{sub}]$. Similarly, the relation between the nodal mass flux densities over a riser node (Eq. 3.35) is expressed as

$$G^*_{R,n-1}(t^*)[1 + j_{2Rav,n-1}(t^*)] = G^*_{R,n}(t^*)[1 + j_{2Rav,n}(t^*)] \tag{5.5}$$

where, $j_{2Rav,n,j}(t^*) = X^*_{Rn,j}(t^*)[N_{Zu,j} - N_{sub}]$. The relation between the average void frac-

tion (in the core) and the core exit quality is given by Eq. 3.41 as

$$j_{1cav,j}(t^*) = \left[1 - z^*_{bb,j}(t^*)\right]\left[1 - \frac{ln\left(1 + j_{2cav,j}(t^*)\right)}{j_{2cav,j}(t^*)}\right] \tag{5.6}$$

Similarly, in the riser, the relation between the average void fraction (over a riser node) and the nodal steam quality is given by Eq. 3.42 as

$$j_{1Rav,n,j}(t^*) = \left[1 - \frac{1}{(j_{2Rav,n,j} - j_{2Rav,n-1,j})} ln\left\{1 + \frac{j_{2Rav,n,j} - j_{2Rav,n-1,j}}{1 + j_{2Rav,n-1,j}}\right\}\right] \tag{5.7}$$

Now, differentiating the algebraic Eq. 5.6 with respect to non-dimensional time and re-arrangement of the terms, the dynamics of the core exit quality in the two-phase region (3.47) is given as

$$\frac{dX^*_{ce,j}}{dt^*} = \frac{\left[\frac{dj_{1c,j}}{dt^*} + \left(\frac{j_{2c,j} - \ln\left(1+j_{2c,j}\right)}{j_{2c,j}}\right)\frac{dz^*_{bb,j}}{dt^*}\right]\left(1 + j_{2c,j}\right) j^2_{2c,j}}{\left(1 - z^*_{bb,j}\right)\left(N_{Zu,j} - N_{sub}\right)\left[\left(1 + j_{2c,j}\right)\ln\left(1 + j_{2c,j}\right) - j_{2c,j}\right]} \tag{5.8}$$

Similarly, differentiating the algebraic Eq. 5.7 with respect to non-dimensional time, the dynamics of vapor mass quality in a riser node is given by

$$\frac{dX^*_{R,n,j}}{dt^*} = \frac{A_{n,j}\left(\frac{dXR,n-1,j^*}{dt^*}\right) - B_{n,j}\left(\frac{dj_{1R,n,j}}{dt^*}\right)}{1 + \left[1 + \left(N_{Zu,j} - N_{sub}\right)X^*_{R,n,j}\right]\left(j_{1R,n,j} - 1\right)} \tag{5.9}$$

where, $A_{n,j} = \left(j_{1R,n,j} - 1\right)\left[1 + \left(N_{Zu,j} - N_{sub}\right)X^*_{R,n,j}\right] + \left[1 + \frac{\left(N_{Zu,j} - N_{sub}\right)\left(X^*_{R,n,j} - X_{R,n-1,j}\right)}{\left[1 + \left(N_{Zu,j} - N_{sub}\right)X^*_{R,n,j}\right]}\right]$ and $B_{n,j} = \left[\left(X^*_{R,n,j} - X^*_{R,n-1,j}\right)\left(1 + \left(N_{Zu,j} - N_{sub}\right)X^*_{R,n,j}\right)\right]$.

In the double-channel system, there are two closed loops each consisting of the core, the riser and a common downcomer (Figure 5.1). Since both the loops are closed, the integral of the LHS in the momentum Eq. 3.25 becomes zero and the RHS expresses various contributions (inertial, frictional, gravitational,acceleration and minor losses) to the pressure drop in different sections of each closed loop. These pressure drop terms are derived by integrating the respective terms of the one-dimensional momentum Eq. 3.25 along the components of each channel and the common downcomer of the double-channel boiling system. Detailed derivations of these pressure drop terms are discussed in Appendix B. The flow in the downcomer is considered to be in single phase and frictional effects are

neglected. In a natural circulation double channel system, two boundary conditions must be satisfied (as discussed in Section 3.2.3). That is the summation of the dynamic pressure drop through each closed loop is equal to zero (Eq. 3.44). Imposing this boundary condition in a double channel system yields two algebraic equations (any one of the equations can be used). Hence, for one of the closed loops (say channel one, riser and downcomer) of the double channel system, the Eq. 3.44 can be written as

$$\left(\sum \Delta P\right)_{C,1} + \left(\sum \Delta P\right)_{R,1} + \left(\sum \Delta P\right)_{D} = 0 \tag{5.10}$$

where, $(\sum \Delta P) = \Delta P_i + \Delta P_a + \Delta P_g + \Delta P_f + \Delta P_m$. The expression for each term is derived in Appendix B. The coupling between the two closed loops is given by Eq. 3.45, which, for a double-channel system, reduces to

$$G^*_{Di} A^*_D = G^*_{ci,1} + G^*_{ci,2} \left(\frac{A_{C,2}}{A_{C,1}}\right) \tag{5.11}$$

furthermore, since the two channels are geometrically identical and share the common lower and upper plena, the pressure drop across each channel must be the same. Hence, for the two channels,

$$\left(\sum \Delta P\right)_{C,1} + \left(\sum \Delta P\right)_{R,1} = \left(\sum \Delta P\right)_{C,2} + \left(\sum \Delta P\right)_{R,2} \tag{5.12}$$

Substituting the expressions for pressure drop terms (inertial, frictional, gravitational acceleration and minor losses) in the above equations (Eq. 5.10 and Eq. 5.12) and after lengthy algebraic calculations, the dynamic equations of inlet mass flux densities in both the channels are derived as follow.

$$E_{11} \frac{dG^*_{ci,1}}{dt^*} + E_{12} \frac{dG^*_{ci,2}}{dt^*} = F_1 \tag{5.13}$$

and

$$E_{21} \frac{dG^*_{ci,1}}{dt^*} - E_{22} \frac{dG^*_{ci,2}}{dt^*} = F_2 \tag{5.14}$$

Further simplifying the equations (Eq. 5.13 and Eq. 5.14), the dynamic equations in terms

of inlet mass flux densities of each channel are given as

$$\frac{dG^*_{ci,1}}{dt^*} = \left[\left(\frac{F_1}{E_{12}} + \frac{F_2}{E_{22}}\right) / \left(\frac{E_{11}}{E_{12}} + \frac{E_{21}}{E_{22}}\right)\right] \tag{5.15}$$

and

$$\frac{dG^*_{ci,2}}{dt^*} = \left[\left(\frac{F_1}{E_{11}} - \frac{F_2}{E_{21}}\right) / \left(\frac{E_{12}}{E_{11}} + \frac{E_{22}}{E_{21}}\right)\right] \tag{5.16}$$

where,

$$E_{11} = \left[z^*_{bb,1} + \left\{\frac{(1 - z^*_{bb,1})}{1 + X^*_{ce,1}(N_{Zu,1} - N_{sub})}\right\} + \sum_{n=1}^{N_R}\left\{\frac{L^*_R}{A^*_R N_R(j_{3,R,n,1})}\right\} + \frac{L^*_D}{A^*_D}\right] \tag{5.17}$$

$$E_{12} = \frac{L^*_D}{A^*_D} \tag{5.18}$$

$$E_{2j} = \left[z^*_{bb,1} + \left\{\frac{(1 - z^*_{bb,1})}{1 + X^*_{ce,1}(N_{Zu,1} - N_{sub})}\right\} + \sum_{n=1}^{N_R}\left\{\frac{L^*_R}{A^*_R N_R(j_{3,R,n,1})}\right\}\right] \tag{5.19}$$

Further, the terms F1 and F2 are given as

$$F_1 = (w_{51} - w_{41}) - DP_1 \tag{5.20}$$

$$F_2 = (w_{42} - w_{41}) + (w_{51} - w_{52}) + (DP_{c1} - DP_{c2}) \tag{5.21}$$

where,

$$w_{4,j} = \left[(G^*_{ce,j} - G^*_{ci,j}) - \frac{(1 - Z^*_{bb,j})N_{Zu,j}}{1 + j_{2cav,j}}\right]\frac{dZ^*_{bb,j}}{dt^*} - \left[\frac{(G^*_{ci,j} + N_{Zu,j}(1 - Z^*_{bb,j}))((1 - Z^*_{bb,j})(N_{Zu,j} - N_{sub}))}{(1 + j2cav,j)^2}\right]\frac{dX^*_{R,n,j}}{dt^*} \tag{5.22}$$

$$w_{5,j} = \sum_{n=1}^{n=N_R} \left[\frac{N_{Zu,j}(dZ^*_{bb,j}/dt^*)}{A^*_R(1 + X^*_{R,n,j}(N_{Zu,j} - N_{sub}))} \right]$$
$$+ \sum_{n=1}^{n=N_R} \left[\frac{G^*_{ci,j} + N_{Zu,j}(1 - Z^*_{bb,j})}{A^*_R(1 + X^*_{R,n,j}(N_{Zu,j} - N_{sub}))^2} \left\{ 1 + (N_{Zu,j} - N_{sub}) \frac{dX^*_{R,n,j}}{dt^*} \right\} \right] \quad (5.23)$$

for j = 1,2. Further, DP_1 in the expression for $F1$ is the pressure drop (frictional, gravitational, acceleration and minor losses) in closed loop comprising one channel (core and riser) and downcomer. It is given as

$$DP_1 = \left(\sum \Delta P\right)_{C,1} + \left(\sum \Delta P\right)_{R,1} + \left(\sum \Delta P\right)_D = 0 \quad (5.24)$$

This expression is similar to the expression described in Eq. 5.10 but does not include inertial term. That is, here $\sum \Delta P$ is defined as $\sum \Delta P = \Delta P_a + \Delta P_g + \Delta P_f + \Delta P_m$. The term $DP_{c,j}$ in the expression for $F2$ (Eq. 5.21) is the pressure drop in j^{th} channel comprising core and riser and its is given as $DP_{c,j} = \Delta P_{a,j} + \Delta P_{g,j} + \Delta P_{f,j} + \Delta P_{m,j}$.

In natural circulation, the Zuber number and subcooling number are coupled. Assuming steady drum dynamics, with no carry-under in downcomer and applying steady state mass and energy balances, an expression (Eq. 3.43) for the feedwater inlet subcooling is given as

$$N_{sub} = \left(\frac{h_l - h_{fi}}{h_g - h_{fi}} \right) N_{Zu1} \quad (5.25)$$

In comparison studies (Section 5.3), the feedwater system is considered using Eq. 5.25. The stability map is plotted on feed water inlet temperature - reactor power parameter plane. In stability analysis (Section 5.4), a constant core inlet subcooling is assumed.

5.2.2 RELAP5 model

The primary heat transport loop (PHT) of boiling system consists of core, riser, steam drum, downcomer etc. Sub-cooled water enters the core and the two-phase mixture enters

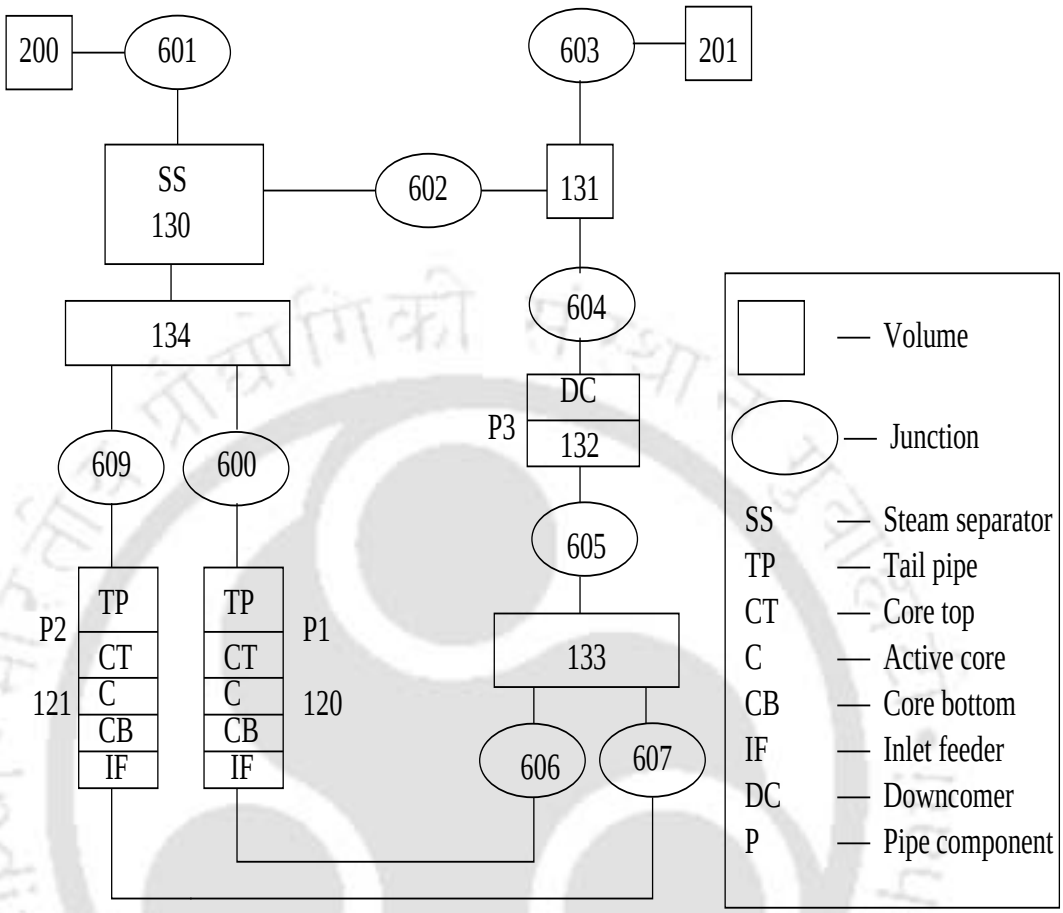

Figure 5.2: Nodalization scheme of double channel RELAP5 model

the steam drum through riser. The steam is separated in the steam drum and the saturated liquid mixes with sub-cooled feedwater and enters the downcomer. The heat supply is assumed to be constant and uniform along the active core. The nodalization scheme of the double channel system is shown in Figure 5.2. The inlet feeder pipes, core bottom, active core and the riser are modeled using the pipe components (cards 120 and 121) represented by P1 and P2. Based on a detailed nodal sensitivity test (discussed in Section 5.3.1), the pipe components P1 and P2 are divided into 17 volumes. The first two volumes represent inlet feeders (0.0074 m^2 flow area, 10.0 m vertical and 7.0 m horizontal length) and third volume represent core bottom (0.0027 m2 flow area and 4.9m vertical length). Volumes 4 to 13 represent active core (0.00483 m^2 flow area and 3.5 m length) and the volumes 14 to 17 model the riser (0.01170 m^2 flow area and 5.0 m length).

Junctions 600 and 609 connect the pipe components 120 and 121 respectively to the outlet header (single volume component 134). The steam drum of the boiling system

is modeled using a steam separator (component 130). A steam separator has one inlet and two outlets (one each for steam and saturated water). The steam from the separator passes to a sink modeled by a time dependent volume (component 200). The saturated liquid flows to the single volume 131 where it mixes with feedwater and through junction 604, the single phase liquid passes into downcomer (0.0120 m2 flow area) modeled using pipe component 132. The feedwater inlet is modeled using a time dependent volume 201. The inlet header (0.25 m2 flow area and 0.1m length) is modeled as a single volume (component 133). The inlet feeders (first two volumes of pipe components 120 and 121) are connected to the inlet header by junctions 606 and 607, respectively. The two single channels modeled by pipe components 120 and 121 have the same volume flow area and length. The heat supply to the active core is modeled using heat structures. The heat structure is divided into volumes equivalent to the volumes of active core and constant power option (no neutronics) is used.

5.3 Nodal sensitivity and model comparison

5.3.1 Nodal sensitivity test

As discussed in Section 3.3, RELAP5 uses a one-dimensional, transient, two-fluid model for the flow of a two-phase steam-water mixture. In the two-fluid non-equilibrium model, each phase is defined by separate mass, momentum and energy balance equations resulting in six basic field equations. The system of differential equations along with the linear equations of state and additional constitutive relations, are solved simultaneously by a forward elimination scheme and subsequent direct solution for the pressure field. The numerical solution method for the hydrodynamic model uses a finite difference scheme having fixed, but staggered, spatial nodes. The predictions are generally sensitive to nodalization and the uncertainty in the results has to be kept within tolerable limits by an appropriate choice of nodalization. In this section the effect of nodalization on the predictions is studied. Parametric studies are carried out at 7 MPa and 4 MPa pressures. Five different nodalization schemes (denoted A, B, C, D and E in Figures 5.3 – 5.5) having different nodalizations of the active core and riser sections have been considered. Figures 5.3 – 5.4(b) show the mass flow rate, void fraction and exit quality calculated at different pow-

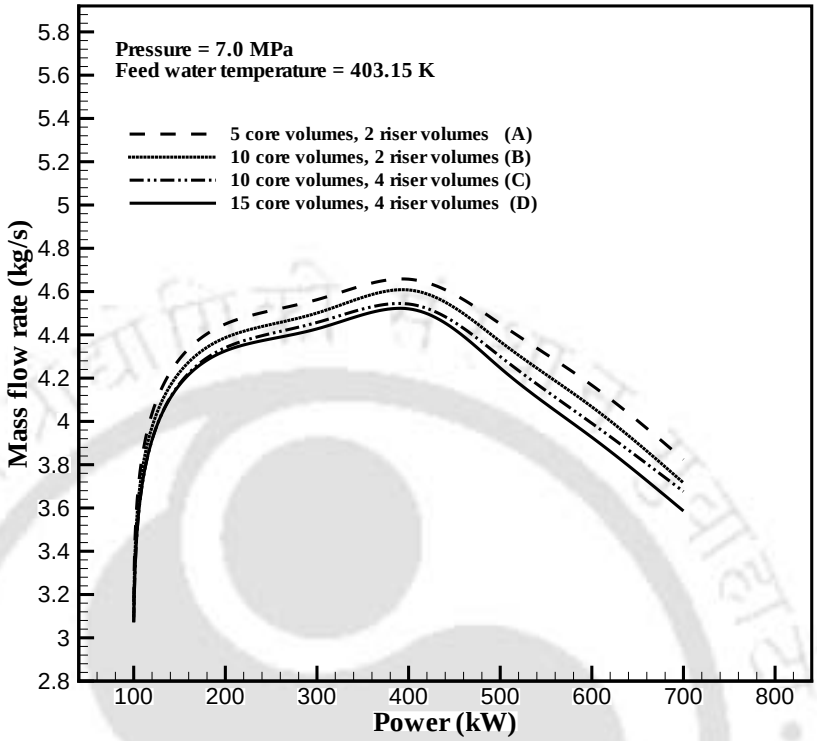

Figure 5.3: Parametric study with different nodalization schemes at 7 MPa

ers for four different nodalization schemes (A, B, C and D) at 7 MPa pressure. At low powers, all the schemes predict very close values of the mass flow rate, the difference being in the third and fourth decimals (Figure 5.3). However, the difference in the predictions widens as the power increases. The effect of nodalization schemes on void fraction and core exit quality is shown in Figures 5.4(a) and 5.4(b), respectively.

It can be observed that the nodalization scheme affects quality at higher powers, but the void fraction is not much affected. However, there is considerable increase in CPU time for finer nodalization schemes. It is also observed that as the number of nodes increases, the marginal stability boundary or the occurrence of oscillatory behavior shifts towards the high power region. Thus, within the stable region, the steady state values obtained by all the four schemes considered match with each other, albeit there are differences in the marginal stability boundary. It is observed that the predictions of scheme C are close to those of scheme D (which has finer nodalization in the core). Further parametric studies are carried out at pressure 4 MPa with three nodalization schemes (A, C and E). It can be observed from Figure 5.5 that the results of Scheme C are very close to those of scheme E (which has finer nodalization in the riser section). Based on this study,

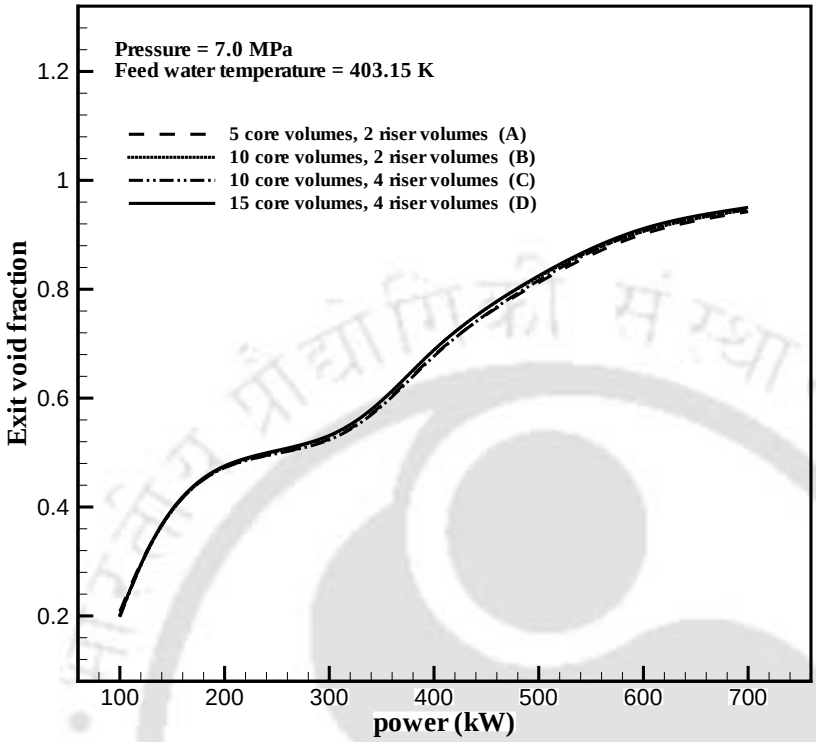

(a) Void fraction calculated for different powers using different nodalization schemes at 7 MPa

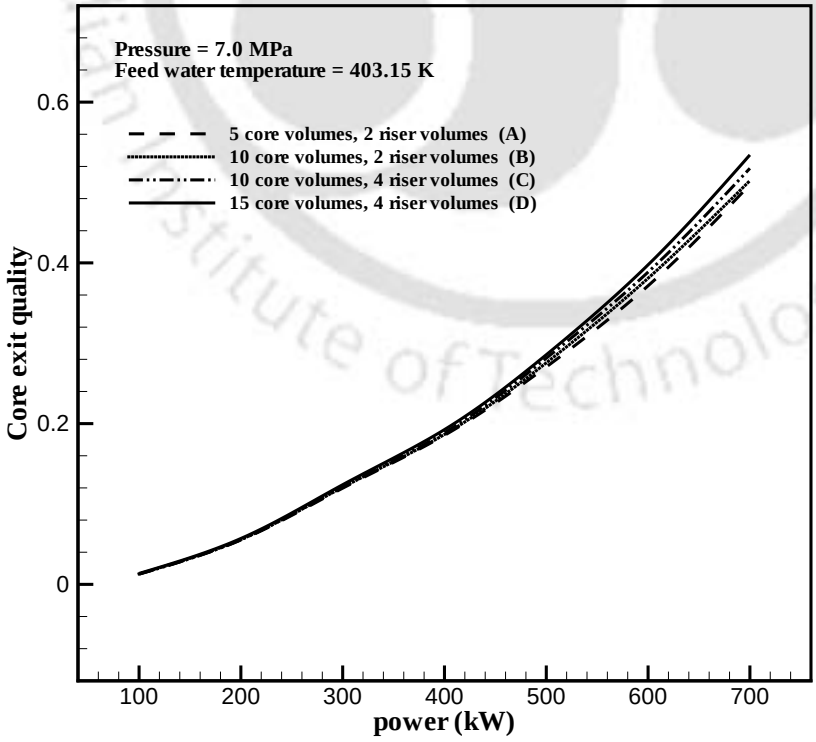

(b) Exit quality calculated for different powers using different nodalization schemes at 7 MPa

Figure 5.4: Void fraction and exit quality calculated for different powers using different nodalization schemes at 7 MPa

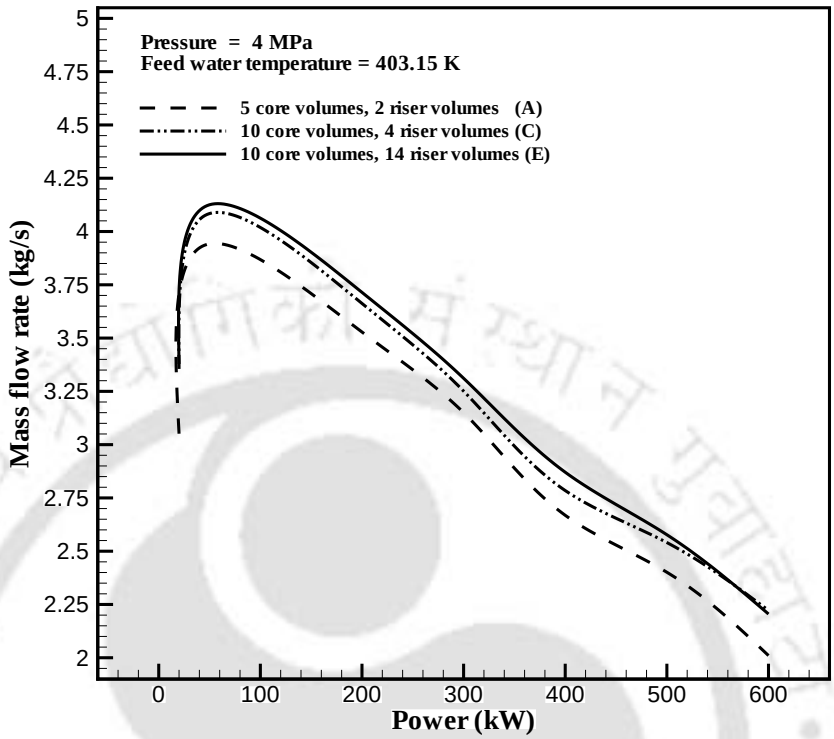

Figure 5.5: Mass flow rate calculated for different powers using different nodalization schemes at 4 MPa

scheme C (10 core volumes and 4 riser volumes) is selected for analysis in the present work.

5.3.2 Comparison of LPM and RELAP5 models

RELAP5 transient simulations are carried out at various operating conditions and pressures. Initially, parametric studies are conducted at 7 MPa pressure using RELAP5 and steady state lumped parameter model and the results are compared. The core inlet mass flow rate at various channel powers simulated by LPM and RELAP5 is shown in Figure 5.6(a). It can be observed that the lumped parameter model predicts trends similar to those observed in RELAP5 simulations. The LPM underpredicts the mass flow rate at lower powers and overpredicted at powers higher than 400 kW. As the power is increased, the mass flow rate increases first and then decreases at higher powers as discussed in 3.4.

The core exit quality predictions using lumped parameter model are in very good agreement with RELAP5 predictions at low powers, but deviate at high powers as shown

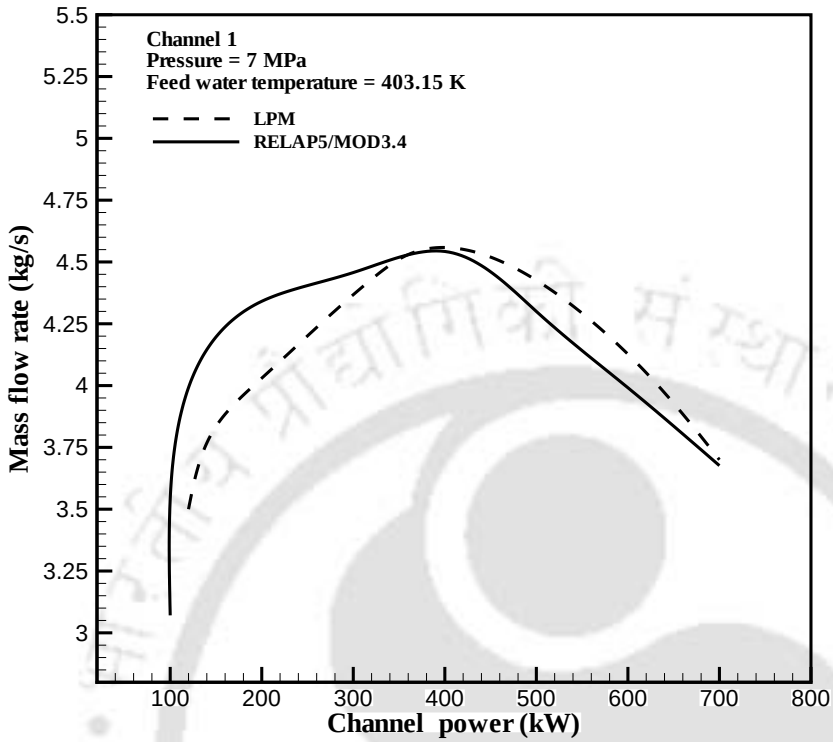

(a) Variation of mass flow rate with channel power at 7 MPa using RELAP and LPM

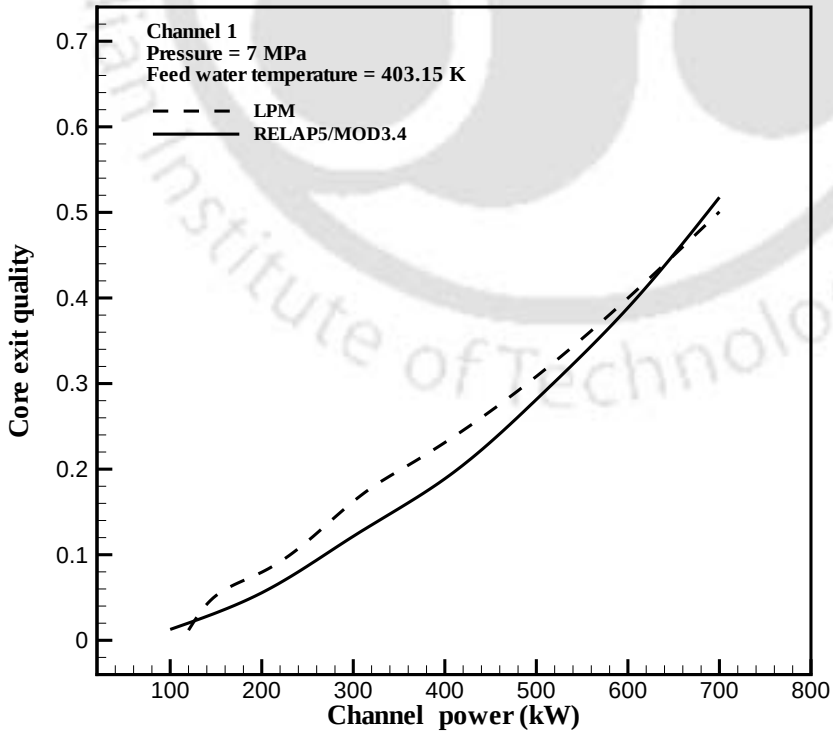

(b) Variation of core exit quality with channel power at 7 MPa using RELAP and LPM

Figure 5.6: Variation of mass flow rate and exit quality with channel power at 7 MPa using RELAP and LPM

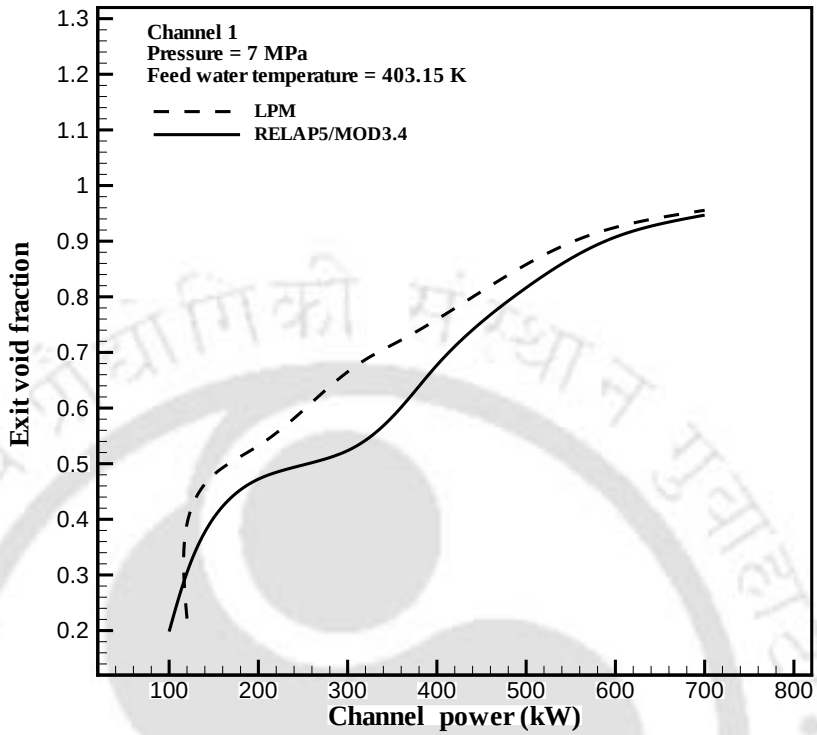

Figure 5.7: Variation of void fraction with channel power at 7 MPa

in Figure 5.6(b). The void fraction predictions by RELAP5 and LPM are shown in Figure 5.7. It can be observed that the core void fraction is overpredicted by LPM when compared with RELAP5 simulations, albeit the trends are similar. It is observed that the LPM overpredicts the void fraction and exit quality as compared to RELAP5 predictions, although the trends obtained with LPM are similar to those simulated with RELAP5. The differences can be due to the various simplifying assumptions made in LPM.

The lumped parameter model is linearised about its steady-state point and the eigenvalues of the Jacobian matrix are evaluated. The stability is determined by the nature of the eigenvalues of the Jacobian matrix. A marginal stability boundary is plotted on a channel power-feedwater inlet temperature (i.e. water temperature in volume 201) plane at pressure 7 MPa. Similarly, RELAP5 transient simulations are carried out at various powers and feedwater inlet temperatures. The stability of the system is inferred from the nature of time evolutions of different variables such as void fraction, quality and mass flow rate and a marginal stability boundary is plotted accordingly. The marginal stability boundaries computed by LPM and RELAP5 are shown in Figure 5.8. It can be observed that the stability boundaries developed by using LPM and RELAP5 have similar trends

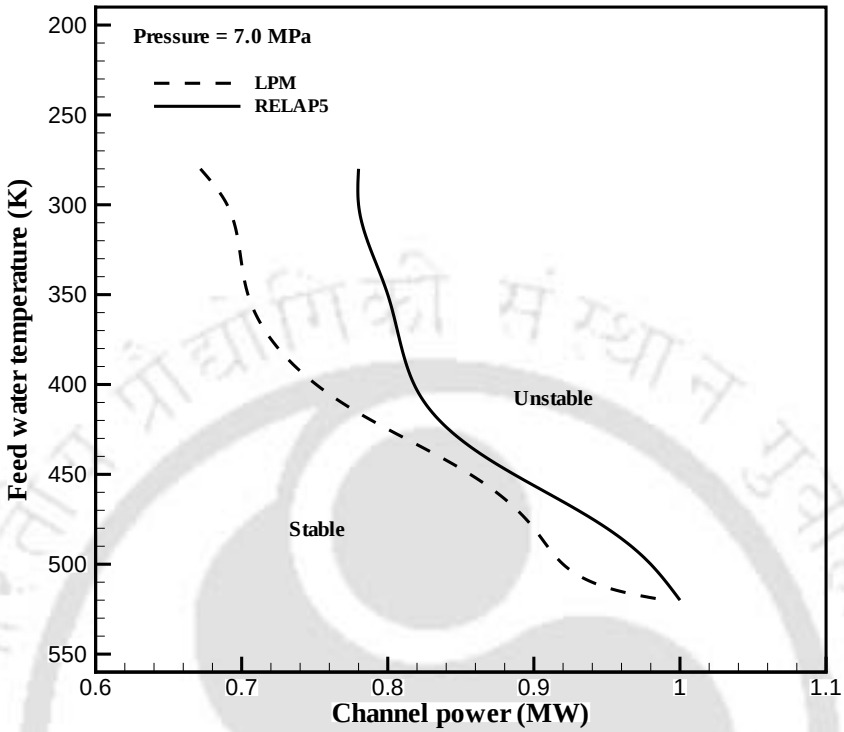

Figure 5.8: Comparison of marginal stability boundary at 7.0 MPa

and the lumped parameter model is conservative.

5.4 Stability analysis with LPM

The lumped parameter model (system of nonlinear ordinary differential equations) is linearized about its steady-state point and the eigenvalues of the Jacobian matrix are evaluated. In this analysis, the feedwater modeling is not considered instead a constant core inlet subcooling is considered. The stability is determined by the nature of the eigenvalues of the Jacobian matrix. A marginal stability boundary is plotted on a $N_{Zu} - N_{sub}$ plane as shown in Figure 5.9. Complex eigenvalue crossing is observed across the marginal stability boundary (MSB), which confirms Hopf bifurcation and the presence of periodic orbits in the neighborhood of the MSB. Transient simulations are carried out in the unstable regions (both Type I-and Type-II regions) and stable periodic orbits (limit cycles) are located. A small perturbation from the steady state causes the system to exhibit sustained periodic oscillations. This confirms that the system undergoes supercritical Hopf

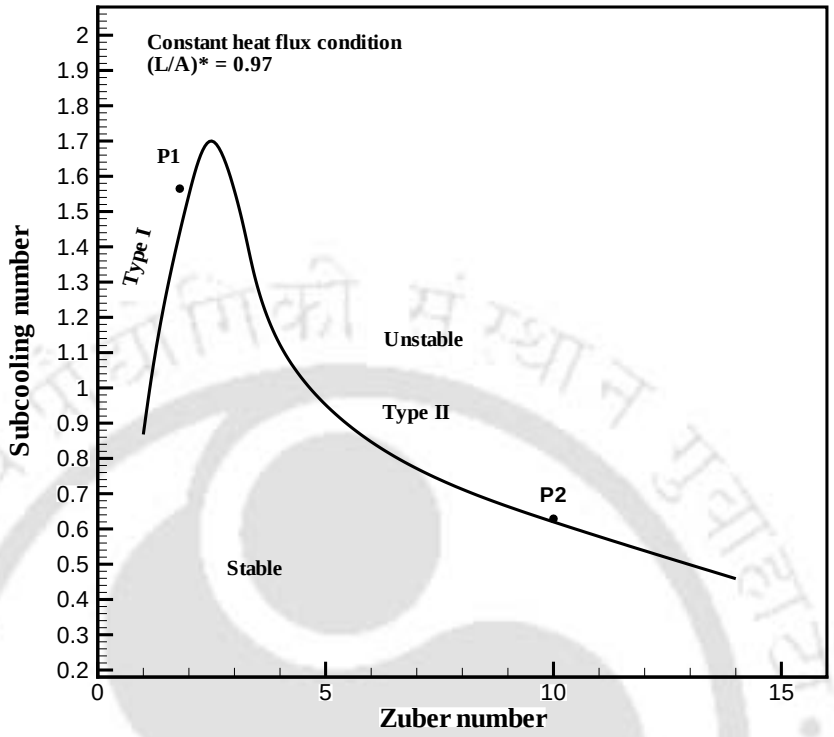

Figure 5.9: Marginal stability boundary plotted using lumped parameter model

bifurcation.

A double channel system consisting of two identical and equal-heating channels with constant heat flux condition has two modes of oscillation: in-phase and out-of-phase, depending on the feedback effect of recirculation loop dynamics. The dominance of gravitational and frictional pressure drops and the inertial effects in downcomer influence the in-phase and out-of-phase modes of oscillations at different operating conditions. The downcomer inertia characterized by (L_D^*/A_D^*) depends on the geometrical parameters such as riser length, length and area of core, length and area of downcomer. The influence of the above quantities on the in-phase and out-of-phase oscillations in equal powered double channels is investigated with the help of transient simulations in Type-I and Type-II regions. In Type-I region (low power and low to medium subcooling), the gravitational pressure drop in the unheated riser section plays a dominant role. The fractional contribution of pressure drops at N_{sub} = 1.565 in Type-I region and N_{sub} = 0.630 in Type-II region are shown in Figures 5.10 and 5.11. It can be observed that the gravitational pressure drop contributes about 90 percent in Type-I region (Figure 5.10), whereas frictional pressure drop has significant contribution of nearly 50 percent in Type-II region (Figure 5.11). The

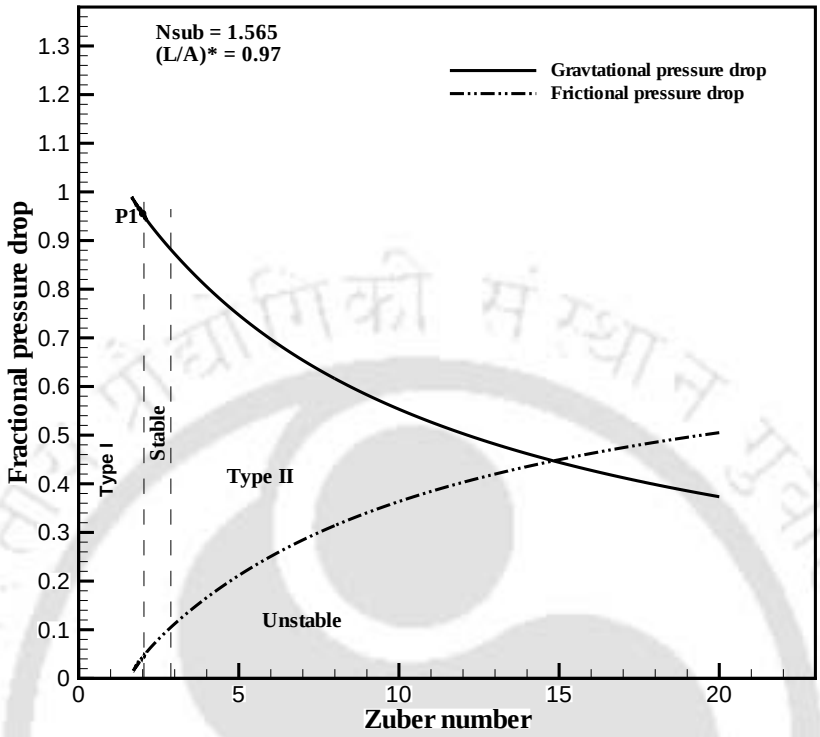

Figure 5.10: Contribution of gravitational and frictional pressure drops at $N_{sub} = 1.565$

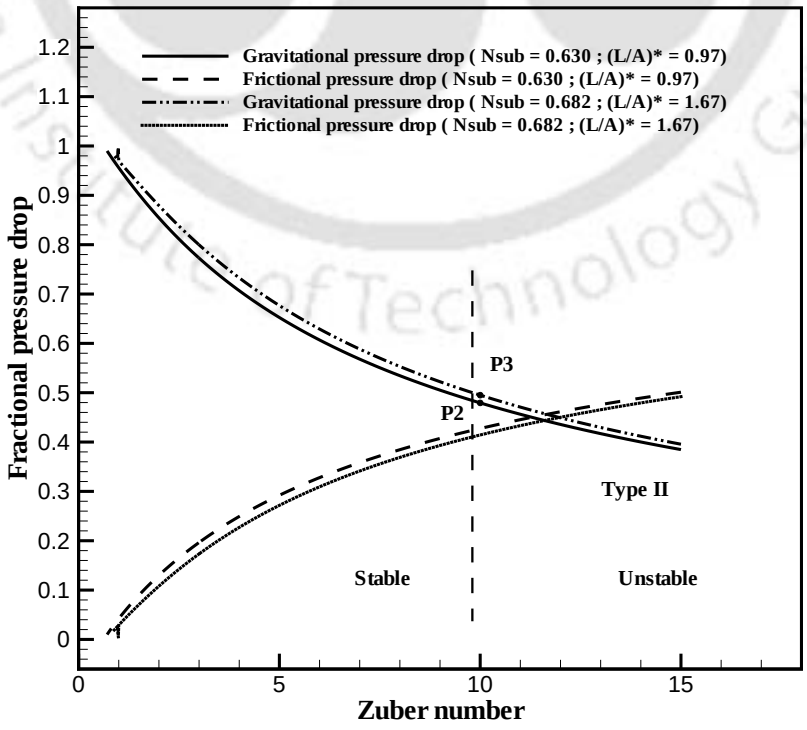

Figure 5.11: Contribution of gravitational and frictional pressure drops at $N_{sub} = 0.630$

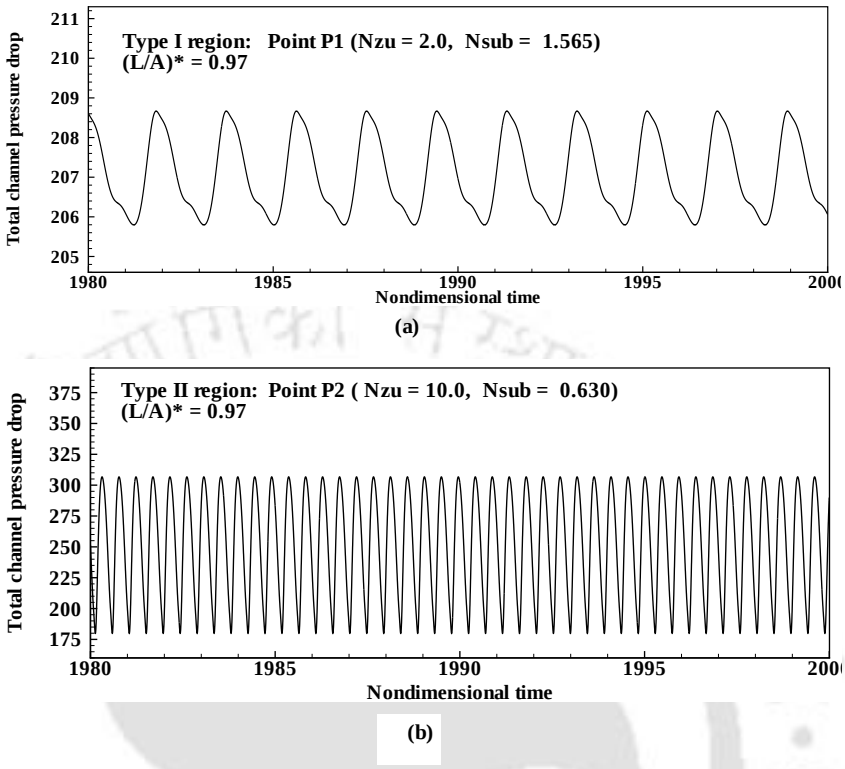

Figure 5.12: Comparison of channel pressure drops in Type-I and Type-II regions

oscillations in channel pressure drops in Type-I and Type-II regions are shown in Figure 5.12. The amplitude and frequency of the channel pressure drop in Type-I region are small compared to those in Type-II region. Thus, the channel pressure drop in Type-I region is nearly constant (with very small oscillations) and unaffected by flow fluctuations. Hence, when there is increase in mass flux density in one channel, then the velocity in the other channel reduces such that the net pressure drop remains constant. Consequently, in Type-I region, the two channels (identical and equal-heating) oscillate out-of-phase with each other. Figure 5.13(a) shows the out-of-phase oscillations in Type-I region at $N_{Zu} = 2.0$ and $N_{sub} = 1.565$ (point P1 of Figures 5.9 and 5.10).

In Type-II region, the frictional pressure drop is significant (Figure 5.11). An increase in inlet mass flux density in one channel significantly increases the pressure drop. Accordingly, the inlet mass flux density in the other channel also increases. This causes in-phase oscillations. Figure 5.13(b) shows in-phase oscillations at $N_{Zu} = 10.0$ and $N_{sub} = 0.630$ in Type-II region (point P2 of Figures 5.9, 5.11 and 5.14). The effect of downcomer inertia on in-phase and out-of phase oscillations is shown in Figure 5.14. Downcomer inertia influences the mode of oscillation in Type-II region. It can be seen from Figure 5.14 that

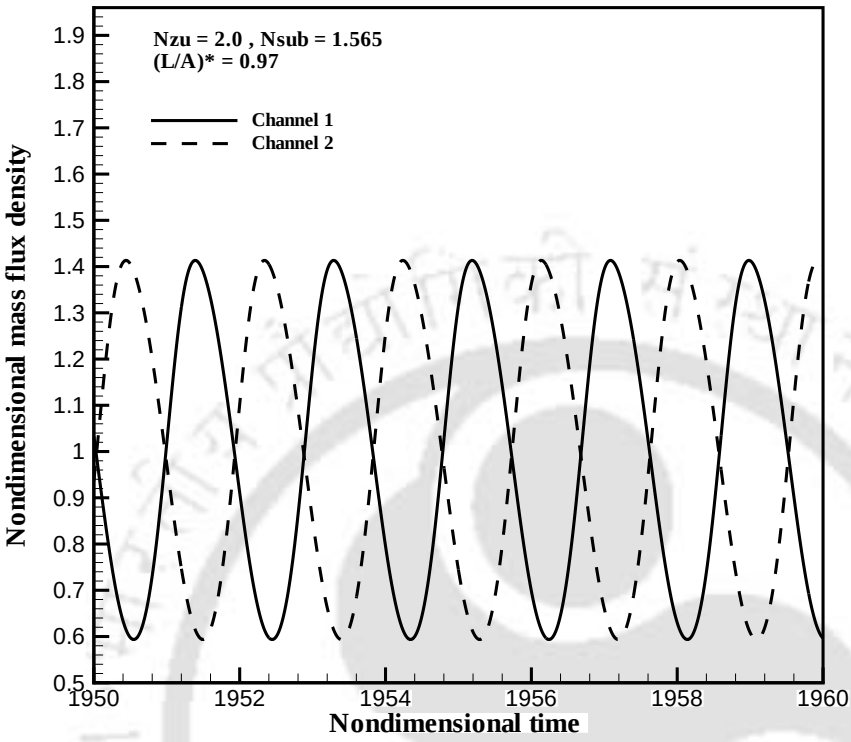

(a) Out-of-phase oscillations at point P1 (NZu = 2.0, Nsub = 1.565) in Type I region.

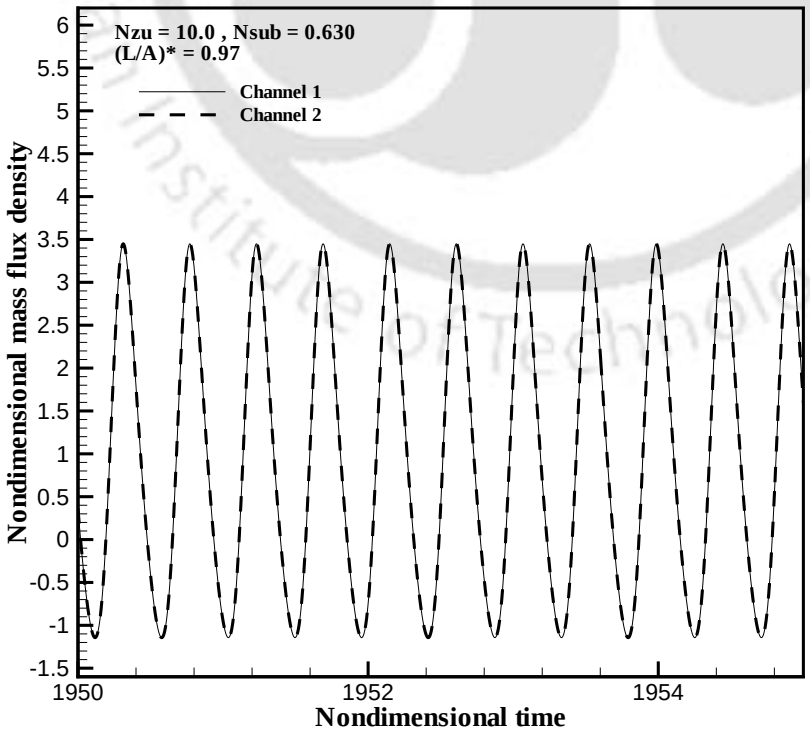

(b) In-phase oscillations at point P2 (NZu = 10.0, Nsub = 0.630) in Type-II region.

Figure 5.13: Modes of oscillations in Type-I and Type-II regions

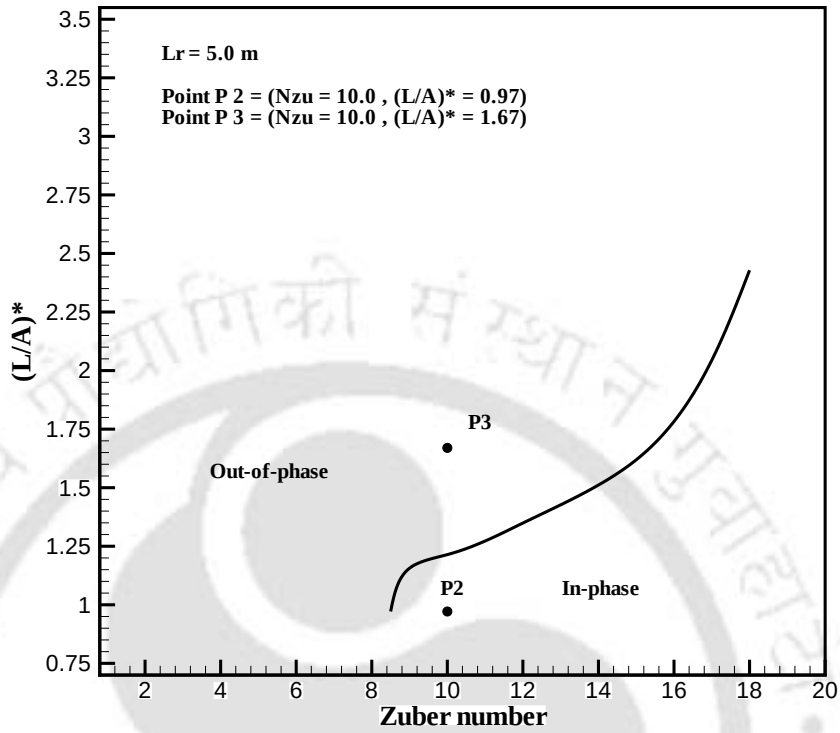

Figure 5.14: Effect of downcomer inertia $(L/A)^*$ on the in-phase and out-of-phase oscillations.

as the downcomer inertia is increased (by increasing (L_D^*/A_D^*)), the two channels oscillate out-of-phase in Type-II region. This happens because oscillations in the downcomer flow rate are suppressed when the downcomer inertia is high.

The term (L_D^*/A_D^*) can be increased either by increasing the riser length and the flow areas of channels in the core, or by decreasing the length of the core and cross sectional area of the downcomer. Thus, the geometrical configuration of the boiling system influences the mode of oscillation in Type-II region. The out-of-phase oscillation at $N_{Zu} = 10.0$ and $N_{sub} = 0.682$ in Type-II region (point P3 of Figures 5.11 and 5.14) is shown in Figure 5.15.

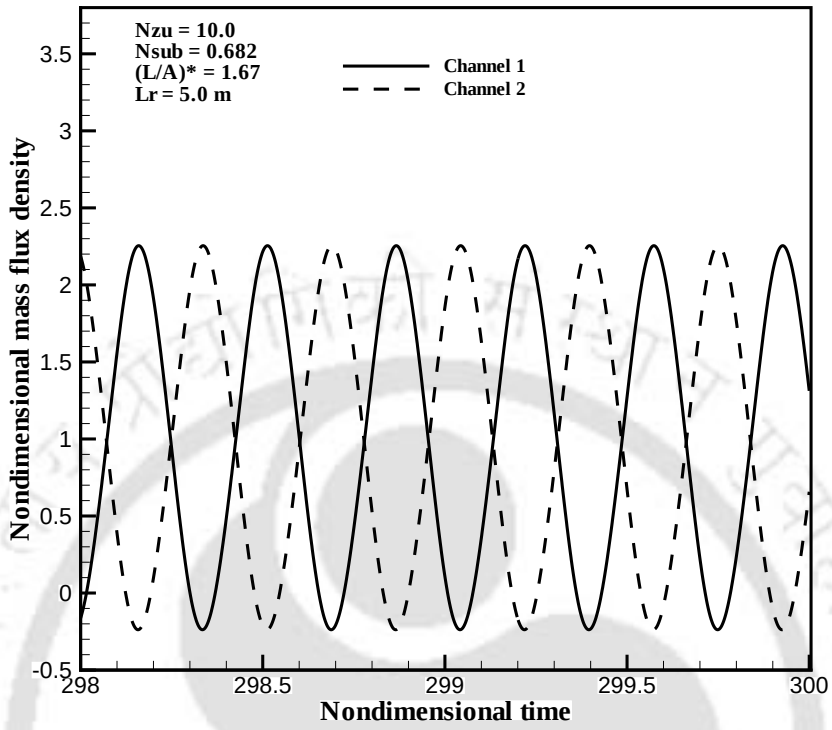

Figure 5.15: Out-of-phase oscillations in Type-II region at point P3.

5.5 Channel-to-channel interaction and on-power refueling

In multi-channel systems, interaction between the channels exists due to closed loop boundary conditions. Fluctuations (generally power) in one channel disturb the other channels. The channel-to-channel interaction in a double channel system is studied using RELAP. Here, the two channels are referred to as C1 and C2. Initially, the two channels are given the same power. Once the system stabilizes, the power in channel C2 is increased by 20 percent and transient simulations are continued for a sufficiently long time. The interaction between the channels is investigated at different operating conditions.

The effect of power fluctuations in C2 at low and high powers (100 and 500 kW per channel) is shown in Figures. 5.16(a) and 5.16(b), respectively. Figure 5.16(a) shows the effect of 20 percent power increase in C2 on mass flow rate and core exit void fraction for feedwater temperature 403.15 K, pressure 7 MPa and power 100 kW per channel. It can be seen that, as power is increased in C2 by 20 percent, the mass flow rate and void

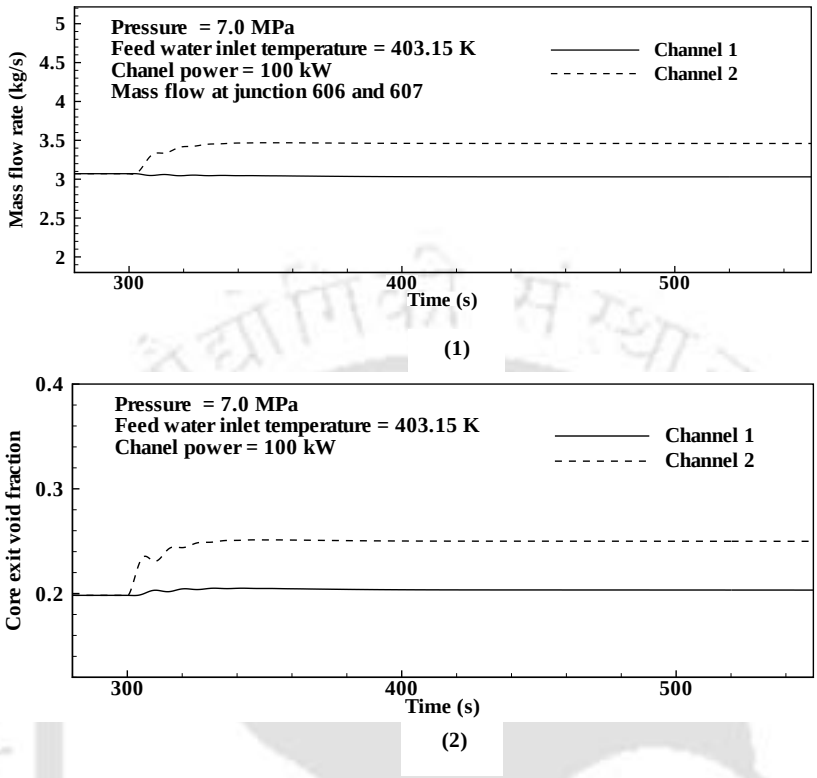

(a) Effect of 20 percent power increase in C2 at feedwater temperature 403.15 K at power 100 kW.

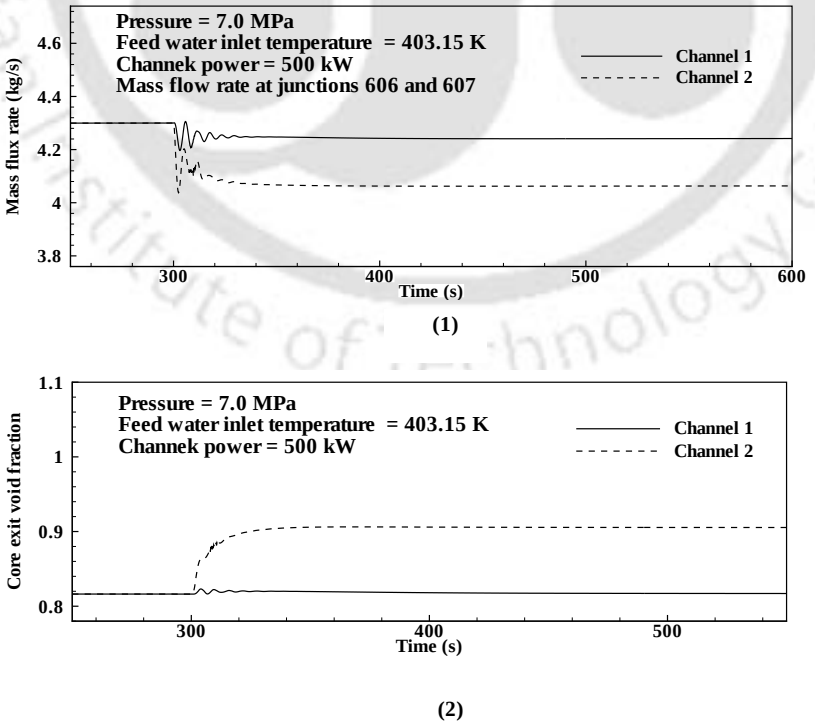

(b) Effect of 20 percent power increase in C2 at feedwater temperature 403.15 K at power 500 kW.

Figure 5.16: Effect of 20 percent power increase at different powers

fraction in C2 are increased. However, there is no significant effect on the mass flow rate and void fraction in C1. This is because, at low powers, the gravitational pressure drop is dominant and the contribution of frictional pressure drop is not significant (Figure 5.10). The total channel pressure drop in C2 is unaffected by small power fluctuations at low powers, hence the flow rate in C1 is undisturbed. However, at higher power (500 kW), the dynamics is different. Figure 5.16(b) shows the effect of 20 percent increase in power on mass flow rate and core exit void fraction in C2 at 500 kW. It can be observed that as power is increased in C2, the mass flow rate in C2 decreases but the void fraction increases. The mass flow rate in C1 also decreases after initial disturbance, but the void fraction in C1 is unaffected. The reason for decrease in mass flow rate at higher powers is discussed in Section 3.2. At high powers, when there is increase in power in C2, the void fraction in C2 increases (Figure 5.16(b)(2)). This results in increase in frictional pressure drop, which is dominant at high powers. Thus, the total pressure drop in C2 increases, resulting in decrease in mass flow rate. To enforce the constant pressure drop boundary condition across the two identical channels, the increase in pressure drop is compensated by reduction in mass flow rate in channel 1.

On-power refueling is a process in which fuel rod in one of the channels is removed and a new fuel rod is inserted. During this process, there is no heat supplied in the channel and the flow area in the said channel increases. In the present study, the effect of refueling on the dynamics of the system at different powers and pressures is investigated in a double channel system. It may be noted that, in a real reactor, there will be hundreds of channels and refueling in one of the channels may not have a significant effect on the other channels, except a few neighboring channels. However, in the present study, a double channel system is considered in order to know the maximum possible effect of refueling. The system behavior during refueling is studied at operating pressures 7 and 4 MPa for different powers. The feedwater inlet temperature is kept constant at 403.15 K. Initially, RELAP5 code is run with the same power for the two channels C1 and C2. Once the steady state is reached, the fuel rod is removed from channel C2 and the simulation is continued. This is implemented in the restart file by setting the power in channel C2 to zero and modifying the flow area and the hydraulic diameter in the corresponding hydrodynamic component. Thus, the power reduction (to zero) and the area increase in channel C2 are assumed to occur at the time $t = 0^+$ in the simulation. This is a conservative analysis because the transients during the refueling process will be less severe due to the gradual removal of

the fuel rod from the channel.

There are three possibilities when fuel rod is removed from a channel: forward flow of cold water, reverse flow of hot water, or stagnation. Forward flow will occur in channel C2 (even after removal of fuel rod) if the external pressure drop imposed on the channel is greater than the hydrostatic pressure drop in the channel (which can never happen due to the frictional pressure drop in the downcomer). Flow reversal will occur in channel C2 when the external pressure drop imposed on the channel is less than the hydrostatic pressure drop in the channel. Stagnation will occur in C2 if the external pressure drop imposed on the channel is less than the hydrostatic pressure drop for cold water (at the bottom of the channel) but greater than the hydrostatic pressure drop for hot water (at the top of the channel). It is important to study stagnation from the safety point of view, because it may lead to cold pressurization in the channel due to heat loss to the moderator.

Figure 5.17(a) shows the effect of refueling at low and high powers (100 kW and 700 kW, respectively). The pressure is maintained at 7 MPa. Figure 5.17(a) shows the effect of refueling at high power (700 kW). The inlet mass flow rates in channels C1 and C2 are shown in Figure 5.17(a) (1). When fuel rod is removed in channel C2, more liquid is drawn into the channel from the inlet header due to increase in flow area and consequent reduction in frictional resistance. Thus, there is a sudden rise in the mass flow rate at the inlet to channel C2 (Figure 5.17(a)(1)). Subsequently, as the channel C2 is filled with water from inlet header, the flow rate gradually decreases and eventually reaches a near-stagnation condition. On the other hand, there is a sudden reduction in the mass flow rate at the outlet of C2 (Figure 5.17(a)(2)). This is because the upward flow has decreased due to increase in the flow area in the active core. It can also be observed from Figure 5.17(a)(1) that the mass flow rate in channel C1 fluctuates significantly. Figure 5.17(a)(3) shows the effect of refueling at low power (100 kW). It can be observed that the behavior of refueled channel C2 is similar to that observed at higher power (Figure 5.17(a)(1)); however, there is no significant disturbance in channel C1. Hence, at higher powers, the disturbances in C1 are more compared to the disturbances observed at low powers. Refueling studies are also carried out at pressure 4 MPa to study the effect of pressure. Figures 5.17(b) (1) and 5.17(b) (2) show the mass flow rate at the inlets to channels C1 and C2 at powers 500 and 50 kW per channel. It can be observed that there is steady reverse flow in channel C2 with a very low mass flux (an order of magnitude lower than

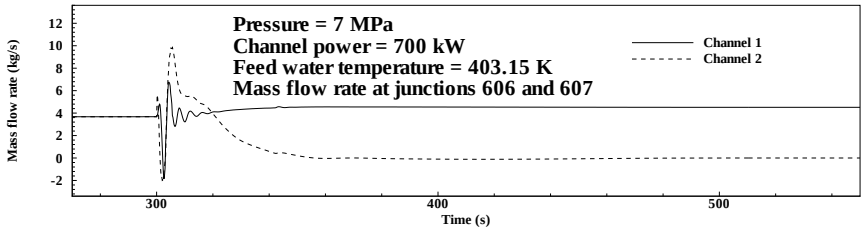

(1)

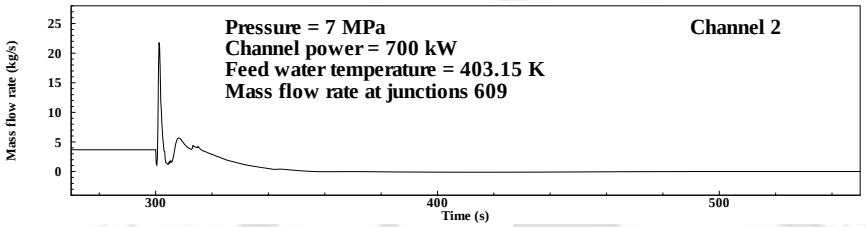

(2)

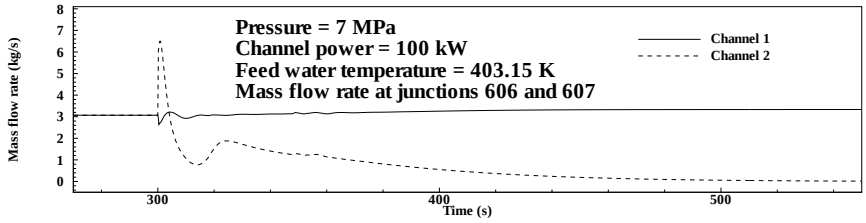

(3)

(a) Effect of on-power refueling in channels C1 and C2 at 7 MPa pressure on the mass flow rates in the two channels.

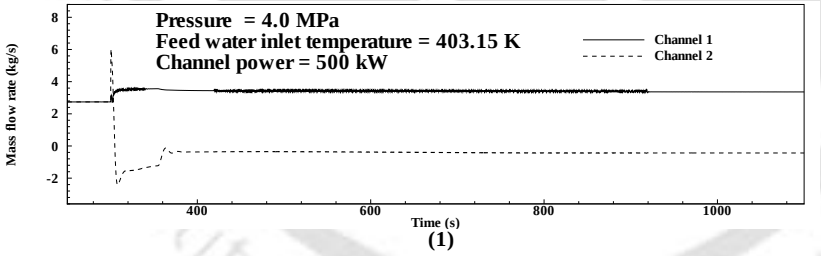

(1)

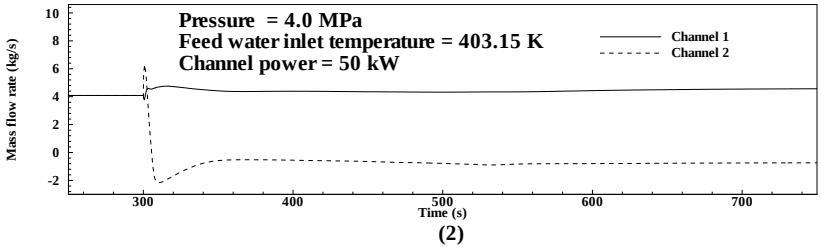

(2)

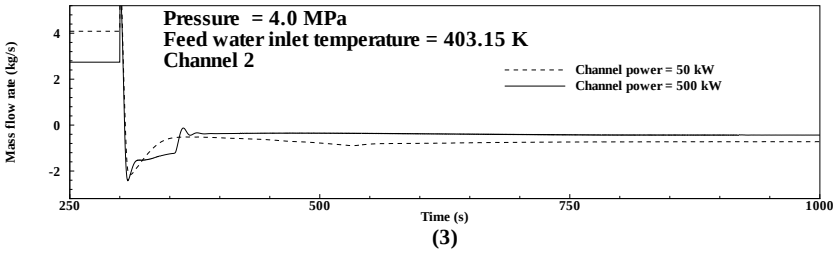

(3)

(b) Effect of online refueling at 4 MPa pressure on the mass flow rates in the two channels.

Figure 5.2: Effect of on-power refueling in channels C1 and C2 at 7 and 4 MPa pressures

that in C1). Figure 5.17(b)(3) compares the flow in channel C2 at powers 500 and 50 kW per channel. It can be observed that the flow reversal is less at higher power due to higher driving force. In the cases studied (7 MPa and 4 MPa), the external pressure drop is found to be very close to the hydrostatic pressure drop (the difference being of the order of 0.1 kPa). Therefore, a near-stagnation condition or low-velocity reverse flow can be expected, which is confirmed by the numerical simulations discussed above.

5.6 Channel-to-channel interaction and on-power refueling in NCBWR

A detailed description of the primary heat transport loop (PHT) of a pressure tube type NCBWR is given in Section 3.4.1 where the NCBWR was modeled as a single channel (volume flow area equivalent to that of 113 channels) system . However, in the present study to facilitate the analysis of on-power refueling, the pressure tube type NCBWR is modeled as a three channel system comprising two hot channels (HC1 and HC2) and one average channel (AC) with volume flow area equivalent to the volume flow area of 111 channels. The geometrical configuration and the division of pipe components into number of nodes are same as presented in Section 3.4.1. The nodalization of the NCBWR is shown in Figure 5.18. The channels and risers are modeled as pipes represented by components 120, 121 and 122. The pipe components 121 and 122 model two single hot channels (HC1 and HC2, respectively) having same volume flow area and length. However, the volume flow area of average channel modeled by pipe component 120 is equivalent to 111 coolant flow channels.

The system behavior during refueling is studied at operating pressures 7 and 5 MPa for different powers. The feedwater inlet temperature is kept constant at 403.15 K. In this study the hot channel HC2 is considered for refueling. The trends observed are similar to those observed in the refueling studies of double channel system. The mass flow rate at junction 608 (inlet to hot channel HC2 in Figure 5.18) is shown in Figure 5.19 at three different powers. It is observed that at all powers when the fuel rod is removed in the channel HC2, there is a sudden rise in the flow rate due to the inflow of hot and cold liquids from the steam drum and the inlet header, respectively. Once the channel filled,

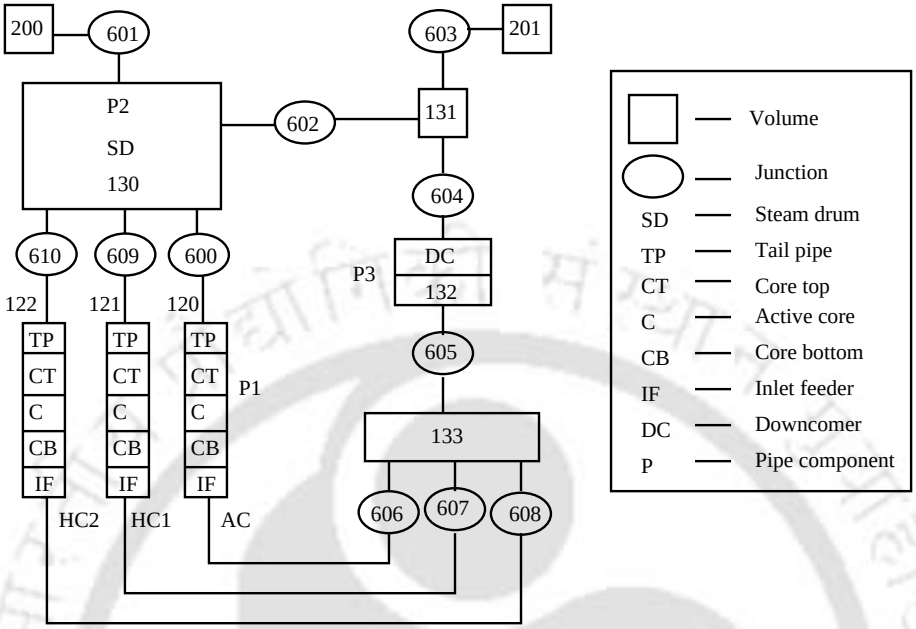

Figure 5.18: Nodalization scheme of pressure tube type NCBWR.

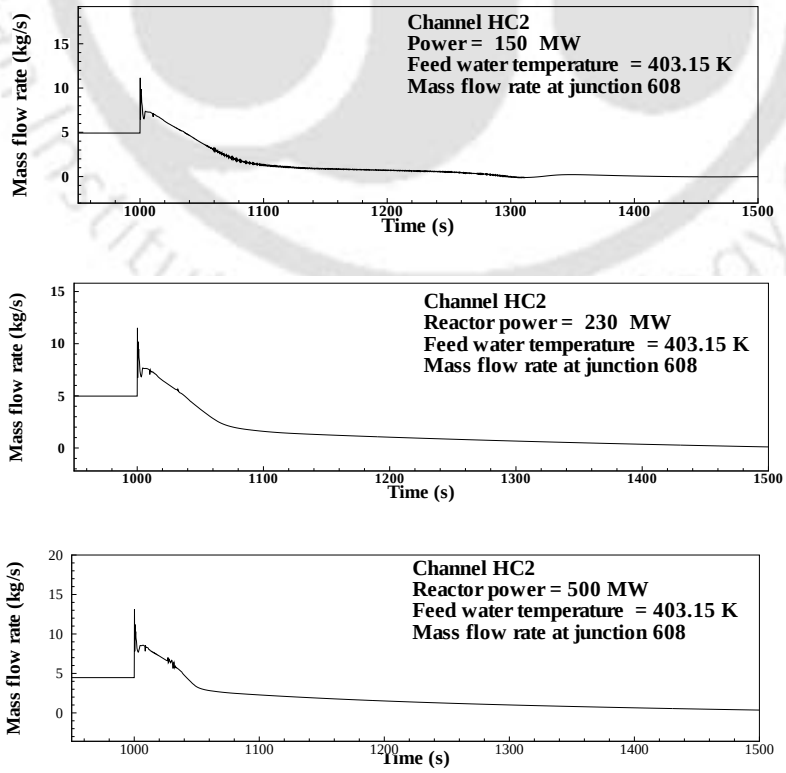

Figure 5.19: Mass flow rate at junction 608 (inlet of refueled channel HC2).

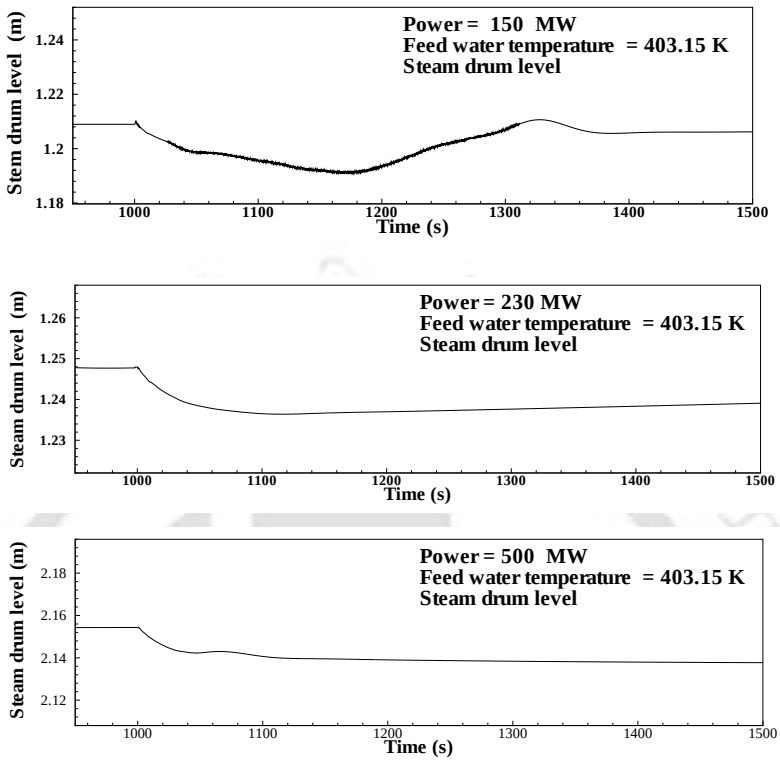

Figure 5.20: Steam drum level at different power during refueling.

the flow stagnated. The reduction in the drum level during refueling at three different powers is shown in Figure 5.20 which is an evidence for the down flow of hot water due to gravity. The reduction in drum level is very little because of the large volume of the steam drum. Comparing Figures 5.19 and 5.17(a), the behavior of the refueled channels HC2 of NCBWR and C2 of double channel system are observed to be similar and stagnation occurred in both the systems. The effect of refueling on the other channels AC and HC1 is shown in Figure 5.21. It can be observed that during refueling, the disturbance in mass flow rate observed in the channels AC and HC1 was of the order of 0.5 to 1.0 percent of the mass flow rate in the respective channels. It is also observed that at higher powers, the disturbances are more compared to the disturbances observed at low powers. However, in the case of double channel system it can be observed that the disturbance in mass flow rate in the channel C1 is nearly of the order of the mass flow rate in the channel Figure (5.17(a)). Hence, during refueling of channel HC2, the other channels AC and HC1 of the pressure tube type NCBWR are not much disturbed as compared to the disturbance observed in channel C1 (Figure 5.17(a)) for the double channel system. This can be explained as below.

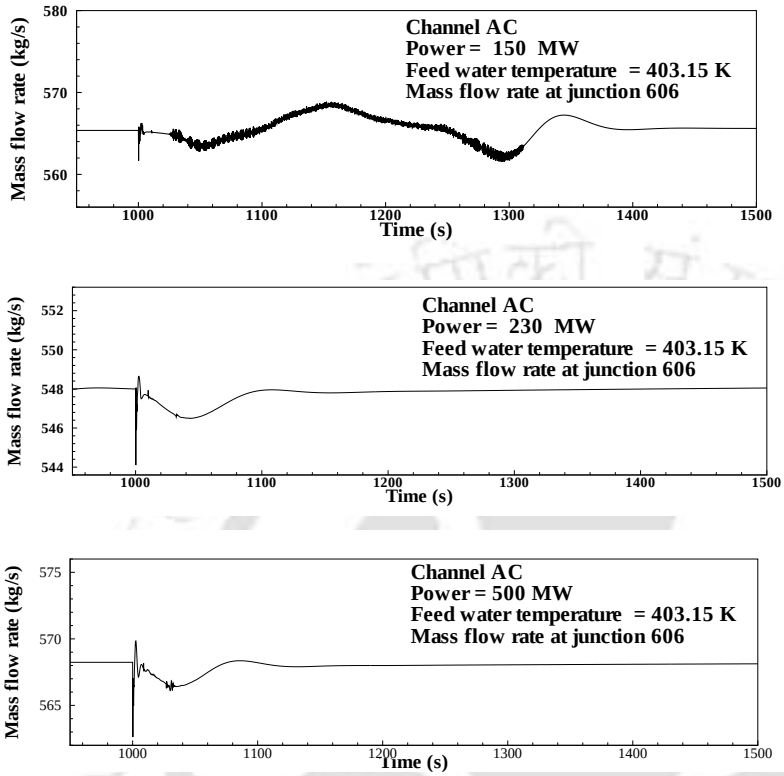

(a) Mass flow rate at junction 606 in average channel AC.

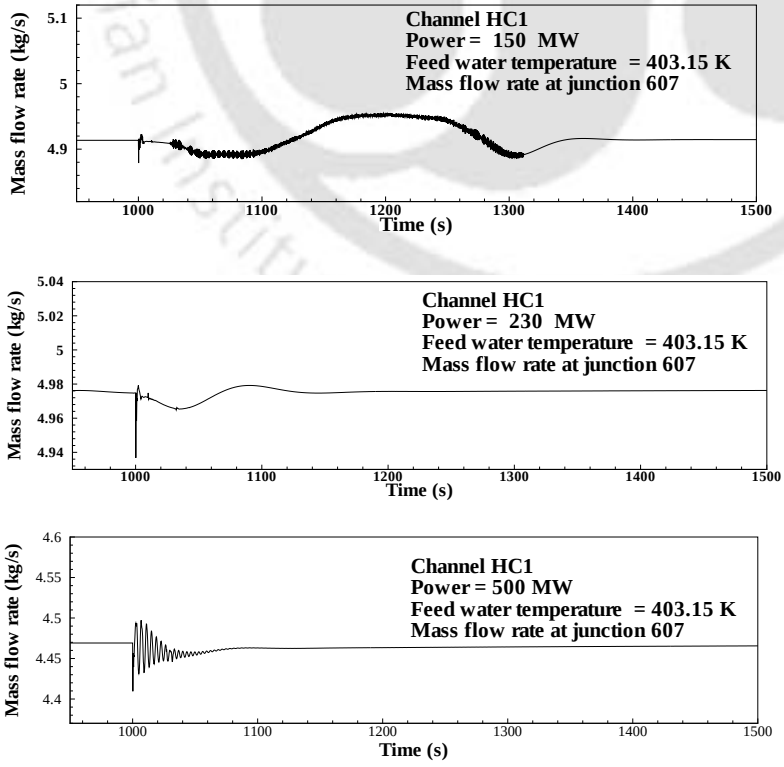

(b) Mass flow rate at junction 607 in average channel HC1.

Figure 5.21: Effect of refueling in channels AC and HC1

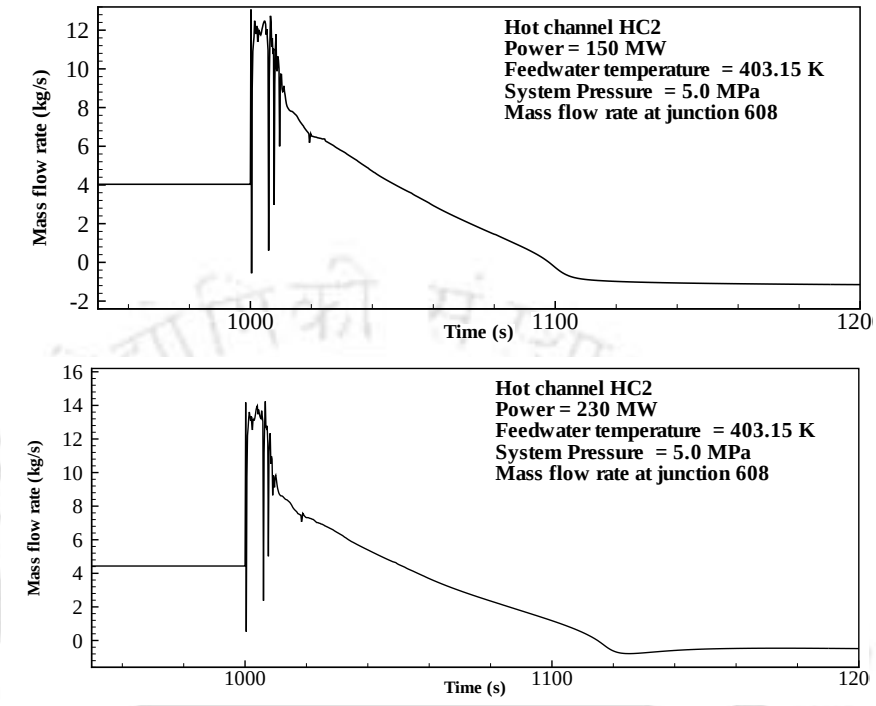

Figure 5.22: Mass flow rate at junction 608 for channel HC2 at 5 MPa.

In double channel system, the two channels are identical and share the same lower and upper plenum. Each channel has a significant contribution in the total pressure drop across the channels. Hence, a disturbance in one of the channels significantly affects the total pressure drop across the system, due to which, the mass flow rate in other channel also varies to compensate for the change in the total pressure drop across the system. However, in pressure tube type NCBWR, 113 channels are present. During refueling, the effect of pressure drop variation in the channel HC2 on the total pressure drop across the system was not significant. Hence, the other channels HC1 and AC are not much disturbed.

In order to study the effect of refueling at lower pressures, studies are carried out at 5 MPa. Figure 5.22 shows the mass flow rate at junction 608 (inlet of hot channel HC2) for two powers (150 MW and 230 MW) corresponding to refueled channel HC2. It can be observed that there is reverse flow in junction 608 at both the powers (150 and 230 MW). The reverse flow at 230 MW is less compared to that at 150 MW similar to that observed in the case of double channel system at pressure 4 MPa (Figure 5.17(b)). Hence, when refueling is done at low pressures, reverse flow can be observed in the boiling systems.

5.7 Summary

In this chapter, thermal-hydraulic instabilities in a double channel system and a pressure tube type NCBWR are investigated. Initially, a simple double channel natural circulation boiling system is modeled separately using lumped parameter mathematical model and RELAP5/MOD3.4. Nodal sensitivity test is carried out at two pressures using different nodalization schemes for core and riser. At low powers, all the schemes predict very close values of the mass flow rate, the difference being in the third and fourth decimals. However, the difference in the predictions widens as the power increases. It can be observed that the nodalization scheme affects quality at higher powers, but the void fraction is not much affected. As the number of nodes increases, the marginal stability boundary or the occurrence of oscillatory behavior shifts towards the high power region. Within the stable region, the steady state values obtained by all the four schemes considered match with each other. Parametric studies are conducted at 7 MPa pressure using RELAP5 and steady state lumped parameter model and the results are compared. The lumped parameter model predicts trends similar to those observed in RELAP5 simulations.

Stability and nonlinear dynamic analysis for the double channel system was carried out using lumped parameter model. The oscillation modes of the two equal powered geometrically identical parallel channels are investigated in Type-I and Type-II regions. The effects of gravitational and frictional pressure drops, and geometrical parameters on the oscillation modes are investigated. The two channels oscillate out-of-phase in Type-I region due to dominant gravitational pressure drop at low powers. In Type-II region, the channels oscillate in both in-phase and out-of-phase modes depending on the dominance of two-phase frictional pressure drop and the downcomer inertia. The downcomer inertia can be varied by varying the dimensions of the boiling system. Thus, geometrical parameters influence the mode of oscillations in Type-II region, but not in Type-I region.

Channel-to-channel interaction and on-power refueling studies are carried out for a double channel system using RELAP model. It is observed that at low powers, disturbance in one channel does not have significant effect on the other channel. At higher powers, disturbances in one channel significantly affect the dynamics of other channels. During on-power refueling, a near-stagnation condition or a low-velocity reverse flow can occur; the possibility of reverse flow being higher at lower pressures and lower pow-

ers. Further, the effects of power fluctuations and on-power refueling in a simple double channel natural circulation system have been investigated. The refueling study was then extended to a pressure tube type NCBWR. The trends observed are similar to those observed in the case of double channel system. Reverse flow was observed at low pressures. This study can be useful in the design and safety analysis of reactors.

Chapter 6

Coupled-Neutronic Instabilities in Double Channel Systems

6.1 Introduction

In NCBWRs, a strong coupling exists between the thermal-hydraulic and neutronics which increases the number of feedback loops in addition to the recirculation loop feedback. This coupling strongly influences the modes of oscillations in multi channel systems. These instabilities are called reactivity instabilities which are of two types: The core-wide oscillation mode during which the whole core behaves as one and the oscillations are in-phase across the core; The out-of-phase or regional oscillation mode, during which one half of the core oscillates out-of-phase from the other half (March-Leuba and Rey, 1993) . Different feedback loops that exist in a nuclear coupled double channel natural circulation system are shown in Figure 6.1.

The thermal-hydraulic equations in a particular channel are essentially the same for both the modes of oscillations but the boundary conditions (i.e., inlet flow and pressure drop) are different. For in-phase mode the boundary conditions are determined by the recirculation loop dynamics, whereas for out-of-phase mode, the boundary conditions are fixed and they determine the necessary inlet flow to maintain a constant pressure drop across the core (March-Leuba and Rey, 1993). According to March-Leuba and Rey (1993), the in-phase oscillations are favored when the gain of neutronic feedback is large

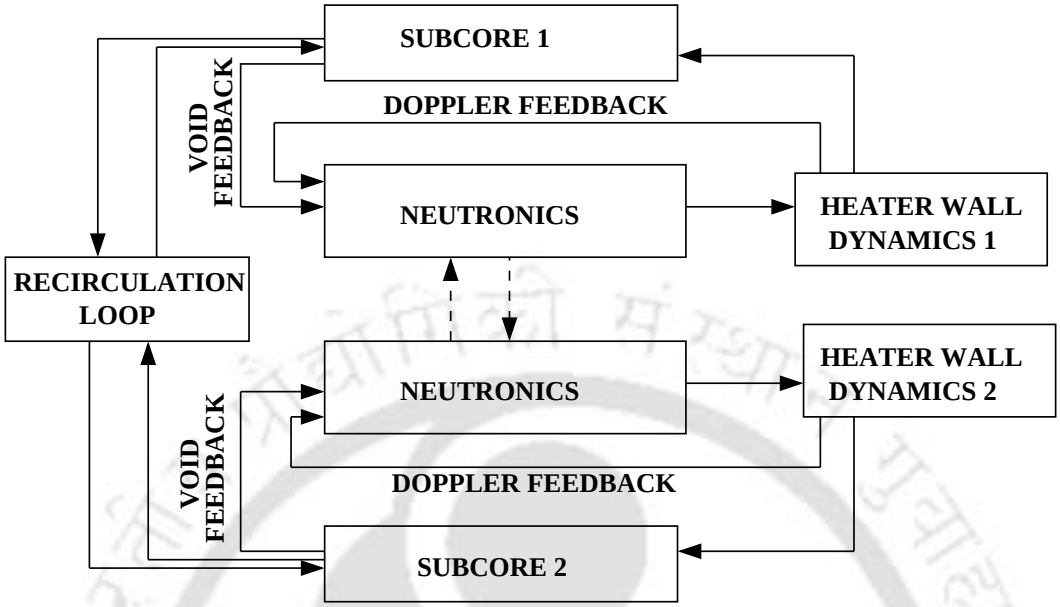

Figure 6.1: Schematic view of feedback loops in nuclear coupled double channel system

compared to the gain of thermal-hydraulic feedback. On the other hand, out-of-phase oscillations are favored when the gain of thermal-hydraulic feedback is large compared to the gain of neutronic feedback.

The neutron diffusion from one subcore to other subcore due to variation of void has a significant influence on the out-of-phase modes of oscillations and stability of the system. The core-wide reactivity instabilities can be investigated using single channel lumped parameter thermal-hydraulic model, coupled with a point neutron kinetics which considers the whole core as a single lump or point. However, in order to investigate the out-of-phase reactivity instabilities in NCBWR, a double channel thermal hydraulic lumped parameter model, coupled with a neutron kinetic model which includes the effect of spatial variation of neutrons is needed.

In this chapter, the parametric effects on stability of the system, frequency, and the oscillation modes (reactivity instabilities) are investigated. Further, nonlinear analysis is carried out to investigate the parametric effects on the bifurcation characteristics, transition from one mode to the other mode and chaotic oscillations. For this purpose, a double channel natural circulation boiling system is modeled using a lumped parameter thermal-hydraulic model (LPM2) with heater wall dynamics. The reactor kinetics is represented by multi-point neutron kinetics. A detailed derivation of LPM2 and the multi-point reac-

tor kinetics is discussed in Section 3.2.1. In the present study, these models are applied to a double channel system. The final state equations are briefly discussed in Section 6.2.

6.2 Modeling of double channel system

The schematic view of the simple double channel system is shown in Figure 5.1. As discussed in Section 5.2 the double channel system (in which only 2 channels of the core are considered for modeling), is a simplified version of the pressure tube type NCBWR (discussed in Section 3.4.1). In the present analysis the whole core comprising 113 channels is modeled as a double channel system (each channel representing half of the reactor core). The geometrical configuration of the double channel system in the present study is given in Section 5.2.2. The length of the downcomer is adjusted according to the riser length. Further, the area of the downcomer and the inlet header are given in Table 3.1.

The power dynamics is represented by multi-point reactor kinetics. The dynamic equations for the neutron density and delayed neutron precursors in the j^{th} subcore are given by equations 3.13 and 3.14 as given below

$$\frac{dq_j'^*(t^*)}{dt^*} = t_{ref}\left[\frac{\rho_j(t^*)+H_{jj}-\beta-1}{\Lambda}q_j'^*(t^*)+\frac{\beta}{\lambda}c_j^*(t^*)+\frac{\rho_j(t^*)+H_{jj}-1}{\Lambda}\right] + t_{ref}\left[\sum_{m\neq j}^{M}\frac{q'_{m0}H_{jm}}{q'_{j0}\Lambda}q_m'^*(t^*)+\sum_{m\neq j}^{M}\frac{q'_{m0}H_{jm}}{q'_{j0}\Lambda}\right] \quad (6.1)$$

$$\frac{dc_j^*(t^*)}{dt^*} = \lambda t_{ref}[q_j'^*(t^*)-c_j^*(t^*)] \quad (6.2)$$

where, the suffix j = 1,2 and M=2. This results in a set of four equations in a double channel system. The reactivity $\rho(t^*)$ is given by Eq. 3.7. The coefficient H_{jm}, accounts for the fraction of neutrons generated in the m^{th} subcore that migrate to the j^{th} subcore which can be expressed as

$$H_{jm} = \frac{q'_{j0}exp(-\varepsilon_{jm})}{\sum_{k=1}^{M}q'_{k0}exp(\varepsilon_{jk})} \quad (6.3)$$

where, ε_{jm} is the neutron interaction coefficient which is expressed as $\varepsilon_{jm} = \frac{|r_j - r_m|}{L_n}$. The term $|r_j - r_m|$ is the distance between the j^{th} and m^{th} subcores and L_n is the neutron migration length. In the present study only one neutron interaction coefficient is used i.e., $\varepsilon_{12} = \varepsilon_{21}$. Therefore, the term ε_{jm} is referred as ε for simplicity. Under steady state conditions, from the equations 3.8 and 3.9, the term H_{jj} is given as

$$H_{jj} = 1 - \sum_{m \neq j}^{M} H_{jm} \frac{q'_{m0}}{q'_{j0}} \tag{6.4}$$

The heater wall dynamics for j^{th} subcore is given by Eq. 3.19 as

$$\frac{dT^*_{f,j}}{dt^*} = N_S[q'^*_j - T^*_{f,j} + 1] \tag{6.5}$$

where, $N_S = \frac{t_{ref}}{\tau_f}$ is the ratio of reference time to the fuel time constant. Here the reference time is given as $t_{ref} = \frac{L\rho_l}{G_0}$ where, G_0 is the steady state inlet mass flux density of channel 1 of the double channel system. The thermal-hydraulics is represented by the lumped parameter model (LPM2) derived in Section 3.2.3.

6.3 Stability analysis

The lumped parameter model (system of nonlinear ordinary differential equations) is linearized about its steady-state point and the eigenvalues of the Jacobian matrix are evaluated. The stability is determined by the nature of the eigenvalues of the Jacobian matrix. Marginal stability boundaries (MSB) are plotted on a $N_{Zu} - N_{sub}$ plane for different parametric values. Complex eigenvalue crossings are observed across the MSB, which confirms Hopf bifurcation and the presence of periodic orbits in the neighborhood of the MSB. The oscillation frequency of the periodic orbits near the MSB is estimated from the imaginary part of the eigenvalues of the Jacobian matrix. The effects of different parameters such as void reactivity coefficient (VR), fuel time constant and neutron interaction coefficient ε, on the stability and frequency of oscillations of the system are investigated. The void reactivity coefficient was varied from -0.005 to -0.5 and the fuel time constant was varied from 2.0s to 18.0s. The neutron interaction coefficient ε is the ratio of the distance between the subcores and the neutron migration length, and it depends on the

core design and reactor physics. In the present study ε is varied from 1.0 to 15.0. It is to be noted that, while studying the effect of one parameter, all the other parameters are kept constant. In stability analysis the base values of the parameters are set as VR = -0.1, fuel time constant = 5.0s and ε = 5.0. The downcomer inertia which is characterized by the parameter (L_D^*/A_D^*) is taken as $(L_D^*/A_D^*) = 1.54$, and the number of channels is equal to 113.

The effect of void reactivity coefficient on the stability of the system in Type-I and Type-II regions is shown in Figure 6.2(a). Increase in the absolute value of void reactivity coefficient has a stabilizing effect in Type-I region and destabilizing effect in Type-II region. From Figure 6.2(b) it can be observed that the frequency of oscillations increases in both Type-I and Type-II regions as the absolute value of the void reactivity coefficient increases. On the other hand, the fuel time constant has a stabilizing effect in Type-II region and destabilizing effect in Type-I region as shown in Figure 6.3(a). It can be observed that the effect of VR and fuel time constant on the Type-I and Type-II regions in the present study match with the stability studies carried out using single channel model with geometrical configuration 1 in Section 4.3.2. Furthermore, the effect of fuel time constant on the frequency of oscillations is shown in Figure 6.3(b). At low powers, the frequency of oscillations increases with fuel time constant and at higher powers (Type-II region) the frequency decreases with increase in fuel time constant. It can also be observed that the frequency of oscillations increases with increase in Zuber number.

The effect of neutron interaction coefficient ε on the stability and frequency of oscillations is shown in Figure 6.4. Increase in ε characterizes reduction in neutron interactions between channels. It can be observed from Figure 6.4(a) that increase in ε has a destabilizing effect on Type-II region and stabilizing effect on Type-I region. Lower the interaction coefficient, higher is the neutron interaction between the channels and increase in the stability of the system. Thus, it can be inferred that at high powers, compact cores will be more stable compared to larger cores, while opposite will be the case at low powers. The effect of ε on the frequency of oscillations is shown in Figure 6.4(b). The frequency of oscillations increases slightly with the increase in the neutron interaction coefficient.

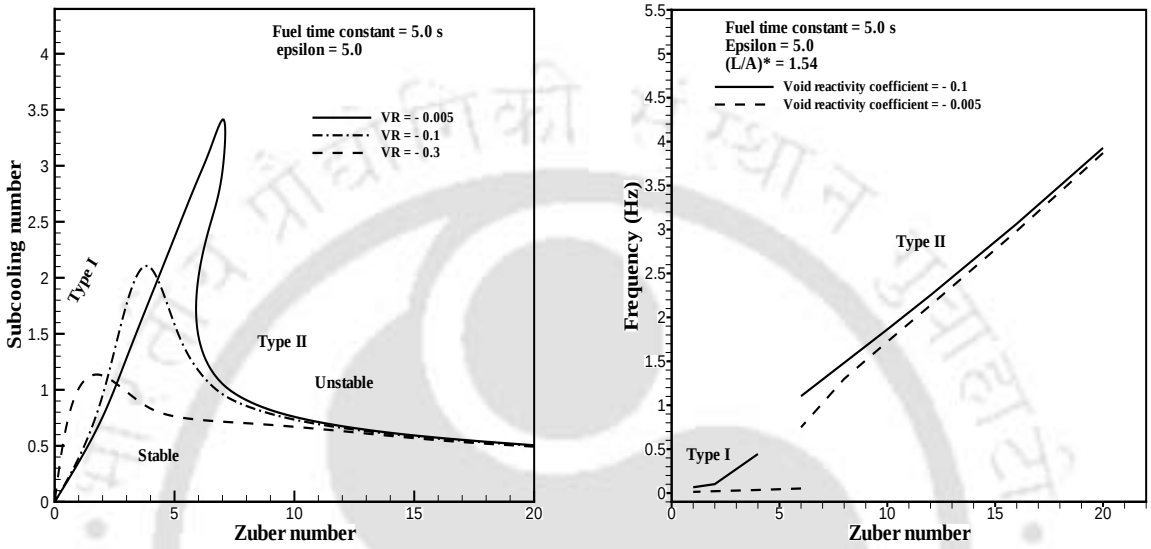

(a) Effect of VR on stability of the system

(b) Effect of VR on frequency of the system

Figure 6.2: Effect of void reactivity coefficient on stability and frequency of oscillations

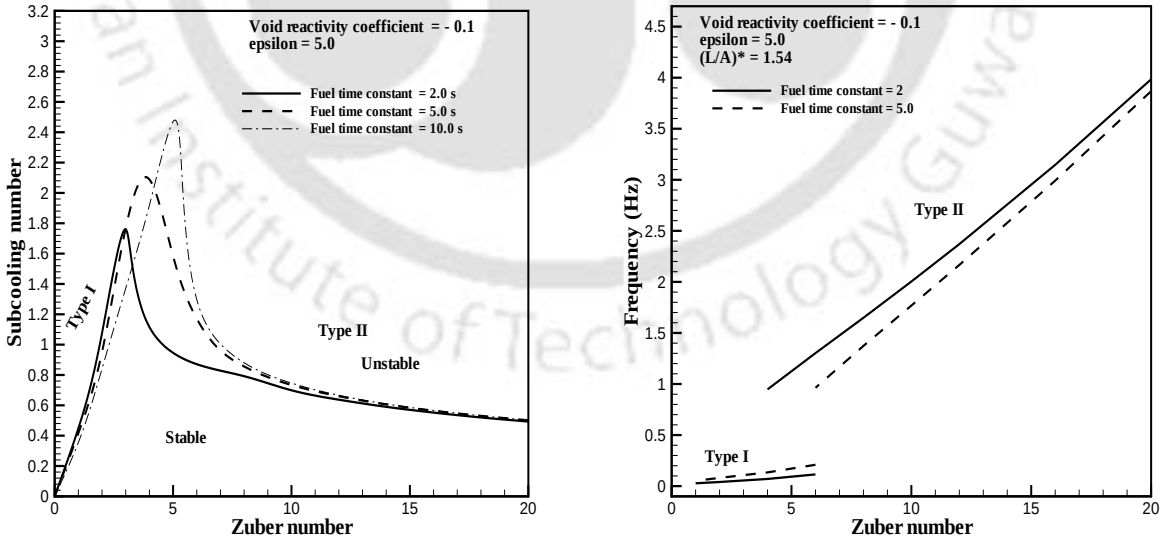

(a) Effect of fuel time constant on stability of the system

(b) Effect of fuel time constant on frequency of oscillations of the system

Figure 6.3: Effect of fuel time constant on stability and frequency of oscillations

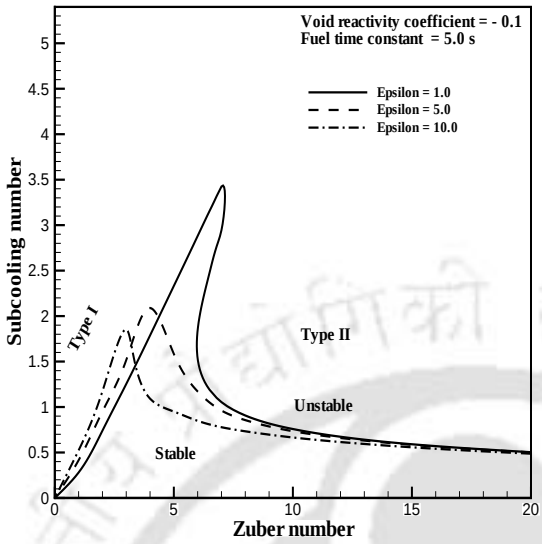

(a) Effect of ε on stability of the system

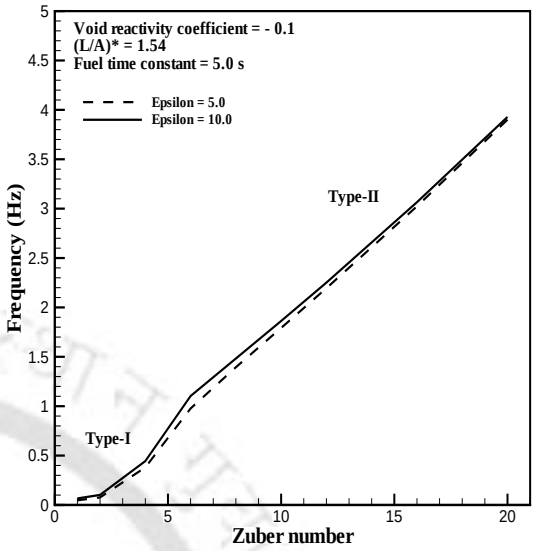

(b) Effect of ε on frequency of oscillations of the system

Figure 6.4: Effect of ε on stability and frequency of oscillations

6.4 Parametric effects on modes of oscillations

The regional and core-wide oscillations are influenced by the geometrical and feedback parameters. In this section, the effects of various parameters on the in-phase and out-of-phase modes are studied. Transient simulations are carried out in Type-II region at different parametric values. Figure 6.5(a) shows the effect of Zuber number on the modes of oscillations in Type-II region, plotted on VR - fuel time constant parameter plane. It can be observed that, increase in Zuber number favors out-of-phase oscillations. The in-phase oscillations are favored by increase in absolute value of void reactivity coefficient. This is because the gain of neutronic feedback increases with increase in absolute value of void reactivity coefficient. It can also be observed that the out-of-phase oscillations are favored by increase in fuel time constant. Fuel time constant characterizes delay in the heat transfer. The more the fuel time constant, the higher is the delay in heat transfer from fuel rod to the coolant.

Figure 6.5(b) shows the effect of void reactivity coefficient at different Zuber numbers. In-phase oscillations prevail at low powers under strong reactivity feedback. At low Zuber numbers, the mass flow rate is very less and cannot dominate the frictional effects in downcomer. This reduces the gain of thermal-hydraulic feedback and in-phase oscillations are favored. However, at high Zuber numbers, the delay effects are dominant

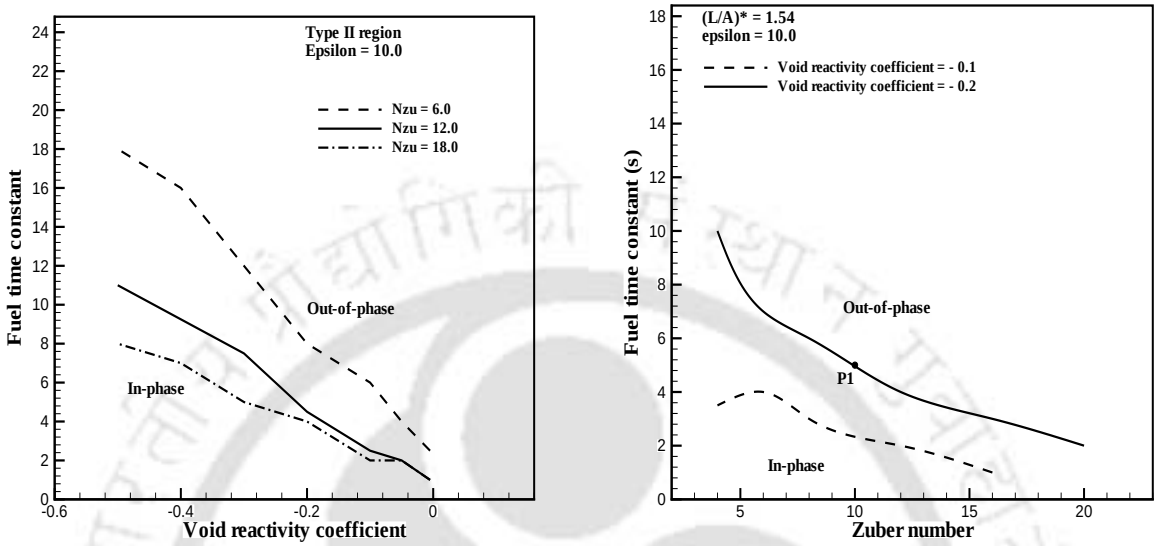

(a) Effect of Zuber number on modes of oscillations (b) Effect of VR on modes of oscillations

Figure 6.5: Effect of Zuber number and VR on modes of oscillations

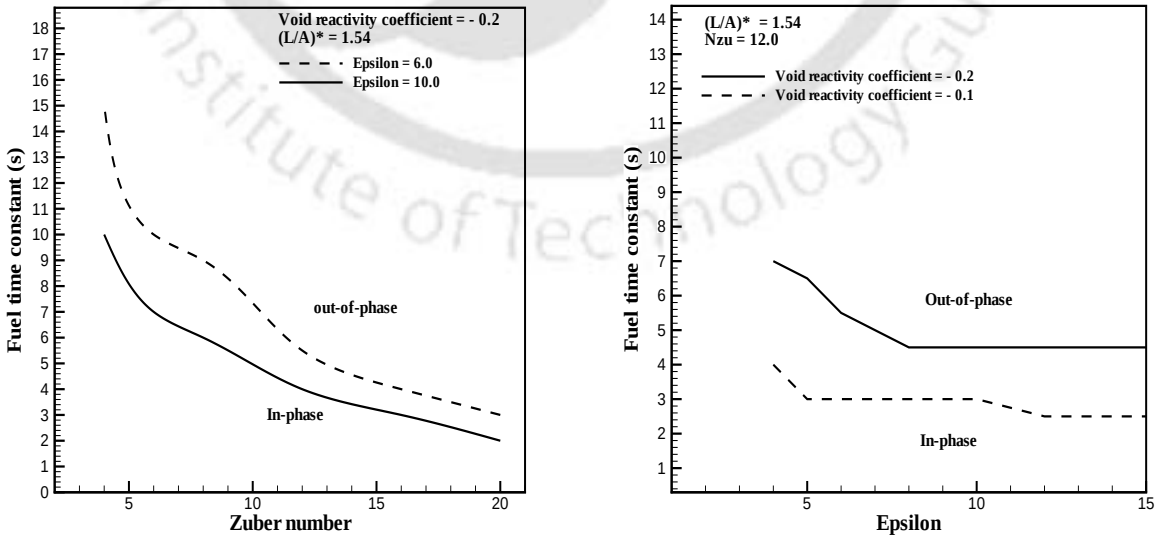

(a) Effect of ε number on modes of oscillations at different Zuber numbers (b) Effect of VR on modes of oscillations at different ε

Figure 6.6: Effect of Zuber number and VR on modes of oscillations

and suppress the gain of neutronic feedback and favors out-of-phase oscillations. It can be observed that at high Zuber numbers, the out-of-phase oscillations occur at relatively lower values of fuel time constant compared to lower Zuber numbers. The effect of ε is shown in Figure 6.6(a) at different powers. It can be observed that higher values of ε favor out-of-phase oscillations. In large cores, the distance between the subcores is large and the neutron interaction between the subcores reduces. The gain of neutronic feedback is large under strong neutronic interactions between channels (i.e., at lower values of ε). Thus, in-phase oscillations are favored with lower values of ε. Figure 6.6(b) further shows the effects of ε on oscillation modes at two different values of void reactivity coefficient. The boundaries appear to be flat at higher values of ε. Thus, in large cores the neutron interaction between the subcores (or interaction coefficient ε) has negligible effect on the modes of oscillations. However, in compact cores, the distance between the subcores is short and hence, the ε has a significant effect on the modes of oscillations (6.6(b)).

The effect of riser length in Type-II region ($N_{Zu} = 12.0$) for different values of VR is shown in Figure 6.7(a). In Type-II region, two-phase frictional pressure drop plays a dominant role. Increase in riser length increases gravitational pressure drop and favors out-of-phase oscillations. Figure 6.7(b) shows the effect of downcomer inertia on the oscillation modes. The downcomer inertia is characterized by (L_D^*/A_D^*). The effects of geometrical parameters such as area and length of core, area and length of downcomer, on the oscillation modes can be interpreted by the study of effect of (L_D^*/A_D^*). In Figure 6.7(b), the value of (L_D^*/A_D^*) is increased by reducing the area of downcomer. An increase in downcomer inertia suppresses the flow rate fluctuations in the downcomer. Hence, when the flow rate in one channel increases, then the flow rate in the other channel reduces, such that the total flow rate in the downcomer is unaffected. Therefore, increase in the downcomer inertia favors out-of-phase oscillations as shown in Figure 6.7(b). This result is in agreement with the observations made by (van Bragt, 1998). It can also be inferred that, increase in the flow area and the length of core favors the out-of-phase oscillations.

The effect of (L_D^*/A_D^*) at different powers and VR = -0.1 is shown in Figure 6.8. It can be observed that increase in the downcomer inertia favors out-of-phase oscillations at all values of Zuber number. In Section 5.4 the effect of downcomer inertia on the modes of oscillations in a double channel system is studied with constant heat flux condition (no neutronics). In the absence of neutronic feedback and delay effects (no heater wall dy-

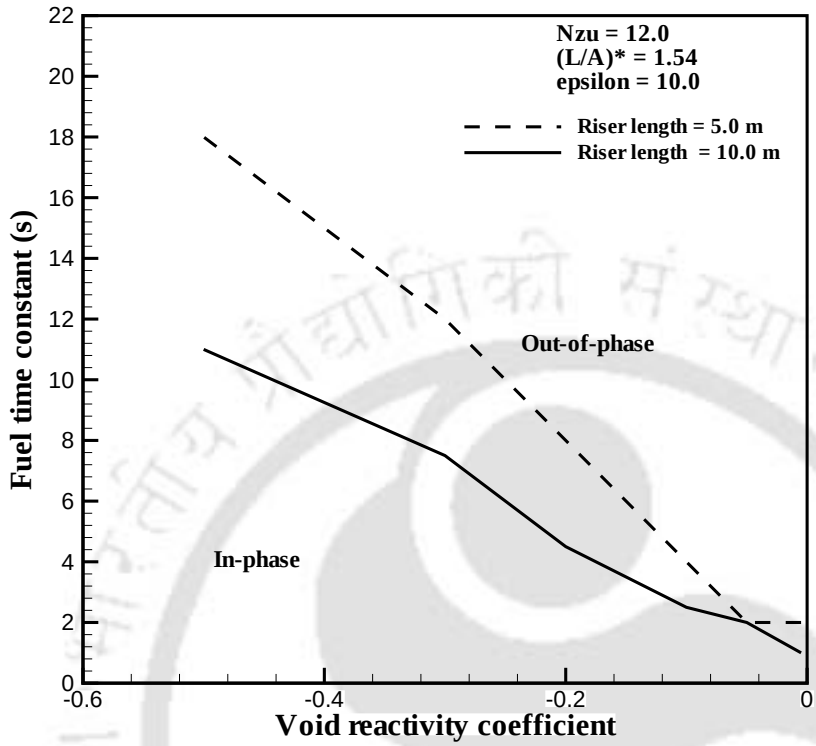

(a) Effect of riser length on modes of oscillations at different values of VR

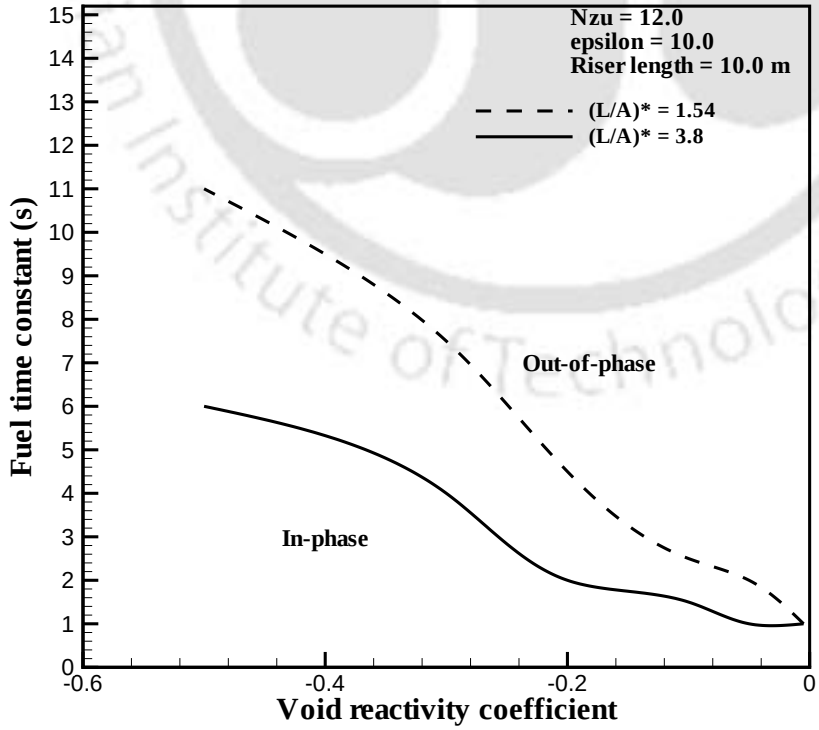

(b) Effect of downcomer inertia on modes of oscillations at different values of VR

Figure 6.7: Effect of riser length and downcomer inertia on modes of oscillations at different values of VR

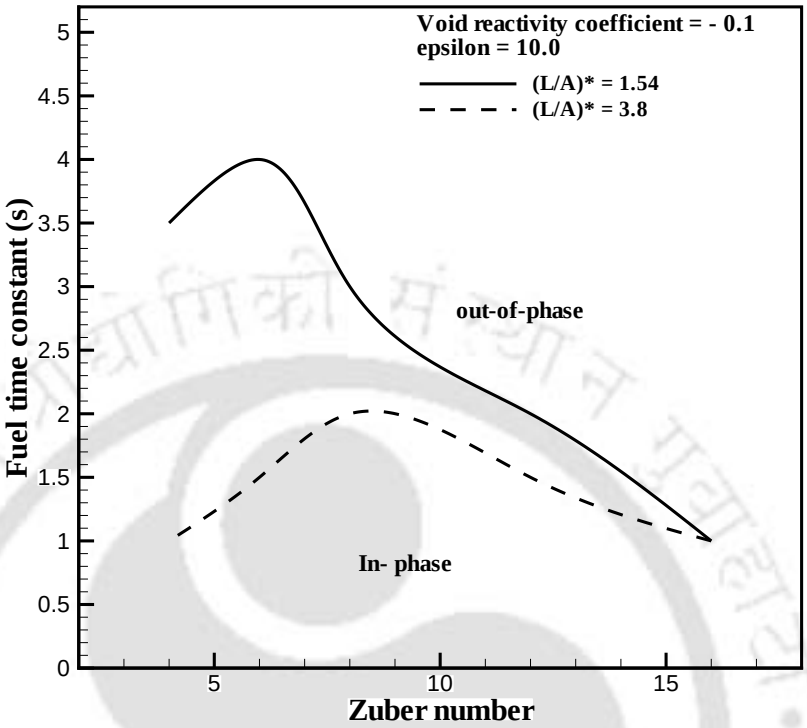

Figure 6.8: Effect of downcomer inertia on modes of oscillations at different Zuber numbers

namics), it was observed that in Type-I region (low Zuber numbers) the channels oscillate in out-of-phase mode and in Type-II region (high Zuber numbers) the channels oscillate in-phase (Figure 5.13). It was also observed that an increase in downcomer inertia favors out-of-phase oscillations in Type-II region, but has no effect in Type-I region (Figure 5.14). Though an increase in the downcomer inertia favors out-of-phase oscillations in the absence of neutronics, its effect is not seen in Type-I region because the out-of-phase oscillations in Type-I region occur due to the dominant gravitational pressure drop as discussed in Section 5.4.

However, when the neutronic feedback and delay effects are considered as in the present study (Figure 6.8), the effect of downcomer inertia at low Zuber numbers (Type-I region) can be studied. This is because the neutronic feedback favors in-phase oscillations which can be observed in Figure 6.8. However, when the downcomer inertia is increased and (or) the delay in heat transfer is increased (increase in fuel time constant), the out-of-phase oscillations are favored at all Zuber numbers.

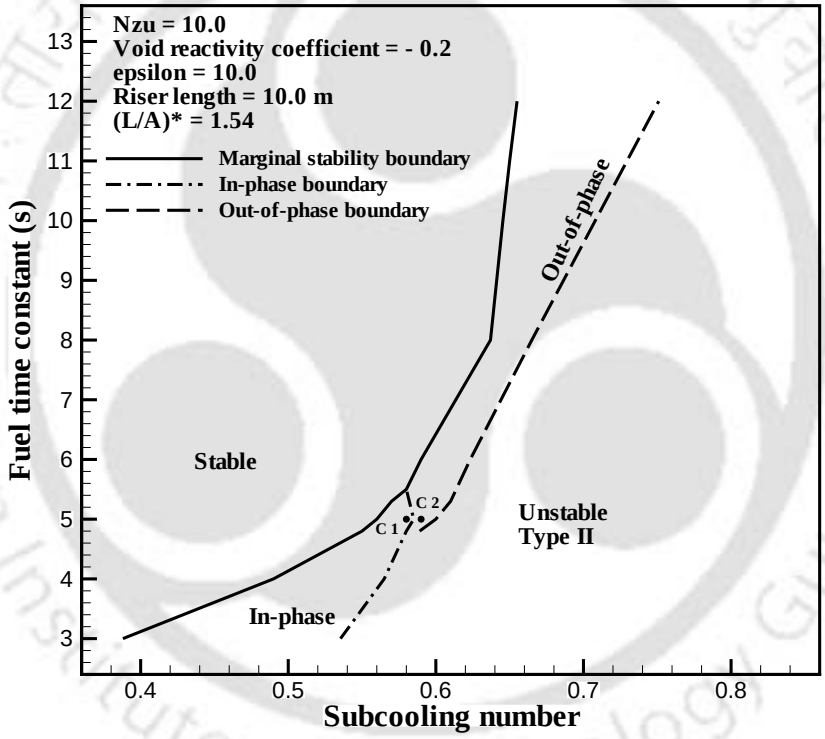

Figure 6.9: Bifurcation characteristics at point P1 (Figure 6.5(b)) during transition from in-phase to out-of-phase.

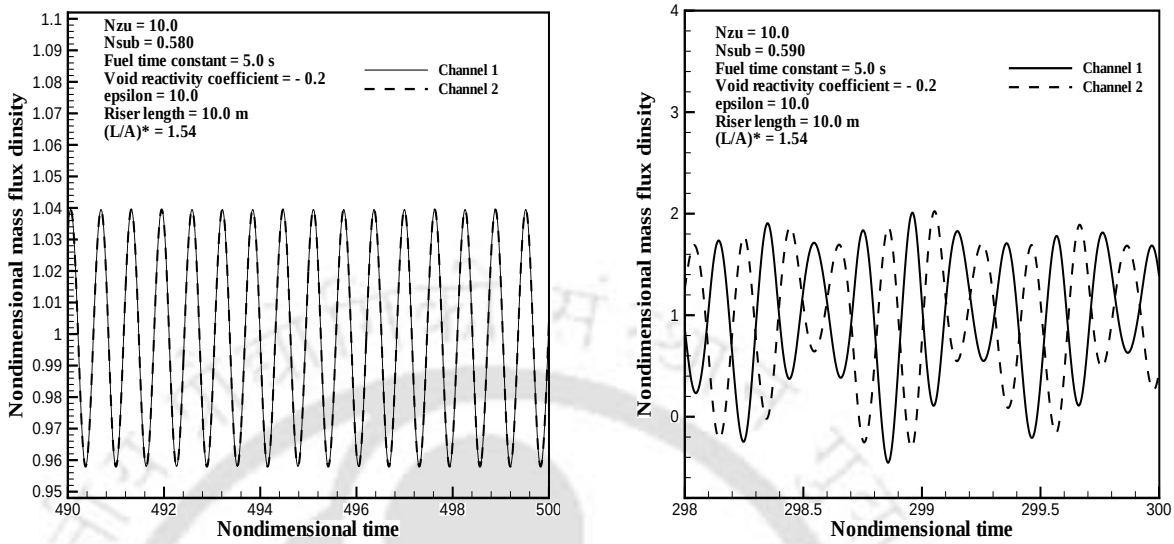

(a) Transient simulations at point C1 of Figure 6.9 (b) Transient simulations at point C2 of Figure 6.9

Figure 6.10: Transient simulations at point C1 and C2 of Figure 6.9

6.5 Nonlinear dynamics and bifurcation studies

As discussed in Section 6.3, when the stability boundary is crossed in the parameter plane, a pair of complex conjugate eigenvalues crosses the imaginary axis in the complex plane. Therefore, according to the Hopf bifurcation theorem, there is a possibility of existence of stable limit cycles (supercritical Hopf bifurcation) in the unstable region or unstable limit cycles (subcritical Hopf bifurcation) in the stable region. Transient simulations are carried out at different parameter values and the presence of periodic orbits, period doubling sequence, and chaotic oscillations (strange attractors) are investigated for both the in-phase and out-of-phase oscillation modes. The periods of stable and unstable periodic orbits are calculated using the limit cycle shooting technique (Parker and Chua, 1989) and cross checked with direct transient simulations. The presence of chaotic orbits is confirmed by plotting Poincaré sections, and by evaluating Lyapunov exponents.

Figure 6.9 shows the bifurcation characteristics at point P1 (Figure 6.5(b)) during transition from the in-phase to the out-of-phase mode. Transient simulations are carried out at N_{Zu} = 10.0 and VR = -0.2 in Type-II region for different values of fuel time constant. The study is carried out with riser length ($L_R = 10.0$ m) and downcomer inertia $(L_D^*/A_D^*) = 1.54$. The fuel time constant is varied form 2 to 15s. It is observed that the system undergoes supercritical Hopf bifurcation across the MSB (solid line in Figure 6.9)

for all values of fuel time constant. In the unstable region, for the values of fuel time constant lower than about 5s, the channels experience sustained in-phase oscillations, and for values higher than 5s, the channels oscillate out-of-phase. The transition from in-phase to out-of-phase oscillations takes place around fuel time constant equal to 5s where the subcooling number plays an important role in changing the mode of oscillations. It can be observed that at fuel time constant equal to 5s in-phase oscillations occurred initially at point C1 and on further increase in subcooling number, out-of-phase oscillations occurred at C2. Transient simulations are carried out at the two points C1 and C2. At point C1, the channels oscillate in-phase (Figure 6.10(a)) and it can be observed that it is a simple limit cycle. However, at point C2 (Figure 6.10(b)), it can be observed that the channels oscillate out-of-phase and have experienced period multiplication.

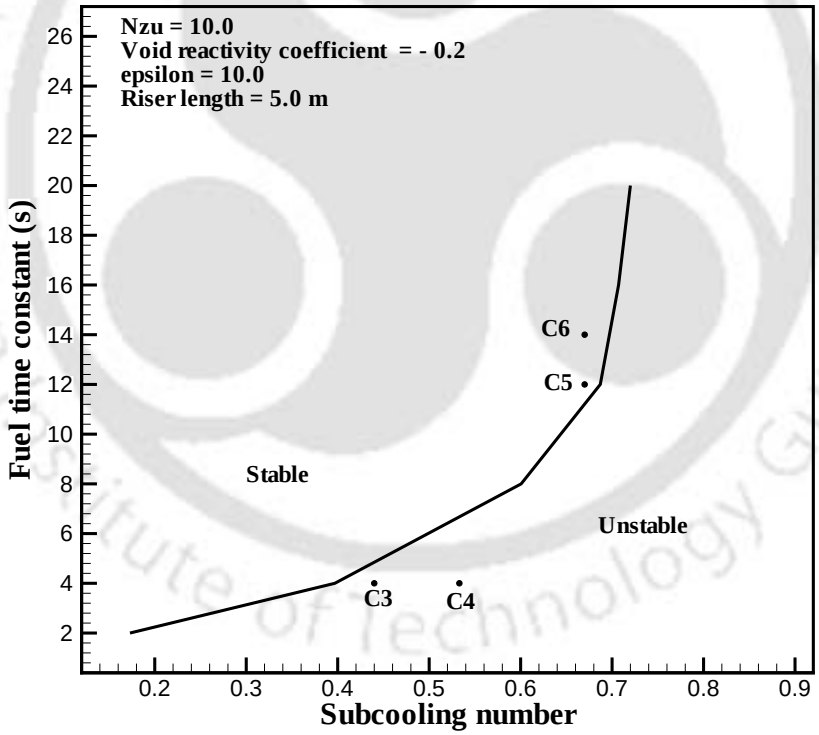

Figure 6.11: Bifurcation characteristics at riser length $L_R = 5.0$ m .

The effect of riser length on bifurcation characteristics is shown in Figure 6.11. The riser length is reduced to 5.0 m and the other operating conditions are the same as those in Figure 6.9. It is observed that the system experiences supercritical Hopf bifurcation at fuel time constant values below 5 seconds, approximately. A stable limit cycle at point C3 (Fuel time constant = 4.0s, $N_{sub} = 0.44$) is shown in Figure 6.12(a). The channels

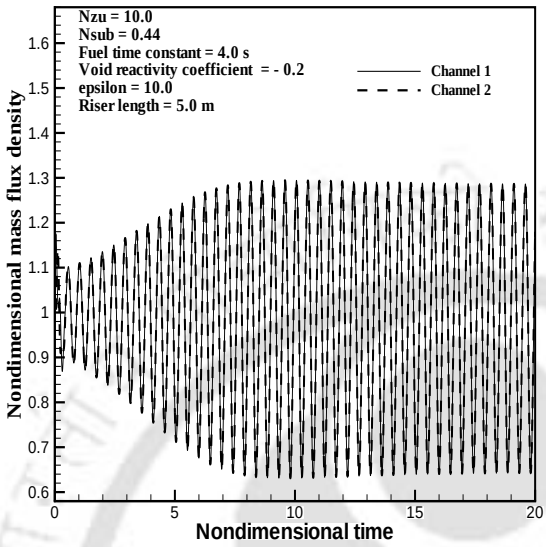

(a) Stable limit cycle at point C3 of Figure 6.11

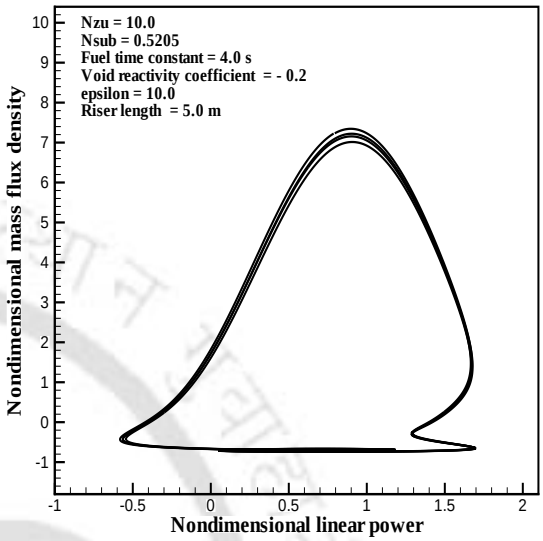

(b) Second period doubling observed at C4 of Figure 6.11

Figure 6.12: Transient simulations at points C3 and C4 of Figure 6.11

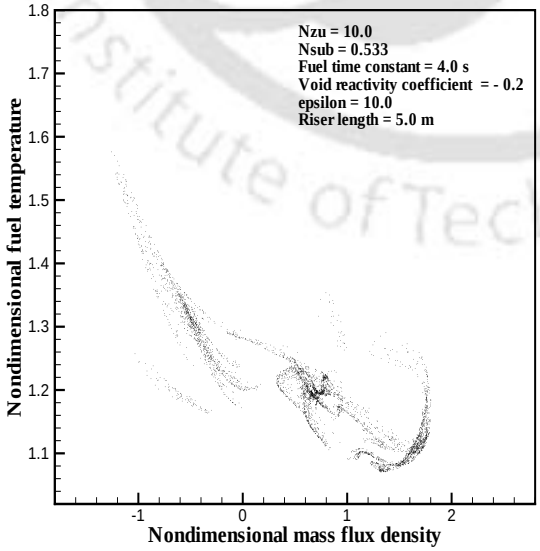

(a) Poincaré section at $N_{sub} = 0.533$

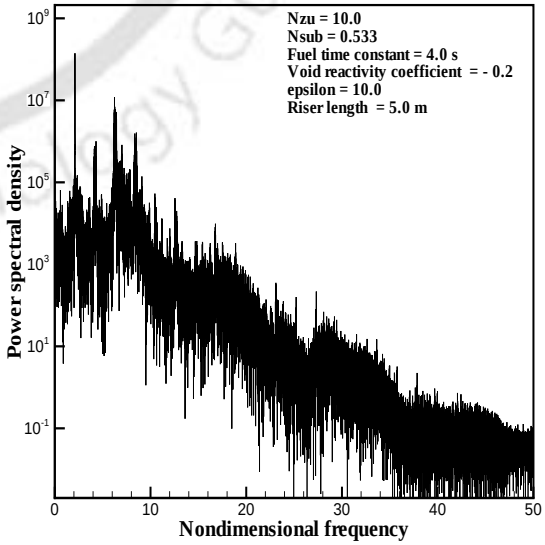

(b) Power spectral density at $N_{sub} = 0.533$

Figure 6.13: Poncare section and power spectral density at $N_{sub} = 0.533$

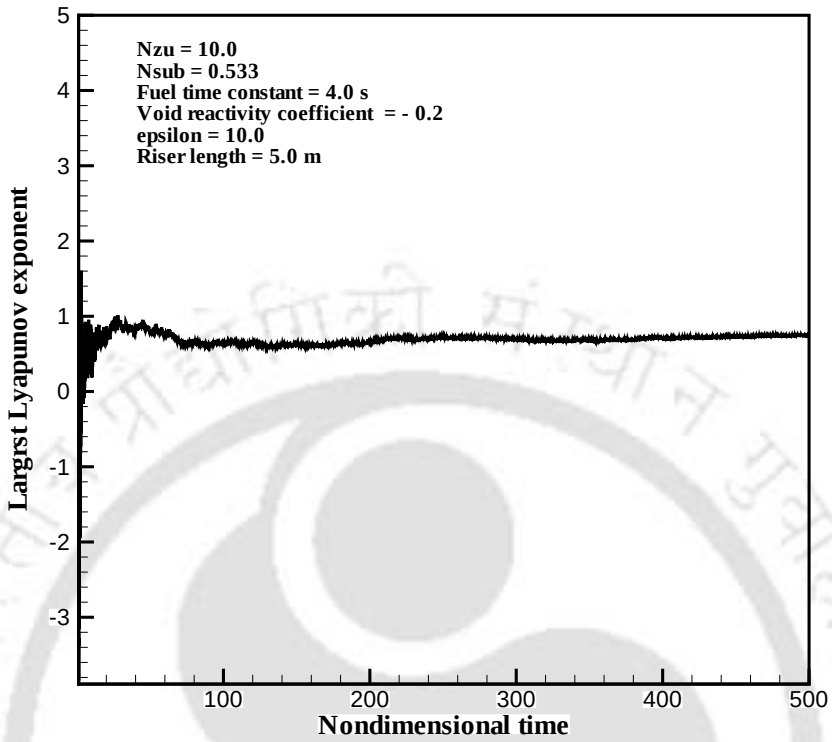

Figure 6.14: Largest Lyapunov exponent at $N_{sub} = 0.533$ for riser length = 5 m.

are observed to oscillate in-phase. As the subcooling number is slowly increased the period has quadrupled at point C4 ($N_{sub} = 0.5205$). The phase portrait of the quadrupling is shown in Figure 6.12(b). On further increase in N_{sub} a series of period doublings occurred and eventually the system became chaotic at $N_{sub} = 0.533$. A Poincaré section of the chaotic attractor is shown in Figure 6.13(a). The scattered nature of the points indicates chaotic behavior. Power spectral density and the largest Lyapunov exponent, are shown in Figures 6.13(b) and 6.14, respectively. The continuous power spectrum indicates the chaotic nature of oscillations. This is confirmed by the observation that one of the Lyapunov exponents is positive.

Further transient simulations are carried out by varying the fuel time constant between 5s and 20s to test the presence of periodic orbits near the MSB. It is observed that for fuel time constant values above 5s, the system experiences subcritical Hopf bifurcation (i.e., presence of unstable limit cycles in the stable region) and out-of-phase with each other. Transient simulations indicating the presence of unstable limit cycles at points C5 (fuel time constant = 12.0s, $N_{sub} = 0.67, N_{Zu} = 10.0$) and C6 (fuel time constant = 14.0s, $N_{sub} = 0.67, N_{Zu} = 10.0$) are shown in Figure 6.15(1) and 6.15(2), respectively. Unlike

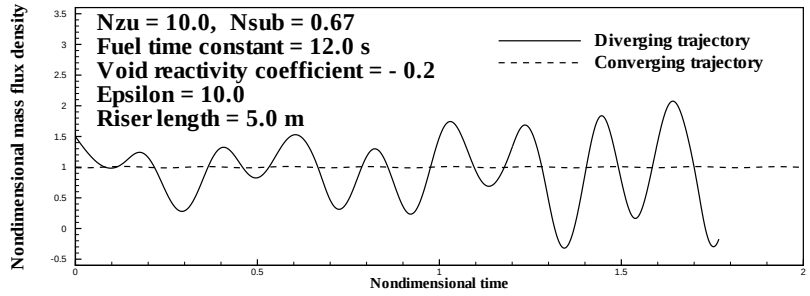

(1): Unstable limit cycle at point C5

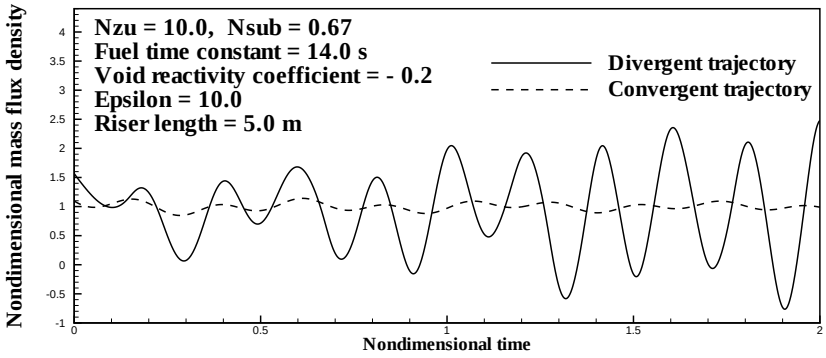

(2): Unstable limit cycle at point C6

Figure 6.15: Determination of unstable limit cycles at C5, C6 of Figure 6.11.

stable limit cycles, it is not possible to obtain the phase-portraits of unstable limit cycles by numerical integration, unless the initial point is exactly on the limit cycle. Therefore, trajectories emanating from two initial conditions are shown in Figure 6.15. The trajectory emerging from one initial condition diverges out (solid line in Figure 6.15), whereas the trajectory from other initial condition (dashed line in Figure 6.15) converges to the fixed point, which is locally stable. This shows that the system can be unstable for large disturbances even though it is stable for small perturbations about its steady-state.

The effect of riser length on chaotic oscillations is shown in Figure 6.16(a). The period doubling sequence with respect to the variation of N_{sub} is plotted for two different riser lengths (5m and 10 m) at $N_{Zu} = 10.0$ at VR = -0.2 and fuel time constant equal to 4.0s. The bifurcation parameter N_{sub} was increased slowly and the exact point of period doubling on the parameter plane was located using the method of limit cycle shooting and confirmed with transient simulations. The region between vertical lines A and B denotes a cascade of period doublings, the line B represents the onset of chaos, and the region between lines B and C is that in which the system was found to be chaotic. At riser length $L_R = 10$ m the difference between the occurrences of period doublings was very small,

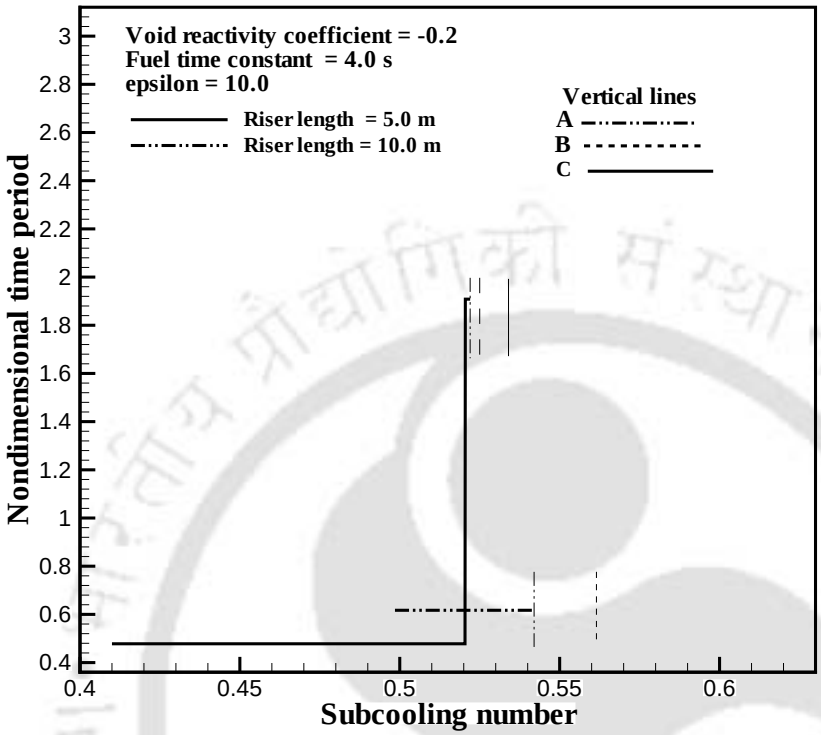

(a) Effect of riser length on chaotic oscillations

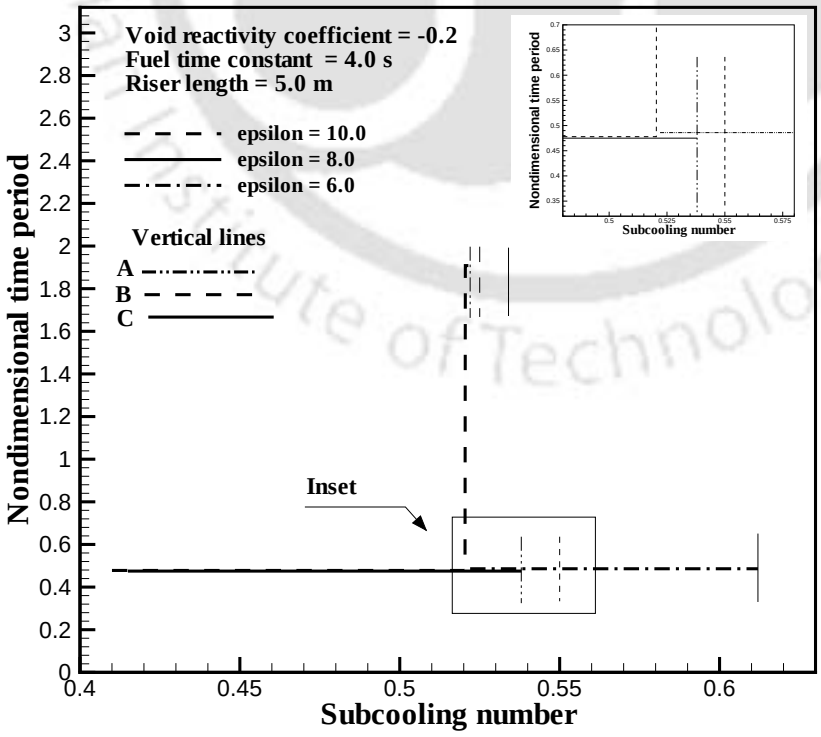

(b) Effect of ε on chaotic oscillations

Figure 6.16: Effect of riser length and ε on chaotic oscillations.

making it difficult to distinguish the exact points of period doublings in Figure 6.16(a). Hence, the region of higher periods is simply marked by vertical lines A and B. Lyapunov exponents are evaluated at line B (N_{sub} = 0.5615) for riser length $L_R = 10.0$ m. It is found that one of the Lyapunov exponents is zero and all the other exponents are negative, which means that the system is not chaotic. Thus, at riser length = 10m, the chaotic oscillations did not occur for the geometrical configuration considered in the present study. It can be observed that due to increase in riser length, the occurrence of Hopf bifurcation and the period doublings are delayed. Hence, it can be expected that if chaotic oscillations occur for some geometrical configurations, they will be delayed when the riser length is increased. The effect of neutron interaction coefficient on chaotic oscillations is shown in Figure 6.16(b). Period doubling studies are carried out for three different values of ε (i.e. ε = 6.0, 8.0, 10.0). It can be observed that the chaotic oscillations are delayed at lower values of ε. At ε = 6.0 the period doubling and chaos did not occur. Thus, strong neutron interaction among channels delays chaotic oscillations.

6.6 Summary

In the present chapter, a natural circulation double channel boiling system is modeled using the lumped parameter approach. The reactor kinetics is represented by multi-point neutron kinetics which includes the spatial variation of neutrons. The thermal-hydraulics is represented by LPM2. Stability analysis is carried out and parametric effects on modes of oscillations have been investigated. Furthermore, the parametric effects on bifurcation characteristics and chaos are investigated.

Increase in the absolute value of void reactivity coefficient has a stabilizing effect in Type-I region and destabilizing effect on Type-II region, and increases the frequency of oscillations in both Type-I and Type-II regions. The fuel time constant has a stabilizing effect on Type-II region and destabilizing effect on Type-I region. The frequency of oscillations increases with fuel time constant at low powers, and at higher powers (Type-II region) the frequency decreases with increase in fuel time constant. Increase in ε has a destabilizing effect on Type-II region and stabilizing effect on Type-I region. Lower the interaction coefficient, higher is the neutron interaction between the channels and increase in the stability of the system. Thus, it can be inferred that at high powers, compact

cores will be more stable compared to larger cores, while opposite will be the case at low powers.

Increase in Zuber number favors out-of-phase oscillations. The in-phase oscillations are favored by increase in the absolute value of void reactivity coefficient. This is because the gain of neutronic feedback increases with increase in absolute value of void reactivity coefficient. The delay in heat transfer from fuel rod to the coolant reduces the gain of neutronic feedback and favors out-of-phase oscillations. The delay effects are dominant at high powers. The out-of-phase oscillations occur at relatively lower values of fuel time constant at high Zuber numbers compared to lower Zuber numbers. In large cores, the distance between the subcores is large and the neutron interaction between the subcores reduces and favors out-of-phase oscillations. However, the gain of neutronic feedback is large under strong neutronic interactions between channels (i.e. at lower values of ε). Thus, in-phase oscillations are favored with lower values of ε. Furthermore, in large subcores or if the distance between the subcores is large, the neutron interaction between the subcores (or interaction coefficient ε) has negligible effect on the modes of oscillations. However, in compact cores, the distance between the subcores is very less and hence, ε has a significant effect on the modes of oscillations. Increase in riser length favors out-of-phase oscillations. The effects of geometrical parameters such as area and length of core, area and length of downcomer, on the oscillation modes can be interpreted by the study of effect of (L_D^*/A_D^*). An increase in the downcomer inertia suppresses the flow rate fluctuations in the downcomer and favors out-of-phase oscillations. It can also be inferred that, increase in the flow area and the length of core favors out-of-phase oscillations.

At riser length = 10 m, and VR = -0.2, the system was observed to undergo supercritical Hopf bifurcation at all values of fuel time constant. In the unstable region, as the fuel time constant is varied from 2s to 15s, there is a transition from in-phase to out-of-phase oscillation mode around fuel time constant equal to 5s. During this transition, it is observed that the subcooling number plays an important role in changing the mode of oscillations. At riser length = 5 m, supercritical Hopf bifurcation was observed for fuel time constant below 5s and the channels oscillate in-phase to each other. On the other hand, subcritical Hopf bifurcation was observed for fuel time constant values higher than 5s and the channels were observed to oscillate out-of-phase. The chaotic oscillations can be delayed by increasing the riser length. The chaotic oscillations are delayed at lower

values of ε. Thus, compact cores are more susceptible to chaotic oscillations compared to large cores.

Chapter 7

Summary and Conclusions

The present work consists of numerical studies on flow instabilities in natural circulation boiling systems. Thermal-hydraulic as well as coupled neutronic-thermohydraulic instabilities have been studied in single and double channel systems. Nonlinear oscillations, bifurcations and chaotic oscillations have also been investigated. Parametric effects on the stability, oscillation modes, bifurcation characteristics, and chaos in natural circulation boiling water reactors have been investigated.

7.1 Summary

Some of the salient features of the present work are summarized below

- A detailed review of the research carried out on instabilities in natural circulation boiling systems, is conducted. Work done on instabilities due to channel thermal hydraulics as well as neutronics thermal-hydraulics coupling has been reviewed. Different methods of analysis used by researchers and results obtained by them have been discussed. Various mathematical models and numerical techniques adopted for developing computer codes have also been discussed. The findings reported in the past three decades have been summarized to present the state of the art of the understanding of flow instabilities in natural circulation boiling systems.

- A lumped parameter mathematical model of a simple NCBWR is derived. The

power dynamics is represented by point neutron kinetics and multi-point kinetics. The heater wall dynamics is represented by a lumped parameter model. A non-dimensionalized lumped parameter thermal-hydraulic model based on homogeneous equilibrium mixture method is derived from the basic governing equations of mass momentum and energy. The one-dimensional PDEs are integrated along the boiling system and a generalized lumped parameter thermal-hydraulic model for a multi-channel system is developed. The model is derived with different state variables and compared.

- A pressure tube type natural circulation boiling water reactor is modeled using LPM as well as RELAP5/MOD3.4 which is based on a two-fluid model. Nodal sensitivity test of the RELAP5 model is carried out and a suitable nodalization scheme is selected. Stability analysis and parametric studies are carried out for the pressure tube type NCBWR using LPM1 and RELAP5 and the results are compared.

- Stability analysis and nonlinear dynamics of a single channel natural circulation boiling water reactor is done using lumped parameter model (LPM1). Parametric effects on the stability of a natural circulation boiling water reactor are studied. The influence of system parameters on the stabilizing and destabilizing effects of parameters like void reactivity feedback (VR) and fuel time constant are investigated. Stability maps are plotted on $N_{Zu} - N_{sub}$ parameter plane.

- Different, seemingly contradictory parametric trends reported earlier in literature about the effects of parameters such as void reactivity coefficient and fuel time constant on the stability of the system are resolved. For this purpose, three different system configurations have been analyzed using the same mathematical model. The influence of neutronic parameters, such as β, λ and Λ on the stabilizing or destabilizing effects of void reactivity coefficient and fuel time constant is also investigated. Further, in order to investigate the influence of neutronic parameters, the effect of void reactivity coefficient and fuel time constant was investigated for system 1 with the neutronic parameters of system 2.

- Nonlinear analysis has been carried out for the boiling channels with and with out riser. Both constant heat flux and coupled neutronic cases are considered. For constant heat flux case, transient simulations are carried out across the MSB in the Type-I and Type-II regions. Nonlinear analysis for coupled-neutronics case has

been done using one of the system configurations (system 1) to study the effects of parameters in Type-I and Type-II regions. The nature of Hopf bifurcation in both the regions has also been investigated. Further, nonlinear analysis has been carried out to study the effect of parameters such as VR, fuel time constant, core inlet and exit loss coefficients on the bifurcations and chaotic behavior of the system in Type-II region. Poincaré sections, Fourier power spectra and Lyapunov exponents were computed to confirm the chaotic behavior.

- The transient simulations were done using a modified Bulirsch-Stoer algorithm applicable for stiff systems of ODEs. This algorithm based on Richardson extrapolation technique is one of the best ways to obtain high-accuracy solutions to ODEs. The stable and unstable periodic solutions were located using the limit cycle shooting technique. This technique, based on the Newton-Raphson method and the orthogonality condition (Mees criterion), locates a point on a periodic orbit of an autonomous system and determines its period. Fourier power spectra were computed using an FFT algorithm with the sampling interval carefully chosen to avoid the aliasing problem. Poincaré sections (Parker and Chua, 1989) were computed by locating crossings of the trajectory with a hyperplane in the state-space.

- Channel thermal-hydraulic instabilities in a double channel system are investigated using LPM2 and RELAP5 models. A detailed study of instabilities and nonlinear oscillations are carried out using LPM. Parametric effects on the modes of oscillations are investigated. Channel-to-channel interaction and on-power refueling studies are carried out using RELAP5. Further, the channel-to-channel interaction and on-power refueling studies are extended to a pressure tube type natural circulation boiling water reactors.

- Coupled neutronic and thermal-hydraulic instabilities in a double channel system are investigated using LPM2. The core comprising a number of channels is modeled as a double channel system (each channel representing half of the reactor core). The power dynamics is represented by multi point reactor kinetics which accounts for the neutron diffusion between the sub-cores.

- Parametric effects on stability, modes of oscillations, and bifurcation characteristics are investigated for double channel system. Further, the effects of parameters such

as neutron interaction coefficient and riser length on the chaotic oscillations are investigated.

7.2 Conclusions

As summarized in the preceding section, a detailed investigation of parametric effects on the stability, and nonlinear oscillation in natural circulation systems has been presented in this work. Based on these results the following conclusions can be drawn.

- Extensive research has taken place on linear analysis of instabilities in natural circulation boiling systems. Different types of instabilities have been studied separately, experimentally and numerically, which makes it desirable to develop a unified stability map covering the entire parameter space and all types of instabilities. Many numerical codes have been developed to simulate neutronics and thermal-hydraulics, but development of user-friendly software with graphic user interface remains to be done. This will facilitate extensive numerical simulations of instabilities and thus help in improving reactor safety.
- The stability boundaries predicted by the lumped parameter models LPM1 and LPM2 perfectly matched as expected because both the models are mathematically equivalent. However, LPM2 is much faster than the LPM1. The elimination of quadratic equations in the LPM2 model makes it computationally faster than the LPM1.
- From the nodal sensitivity test of the pressure tube type NCBWR (Section 3.4), it is observed that the nodalization scheme has a significant effect on the parametric predictions and stability boundaries though the trends predicted by all the schemes are similar. Optimum selection of a nodalization scheme should be made on the basis of accuracy requirements and computational time. The parametric trends and stability boundaries predicted by LPM and RELAP5 models matched well. The differences in the parametric predictions can be attributed to various simplifying assumptions used in LPM.
- The difference in the way the VR and the fuel time constant effect the system stability can be either due to the influence of various geometric and neutronic parameters

or due to the difference in the modeling approaches. Since the present study has been conducted by using the same mathematical model with three different system configurations, and the results agree with the findings reported in literature, it is confirmed that the difference observed is not attributable to model uncertainties. It was also observed that the neutronic parameters such as β, λ, and Λ do not influence the nature of the effects of VR and fuel time constant on the system stability.

- For constant heat flux case, it is observed the system experienced supercritical Hopf bifurcation across the MSB in Type-I and Type-II regions. Stable limit cycles are located but there is no period doubling scenario. For coupled-neutronics case, in Type-I region fuel time constant has a strong influence on the bifurcation characteristics of the system. For fuel time constant values lower than 4.0s, the system experiences a subcritical Hopf bifurcation for all the values of VR explored. On the other hand for values of fuel time constant above 4.0s, the bifurcation was subcritical at values of VR greater (algebraically) than -0.09 and supercritical at values of VR less (algebraically) than -0.10. However, period doubling scenario and chaos was not observed in Type-I region.

- In Type-II region, the boiling channels with and without riser experience chaotic oscillations under strong reactivity feedback. Boiling channel with riser experiences chaotic oscillations at lower values of VR (in absolute sense) compared to boiling channel without riser. It is observed that, an increase in VR (absolute value) and core exit loss coefficient aggravates the chaotic oscillations. On he other hand, an increase in parameters such as fuel time constant and core inlet loss coefficient delayed the occurrence of period doubling and chaos. in other words, the parameters which have a stabilizing effect on the system delays the occurrence of period doubling and chaotic oscillations, and the parameters which destabilize the system aggravates the chaotic oscillations.

- In double channel (identical) system with equal power, the two channels oscillate out-of-phase in Type-I region due to dominant gravitational pressure drop at low powers. In Type-II region, the channels oscillate in both in-phase and out-of-phase modes depending on the dominance of two-phase frictional pressure drop and the downcomer inertia. Increase in the downcomer inertia favors out-of-phase oscillations. The downcomer inertia can be varied by varying the dimensions of the

boiling system. Thus, geometrical parameters influence the mode of oscillations in Type-II region, but not in Type-I region.

- Channel-to-channel interaction and on-power refueling studies are carried out for a double channel system using RELAP model. It is observed that at low powers, disturbance in one channel does not have significant effect on the other channel. At higher powers, disturbances in one channel significantly affect the dynamics of other channels. During on-power refueling, a near-stagnation condition or a low-velocity reverse flow can occur; the possibility of reverse flow being higher at lower pressures and lower powers.

- In the pressure tube type NCBWR, during refueling of one hot channel (HC1), the disturbance in mass flow rate observed in the average channel (AC) and other hot channel (HC2) was of the order of 0.5 to 1.0 percent of the mass flow rate in the respective channels. However, in the case of the double channel system it can be observed that during refueling in one channel (C2), the disturbance in mass flow rate in the other channel (C1) is nearly of the order of the mass flow rate in the channel.

- Increase in absolute value of void reactivity coefficient has a stabilizing effect in Type-I region and destabilizing effect on Type-II region, and increases the frequency of oscillations in both Type-I and Type-II regions. The fuel time constant has a stabilizing effect on Type-II region and destabilizing effect on Type-I region. The frequency of oscillations increases with fuel time constant at low powers, and at higher powers (Type-II region) the frequency decreases with increase in fuel time constant. Increase in ε has a destabilizing.

- Increase in Zuber number favors out-of-phase oscillations. The in-phase oscillations are favored by increase in absolute value of void reactivity coefficient. This is because the gain of neutronic feedback increases with increase in absolute value of void reactivity coefficient. The delay in heat transfer from fuel rod to the coolant reduces the gain of neutronic feedback and favors out-of-phase oscillations. The delay effects are dominant at high powers. The out-of-phase oscillations occur at relatively lower values of fuel time constant at high Zuber numbers compared to lower Zuber numbers.

- In large cores, the distance between the subcores is large and the neutron interaction between the subcores reduces and favors out-of-phase oscillations. However, the gain of neutronic feedback is large under strong neutronic interactions between channels (i.e. at lower values of ε). Thus, in-phase oscillations are favored with lower values of ε. Furthermore, in large subcores or if the distance between the subcores is large, the neutron interaction between the subcores (or interaction coefficient ε) has negligible effect on the modes of oscillations. However, in compact cores, the distance between the subcores is very less and hence, ε has a significant effect on the modes of oscillations.

- The effects of geometrical parameters such as area and length of core, area and length of downcomer, on the oscillation modes can be interpreted by the study of effect of (L_D^*/A_D^*). An increase in downcomer inertia suppresses the flow rate fluctuations in downcomer and favors out-of-phase oscillations. It can also be inferred that, increase in flow area and length of core favors out-of-phase oscillations.

- At riser length = 10 m, and VR = -0.2, the system was observed to undergo supercritical Hopf bifurcation at all values of fuel time constant. In the unstable region, as the fuel time constant is varied from 2s to 15s, there is a transition from in-phase to out-of-phase oscillation mode around fuel time constant equal to 5s. During this transition, it is observed that, the subcooling number plays an important role in changing the mode of oscillations. At riser length = 5 m, supercritical Hopf bifurcation was observed for fuel time constant below 5s and the channels oscillate in-phase to each other. On the other hand, subcritical Hopf bifurcation was observed for fuel time constant values higher than 5s and the channels were observed to oscillate out-of-phase. The chaotic oscillations can be delayed by increasing the riser length. The chaotic oscillations are delayed at lower values of ε. Thus, compact cores are more susceptible to chaotic oscillations compared to large cores.

7.3 Observations

A few observations and suggestions which may be useful in future extensions of the present work are given below.

- This thesis presents a detailed analysis of instabilities and nonlinear oscillations in natural circulation boiling systems. The knowledge generated by this study is likely to be useful for the design and operation of natural circulation boiling water reactors. Based on these studies, a suitable combination of geometrical, feedback, and neutronic parameters can be selected.

- It is suggested that, design optimization studies be carried out to develop better reactors and to choose the best operating conditions, from the point of view of performance, economy and safety. One such work has been carried out by Durga Prasad et al. (2008).

- Many numerical codes have been developed to simulate neutronics and thermal-hydraulics, but development of user-friendly software with graphic user interface remains to be done. This will facilitate extensive numerical simulations of instabilities and thus help in improving reactor safety.

- Nonlinear analysis of start-up transients: In the present study a high pressure lumped parameter model is used. The fluid properties are evaluated at constant system pressure. This restricts the use of this model to high pressure conditions and operational transients. In order to investigate the nonlinear dynamics of start-up-transients, a lumped parameter model in which fluid properties are evaluated at local pressure is to be used.

- Nonlinear dynamic analysis of the natural circulation boiling water system using three equation drift flux model: The drift flux model can be developed by incorporating minor changes in the lumped parameter model (which is based on homogeneous equilibrium mixture model) used in the present study. This analysis can give an insight into the modeling uncertainties in the predictions of the period doublings and chaotic oscillations.

- Effect of instabilities and chaotic oscillations on CHF: In the present the parametric effects on stability period doubling scenario and chaotic oscillations have been studied. In boiling systems, sustained flow oscillations can reduce the critical heat flux drastically. Experimental studies can be conducted to investigate the effect of instabilities and chaotic oscillations on critical heat flux

Appendix A

Steam drum statics

In steam drum, the saturated steam is separated and the saturated water mixes with feedwater and flows into downcomer. The steam drum dynamics is very slow compared to channel thermal-hydraulics because of its large volume. Hence, a steady mass balance is applied to the steam drum. Under steady state, the amount of subcooled feedwater is equal to the amount of saturated steam flow at steam drum outlet.

Applying steady mass and energy balances to steam drum, we get

$$m_{fi} - m_D + m_{Re}(1 - X_{Re}) = 0 \tag{A.1}$$

$$m_{fi}h_{fi} - m_s h_g - m_D h_D + m_{Re}h_{Re} = 0 \tag{A.2}$$

where,

m_{fi}: Mass flow rate (kg/s) of makeup feedwater.

m_D: Mass flow rate of subcooled water flowing into downcomer .

m_{Re}: Mass flow rate (kg/s) of two-phase mixture at riser exit.

m_s: Mass flow rate (kg/s) of saturated steam.

h_{fi}: Specific enthalpy (kJ/kg.s) of inlet feedwater .

h_D: Specific enthalpy (kJ/kg.s) of subcooled water in the downcomer. This is equal to the enthalpy of water at core inlet (i.e. $h_D = h_{ci}$).

The enthalpy at riser exit can be expressed as

$$h_{Re} = (1 - X_{Re})h_l + X_{Re}h_g \tag{A.3}$$

In natural circulation systems, it can be observed from equations A.1 and A.2 that, the core inlet subcooling depends on the power generated in the core. For instance, when power (or the Zuber number) increases, the core exit quality increases, and the circulation flow reduces (i.e. flow of saturated liquid into the feedwater mixer reduces due to increase in outlet steam flow). This affects the core inlet subcooling which is clear from the steady-state energy balance Eq. A.2. At low powers, the exit quality deminishes and the mass flow rate of saturated steam at the drum outlet reduces, which in turn results in reduction of feedwater flow. A simple relation between the feedwater inlet enthalpy and the core inlet enthalpy can be derived as below.

Under steady state conditions, as there is no mass accumulation, the mass flow rate into the downcomer is equal to the mass flow of two-phase mixture at the riser exit (i.e. $m_D = m_{Re}$). Hence, from equation A.1 we have,

$$m_{fi} = m_D X_{Re} \tag{A.4}$$

also, under steady state condition, the amount of feedwater supplied is equal to the amount of steam produced. Hence,

$$m_s = m_{fi} \tag{A.5}$$

substituting equations A.3, A.4 and A.5 in Eq. A.2 and simplifying, the relation between the feedwater inlet enthalpy and the enthalpy at the core inlet is given as

$$(h_l - h_{ci}) = X_{Re}(h_l - h_{fi}) \tag{A.6}$$

This Eq. A.6 can be expressed in non-dimensional form as

$$N_{sub} = N_{Zu}\left(\frac{h_l - h_{fi}}{h_g - h_{fi}}\right) \tag{A.7}$$

Hence, in natural circulation systems, the subcooling number depends on the Zuber number and the feedwater inlet enthalpy.

Appendix B

Derivation of momentum balance

Non-dimensional 1-D momentum equation is given as

$$-\frac{\partial P^*}{\partial z^*} = -\frac{\partial G^*}{\partial t^*} - \frac{1}{\rho^*}\left[\frac{\partial G^{*2}}{\partial z^*}\right] - \Lambda\frac{(G^*)^2}{\rho^*} - \frac{\rho^*}{N_{Fr}} \tag{B.1}$$

Each term in the momentum equation is integrated along each component of the boiling system to obtain the dynamic momentum balance in ODE form. The integration process is discussed here in detail.

INERTIAL PRESSURE DROP

Core

From momentum equation the inertial pressure drop term can be written as

$$-\frac{\partial P^*}{\partial z^*} = \frac{\partial G^*}{\partial t^*} \tag{B.2}$$

Integrating the Eq. B.2 from core inlet to outlet

$$-\int_0^1 \frac{\partial P^*}{\partial z^*}\, dz^* = \int_0^{z^*_{bb}} \frac{\partial G^*}{\partial t^*}\, dz^* + \int_{z^*_{bb}}^1 \frac{\partial G^*}{\partial t^*}\, dz^* \tag{B.3}$$

Applying Leibnitz's rule to the Eq. B.3, the inertial pressure drop in j^{th} channel can be written as

$$(\Delta P_i)_{c,j} = \left[\frac{d}{dt^*}\int_0^{z^*_{bb,j}} G^*_{ci,j}\, dz^*_{bb,j} - G^*_{ci,j}\frac{dz^*_{bb,j}}{dt^*}\right] + \left[\frac{d}{dt^*}\int_{z^*_{bb,j}}^{1} G^*_{ce,j}\, dz^*_{bb,j} - G^*_{ci,j}\frac{dz^*_{bb,j}}{dt^*}\right] \tag{B.4}$$

Simplifying and rearranging, the inertial pressure drop in core is given as

$$(\Delta P_i)_{C,j} = z^*_{bb,j}\frac{dG^*_{ci,j}}{dt^*} + \left(1 - z^*_{bb,j}\right)\frac{dG^*_{ce,j}}{dt^*} + \left(G^*_{ci,j} - G^*_{ce,j}\right)\frac{dz^*_{bb,j}}{dt^*} \tag{B.5}$$

Substituting the relation between $G^*_{ce,j}$ and $G^*_{ci,j}$ given by the Eq. 3.33 and after simplifications, the inertial pressure drop in core can be expressed in terms of core inlet mass flux density $G^*_{ci,j}$ as

$$(\Delta P_i)_{C,j} = \left[z^*_{bb,j} + \frac{(1 - z^*_{bb,j})}{1 + X^*_{ce,j}(N_{Zu,j} - N_{sub})}\right]\frac{dG^*_{ci,j}}{dt^*} + W_{2,j} \tag{B.6}$$

Where,

$$W_{2,j} = \left[(G^*_{ce,j} - G^*_{ci,j})\frac{dz^*_{bb,j}}{dt^*} - (1 - z_{bb,j})W_{1,j}\right] \tag{B.7}$$

$$W_{1,j} = \frac{N_{Zu,j}}{1 + X^*_{ce,j}(N_{Zu,j} - N_{sub})}\left[(1 - z^*_{bb,j})\frac{dT^*_{f,j}}{dt^*} - T^*_{f,j}\frac{dz_{bb,j}}{dt^*}\right] + \left[\frac{\left[G^*_{ci,j} + \left\{N_{Zu,j}(1 - Z^*_{bb})T^*_{f,j}\right\}\right](N_{Zu,j} - N_{sub})}{\left[1 + X^*_{ce,j}(N_{Zu,j} - N_{sub})\right]^2}\right]\frac{dX^*_{ce,j}}{dt^*} \tag{B.8}$$

Under constant heat flux assumption, $W_{1,j}$ reduces to

$$W_{1,j} = \left[\frac{-N_{Zu,j}}{1 + X^*_{ce,j}(N_{Zu,j} - N_{sub})}\right]\frac{dz_{bb,j}}{dt^*} + \left[\frac{\left[G^*_{ci,j} + \left\{N_{Zu,j}(1 - Z^*_{bb})\right\}\right](N_{Zu,j} - N_{sub})}{\left[1 + X^*_{ce,j}(N_{Zu,j} - N_{sub})\right]^2}\right]\frac{dX^*_{ce,j}}{dt^*} \tag{B.9}$$

Riser

Riser is divided into N_R nodes of equal length. Integrating Eq. B.2 over a riser node,

$$-\int_{R_{n-1}}^{R_n} \frac{\partial P^*}{\partial z^*}\, dz^* = \int_{R_{n-1}}^{R_n} \frac{\partial G^*}{\partial t^*}\, dz^* = \frac{d}{dt^*}\int_{R_{n-1}}^{R_n} G^*\, dz^* \tag{B.10}$$

If L_R^* is the length of each node, then $\int_{R_{n-1}}^{R_n} G^*\, dz^* = G_{Rav}^*$ and hence the inertial pressure drop in riser for j^{th}, channel can be expressed as

$$(\Delta P_i)_{R,j} = \frac{dG_{Rav,j}^*}{dt^*} \tag{B.11}$$

Where the average mass flux density in a riser with N_R nodes is given as

$$G_{Rav,j}^* = \frac{L_R^*}{N_R}\left[\sum_{N_R=1}^{N_R} G_{R,n,j}^*\right] \tag{B.12}$$

Further the mass flux density at the core and riser junction is defined as $G_{R,0,j}^* = G_{ce,j}^*/A_R^*$. Hence, using the relation between $G_{ce,j}^*$ and $G_{ci,j}^*$ (given by Eq. 3.33) and the relation between mass flux densities along a riser node (given by Eq. 3.35), the nodal mass flux density in riser can be expressed in terms of core inlet mass flux density $G_{ci,j}^*$as

$$G_{R,n,j}^* = \frac{G_{ci,j}^* + N_{Zu,j}T_{f,j}^*(1-z_{bb,j}^*)}{A_R^*(j_{3,R,n,j})} \tag{B.13}$$

Differentiation Eq. B.13 with respect to time and using equations B.11 and B.12 , the inertial pressure drop in riser can be expressed as

$$(\Delta P_i)_{R,j} = \sum_{n=1}^{N_R}\left[\frac{L_R^*}{A_R^*(j_{3,R,n,j})N_R}\right]\frac{dG_{ci,j}^*}{dt^*} + C_{n,j} \tag{B.14}$$

Where, $C_{n,j}$ is defined as

$$\begin{aligned} C_{n,j} = &\sum_{n=1}^{N_R}\frac{L_R^*}{N_R}\left[\frac{N_{Zu,j}}{A_R^*(j_{3,R,n,j})}\left\{(1-z_{bb,j}^*)\frac{dT_{f,j}^*}{dt^*} - T_{f,j}^*\frac{dz_{bb,j}^*}{dt^*}\right\}\right] \\ &-\sum_{n=1}^{N_R}\frac{L_R^*}{N_R}\left[\left\{\frac{(G_{ci,j}^* + N_{Zu,j}T_{f,j}^*(1-z_{bb,j}^*))}{A_R^*(j_{3,R,n,j})^2}\right\}\frac{dj_{3,R,n,j}}{dt^*}\right] \end{aligned} \tag{B.15}$$

and the time derivative for $j_{3,R,n,j}$ is given as

$$\frac{dj_{3,R,n,j}}{dt^*} = (N_{Zu,j} - N_{sub})\frac{dX^*_{R,n,j}}{dt^*} \tag{B.16}$$

where, the time derivative for $X^*_{R,n}$ is given by Eq. 3.48. For constant heat flux condition, the expression for C_n reduces to

$$C_{n,j} = \sum_{n=1}^{N_R} \frac{L^*_R}{N_R}\left[\frac{N_{Zu,j}}{A^*_R(j_{3,R,n,j})}\left\{-\frac{dz^*_{bb,j}}{dt^*}\right\}\right] - \sum_{n=1}^{N_R} \frac{L^*_R}{N_R}\left[\left\{\frac{(G^*_{ci,j} + N_{Zu,j}(1 - z^*_{bb,j}))}{A^*_R(j_{3,R,n,j})^2}\right\}\frac{dj_{3,R,n,j}}{dt^*}\right] \tag{B.17}$$

Downcomer

A constant area downcomer is considered and it is assumed that there is no carry under, hence, only single phase subcooled liquid flows.Integrating the Eq. B.2 along the length of downcomer, the inertial pressure drop in downcomer can be derived as

$$(\Delta P_i)_{D,j} = L^*_D \frac{dG^*_{Di}}{dt^*} \tag{B.18}$$

Where,G^*_{Di} is mass flux density at downcomer inlet. In a multichannel system (say M channels) , G^*_{Di} can be expressed as

$$G^*_{Di}A^*_D = G^*_{ci,1} + \sum_{j=2}^{M} G^*_{ci,j}\left(\frac{A_{C,j}}{A_{C,1}}\right) \tag{B.19}$$

Hence, the total inertial pressure drop is given as

$$(\Delta P_i)_j = (\Delta P_i)_{C,j} + (\Delta P_i)_{R,j} + (\Delta P_i)_{D,j} \tag{B.20}$$

Substituting equations B.6, B.14 and B.18 in Eq. B.20, the inertial pressure drop in terms of core inlet mass flux density $G_{ci,j}$ for a single channel system (put suffix $j = 1$) is derived as

$$(\Delta P_{i,1}) = \left[z^*_{bb,1} + \left\{\frac{(1 - z^*_{bb,1})}{1 + X^*_{ce,1}(N_{Zu,1} - N_{sub})}\right\} + \sum_{n=1}^{N_R}\left\{\frac{L^*_R}{A^*_R N_R(j_{3,R,n,1})}\right\} + \frac{L^*_D}{A^*_D}\right]\frac{dG^*_{ci,1}}{dt^*} + W_{2,1} + C_{n,1} \tag{B.21}$$

Where, the terms $W_{2,1}$ and $C_{n,1}$ are given by equations B.7 and B.17 respectively.

ACCELERATION PRESSURE DROP

From momentum equation the acceleration pressure drop term can be written as

$$-\frac{\partial P^*}{\partial z^*} = \frac{1}{\rho^*}\frac{\partial G^{*2}}{\partial z^*} \tag{B.22}$$

Core

Core is divided into single and two-phase regions. In single phase region $\rho^* = 1$ and in two-phase region $\rho^* = \frac{1}{(1+j_{2c,j})}$. Integrating the Eq. B.22from core inlet to outlet gives,

$$(\Delta P_a)_{C,j} = \left[G^{*2}_{ce,j}(1+j_{2c,j}) - G^{*2}_{ci,j}\right] \tag{B.23}$$

Riser

In riser, the mixture density ρ^* is defined as $\rho^* = \frac{1}{1+j_{2R,n,j}}$ where, $j_{2R,n,j} = (N_{Zu,j} - N_{sub})X^*_{R,n,j}$. Hence, integrating the Eq. B.22 from riser inlet to outlet gives,

$$(\Delta P_a)_{R,j} = \left[G^{*2}_{Re,j}(1+j_{2Re,j}) - G^{*2}_{Ri,j}(1+j_{2Ri,j})\right] \tag{B.24}$$

Downcomer

As stated above, a constant area downcomer is considered in the present study. Hence, the acceleration pressure drop in downcomer is zero.

$$(\Delta P_a)_D = 0 \tag{B.25}$$

GRAVITATIONAL PRESSURE DROP

From momentum equation the gravitational pressure drop term can be written as

$$-\frac{\partial P^*}{\partial z^*} = \frac{\rho^*}{N_{Fr}} \tag{B.26}$$

Core

The mixture density can be defined in terms of α_{cav} as $\rho = \rho_g \alpha_{cav} + (1 - \alpha_{cav})\rho_l$. This can be written in non-dimensional form as $\rho^* = \left[1 - j_{1c,j}\right]$. Integrating Eq. B.26 from core inlet to outlet gives,

$$(\Delta P_g)_{C,j} = \left[\frac{(1 - j_{1c,j})}{N_{Fr}}\right] \tag{B.27}$$

Riser

Similarly, the mixture density can be defined in riser as $\rho^* = \left[1 - j_{1R,n,j}\right]$. Integrating the Eq. B.26 from riser inlet to exit gives,

$$(\Delta P_g)_{R,j} = \sum_{n=1}^{N_R} \left[\frac{L_R^*(1 - j_{1R,n,j})}{N_R N_{Fr}}\right] \tag{B.28}$$

Downcomer

In downcomer, $\rho^* = 1$. Hence, integrating the Eq. B.26 from downcomer inlet to outlet, the gravitational pressure drop in downcomer is given as,

$$(\Delta P_g)_D = -\left[\frac{L_D^*}{N_{Fr}}\right] = -\left[\frac{1 + L_R^*}{N_{Fr}}\right] \tag{B.29}$$

Here, negative sign in Eq. B.29 indicates that the flow is in downward direction.

FRICTIONAL PRESSURE DROP

From momentum equation the gravitational pressure drop term can be written as

$$-\frac{\partial P^*}{\partial z^*} = \Lambda \frac{(G^*)^2}{\rho^*} \tag{B.30}$$

Core

Integrating Eq. B.30 from core inlet to outlet

$$-\int_0^1 \frac{\partial P^*}{\partial z^*}\, dz^* = \int_0^{z^*_{bb}} \Lambda \frac{(G^*)^2}{\rho^*}\, dz^* + \int_{z^*_{bb}}^1 \Lambda \frac{(G^*)^2}{\rho^*}\, dz^* \tag{B.31}$$

which gives,

$$(\Delta P_f)_{C,j} = \Lambda_C \left[\left\{ z^*_{bb,j} G^{*2}_{ci,j} \right\} + \left\{ G^{*2}_{ce,j} (1 - z^*_{bb,j}) \left(1 + \frac{1}{2} j_{2c,j} \right) \right\} \right] \tag{B.32}$$

Riser

Integrating the Eq. B.30 along riser which is divided into N_R nodes gives,

$$(\Delta P_f)_{R,j} = \sum_{n=1}^{N_R} \frac{\Lambda_R}{N_R} \left[G^{*2}_{R,n,j} (1 + j^*_{2R,n,j}) \right] \tag{B.33}$$

Single phase region

In components with single phase flow like downcomer, inlet header, inlet feeder pipes etc the density $\rho^* = 1$ and integrating Eq. B.30 along these sections gives the frictional pressure drop in single phase sections as

$$(\Delta P_f) = \Lambda G^{*2} \tag{B.34}$$

Hence, in downcomer, the frictional pressure drop is given as

$$(\Delta P_f)_D = \Lambda G^{*2}_{Di} \tag{B.35}$$

Where, G^*_{Di} is given by Eq. B.19

MINOR LOSSES

Entry and exit losses

The entry and exit losses in single phase region are evaluated using the equation

$$(\Delta P_m) = \frac{kG^{*2}}{2} \tag{B.36}$$

In two-phase region the entry and exit losses can be expressed as

$$(\Delta P_m) = \frac{kG^{*2}(1+j_2)}{2} \tag{B.37}$$

Where, k is loss coefficient, G is mass flux density at the entry or exit of the component and j_2 is given as $j_2 = (N_{Zu,j} - Nsub)X^*$. Here X^* is quality at the entry or exit of the component.

Hence, the dynamic momentum balance of the closed loop is given by the Eq. B.38 as

$$\left(\sum \Delta P\right)_{C,j} + \left(\sum \Delta P\right)_{R,j} + \left(\sum \Delta P\right)_D = 0 \tag{B.38}$$

Where, in each closed loop the term $(\sum \Delta P)$ is defined as

$$\left(\sum \Delta P\right) = \Delta P_i + \Delta P_a + \Delta P_g + \Delta P_f + \Delta P_m \tag{B.39}$$

Substituting the respective pressure drop terms discussed above in Eq. B.38, the dynamic momentum equation in terms of core inlet mass flux density is obtained.

Appendix C

Numerical methods

A dynamical system is one whose state evolves with time t. The evolution is governed by a set of rules that specifies the state of the system for either discrete or continuous values of time t. A continuous-time evolution is usually described by system of differential equations. The nonlinear lumped parameter model derived in Section 3.2 is a continuous time autonomous system which can be written as

$$\dot{Y} = F(Y, M) \tag{C.1}$$

where, Y is the state vector, F is the vector field and M is the vector of control parameters.

C.1 Calculation of fixed points

A fixed point is a point in state space where the vector field F of the Eq. C.1 vanishes i.e.,

$$F(Y, M) = 0 \tag{C.2}$$

At such a point, the integral curve of the vector field F corresponds to the point itself. Fixed points are also called as constant or stationary solutions. The fixed points at different values of parameter M can be evaluated by solving Eq. C.2, which is a system of nonlinear algebraic equations, either analytically or numerically. In the present work, the Eq. C.2 for the lumped parameter model discussed in Chapter 3 is complex and difficult

to solve analytically. Therefore, it is solved numerically.

Different numerical methods to solve nonlinear algebraic equations are discussed by Press et al. (1993). The successful convergence of the scheme depends critically on having a good first guess for the solution (which may or may not be available). Hence, it is desirable to use a globally convergent method which guarantees some progress towards the solution at each iteration (Press et al., 1993). In the present work, globally convergent Newton-Raphson method discussed by Press et al. (1993) is used to solve Eq. C.2. This algorithm first brackets the root and then refines it by a combination of the Newton-Raphson and the bisection methods. This keeps the root within the brackets while taking advantage of the rapid local convergence of the Newton's method. This also ensures an early exit if the root remains unbracketed within the given ranges of the parameter.

C.2 Linear stability analysis

Linear analysis is used to determine the stability of a system at different operating conditions. Stability boundaries can be plotted in the parameter space, in which the stable and unstable operating regions can be determined. Linear stability analysis involves three steps, described as follow.

C.2.1 Linearization and evaluation of Jacobian matrix

Consider Y_0 be the solution of C.1 for $M = M_0$. To determine the stability of this equilibrium solution, we superimpose on it a small disturbance 'y' and obtain

$$Y(t) = Y_0 + y(t) \tag{C.3}$$

Substituting Eq. C.3 in Eq. C.1 yields

$$\dot{y} = F(Y_0 + y, M_0) \tag{C.4}$$

Hence, the fixed point $Y = Y_0$ of Eq.C.1 has been transformed into the fixed point $y = 0$ of Eq. C.4. Expanding Eq. C.4 in a Taylor series about Y_0 and retaining only linear terms

in the disturbance leads to

$$\dot{y} = F(Y_0, M_0) + D_Y F(Y_0, M_0) y + O(||y||^2) \tag{C.5}$$

or

$$\dot{y} \approx D_Y F(Y_0, M_0) y \equiv Ay \tag{C.6}$$

where, 'A' is the Jacobian matrix which is the matrix of the first partial derivatives of the vector field 'F'. For a n-dimensional system, it is of the form

$$A = \begin{bmatrix} \frac{\partial F_1}{\partial Y_1} & \frac{\partial F_1}{\partial Y_2} & - & - & \frac{\partial F_1}{\partial Y_n} \\ \frac{\partial F_2}{\partial Y_1} & \frac{\partial F_2}{\partial Y_2} & - & - & \frac{\partial F_2}{\partial Y_n} \\ - & - & - & - & - \\ - & - & - & - & - \\ \frac{\partial F_n}{\partial Y_1} & \frac{\partial F_n}{\partial Y_2} & - & - & \frac{\partial F_n}{\partial Y_n} \end{bmatrix}$$

In simple systems, the evaluation of analytical Jacobian is simple and straightforward. However, in complex nonlinear systems, evaluation of analytical Jacobian matrix is difficult and error prone. In such situations, it is advisable to evaluate the Jacobian matrix numerically. In the present study, the first partial derivative of the vector field 'F' with respect to the state vector 'Y' is evaluated numerically using central difference scheme

$$F'(Y) = \frac{F(Y+h) - F(Y-h)}{2h} \tag{C.7}$$

The optimal choice of 'h', is given as

$$h \approx \epsilon_F^{\frac{1}{3}} S_\mu \tag{C.8}$$

where, S_μ is the characteristic (curvature) scale of the function 'F' over which it changes, and ϵ_F is the fractional accuracy with which the function 'F' can be evaluated (Press et al., 1993).

C.2.2 Evaluation of eigenvalues and determination of stability

Evaluation of eigenvalues of a matrix numerically, is a fairly complicated business. It is generally advisable to use the canned routines available in public domain. The eigenvalues of the Jacobian matrix for a given set of parameter values are calculated using the QR algorithm. The Jacobian matrices associated with the dynamical systems studied in the present work are, in general, nonsymmetric. Since a nonsymmetric matrix may not be balanced, it is first replaced by a balanced matrix with identical eigenvalues (Press et al., 1993). This reduces the sensitivity of the eigenvalues to rounding errors during numerical computations. The matrix is then reduced to a simpler Hessenberg form and the eigenvalues are calculated by using the standard QR algorithm aplicable to real Hessenberg matrices (Press et al., 1993).

Once the eigenvalues are evaluated, the stability of the system is determined by the nature of the eigenvalues. The system is said to be stable, if the real parts of all the eigenvalues are negative, and unstable if all or some of the eigenvalues have positive real parts.

C.2.3 Location of bifurcation points

The Jacobian matrix 'A' in Eq. C.6 and the associated eigenvalues are function of the control parameter vector 'M'. If one or more control parameters are slowly varied, a fixed point becomes nonhyperbolic (one or more eigenvalues have zero real part) at a certain location in the parameter space. then, if the stability of the system before and after this location is qualitatively different, this location is called bifurcation point, and the accompanying qualitative change is called bifurcation.

Several techniques have been discussed for the location of bifurcation point. In general the algorithms are iterative in nature and make use of the numerical techniques such as Newton-Raphson method, and bisection method to find the critical value of the parameter for which the Jacobian matrix has a pair of eigenvalues with zero real part. In the present work, an iterative algorithm with bisection method is used. The several steps involved in the iterative algorithm are listed below.

1. Select two initial values M_1, M_2 of the control parameter M in the parameter space. Set an error criterion $(E = 10^{-5} to 10^{-10})$ depending on the complexity of the system and the machine precision.

2. Compute the eigenvalues of the Jacobian matric at each value of control parameter.

3. Check the real parts of the eigenvalues computed at each value of control parameter

- If the real parts of all the eigenvalues computed at each of the control parameters are negative. Give flag integer I = 1 and go to Step 4
- If the real parts of all (or some) of the eigenvalues computed at each of the control parameters are positive. Set flag integer I = 2 and go to Step 4
- If the real parts of all the eigenvalues computed at one parameter value are negative but the real parts of all (or some) of the eigenvalues computed at other parameter value are positive. Set flag integer I = 3 and go to Step 5

4. If the flag integers from step 3 are I = 1 or 2

- The initial parameter values $M_1 and M_2$ do not bracket the critical parameter M_{cric}.
- Modify the initial guess values $M_1 and M_2$. A proper guess of these initial values can be made from the marginal stability boundary plots in the parameter space. In the present work the initial guess of the parameter values $M_1 and M_2$ is made from the stability plots on $N_{Zu} - N_{sub}$ parameter space where N_{sub} was the control parameter.
- Go to Step 2 and repeat.

5. If the flag integer is from step 3 is I = 3.

- We reach this step only when the guess values M_1 and M_2 bracket the critical value M_{cric}. Hence, the critical value M_{cric} lies somewhere between $M_1 and M_2$.
- Now compute $M_0 = (M_1 + M_2)/2$. Go to Step 6

6. Repeat the Steps 2 and 3 with parameter values M_1 and M_0. Then from Step 3

- If flag integers are I = 1 or 2. Then set $M_1 = M_0$
- Else if, the flag integer I = 3. Then set $M_2 = M_0$
- Go to Step 7

7. Compute the eigenvalues at M_0 and find the eigenvalue whose real part has the least absolute value (say IV_0).

- If $IV_0 \leq E$. Then it is the critical value. Set $M_{cric} = M_0$. Go to Step 8
- If, $IV_0 \geq E$. The algorithm has not yet converged. Go to Step 5 and repeat.

8. Print the critical parameter value M_{cric} and the corresponding eigenvalues.

In bisection method, we choose a mid point M_0 in the interval M_1 and M_2. Depending on the nature of the real parts of the eigenvalues computed at the two initial values, M_1 or M_2 are set equal to M_0 such that the new interval contains the critical value M_{cric}. In either case the interval containing the critical value is reduced by a factor of 2. The same procedure is repeated for the new interval. If the procedure is repeated n times, then the interval containing the critical value is reduced to the size

$$\frac{M_2 - M_1}{2^n} = \frac{\Delta M}{2^n} \tag{C.9}$$

Hence, after n, the critical value must lie within $\pm$ $(\Delta M/2^n)$ of the estimate. This means that the error bound at n^{th} iteration is $E_n = |\Delta M/2^n|$ and similarly $E_{n+1} = |\Delta M/2^{n+1}| = E_n/2$. That is, the error decreases linearly with each step ba a factor of 0.5. The bisection method is, therefore, linearly convergent. Since the convergence is slow to achieve a high degree of accuracy, a large number of iterations may be needed.

C.3 Nonlinear analysis

Linear stability analysis is widely used to study the parametric efefcts on the stability of the system. However, the information given by linear analysis is valid for small disturbances only. When larger disturbances occur, the nonlinearities amplify and eventually

lead to limit cycle oscillations and chaos. The time period of the oscillations and chaotic behavior can be studied using nonlinear techniques.

C.3.1 Location of periodic orbits

Once the critical value of the parameter M_{cric} is located where the real part of one (or more) of the eigenvalues are zero, the nature of the eigenvalues with zero real part will determine the type of bifurcation. If one or more eigenvalues are purely real and zero, then the bifurcation is said to static bifurcation. On the other hand, if a pair of complex conjugate eigenvalues with zero real part are present, then the bifurcation is called Hopf bifurcation which is also called dynamic bifurcation. In the present work, complex crossings are observed cross the marginal stability boundary confirming the occurrence of Hopf bifurcation. Hence, stable and unstable periodic orbits may exist in the neighborhood of the marginal stability boundary. The Hopf bifurcation is supercritical, if stable limit cycles exist in unstable region, and subcritical if unstable limit cycles exit in the stable region. The numerical techniques to locate these periodic orbits are discussed below.

Time integration (brute-force method)

One simple way to locate the periodic orbits in the unstable region is simulation of trajectories by numerical integration of the dynamical system defined by Eq. C.1. This method is also called as brute-force approach. A large number of algorithms are available in literature to approximate the behavior of a continuous-time systems. A proper choice of the method and a careful application play a crucial role in the computational accuracy and efficiency. Among the available methods, the major practical choices are the single step methods, the multi-step predictor-corrector methods, and the Bulirsch-Stoer extrapolation methods. the computational efficiency of multi-step methods is high compared to that of single step methods for many smooth problems (Pandey, 1996). The Bulirsch-Stoer methods use the powerful idea of extrapolating to zero step size and are perhaps the best known methods to obtain high accuracy solutions with minimal computational effort. the choice of a suitable method depends on the stiffness of the system to be integrated.

The lumped parameter model used in the present work is stiff due to an order of

magnitude difference between the prompt and delayed neutron life times, and the different time scales involved in the various feedback processes. The Bulirsch-Stoer method is used for transient simulations in the present work. Algorithm based on this method is given in the book by Press et al. (1993).

As said earlier, time integration method is simple and can be used to locate stable periodic orbits (supercritical Hopf bifurcation), period doubling scenario, and chaos. However, this method cannot predict the time period of the limit cycles, exact point of period doubling. Furthermore, this method miserably fails to locate unstable periodic orbits in the stable region.

Shooting method

To overcome the above shortcomings of the brute-force method, direct approaches in frequency and time domain have been proposed in literature. In time domain formulation, finite-difference schemes, shooting technique, and Poincaré map methods are commonly used (ref Nefey and balachandran). In the present study, we limit our discussion to shooting method applicable to autonomous systems. Consider that if one-parameter family of mappings $\phi_t : \Re^n \mapsto \Re^n$ represents the flow associated with the n-dimensional dynamical system (Eq. C.1), then a point Y on the periodic orbit and its period T are yielded by the zeros of

$$H(Y,T) \equiv \phi_T(Y) - Y. \tag{C.10}$$

The above Eq. C.10 is a system of n equations for $(n+1)$ unknowns, and an additional constraint must be used. Parker and Chua (1989) discuss an orthogonality constraint based on Mees criterion. This restricts the state correction term ΔY to be orthogonal to the trajectory at Y. This amounts to restricting ΔY to a hyperplane which changes position and orientation from iteration to iteration. Due to the constraint, the iterative procedure deviates from standard Newton-Raphson method, but inherits its convergence properties. In addition, the procedure requires the evaluation of the fundamental matrix Φ together

with the trajectory.

$$\begin{bmatrix} \dot{Y} \\ \dot{\Phi} \end{bmatrix} = \begin{bmatrix} F(Y) \\ D_Y F(Y)\Phi \end{bmatrix} \tag{C.11}$$

The matrix Φ is needed to evaluate the Jacobian matrix associated with Eq. C.10. The matrix-valued equation governing the evaluation of Φ is sometimes referred to as the variational equation and is integrated with the initial condition $\Phi(0) = I$, where I is the unit matrix. The detailed formulations of the iterative procedures based on the above considerations are discussed by Parker and Chua (1989). The system described by Eq. C.11 comprises of $(n^2 + n)$ equations.

C.3.2 Analysis of nonlinear oscillations

Fourier power spectra

The understanding gained about a dynamical system using the time -domain techniques presented earlier is significantly enhanced by extending the investigation to the frequency domain. It often yields surprisingly valuable information.

The time evolution of a dynamical system is represented by the time variation of $Y(\tau)$ of the state vector, or when sampled at regular intervals, by the time series of its dynamical variables. If we represent the time series of a particular dynamical variable by C.12

$$Y^{(k)}; \qquad k = 0, 1, ..., N-1, \tag{C.12}$$

Then the discrete Fourier transform of the N points $Y^{(k)}$ is given by

$$\hat{Y}^{(l)} = \sum_{k=0}^{N-1} Y^{(k)} e^{\frac{2\pi jkl}{N}}, \tag{C.13}$$

Where, $j = \sqrt{-1}$. For a real time series, we need to consider only L = 0,1,..., $\frac{N}{2}$. The transformation (Eq. C.13) can be carried out efficiently by using a fast Fourier transform (FFT) algorithm (Press et al., 1993). For this purpose, the number of points N in the time series (Eq. C.12) must be a power of 2

The periodogram estimate of the power spectral density (PSD) at $(\frac{N}{2}+1)$ frequencies f_l then is defined as

$$\begin{aligned} PSD(0) \equiv PSD(f_0) &= |\hat{X}^{(0)}|^2 \\ PSD(f_l) = 2|\hat{X}^{(l)}|^2, l &= 1,2,....,(\frac{N}{2}-1) \\ PSD(f_c) \equiv PSD(f_{\frac{N}{2}}) &= |\hat{X}^{(\frac{N}{2})}|^2 \end{aligned} \tag{C.14}$$

where $f_l = \frac{l}{N\Delta\tau}, \qquad l = 0,1,....,\frac{N}{2}$
$\Delta\tau$ = sampling interval for the time series (Eq. C.12), and
$fc = \frac{1}{2\Delta\tau}$, the Nyquist frequency.

A suitable normalizing factor can be included in Eq. C.13 or C.14. With values as above, the discrete form of Parseval's equation is written as

$$N\sum_{k=0}^{N-1}|Y^{(k)}|^2 = \sum_{t=0}^{\frac{N}{2}} PSD(f_l). \tag{C.15}$$

The above Eq.C.15 is useful in checking the overall accuracy of the transformation as well as in detecting any error due to misinterpretation of the output array from an FFT algorithm. This possibility arises as the input real array is replaced by the an output array containing components of a complex transform with some re-arrangement which can be implementation dependent.

While data filtering on smoothing of the spectral estimates is generally not required in numerical simulation studies of dynamical systems governed by ODEs, careful attention must be paid to aliasing the frequency resolution. All the spectral power that lies outside the Nyquist frequency range is aliased (falsely translated or folded back) into that range by discrete sampling. Thus the sampling interval $\Delta\tau$ must be such that the higher frequency harmonics beyond $fc = \frac{1}{2\Delta\tau}$ are negligible. If f_* denotes a characteristic fundamental frequency associated with the time series, then $\Delta\tau$ is selected such that

$$\frac{f_c}{f_*} = L \tag{C.16}$$

is a large number, say between 8 to 64. Once the spectrum has been calculated, one checks

whether or not $PSD(f_c) \rightarrow 0$, or is at least several orders of magnitude smaller than the dominant components of the spectrum. If not a larger value of L is required. For a good resolution in frequency, the frequency interval Δf between two consecutive points of the power spectrum must be small in comparison with f_*, i.e.,

$$\frac{f_*}{\Delta f} = S \tag{C.17}$$

should be large. If S is 16, for example, the higher frequency harmonics in the spectrum will be separated by 16 points each. If subharmonics of f_* are present in the time series, and it is sought to resolve them accurately, S must be increased suitably.

Once f_* is given and L and S are selected as above, the sampling interval and the number of points N in the time series are determined by

$$\Delta\tau = \frac{1}{2Lf_*}, \qquad N = 2LS \tag{C.18}$$

L and S should chosen such that N is a power of 2 as mentioned earlier. An estimate of f_*, the basic frequency associated with the time series, is based on a characteristic time scale, for example, the time spent between two consecutive points on a Poincaré section. In the periodic case, the latter becomes the time period of the orbit.

Poincaré sections

The phase space diagrams of a dynamical system of order n can be simplified by introducing an (n-1)-dimensional surface of sections in the phase space. Hence, instead of studying a complete trajectory, one monitors only the points of its intersection with this surface. This reduces the study of continuous time dynamical systems (flows) to the study of reduced-order discrete-time systems (maps). A set of points of intersection of the trajectory with a hypersurface, as the trajectory crosses the surface from one side to the other, is referred to as the Poincaré section. Mapping an intersection point onto the subsequent intersection point is referred to as Poincaré map. By the use of Poincaré sections or maps, the quantity of the data to be analyzed or manipulated is greatly reduced, since almost all the points on the trajectory can be ignored except the points of intersection with the surface of sections.

The crossings of a trajectory from one side to the other of a hypersurface $\Sigma(Y) = 0$ are located by calculating the value of Σ at each point of the trajectory until two consequitive points Y_1 and Y_2 lie on different sides of the surface, i.e., until $\Sigma(Y_1)$ and $\Sigma(Y_2)$ are of opposite signs. For one-sided Poincaré sections, the sign of $\Sigma(Y_1)$ must remain fixed. For taking sections with a (hyper) plane, we define it by a (unit) vector, $\hat{n}$, normal to the lane and a point Y_Σ on the plane:

$$\Sigma(Y) = \langle \hat{n}, Y - Y_\Sigma \rangle = 0, \tag{C.19}$$

where $\langle -, - \rangle$ denotes the inner product. If the components of $\hat{n}$ and Y_Σ other than those which are in the direction of Y_i are taken zero, we have a hyperplane defined by

$$Y_i = a, \tag{C.20}$$

where a is a constant which may be taken zero if the state variable X_i takes both positive and negative values. Such hyperplanes are the simplest to define and can also establish the fractional time for which the value of a state variable, e.g., temperature of fuel rod, is above the steady state value during an oscillation. Use of such hyperplanes requires minimum of calculation for locating a crossing as well as for obtaining the points of intersection, and these have been generally used in this work.

It should, however, be noted that the algorithms for locating the points of intersection are more accurate if the hyperplane is orthogonal to the trajectory (Parker and Chua, 1989). For hyperplanes defined by Eq. C.20 this will generally not be true.The condition of orthogonality can be satisfied by taking in Eq. C.19, Y_Σ a point on the trajectory and $\hat{n}$ in the direction of the vector field at that point. Even when the trajectory is known only approximately, this results in near orthogonal crossings. As the trajectory is more accurately calculated, both Y_Σ and $\hat{n}$ can be approximately updated. In the limit cycle shooting and the calculation of characteristic multipliers, we have used a hyperplane normal to the trajectory at the point where the magnitude of the vector field is maximum. This yields best accuracy, although the simpler option of using hyperplanes defined by Eq. C.20 is normally adequate.

Once the crossing is located, the simplest option for solving for $\Sigma(Y) = 0$ is by interpolation (Parker and Chua, 1989). The point of intersection can be located by Bisection

method as discussed earlier.

Lyapunov exponents

Aperiodicity (chaoticity) observed in different models of the BWR, with certain parameter range results from the exponential divergence of initial close points on the limit set (asymptotic orbit). The rate of this divergence is characterized by Lyapunov exponents. These are numerically computable - albeit expensive in terms of CPU time and give a precise quantitative definition of sensitive dependency on initial condition. The Lyapunov exponents are computed by numerically integrating the variational equations C.11. Starting from the initial condition (Y_0, I) integration of Eq. C.11 yields the state transition matrix $\Phi(t)$. Let m_i(t) denote the eigenvalues of $\Phi(t)$ then the Lyapunov exponents σ_i of the trajectory at Y_0 are given by (Parker and Chua, 1989):

$$\sigma_i := \lim_{t\to\infty} \frac{1}{t} \ln |m_i(t)|, \qquad i = 1, ..., n \tag{C.21}$$

In practice the above limit is computed by taking t large but finite, say, a few thousand times the characteristic time scale of the system. Integration of the variational equation for such large times can lead to numerical problems as $\Phi(t)$ may be unbounded at $t \to \infty$. Furthermore, for large t, all columns of $\Phi(t)$ tend to line up with the eigenvector corresponding to the largest $|\sigma_i|$ (Parker and Chua, 1989). This implies that for large t, the matrix $\Phi(t)$ becomes ill-conditioned, making a direct approach based on Eq. C.21 unworkable.

In the present work, the algorithm developed by Wolf et al. (1985) is used which overcomes both the problems mentioned above by the repeated use of the Gram-Schmidt orthonormalization procedure at fixed intervals of time. This algorithm can simultaneously find all the Lyapunov exponents of any asymptotically stable limit sets.

Bibliography

Achard, J.L., Donald, D. A., Lahey, R.T., 1985. The analysis of nonlinear density wave oscillations in boiling channels. J. Fluid Mechanics 155, 213–232.

Aguirre, C., Caruge, D., Castrillo, F., Dominicus, G., Geutjes, A.J., Saldo, V., van der Hagen, T.H.J.J., Hennigg, D., Huggenberger, M., Ketelaar, K.C.J., Manera, A., Munoz-Cobo, J.L., Prasser, H.M., Rohdei, U., Royerb, E., Yadigaroglu, G., 2005. Natural circulation and stability performance of BWRs (NACUSP). Nucl. Engg. Des. 235, 401–409.

Allison, C. M., Siefken, L. J., Coryell, E. W., 1992. SCDAP/RELAP5/MOD3 Code Development. Proc. of USNRC Twentieth Water Reactor Safety Information Meeting ,Maryland 2, 343–362.

Aritomi, M., Chiang, J. H., Nakahashi, T., Wataru, M., Mori, M., 1992. Fundamental study on thermo-hydraulics during startup in natural circulation boiling water reactor (I) Thermo-hydraulic instabilities. J. Nucl. Sci. Tech. 29 (7), 631–641.

Aritomi, M., J.H.Chiang, M.Mori, 1993. Geysering in parallel boiling channels. Nucl. Engg. Des. 141, 111–121.

Astrom, K.J., Bell, R.D., 2000. Drum boiler dynamics. Automatica 36, 363–378.

Bixer, N.E., Heames, T.J., Powers, D.A., 1992. VICTORIA-92 and its application to the PHEBUS-FPTO test. Proc. of USNRC Twentieth Water Reactor Safety Information Meeting ,Maryland 2, 323–342.

Boure, J. A., Bergles, A. E., Tong, L. S., 1973. Review of Two phase flow instability. Nucl. Engg. Des. 25, 165–192.

Bousbia-Salah, A., D'Auria, F., 2007. Use of coupled code technique for best estimate safety analysis of nuclear power plants. Progress in Nuclear Energy 49, 1–13.

Chaiko, M. A., Blythe, P. A., 1993. Influence of nuclear heating on two phase channel instabilities. Int. J. of Engg. Sci. 31 (2), 271–292.

Chang, C.-J., Lahey Jr, R. T., 1997. Analysis of chaotic instabilities in boiling systems. Nucl. Engg. Des. 167, 307–334.

Chiang, J. H., Aritomi, M., Mori, M., 1993. Fundamental study on thermo-hydraulics during startup in natural circulation boiling water reactor (II) Natural circulation oscillation induced by hydrostatic head fluctuation. J. Nucl. Sci. Tech. 30 (3), 203–211.

Chiang, J. H., Aritomi, M., Mori, M., Higuchi, M., sep 1994. Fundamental study on thermo-hydraulics during startup in natural circulation boiling water reactor (III) Effects of system pressure on Geysering and natural circulation oscilation. J. Nucl. Sci. Tech. 31 (9), 883–893.

Clausse, A., Lahey, Jr. R. T., 1990. An investigation of periodic and strang attractors in boiling flows using chaos theory. Ninth International Heat Transfer Conference,Jerusalum 2, 3–8.

Clausse, A., Lahey, Jr. R. T., 1991. The analysis of periodic and strange attractors during density-wave oscillations in boililng channels. Chaos, Solitons and Fractals. 1 (2), 167–178.

Clausse, Jr. A., Lahey, R.T., Podowski, M., 1989. An analysis of stability and oscillation modes in boiling multichannel loops using parameter perturbation methods. Int. J. Heat Mass Transfer 32 (11), 2055–2064.

Coddington, P., Macian, R., 2002. A study of the performance of void fraction correlations used in the context of drift-flux two-phase flow models. Nucl. Engg. Des. 215, 199–216.

Collier, J. G., 1994. Convective Boiling and Condensation. McGraw Hill Book Company.

de Kruijf, W.J.M., Ketelaar, K.C.J., Avakian, G., Gubernatis, P., Caruge, D., Manera, A., van der Hagen, T. H. J. J., Yadigaroglu, G., Dominicus, G., Rohde, U., Castrillo, H.-M. Prasserand F., Huggenberger, M., Hennig, D., Munoz-Cobo, J.L., Aguirre, C., 2003. Planned experimental studies on natural-circulation and stability performance of

boiling water reactors in four experimental facilities and first results (NACUSP). Nucl. Engg. Des. 221, 241–250.

de Kruijf, W.J.M., Sengstag, T., de Haas, D.W., van der Hagen, T. H. J. J., 2004. Experimental thermohydraulic stability map of a Freon-12 boiling water reactor facility with high exit friction. Nucl. Engg. Des. 229, 75–80.

Dijkman, F. J. M., 1971. Void fraction and stability of natural circulation water boiling in a vertical annulus heated internally. Nucl. Engg. Des. 15, 77–95.

Durga Prasad, G.V., Gopa Kishor, G., Pandey, M., Dixit, U. S., 2008. Numerical Simulations and Design Optimization of the PHT Loop of Natural Circulation BWR. Science and Technology of Nuclear Installations 2008 (Article ID 690357).

Dykhuizen, R. C., Roy, R. P., Kalra, S. P., 1986. Two fluid model simulation of density wave oscillations in a boiling flow system. Nucl. Sci. and Engg. 94, 167–179.

France, D. M., Carlson, R. D., Roy, R. P., 1986. Measurement and analysis of dynamic instabilities in fluid heated two phase flow. Int. J. Heat Mass Transfer 29 (12), 1919–1929.

Fukuda, K., Kobori, Tetsuo, 1979. Classification of two-phase flow instability by density wave oscillation model. J. Nucl. Sci. Tech. 16 (2), 95–108.

Furuya, M., Inada, F., van der Hagen, T.H.J.J., 2005a. Development of SIRIUS-N facility with simulated void reactivity feedback to investigate regional and core-wide stability of natural circulation BWRs. Nucl. Engg. Des. 235, 1635–1649.

Furuya, M., Inada, F., van der Hagen, T.H.J.J., 2005b. Flashing-induced density wave oscillations in a natural circulation BWR-mechanism of instability and stability map. Nucl. Engg. Des. 235, 1557–1569.

Guanghui, S., Dounan, J., Fukuda, K., Guo, Y., 2001. Theoretical study on density wave oscillation of two-phase natural circulation under circulation under low quality conditions. J. Nucl. Sci. Tech. 38 (8), 607–613.

Guanghui, S., Dounan, J., Fukuda, K., Guo, Y., 2002. Theoretical and experimental study on density wave oscillation of two phase natural circulation of low equilibrium quality. Nucl. Engg. Des. 215, 187–198.

Guido, G., Converti, J., Clausse, A., 1991. Density-wave oscillation in parallel channels-an analytical approach. Nucl. Engg. Des. 125, 121–136.

Guo, L. J., Feng, Z. P., Chen, X. J., 2001. Pressure drop oscillations of steam-water two-phase flow in a helically coiled tube. Int. J. Heat Mass Transfer 44, 1555–1564.

Hanggi, P., 2001. Investigating BWR Stability with a New Linear Frequency-Domain Method and Detailed 3D Neutronics. Ph.D. Thesis, Swiss Federal Institute of Technology Switzerland.

Hassard, B. D., 1981. Theory and applications of Hopf bifurcation. Vol. 41. London mathematical society Lecture note series.

Henry, A. F., 1975. Nuclear reactor analysis. MIT Press.

Hinds, D., Maslak, C., 2006. Next-generation nuclear energy: the ESBWR. Nuclear News 49, 35–40.

Inada, F., Furuya, M., Yasuo, A., 2000. Thermo-hydraulic instability of boiling natural circulation loop induced by flashing (analytical consideration). Nucl. Engg. Des. 200, 187–199.

Ishii, M., Kataoka, I., 1984. Scaling laws for thermal hydraulic system under single phase and two-phase natural circulation. Nucl. Engg. Des. 81, 411–425.

Iyer, K.N., Kadengal, A., 2003. Scaling of natural circulation boiling systems. Proc. of 2003 ASME Summer Heat Transfer Conference, Lasvegas, Nevada, USA.

Jain, K. C., Petrick, M., Miller, D., Bankoff, S. G., 1966. Self-sustained hydrodynamic oscillations in a natural-circulation boiling water loop. Nucl. Engg. Des. 4, 233–252.

Jeng, H. R., Pan, C., 1999. Analysis of two-phase flow characteristics in a natural circulation loop using the drift flux model taking flow pattern change and subcooled boiling into consideration. Annals of Nuclear Energy 26, 1227–1251.

Jiang, S. Y., Yao, M. S., Bo, J. H., Wu, S. R., 1995. Experimental simulation study on start-up of the 5 MW nuclear heating reactor. Nucl. Engg. Des. 158, 111–123.

Kaliatka, A., Uspuras, E., 2000. Benckmark analysis of main circulation pump trip events at the Ignalina NPP using RELAP5 code. Nucl. Engg. Des. 202, 109–118.

Kaliatka, A., Uspuras, E., 2002. Thermal-hydraulic analysis of accidents leading to local-coolant flow decrease in the main circulation circuit of RBMK-1500. Nucl. Engg. Des. 217, 91–101.

Karve, A. A., Rizwan-Uddin, Dorning, J. J., 1997. Stability analysis of BWR nuclear-coupled thermal hydraulics using a simple model. Nucl. Engg. Des. 177, 155–177.

Kengo, H., Akitoshi, H., Toshikazu, T., 1997. Neutronic model for modal multichannel analysis of out-of-phase instability in boiling water reactor cores. Annals of Nuclear Energy 24 (2), 99–111.

Kim, Y. I., Baek, W.P., Chang, S. H., 1999. Critical heat flux under flow oscillation of water at low-pressure low-flow conditions . Nucl. Engg. Des. 193, 131–143.

Kleinstreuer, C., 2003. Two-Phase Flow: Theory and Applications. Taylor & Francis Group.

Kmetyk, L.N., 1994. MELCOR 1.8.3 assessment: GE large vessel blowdown and level swell experiments. OSTI web site SAND-94-2316.

Kubicek, M., Marek, M., 1983. Computational methods in bifurcation theory and dissipative structures. Springer Verlag.

Kyung, I. S., Lee, S. Y., 1994. Experimental observation on flow characteristics in an open two phase natural circulation loop. Nucl. Engg. Des. 159, 163–176.

Lee, J.D., Pan, C., 2005a. Dynamic analysis of multiple nuclear coupled boiling channels based on a multi-point reactor model. Nucl. Engg. Des. 235, 2358–2374.

Lee, J. D., Pan, C., 1999. Dynamics of multiple parallel boiling chanel system with forced flows. Nucl. Engg. Des. 192, 31–44.

Lee, J. D., Pan, C., 2005b. Non linear analysis for a doble-channel two-phase natural circulation loop under low-pressure conditions. Annals of Nuclear Energy 32, 299–329.

Lee, J. D., Pan, C., 2005c. Nonlinear analysis for a nuclear-coupled two-phase natural circulation loop. Nucl. Engg. Des. 235, 613–626.

Leonard, M. T., Ashbaugh, S. G., Cole, R. K., Bergeron, K. D., Nagashima, K., 1996. A direct comparison of MELCOR 1.8.3 and MAAP4 results for several PWR and BWR accident sequences. OSTI web site.

Lewins, J., 1977. Nuclear Reactor Kinetics. Pergamon Press.

Lin, Y.N., Lee, J.D., Pan, C., 1998. Nonlinear dynamics of a nuclear-coupled boiling channel with forced flows. Nucl. Engg. Des. 179, 31–49.

Lorenzini, E., Spiga, M., Iadarola, G., D'Auria, F., 1991. Density wave instabilities in steam generators. Annals of Nuclear Energy 18 (1), 31–42.

Madni, I. K., 1992. MELCOR verification, benchmarking, and applications experience at BNL. Proc. of USNRC Twentieth Water Reactor Safety Information Meeting ,Maryland 2, 383–400.

Manera, A., 2003. Experimental and analytical investigations on flashing-induced instabilities in natural circulation two-phase systems - application to the startup of boiling water reactors. Ph.D. Thesis, Delft University of Technology Netherlands.

Manera, A., Prasser, H. M., van der Hagen, T. H. J. J., Mudde, R. F., de Kruijf, W. J. M., june 2001. A comparison of void-fraction measurements during flashing-induced instabilities obtained with a wire-mesh sensor and a gamma-transmission set-up. Proc. 4th International Conference on Multiphase Flow (ICMF-2001).

Manera, A., Rohde, U., Prasser, H.M., van der Hagen, T.H.J.J., 2005. Modeling of flashing-induced instabilities in the start-up phase of natural-circulation BWRs using the two-phase flow code FLOCAL. Nucl. Engg. Des. 235, 15171535.

Marcel, C.P., Rhode, M., van der Hagen, T. H. J. J., 2008. Fluid-to-fluid modeling of natural circulation boiling loops for stability analysis. Int. J. Heat Mass Transfer 51, 566–575.

March-Leuba, J., Blakeman, E. D., 1991. A mechanism for out-of-phase power instabilities in boiling water reactors. Nucl. Sci. and Engg. 107, 173–179.

March-Leuba, J., Cacuci, D. G., Perez, R. B., 1986a. Nonlinear dynamics and stability of boiling water reactor:Part1-Qualitative analysis. Nucl. Sci. and Engg. 93, 111–123.

March-Leuba, J., Cacuci, D. G., Perez, R. B., 1986b. Nonlinear dynamics and stability of boiling water reactor:Part2-Quantitive analysis. Nucl. Sci. and Engg. 93, 124–136.

March-Leuba, J., Rey, J. M., 1993. Coupled thermohydraulic-neutronic instabilities in boiling water nuclear reactors: a review of the state of the art. Nucl. Engg. Des. 145, 97–111.

Munoz-Cobo, J. J., Perez, R. B., Ginestar, D., Escriva, A., 1996. Nonlinear analysis of out of phase oscillations in boiling water reactors. Annals of Nuclear Energy 23 (16), 1301–1335.

Munoz-Cobo, J. L., Rosella, O., Miro, R., Escrira, A., Ginestar, D., Verdu, G., 2000. Coupling of density wave oscillations in parallel channels with high order model kinetics: Application to BWR out of phase oscillations. Annals of Nuclear Energy 27, 1345–1371.

Munoz-Cobo, J. L., Verdu, G., 1991. Aplicatlon of Hopf bifurcation Theory and Variational methods to the study of Limit Cycles in Boiling Water Reactors. Annals of Nuclear Energy 18 (5), 269–302.

Nair, S., Lee, S., Ishii, M., Revankar, S. T., 1996. Analysis of flow instabilities and their role on critical heat flux for two-phase down flow and low pressure systems. Int. J. Heat Mass Transfer 39 (1), 39–48.

Nayak, A. K., Vijayan, P. K., Saha, D., Raj, V. Venkat, 1998. Linear analysis of thermohydraulic instabilities of the advanced heavy water reactor (AHWR). J. Nucl. Sci. Tech. 35, 768778.

Nayak, A. K., Vijayan, P. K., Saha, D., Raj, V. Venkat, Aritomi, M., 2000. Analytical study of nuclear-coupled density-wave instability in a natural circulation pressure tube boiling water reactor. Nucl. Engg. Des. 195, 27–44.

OECD, Report, 2004. Neutronics/Thermal-Hydraulics coupling in LWR Technology: State of the art report. Nuclear Energy Agency.

Padki, M. M., Palmer, K., Kakac, S., Vegiroglu, T. N., 1992. Bifurcation analysis of pressure drop oscillations and the Ledinegg instability. Int. J. Heat Mass Transfer 35 (2), 525–532.

Pandey, M., 1996. Nonlinear reactivity interactions in fission reactor dynamical systems. Ph.D. Thesis, Indian Institute of Technology Kanpur.

Paniagua, J., Rohatgi, U. S., Prasad, V., 1999. Modeling of thermal hydraulic instabilities in single heated channel loop during startup transients. Nucl. Engg. Des. 193, 207–226.

Parker, T. S., Chua, L. O., 1989. Practical Numerical Algorithms for Chaotic Systems. Springer-Verlag.

Prasad, R. O. S., Doshi, J. B., Iyer, K.N., 1995. A numerical investigation of nuclear coupled density wave oscillations . Nucl. Engg. Des. 154, 381–396.

Press, W. H., Teukolsky, S. A., Wetterling, W.T., Flannery, B.P., 1993. Numerical Recipes in C. Cambridge University Press.

Qui, Suizhing, Takahashi, Minoru, Jia, Dounan, Su, Guanghui, jly 2003. Density wave instability of sodium boiling two-phase flow in a vertical annulus at low pressure. J. Nucl. Sci. Tech. 40 (7), 493–500.

Rao, Y. F., Fukuda, K., Kaneshima, R., 1995. Analytical study of coupled neutronic and thermodynamic instabilities in a boiling channel. Nucl. Engg. Des. 154, 133–144.

RELAP, RELAP Team, june 1995. Code manual volume1:Code structure, system models, and solution methods. NUREG/CR-5535.

RELAP, TEAM, 2001a. RELAP5/MOD3.3 Code manual volume I: Code structure, system models, and solution methods.

RELAP, TEAM, 2001b. RELAP5/MOD3.3 Code manual volume II: User's guide and input requirements.

Rizwan-Uddin, 2006. Turning points and sub-critical bifurcations in a simple BWR model. Nucl. Engg. Des. 236, 267–283.

Rohatgi, U. S., Chen, H. S., Khan, H. J., Mallen, A. N., Neymotin, L. Y., 1997. RAMONA 4B: A computer code with three-dimensional neutron kinetics for BWR and SBWR system transient-models and correlations. NUREG/CR-4356 1.

Saha, P., Ishi, M., Zuber, N., 1976. An experimental investigation of the thermally induced flow oscillations in two-phase systems. Trans. ASME, J. Heat Transfer, 616–622.

Saha, P., Zuber, N., 1978. An analytical study of the thermally induced two phase flow instabilities including the efect of thermal non-equilibrium. Int. J. Heat Mass Transfer 21, 415–426.

SCDAP/RELAP5, Development Team, 1997. SCDAP/RELAP5/MOD3.2 Code Manual Volume I: SCDAP/RELAP5 interface theory. NUREG/CR-6150 1.

Schuster, C., Ellinger, A., Knoor, J., 2000. Analysis of flow instabilities at the natural circulation loop DANTON with regard to non linear effects. Heat and Mass Transfer 36, 557–565.

Shieh, A.S., Ransom, V.H., Krishnamurthy, R., 1994. RELAP5/MOD3.0 code manual volume6: Validation of numerical techniques in RELAP5/MOD3.0.

Sinha, R.K., Kakodkar, A., 2006. Design and development of the AHWR– the Indian thorium fuelled innovative nuclear reactor. Nucl. Engg. Des. 236, 683700.

Summers, R.M., Jr, R.K. Kole., Smith, R.C., Stuart, D.S., Thompson, S.L., Hodge, S.A., Hyman, C.R., Sanders, R.L., 1992. MELCOR computer code manual. NUREG/CR-6119 2, 383–400.

Tsuji, M., Nishio, K., Narija, M., nov 1993. Stability analysis of BWRs using bifurcation theory. J. Nucl. Sci. Tech. 30 (11), 1107–1119.

Turso, J.J., March-Leuba, J., Edwards, R.M, 1997. A modal-based reduced order model of BWR out-of-phase instabilities. Annals of Nuclear Energy 24 (12), 921–934.

Uehiro, M., Rao, Y. F., Fukuda, K., 1996. Linear stability analysis on instabilities of in-phase and out-of-phase modes in boiling water reactors 33, 628–635.

Unal, H. C., 1980. Correlations for determination of the inception conditions of density wave oscillations for forced and natural circulation steam generator tubes. J. of Heat Transfer 102, 14–19.

Unal, H. C., 1981. Density wave oscillations in sodium heated once-through steam generator tubes. J. of Heat Transfer 103, 485–491.

Unal, H. C., 1985. Two simple correlations for the inception of density wave oscillations in long sodium heated steam generator tubes. Int. J. Heat Mass Transfer 28 (7), 1385–1392.

Urbonas, R., Uspuras, E., Kaliatka, A., 2003. State-of-the-art computer code RELAP5 validation with RBMK-related separate phenomena data. Nucl. Engg. Des. 225, 65–81.

van Bragt, D.D.B., 1998. Analytical modeling of boiling water reactor dynamics. Ph.D. Thesis, Delft University of Technology Netherlands.

van Bragt, D. D. B., Kruijf, W. J. M. De., Manera, A., van der Hagen, T. H. J. J., 2002. Analytical modeling of flashing-induced instabilities in a natural circulation cooled boiling water reactor. Nucl. Engg. Des. 215, 87–98.

van Bragt, D. D. B., Rizwan-Uddin, van der Hagen, T. H. J. J., 1999. Non linear analysis of a natural circulation boiling water reactor. Nucl. Sci. and Engg. 131, 23–44.

van Bragt, D. D. B., Rizwan-Uddin, van der Hagen, T. H. J. J., 2000. Effect of void distribution parameter and axial power profile on BWR bifurcation characteristics. Nucl. Sci. and Engg. 134, 227–235.

van Bragt, D. D. B., van der Hagen, T. H. J. J., 1998a. Stability of natural circulation boiling water reactors: PartI: Desciption stability model and theoretical analysis in terms of dimensionless groups. Nucl. Tech. 121.

van Bragt, D. D. B., van der Hagen, T. H. J. J., jan 1998b. Stability of natural circulation boiling water reactors: PartII: Parametric study of coupled neutronic-thermohydraulic stability. Nucl. Tech. 121.

van der Hagen, T.H.J.J., 1987. Experimental and theoretical evidence for a short effective fuel time constant in a boiling water reactor. Nucl. Tech. 83, 171–181.

van der Hagen, T. H. J. J., Stekelenberg, A. J. C., van Bragt, D. D. B., 2000. Reactor experiments on type-I and type-II BWR stability. Nucl. Engg. Des. 200, 177–185.

van der Hagen, T. H. J. J., van Bragt, D. D. B., Stekelenburg, A. J. C., 1997. Exploring the Dodewaard type I and type II stability; from startup to shutdown, from stable to unstable. Annals of Nuclear Energy 24 (8), 659–669.

Vanttola, T., Hamalainen, A., Kliemb, S., Kozmenkovb, Y., Weissb, F. P., Kereszturie, A., Hadek, J., Strmenskye, C., Stefanovaf, S., Kuching, A., Hlbocky, P., Sikoi, D., Danilin,

S., 2005. Validation of coupled codes using VVER plant experiments. Nucl. Engg. Des. 235, 507–519.

Wallis, G. B., 1969. One-dimensional Two-phase flow. McGraw-Hill.

Wolf, A., Swift, J.B., Swinney, H.L., Vastano, J.A., 1985. Determining Lyapunov exponents from a time series. Physica 16 D, 285–317.

Wu, C. Y., Wang, S. B., Pan, C., 1996. Chaotic oscillations in a low pressure two phase natural circulation loop under low power and high inlet subcoling conditions. Nucl. Engg. Des. 162, 223–232.